

**Thin Film Electroluminescent Displays produced  
using Sol-Gel Methods.**

**A Thesis**

**Submitted to**

**DUBLIN CITY UNIVERSITY**

**For the degree of**

**Doctor of Philosophy (PhD)**

**BY**

**YVONNE LYDON KAVANAGH B Sc , M Appl Sc**

**SCHOOL OF ELECTRONIC ENGINEERING**

**DUBLIN CITY UNIVERSITY**

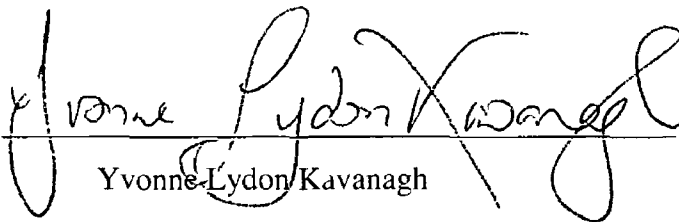
**RESEARCH SUPERVISOR**

**PROFESSOR DAVID CAMERON, BSc PhD CEng, MIEE**

January 2004

## DECLARATION

I hereby certify that this material, which I now submit for the assessment on the programme of study leading to award of Ph D is entirely my own work and has not been taken from the work of others save and to the extent that such work has been cited and acknowledged within the text of my work

Signed   
Yvonne Lydon Kavanagh

ID No 94970581

Date 14/1/04

## **Acknowledgements**

I would especially like to thank Professor David Cameron for his support, advice and encouragement during my time at DCU. Without his inspirational direction and continuous guidance I would not have continued and completed this thesis.

I would also like to thank Professor Charles McCorkell and Mr Jim Dowling for putting the facilities of DCU at my disposal.

I would like to thank Dr Ronan Scarfe, Professor Paul Whelan and Mr John Mallon for the use of their facilities.

I would like to thank Mr Liam Sweeney, Mr Klaus Agersbaek and Mr Kieran Watters, of PEI for their help and discussions during my time at DCU.

Thanks also to Dr Brian Lawless, Professor Brian McCraith, Dr Enda McGlynn, Professor Martin Henry, Gerard Tobin, Brendan Ryan and Dr Greg Hughes for their assistance.

I am grateful to the Physics Department and the Chemistry Department for use of instruments. A special thank you to Ms Veronica Dobbyn and Mr Maurice Burke of the Chemistry Department for their assistance.

Thank you to Mr Martin Johnson, Mr Mike Tyrrell, Mr Micheal May of the Mechanical engineering Department for their help and expertise.

A very special thanks to Ms Theresa Collins, Mr Billy Roarty, Mr Liam Meany, Mr Robert Clare, Mr Conor Maguire, Mr John Whelan, Mr Paul Wogan, and Ms Breda McManus, of the School of Electronic Engineering for their continued help and support.

I am grateful to Dr David Doff, dept of Geology Trinity College Dublin for his help with the X-ray Diffraction Measurements. I am also grateful to the NMRC for the use of their facilities and expertise under the EU Large Scale Facility Usage Scheme and also to Savcor Coatings Oy, Mikkeli, Finland, for the use of their XRD instrument.

I would like to thank Dr Sean Cawley, IT Carlow, Mr Mike Baker, IT Carlow and Dr Patricia Mulcahy, IT Carlow, who facilitated my studies

Thanks to Dr Loranne Vallely whose friendship and support throughout this project will always be appreciated Also a big thank you to Dr Una Ní Ghogain, Ms Aine O'Neill, Ms Anne O'Ruairc, Dr Bridget O'Regan, Dr Dina Brazil, Dr Nuala Eades, Ms Ita Michell, Ms Kíara O'Dea and Ms Breda Fagan for their help and support Also I would like to thank Mr Joe Bennett and Mr Pat Murphy for their mathematical discussions and Mr Kevin Kelly for his support

I would also like to thank Mr Jim Kavanagh, Mr Jim Walsh, Mr Richard Farrell, Mr Bob Stacey, of the Applied Biology and Chemistry Department, Mr Laz Murphy and Mr George Twinem of the Electronic Engineering Department, Mr Fergal Flanagan, Mr Colm O'Connor, Mr John Hegarty, Mr Ger Holohan, Mr Rae Dermody, Mr Jermie Sandot, Ms Gemma O'Meara, Ms Eileen O'Ceilleachair and Mr Matt Givens of Computer Services Department and Ms Yvonne Ffrench and Ms Thelma Keegan for their help

A very special thanks to my sister Jessica, my mother Maureen also sister Olga, Mary and William Kavanagh and Mary-Jo Nolan who were always there to offer help and support throughout this thesis

Last but most importantly, this thesis could not be written without the loving support, encouragement and patience of my husband Billy and children, Kevin and Liam

**To my husband, Billy  
And children,  
Kevin and Liam**

# Thin Film Electroluminescent Displays produced using Sol-Gel

## Methods.

### Abstract

An inverted double insulating thin film electroluminescent (TFEL) display has been fabricated using all sol-gel methods. This involved the production of three film types, an insulating material, a conducting film and a luminescent film. The layers have been evaluated individually and the combination effects are also looked at. The optimised film choice for the display is then given.

This investigation focused on manganese doped zinc sulphide (ZnS:Mn), which has a strong orange emission due to the  $\text{Mn}^{2+} \text{ } ^4\text{T}_1(^4\text{G}) \rightarrow ^6\text{A}_1(^6\text{S})$  transitions. It is produced from sol-gel deposited zinc oxide films. The oxide films are converted to zinc sulphide by annealing in a hydrogen sulphide-containing atmosphere. The conversion process was investigated and it was found that it takes place in a two-step process that is controlled by diffusion. The parameters of the conversion were optimised to produce the doped zinc sulphide having the changes in structure and composition as a function of sulphidation temperature and annealing time. It has been found that, after an initial "dead time", conversion takes place in a two-step manner where, for an initial period of approximately 60 mins. little diffusion takes place followed by faster diffusion with a diffusion coefficient of  $7.8 \times 10^{-18} \text{ m}^2\text{s}^{-1}$ , which is independent of sulphur concentration. It is also found that the sulphide forms the hexagonal, wurtzite phase with a strong (002) orientation.

The emission due to the  $\text{Mn}^{2+} \text{ } ^4\text{T}_1(^4\text{G}) \rightarrow ^6\text{A}_1(^6\text{S})$  transitions has been investigated using photoluminescence (PL), cathodoluminescence (CL), and electroluminescence (EL) and the correlation between the luminescence produced by the various methods has been studied. A comparison of the spectra using PL, CL and EL has shown how these excitation methods can be used to quantify the electroluminescence produced by the zinc sulphide. The luminescent properties of ZnS:Mn films have been investigated for their application as an emission layer in the thin film electroluminescent display. The luminescence of the device depends on the structure of the device and various structures were fabricated and the luminous output investigated. It was found in this case that the optimum structure is a five layer inverted structure. The luminescent properties also depend on the insulating films used in the device and their properties. In this case two insulating materials were investigated.

The insulating films used in the device were both tantalum pentoxide ( $\text{Ta}_2\text{O}_5$ ) and silicon dioxide ( $\text{SiO}_2$ ). Devices using both materials have been produced. The properties and the interaction between the emission layer and the insulating layer were investigated. The effect of the crystal structure of the  $\text{Ta}_2\text{O}_5$  on the luminescent properties of the device was also investigated. The luminescent characteristics of the fabricated devices have been measured and a comparison is made with the characteristics of sol-gel TFEL devices using  $\text{SiO}_2$  insulators. The TFEL devices with the  $\text{Ta}_2\text{O}_5$  insulators have shown higher stability and more reliability in their

operation Therefore  $Ta_2O_5$  is the preferred choice as an insulating material The conducting material chosen for this device is aluminium doped zinc oxide (ZnO Al) as it is a transparent conductor that is compatible with the insulating materials and enhances the performance of the device

# CONTENTS

Declaration	1
Acknowledgements	ii
Dedication	iv
Abstract	v

## Chapter 1 Introduction

1 1	Introduction	1
1 1 1	Cathode Ray Tube	1
1 1 2	Electroluminescent Displays	2
1 1 3	Plasma Displays	4
1 1 4	Liquid Crystal Displays	5
1 1 5	Cathodoluminescence	6
1 1 6	Field Emission Displays	7
1 1 7	Electrochromic Displays	7
1 1 8	Electronic Paper	8
1 2	Performance	8
1 2 1	Lifetime	8
1 2 2	Power, Luminous efficiency	9
1 2 3	Response time, Viewing Angle, Thickness, Gamut	9

## Chapter 2 Thin Film formation Techniques

2 1	Introduction	11
2 2	Evaporative techniques	11
2 3	Glow Discharge Technologies	12
2 3 1	Sputtering	13
2 3 2	Plasma Processes	14
2 4	Gas Phase Chemical Processes	15
2 5	Thermal Oxidation	18
2 6	Atomic Layer Epitaxy	19
2 7	Liquid phase chemical techniques	19
2 7 1	Anodization	19
2 7 2	Electroplating	20
2 7 3	Mechanical Methods	20
2 7	Selection of a coating method	20

## Chapter 3 Sol-Gel Film Formation

3 1	Introduction	21
3 2	History of the sol-gel process	21
3 3	Basic Principles	22



3.3.1	Introduction	22
3.3.2	Precursor Choice	23
	3.3.2.1 All alkoxide method	24
	3.3.2.2 Alkoxide salt method	24
3.3.3	Condensation	25
3.3.4	Gelation	27
3.3.5	Aging of gels	27
3.3.6	Drying of gels	28

## Chapter 4

### Sol- Gel Thin Film Deposition Techniques and Systems

4.1	Introduction	30
4.2	Advantages of sol-gel	30
4.3	Film production methods	30
	4.3.1 Dip coating	30
	4.3.2 Drain coating	32
	4.3.3 Spin coating	32
	4.3.4 Spray Pyrolysis	33
4.4	Film Deposition Systems	33
	4.4.1 Drain coating	33
	4.4.2 Dip coating method	35
4.5	Annealing systems	36
	4.5.1 Sulphidation System Design	37
	4.5.1.1 Heating System Design	38

## Chapter 5

### The Characterization of Thin Films

5.1	Introduction	41
5.2	Film Thickness Measurement	42
	5.2.1 Interferometry	42
	5.2.2 Ellipsometry	43
	5.2.2.1 Instrumentation	45
5.3	Electromagnetic wave interactions with matter	47
	5.3.1 Vibrational Spectrometry	47
	5.3.1.1 Fourier Transform Infrared Spectroscopy	48
	5.3.1.2 Raman spectroscopy	48
	5.3.1.3 Instrumentation	50
	5.3.2 Ultraviolet-Visible Spectroscopy	50
	5.3.3 Photoluminescence	51
	5.3.3.1 Instrumentation	52
	5.3.4 Cathodoluminescence	52
	5.3.4.1 Instrumentation	53
5.4	X-ray Diffraction	54
	5.4.1 Bragg's Law	54
	5.4.2 Instrumentation	56
5.5	Electron Microscopy	56
	5.5.1 Scanning Electron Microscope	56

5 5 2	Energy Dispersive X-rays	58
5 6	Electrical Measurements	59
5 6 1	Thin Film Resistivity measurement	59
5 7	Electroluminescence Measurements	62
5 7 1	Brightness Measurement	63
5 7 2	Electrical Device Characterization	64
5 7 3	Spectral Output Measurement	65

## Chapter 6 Phosphor Films

6 1	Introduction	66
6 2	Theory	66
6 2 1	Host Materials for Luminescence	67
6 2 2	Mechanisms of Luminescence	68
6 3	The isolated luminescent centre	69
6 3 1	Single Configurational Coordinate model	69
6 4	Non-radiative processes	71
6 5	Energy transfer	74
6 6	Luminescence Production	75
6 6 1	Excitons	76
6 6 2	Donor-Acceptor Pairs	76
6 6 3	Deep Level Centres	78
6 6 4	Host materials	79
6 6 5	Luminescent centres	80
6 6 5 1	Mn in ZnS	82
6 7	Production of zinc sulphide thin films	86
6 7 1	Diffusion Process	86
6 7 1 1	Vacancy Diffusion	87
6 7 1 2	Interstitial Diffusion	87
6 7 1 3	Steady State Diffusion	88
6 7 1 4	Non Steady State Diffusion	89
6 7 1 5	Thin Film Solution	90
6 7 2	Conversion of zinc oxide thin films	94
6 7 2 1	Conclusions	104

## Chapter 7 Electroluminescence

7 1	Introduction	105
7 2	Thin film Electroluminescent Devices	105
7 2 1	D C TF Electroluminescence	106
7 2 2	Organic TF Electroluminescence	106
7 2 2 1	Alq Devices	107
7 2 2 2	Polymer Devices	108
7 2 3	A C TF Electroluminescence	108

7.3	Device Physics	111
7.3.1	Tunnel Emission	112
7.3.2	Electron Acceleration	113
7.3.3	Impact excitation/ ionisation	115
	7.3.3.1 Impact excitation	116
	7.3.3.2 Impact ionisation	117
7.3.4	ElectroLuminescence	119
7.4	Luminescence Studies	120

## Chapter 8

### Transparent Insulating and Conducting Thin Films

8.1	Introduction	123
8.2	Film Properties	123
8.2.1	High dielectric constant	123
8.2.2	Dielectric Breakdown strength	124
8.2.3	Film Breakdown Characteristics	124
	8.2.3.1 Propagating Breakdown	125
	8.2.3.2 Self- Healing Breakdown	125
8.2.4	General properties	125
8.2.5	Driving Voltage	125
8.2.6	Stability	126
8.2.7	Insulator-Electrode Interfaces	127
8.2.8	Thermal Conductivity	127
8.2.9	Insulator-semiconductor Interface	127
	8.2.9.1 Bottom Insulator and Active Layer	127
	8.2.9.2 Nature of Insulator-Semiconductor Interface States	128
8.3	Material Choice	128
8.3.1	Silicon Dioxide Thin Films	130
8.3.2	Tantalum Pentoxide Thin Films	133
8.4	Conducting Thin Films	139
8.4.1	Introduction	139
8.4.2	Zinc oxide and doped zinc oxide thin films	140
	8.4.2.1 Optical Properties	145
8.5	Conclusions	146

## Chapter 9

### Display Characteristics

9.1	Introduction	148
9.2	Electro-optical Properties	148
9.2.1	Ideal Model	148
9.2.2	Polarisation Characteristics	152
9.2.3	Charge v Voltage Characteristics	152
9.2.4	Luminance Measurements	155
9.3	Device Results	157
9.3.1	Introduction	157
9.3.2	Structural Properties	157
9.3.3	Electronic Properties	158

9 3 3 1	Threshold voltage	159
9 3 3 2	Charge vs Voltage	159
9 3 4	Optical Properties	162
9 3 4 1	Electroluminescence	162
9 3 4 2	Luminescence	165
9 3 4 3	Brightness	167
9 3 4 4	Stability and Reliability	172

## **Chapter 10**

### **Conclusions and Future work**

10 1	Introduction	174
10 2	Conclusions	174
10 3	Future Work	176
Appendix I		178
Introduction		178
Device 1		178
Device 2		179
Device 3		180
Device 4		180
Device 5		181
Device 6		181
References		183

# Chapter 1

## Introduction

### 1.1 Introduction

The displays industry today is a multi-billion euro industry that is constantly looking for new opportunities and new display types as the markets expand. From mobile phones to projection systems, many different display types are required for the different market areas. The vision that “videophones will also serve as video intercoms and TVs will serve as portals to the ever expanding internet” coupled with “every elevator will have a captive audience and every room will enable a “yahoo” search”<sup>1</sup>, explains how this market is expected to grow over the next decade. The EU currently has a budget of 75 million euro to fund research in the area of display technologies. These new application areas require a variety of flexible display types to meet the market demands since no single display type has been found to satisfy all application areas.

While the CRT is still the favourite for the family home the plasma screens and home projection systems are now challenging it. It is expected that the flat panel display market valued at 34 billion euro will over take the CRT market in value this year and have an overall 65% market share by 2005<sup>1</sup>. The prime flat panel display technologies are plasma, electroluminescent and liquid crystal. These three technologies each have a variety of sub-categories and these will be treated separately. There are many important features<sup>2</sup> required for a flat panel display but only some of them are quantifiable. These are power consumption, resolution, lifetime, size, viewing angle and cost.

In this chapter the details of other possible display types, their applications, limitations and the area of the market targeted by this technology is discussed.

#### 1.1.1 Cathode Ray Tube

The CRT or cathode ray tube is the main display type used today. It is bulky and has limitations in both resolution and size. When comparing the CRT to thin film EL

displays there are fundamental differences in the excitation energy required to produce the light output. In the CRT the luminescent centres of the phosphor are excited by the impact of high-energy electrons, produced by thermionic emission, accelerated in a vacuum. The electrons are focussed on the phosphor screen using electrodes held at varying potentials. A grid is also used to help focus the electrons. The complete assembly is called the electron gun. The electron beam scans across the viewing area in a raster. Displays in Europe have 625 lines (PAL) and in America the displays have 525 lines (NTSC). The screen is scanned at a rate greater than 45Hz to avoid flicker. The luminescence itself is produced by cathodoluminescence of the luminescent centres in the phosphor. This requires both high voltages (20keV) and an accelerating distance. Colour displays are produced using the “shadowmask” principle. Here there are three electron guns that are inclined slightly to each other and their beams coincide in the plane of the shadowmask. This shadowmask is a metal screen with holes in it that is placed in front of the phosphor. The beams then diverge again and hit the phosphor faceplate of the CRT at three distinct positions. The phosphor itself consists of groups of three primary colours that are located in the correct positions for the guns. This leads to a reduced resolution compared to the monochrome devices due to the “dot” size being the area of the three dots<sup>3</sup>

### **1.1.2 Electroluminescent displays**

In contrast to the CRT devices, the electrons in the phosphor that are accelerated by the applied electric field excite luminescent centres in the thin film electroluminescent display. Since the process is confined within the phosphor material itself, this allows these devices to achieve equal resolution in a more compact device than the CRTs. This display type is the focus of this thesis and there are two basic types, AC thin film and DC thick film displays and these can be either organic or inorganic. The organic electroluminescent devices are similar to the inorganic devices studied here but different mechanisms are responsible for the luminescence. This section concentrates on the AC driven devices.

Light emitting diodes (LED) have been used in some display areas where resolution is not the limiting factor. LEDs are based on a low field EL. They require fields in the region of  $10^6$ V/m. The light emission is produced from the potential energy provided during recombination of electron-hole pairs in a p-n junction. The main drawback of

this technology is that for the minority carriers to achieve sufficient diffusion lengths and radiative recombination single crystal materials are required. Thin film EL is a high field process requiring fields in the order of  $10^8 \text{Vm}^{-1}$  achieved with polycrystalline materials and this is a considerable advantage for this technology. An organic EL device is a multilayer diode structure in which the recombination of injected electrons and holes leads to light emission. It incorporates an organic material such as Alq (aluminium tris 8-hydroxyquinoline) or polymer material as the luminescent material. They are also thin and light-weight having self luminescent features that provide a very high picture quality. Another drawback of organic technology is stability. The individual pixel aging leads to latent images and the constant current drivers required currently limit the size achievable by this technology. These devices are also vulnerable to water and oxygen vapour contamination<sup>4</sup> and need appropriate barrier layers.

These organic EL displays are also referred to as organic LEDs (OLED). The polymer section of this technology incorporates ink-jet technology as the deposition method. The core material is a conjugated polymer chain referred to as a dendrimer. Dendrimers are branched snow-flake like molecules that comprise of a light emitting core with branched dendrons that separate luminescent centres and limit quenching. This technology combines the bright pure colours of small-molecule organic LEDs and the solubility for deposition on a flat surface of light emitting polymer materials. Efficiency and low voltage operation of these devices is being investigated<sup>5</sup>. New production technology using lithography is also helping to overcome the resolution limitations. First generation colour OLEDs are being produced as camera viewfinders by Kodak<sup>6</sup>.

Inorganic EL displays have a capacitive structure that requires high fields and low currents limited by the insulators used. In the high fields the electrons are accelerated and impact excite the luminescent centres. The application of ZnS:Mn devices based on filtering of the broadband output have been fabricated<sup>7</sup>.

A comparison of the special features of first generation organic EL and inorganic EL is shown in Table 1.1<sup>8</sup>.

Properties	Alq based organic devices	Inorganic high field devices
Fabrication	Vacuum deposition at low temp.	Vacuum deposition at high temp. / sol-gel
Electrodes	Low work-function materials	Al, Mo. ITO, ZnO:Al
Efficiency	High	Medium
Luminance	High	Medium
Contrast	Low	High
Colour Purity	Poor (filter or colour media required)	"Colour by White" (filter required)
Voltage	Low (dc)	High (ac)
Current	High	Low
Stability	Poor	Very good
Display area with passive driving	Small	Large

**Table 1.1 Comparison of organic molecular EL and inorganic EL devices.**

### 1.1.3 Plasma displays

In the large display market, at the 40 inch plus screen size, plasma displays and rear projection TVs are the only current contenders. EL displays have reached a 17 inch prototype level with plans for a mid 30 inch model soon<sup>9</sup>. LCD displays are available in sizes up to a 40 inch prototype. Therefore plasma displays have, at the moment a niche market area in the large area flat panel display market.

The principle of the plasma display is electric discharge in certain inert gas based mixes. An array of cells arranged in a matrix receives a flow of low pressure xenon



gas that is activated by the electrodes in the cells. Thus the cell structure determines and limits the resolution of the device. The light output is proportional to the discharge current but is a non-linear function of the applied voltage. Also the luminescence efficiency is not as high as that attained in EL devices but this is being addressed and the power consumption is being lowered. The plasma display area can be divided into two categories, ac and dc. AC devices are either memory or refreshed devices and the dc devices are refreshed devices only. The original device is an ac memory device. In the ac devices the electrodes are external to the to the gas cavity while in the dc operated devices the electrodes must be inside the gas cavity. An initial firing voltage in the region of 150V is required but the plasma can be then sustained with a reduced voltage of about 90V.

#### **1.1.4 Liquid Crystal Displays**

While electroluminescent devices are emissive devices, the liquid crystal (LCD) devices modulate light from outside to display images. Even though liquid crystals have been around for over 100 years<sup>10,11</sup> it was not until the discovery of the twisted nematic effect<sup>12</sup> that they found commercial applications. It is the anisotropic physical properties of the liquid crystals that is utilised in the displays. Since the first application of liquid crystals to displays nearly 30 years ago they have achieved major success<sup>13</sup>. There are seven distinct liquid crystal display technologies. These are twisted nematic (TN), super twist (STN), double supertwist, ferroelectric (FLC), thin film transistor (TFT-TN), diode active matrix, and back light structures. All involve the use of liquid crystal material to modulate light and they can be grouped depending on whether they are transmissive or reflective. Transmissive LCD's modulate the light from the back-light at the rear of the liquid crystal panel. This means that the back-light must always be on and therefore the power consumption can be high. The reflective type devices reflect and modulate ambient light such as illumination light or even sunlight when used in mobile phones. There are two types of reflective devices that are classified depending on the auxiliary light source used as reflective and transreflective. The transreflective device used a back-light while the reflective type uses a front-light as the auxiliary light source<sup>14</sup>. LCDs can be defined according to the pixel drive method employed and this determines the resolution of the devices. There are two types of pixel drivers, the passive matrix type and the active matrix

type. The active matrix devices are divided into the metal-insulator-metal (MIM) devices and the thin film transistor (TFT) devices. These devices have high contrast, fast response and a large gamut of available colours but this leads to an increase in the power consumption. The passive devices have low cost and power consumption but they lack the contrast and the response speed of the active devices. These response times are still limited by the liquid crystal fluid switching time, which is around 15ms<sup>15</sup>. Since the response speed of the EL device is dependent on the transitions in the luminescent material it is in the microsecond range and is therefore superior to the LCD devices. Another limitation of the LCD device is its limited viewing angle. Although this is improving it is costly<sup>16</sup> and is not a problem with EL devices.

For the flat panel display market the LCD is used extensively in mobile computers, PCs and TVs. Its picture quality, viewing cone and response times have improved over the last few years allowing it to be successful in these markets.

Liquid Crystal on Silicon (LCoS) devices have been developed to incorporate CMOS and liquid crystal. The use of very large scale integration (VLSI) technology to address the device allows higher electron mobility<sup>17</sup>. The active matrix back plane is either a DRAM or SDRAM with one or more memory cells per pixel. The pixel size is less than ten microns and this gives an apparently unpixelated image with a rapid response time. This is hoped will allow the production of large, inexpensive, high quality, high resolution displays<sup>18</sup>. These devices have found uses in the head-up-display area<sup>19</sup> and are also being developed for microdisplay applications<sup>20</sup>.

### **1.1.5 Cathodoluminescence Displays**

When a beam of energetic electrons strikes a solid the majority of the electrons lose their energy to the atoms in the solid and cause some bound electrons to be ejected from the atom. These secondary electrons will generate further secondary electrons if they have sufficient energy. This can cause cathodoluminescence if bound electron-hole pairs or excitons transfer their recombination energy to activator ions. These displays use ZnS as the material on the anode.

Vacuum fluorescent displays are based on low voltage cathodoluminescence. They generally consist of a filament that produces electrons by thermionic emission that

then strike a phosphor coated anode. The material used here is doped ZnO giving a green colour. Other colours are obtained by using different phosphors. The response time of the devices is in the region of 1ms, which makes them suitable for all applications but the resolution of these devices is dependent on the size of the tubes and hence is limited.

### **1.1.6 Field Emission Displays**

Field Emission Displays (FED) operate in a similar way to CRTs in that phosphors are excited by electrons travelling in a vacuum. Instead of one gun providing electrons, FED use many microscopically small electron emitting cathodes which are matrix-addressed to direct electrons at each pixel. It is this method of electron emission that makes this display type different and allows it to operate at much lower powers than the CRT making it an attractive alternative. The design of the electron emitting cathodes has evolved from microtips that are hard to manufacture because of their small size (1-2  $\mu\text{m}$ ) to 10 $\mu\text{m}$  diameter carbon nanotubes (CNT) and picture element tubes using carbon-film cathodes<sup>21</sup>.

### **1.1.7 Electrochromic Displays**

Electrochromism is the ability of a material to change colour upon oxidation or reduction. The material undergoes a visible and reversible change in the transmittance or reflectance due to the oxidation or reduction reaction. This change is normally between a bleached or clear state and a coloured state. This optical change occurs due to the application of a small electric current at low dc potentials. This display technology has been attracting attention for the last 40 years and lost out to LCD technology in the 1970s<sup>22</sup>. The main application of electrochromic devices today is rear view mirrors in cars. There are four different device types<sup>23</sup> and are classified according to the materials used in the devices and the type of electrodes used. As a display technology this method is limited by the lifetime and degradation problems<sup>24</sup>.

### **1.1.8 Electronic paper.**

This is a relatively new concept in the display industry and was only presented in 2001<sup>25</sup>. This display is produced using the electrophoresis of black or white charged particles. It is flexible enough to permit bending and has lower power consumption than a reflection LCD. This is an area where electrochromic devices may find an application area. These “electric-paint” displays consisting of coloured electrodes and the electrochromic molecules are electrically addressed from the back contact on conductive glass<sup>26</sup>. It has the potential to achieve high contrast and may prove to be a viable display type but it is still in the development stages.

## **1.2 Performance**

Looking at the different types of display technologies discussed it is possible to compare their performance and see where each technology is applied. This discussion is limited to the technologies that are already in production and looks at the use and prospects of each one in terms of the market expectations.

### **1.2.1 Lifetime**

A major factor in the usability of a display is its lifetime. There are two aspects to discuss when looking at the lifetime of a display, differential aging and useful life. Different aging occurs when different pixels emit differing amounts of light over a time period. The eye is very sensitive to this type of aging and will notice variations 2-3%<sup>27</sup>. Useful life is determined by the degradation of the overall luminance over time. Generally the lifetime is defined as the time the display taken for the luminance to fall to 50% of its initial value. Looking at the product market there are generally three areas. Small screen applications such as mobile phones require lifetimes in the order of 10 000hrs. Bigger screens such as PC's require 30 000hrs. For the home TV displays, CRTs have so far led the way in this area and have generally lifetimes in excess of 50 000hrs. OLEDs have been manufactured with lifetimes in excess of 7000hrs<sup>28</sup>. Inorganic EL also has the potential of long lifetimes, showing lifetimes of over 10 000hrs continuous operation<sup>29</sup>, and is therefore a viable technology for most display applications. LCD displays are now reaching lifetimes of 20 000hrs.

ACTFEL displays have shown to lead the way in this area as displays have been produced with lifetimes in excess of 50 000hrs<sup>30</sup>

### **1.2.2 Power, Luminous efficiency**

Power is a deciding factor in the application of a particular display type. Certain markets, especially the mobile industry (both phones and laptops etc.) require displays that require minimal power. This rules out the CRT for these applications. In this area emissive displays have an advantage over non-emissive technologies. Emissive displays only require power when a pixel is activated while non-emissive devices require a backlight that is always active. Therefore the emissive displays are more power efficient in this area. For emissive displays such as electroluminescent devices there is a power requirement to generate the light and this requires voltage levels of 80V<sup>31</sup>. OLEDs require voltage levels similar to logic circuits.

It is important that the display technology chosen is capable of producing a full colour display. Some technologies such as reflective LCD on silicon and some transmissive LCD displays are intrinsically monochrome or field sequential colour. In colour sequential systems the refresh rate has to be high to prevent flicker and therefore these displays require three times the bandwidth of conventional three colour systems. This again adds to the power requirements of these devices. The conventional CRT has a three colour system and EL and OLED can also be manufactured with the full colour gamut. Luminous efficiency compares the technologies based on a power in versus light out basis. OLED's have an operating luminous efficiency of 1.6 lm/W<sup>32</sup> while EL devices have efficiencies of 3 lm/W<sup>33</sup>.

### **1.2.3 Response time, Viewing angle, Thickness, Gamut**

These are some of the additional criteria that are important to consider when looking at the application areas of the displays. In terms of response time or switching speed, the CRT, OLEDs and EL all have microsecond responses based on the lifetimes of the colour responsible material transitions. LCD devices have response times that are dependent on two factors, the LCD cell and the drive circuitry. This leaves its response in the millisecond range and this is not fast enough for full motion videos that need switching times less than 10ms.

Since the CRT, OLED, and EL devices are emissive devices they again have the advantage of having a quasi-lambertian light emission profile resulting in a high viewing angle. Plasma displays also have a large viewing angle and are a truly “flat” screen application. LCDs are limited in their viewing angle due to the optical properties of the liquid crystals although this is being improved by using smaller electronics and improved liquid crystal material.

Coupled with the viewing angle is the actual thickness of the display itself. LCDs and plasma displays are thin display types when compared to the CRTs and even the microdisplays. ACTFEL displays however, allows for possible display thicknesses of 30mm making them the best available.

The colour gamut offered by the emissive technologies is constantly being improved as the materials used in the devices are improved and new phosphor materials are developed. The range of colours that a display can generate is generally given by the CIE (Commission Internationale de l’Eclairage) coordinates<sup>34</sup> for the individual phosphors used.

In the LCD devices better colour filters coupled with tailored outputs of triphosphor backlight cold cathode fluorescent lamps (CCFL) have extended the colour gamut so that it rivals that of cheap CRT’s at the high end of the market but the moderately priced LCDs do not match these specifications.

The significant advantages of ACTFEL over other flat panel display technologies include its wide viewing angle, its solid state construction, making it more shock and vibration resistant, and its long lifetime. Therefore, since a colour ACTFEL device prepared using sol-gel technologies is possible, it could impact the displays industry in the different market areas especially the larger screen area.

## Chapter 2

### Thin Film Formation Techniques.

#### 2.1 Introduction

For the production of a thin film electroluminescent display it is important to look at the types of films needed and how they are produced. In this case insulating, conducting and luminescent thin films are required to complete the display stack. These films are currently produced by a variety of techniques. The thin film deposition techniques can be classified as either purely physical, such as evaporation or purely chemical such as gas and liquid phase chemical processes or a combination of both such as glow discharge and reactive sputtering. Under each of these headings there are many sub-sections. Five general classifications can be used to cover the common deposition methods and these are

- 1) Evaporative methods
- 2) Glow Discharge processes
- 3) Gas phase chemical processes
- 4) Thermal Oxidation
- 5) Liquid phase chemical techniques

Since the deposition method determines many of the film properties it is important to differentiate between the different production methods and see which techniques are suitable for mass production. This chapter gives a brief overview of the various thin film deposition techniques as classified comparing them to the sol gel process, which is a liquid phase chemical technique and will be discussed separately in detail.

#### 2.2 Evaporative Methods

As one of the oldest techniques available, thermal or vacuum evaporation is widely used in the production of metal and metal alloy films<sup>35</sup>. In evaporation a three-step process takes place as follows:

1. the vapour is generated by boiling or subliming a source metal or alloy
2. the vapour is then transported to the substrate and
3. then condensed on to the surface of the substrate where the film is formed.

Since the evaporants can vary dramatically there is a large range of source components and elements available. In order to satisfy step two in the process and to

ensure film uniformity and consistency the process is carried out under high vacuum conditions. Various methods are used to produce the vapour and most of the systems get their name from this.

The most commonly used methods of evaporation are resistive evaporation, electron beam evaporation and molecular beam epitaxy.

In resistive evaporation, placing the metal on a heating element produces the vapour. The element is heated by passing a high current through it. Elements are usually made from refractory metals such as tungsten or tantalum. They are found as coils, boats, or other special designs. This type of evaporation is used to produce the semi-transparent aluminium electrodes for the EL devices produced. This is a simple technology that is limited in the variety of materials that can be deposited.

In electron beam evaporation the heating energy is supplied to the top of the evaporant by the kinetic current of a high-energy electron beam. The evaporant is contained in a water cooled hearth or cell. ZnS Mn has been deposited using this technology<sup>36</sup>. Again the range of materials that can be deposited and the requirement of a vacuum system limit this technology.

Molecular Beam Epitaxy (MBE)<sup>37 38 39</sup> is a finely controlled method for growing single crystal epitaxial films in a high vacuum. It involves using several evaporation sources, or source cells containing the individual elemental or molecular constituents. The constituents are evaporated slowly on to the substrate, which is maintained at the appropriate temperature for the film formation process. The individual constituents are directed at the heated substrate and the amount of each constituent used is determined by controlling shutters. To facilitate epitaxial growth single crystal substrates are used. Doped ZnS films have been produced using this technology but due to the complex operation and expensive equipment the scope of this deposition technology for production applications is limited.

### **2.3 Glow Discharge Technologies**

This area of film deposition methods includes two broad areas, sputtering and plasma processes. The range of applications and methods in the area is large with most of the processes being developed with specific applications in mind.



### 2 3 1 Sputtering

Since it was introduced 130 years ago<sup>40</sup>, this is one of the most basic deposition processes. As well as being a deposition technique, sputtering can also be used as an etching process since surface atoms are ejected from an electrode by momentum transfer from bombarding ions. These surface atoms then form a beam and can be deposited on a substrate. In order for the sputtering to be efficient the incident particle has to be of atomic dimensions. Thus, as electrons do not carry the required momentum and a large particle could be too big to interact with the surface atoms, gases are a convenient source of atomic sized particles or bullets. An inert gas such as Argon is generally used to ensure that there are no unwanted chemical interactions. Since the gas needs to have sufficient momentum to interact with the target, Argon ions are used. Sputter deposition has become a blanket name for a variety of processes that include D C, magnetron, rf bias and ion beam sputtering. D C sputtering uses a plate as the cathode electrode or target in a glow discharge and the substrate as the anode in an Argon environment<sup>41</sup>. The electric field causes electrons to be accelerated and collide with neutral atoms to produce the ions that bombard the target and cause sputtering if the energy of the bombarding ions is sufficient. If the substrate is placed facing the target the film will be deposited. The position and orientation of the anode determined the uniformity of the film produced. A variation of D C sputtering is reactive sputtering where the carrier gas is not inert but will chemically interact with the sputtered beam and a compound is deposited. This requires strict control on the interaction environment as it is preferred if the chemical reaction in the compound takes place close to the substrate to ensure a high quality film.

Another variety of dc sputtering is bias sputtering. This variation involves putting a bias voltage on the anode or substrate. This controls the amount of ion bombardment and therefore the properties of the deposited films. This bias can also be changed during the process to allow different structures to be grown<sup>42</sup>.

Magnetron sputtering uses a magnetic field. The magnetic field,  $B$ , is transverse to the electric field,  $E$ , at the sputtering target surfaces so that the  $E \times B$  drift path of the electrons forms a closed path over the target surface. The magnetic field is used to trap electrons close to the sputtering target both to prevent them from escaping and interacting with the walls thus losing energy and also to cause them to create ions.

close to the sputtering target and increase the ionisation efficiency. This also allows the operation of the system at lower pressures and lower target voltages than the rf sputtering.

Radio Frequency (RF) bias sputtering is a widely used plasma-based method of film deposition. The insulating target electrode has an alternating potential applied with a frequency in the Megahertz region to sustain a glow discharge plasma in the process gas. The substrates are placed on the anode, which may be biased negatively with respect to the plasma. The potential difference between the plasma and the substrate accelerates the ions providing ion bombardment of the film during film deposition. The ion energy and ion flux depend on the geometry of the deposition system, the gas pressure and the target material.

Ion beam sputtering uses an ion beam gun or ion beam source to produce ions. These ions then hit the target and produce the sputtering beam. An ion gun produces the ions from collisions between atoms and electrons. This then allows a plasma to be produced in the vacuum chamber so that the ions are produced close to the target. Due to the nature of the process it is carried out under a high vacuum rather than the previous systems that are high-pressure systems.

Sputtering has been used to produce both the insulating films  $\text{SiO}_2$  and  $\text{Ta}_2\text{O}_5$ , and the luminescent film  $\text{ZnS:Mn}^{43}$ . Here the problems of a high vacuum requirement and problems with the film thickness uniformity make this an expensive option for the deposition of these films. Also in the case of  $\text{ZnS:Mn}$  thin films, high quality films are hard to produce because the sputtering environment during the deposition influences the film quality.

While sputtering is a useful technique it has its limitations. Sputtering is always trying to overcome thickness variations that can form on substrates with complex topographies. Sol gel techniques do not have this problem and do not require the vacuum systems.

### **2.3.2 Plasma Processes.**

A plasma consists of a gas containing large and generally equal numbers of electrons and positive ions. The primary role of the plasma here is to produce chemically active species that will react with the substrate and form a film. Thus electron kinetic energy rather than thermal energy is used thereby limiting excessive heating of the substrate.

It offers the capability of ion bombardment during film growth. The energy from an electric field is coupled into a gas via a few free electrons. These electrons acquire energy rapidly and lose it slowly via elastic collisions. The electrons ionise the gas producing secondary electrons by electron impact reactions. The process avalanches and the discharge starts. In a stable plasma process the number of electrons generated and lost should be about the same. The stability of the system is a function of the plasma pressure, which determines the electron mean free path. Examples of plasma methods of film production are plasma anodization and ion cluster beam deposition. Plasma anodization is used to produce thin oxide films on metals<sup>44</sup>. A dc discharge is set up in an oxygen atmosphere and the substrates are positively biased with respect to the anode. This extracts negative oxygen ions from the discharge to the surface and produces dense, defect free amorphous oxide films.

For the plasma deposition of an inorganic film, generally an RF generated glow discharge is set-up and a volatile reactant is introduced to produce the required inorganic film. This process is also used to produce organic polymers by plasma polymerisation of organic reactants<sup>45</sup>. Plasma deposition is a combination of glow discharge and low-pressure chemical vapour deposition.

The method called ion cluster beam deposition or ICBD, combines a high rate of evaporation with the benefits of ion bombardment. Atomic clusters or macroaggregates having 500-1000 atoms loosely bound together are formed by adiabatic expansion of evaporant material through a nozzle into a high vacuum region. These clusters are then partially ionised by electron bombardment. The positively charged clusters are accelerated towards the substrate by the applied potential and the energy gained by the atoms is assumed to be shared equally between the atoms making up the cluster.

## **2.4 Gas Phase Chemical Processes**

This area involves the formation of the thin film by purely chemical processes in the gas or vapour phases. It includes the areas of chemical vapour deposition (CVD) and thermal oxidation.

The chemical reaction types covered in CVD include thermal decomposition, oxidation, reduction, hydrolysis, nitride and carbide formation, synthesis reactions,

disproportionation, and chemical transport<sup>46</sup>. In producing a given film a sequence of several reaction types may be involved. The overall reaction can be represented by the following simplified equation:



The deposition rate of the film is determined by the deposition variables that include temperature, pressure, gas flow rates, input concentrations and the reactor geometry. Most CVD reactions are designed to take place at the substrate surface rather than in the gas phase as homogeneous reactions in the gas phase nucleate particles to form powdery deposits and contaminate the film.

CVD is a very popular method for the preparation of thin films because a large range of elements and compounds including organic, metalorganic inorganic reactants can be used to prepare a large variety of films including the luminescent film ZnS:Mn. Gases are preferred as they can be readily metered and distributed in the reactor. Therefore the solid and liquid reactants must be vaporized without decomposition and with a suitable carrier gas to the reaction chamber.

In the reactor, decomposition of the gaseous chemicals can be achieved by a variety of methods including, heat, plasma, ultraviolet and other energy sources. This leads to a range of different systems. The following is a brief summary of those systems.

Thermal activation is the conventional CVD activation process. The CVD process is initiated by thermal energy such as resistance heating, RF heating or infrared radiation. The reactive gases are passed over the heated surface. Generally, high temperatures are required for the process and this can cause uniformity and purity problems in processing some compound semiconductors.

CVD Atomic Layer Epitaxy involves the addition and arrangement of individual atoms on the surface of a single crystal using CVD processes. Uniformity of the epitaxial layer refers to both thickness uniformity and a uniform resistivity. The thickness is controlled by the mass transport and the surface reaction rates. In some cases the resistivity is controlled by the dopant incorporation, which is controlled by the local concentration of dopant and the local temperature. These factors are controlled by the reactor design. It is used to deposit elemental semiconductors such as silicon, oxides, nitrides and sulphides.

The basic parameters that require control in the CVD process are

- 1) the rate of transfer of reactant gases from the ambient gas stream to the substrate surface or mass transfer rate  $F$ , and
- 2) the rate of reaction of these gases at the substrate surface,  $R$ .

Thus the observed deposition rate,  $G$  is

$$G = A \frac{1}{1/F + 1/R} \quad (2.1)$$

where  $A$  is a constant.

For Atmospheric Pressure CVD (APCVD) these rates are approximately equal. Both  $F$  and  $R$  are dependent on maintaining a uniform reactant gas concentration over the surface of the substrate and this is accomplished in APCVD through reactor design and appropriate flow velocity. The reactor is designed so that the main gas stream flows over the surface of the substrate. This leads to poor thickness uniformity and low throughput.

Low Pressure CVD (LPCVD) involves the transition from a diffusion controlled process to a surface reaction controlled. By operating at low pressures it is possible to eliminate the diffusion process as a controlling step. This allows the surface reactions to control the process. For each film the surface reactions must be analysed and the reactor designed to suit the process involved.

Plasma Enhanced CVD (PECVD) has been developed to overcome some of the problems associated with thermally activated CVD. PECVD relies on an RF source such as microwaves to ionise the reactive gases. Since the reactants are highly energised their collisions with the surface can transfer enough energy to damage the film or contaminants can be introduced due to collisions with the reactor wall.

Photo-enhanced CVD is a low temperature process that does not damage the surface. Photons from optical sources such as lasers, lamps and plasmas are used to dissociate chemical species. These particles remain electrically neutral, or free radicals. The choice of photons determines the specific chemical bonds that are broken, as a given molecule will only absorb light of a specific energy. Mercury vapour is usually added to the reactant gas mix as a photosensitiser that can be activated with the radiation from a high intensity quartz mercury resonance lamp.

The laser induced CVD (LCVD) process uses a laser beam for highly localized heating of the substrate surface. This induces film deposition by CVD surface reactions. The laser can also be used as photo source to give specific gas phase reactants that lead to very pure films.

Metal-organic CVD (MOCVD) involves growing thin layers of compound semiconducting materials by the co-pyrolysis of organometallic compounds and hydrides. A wide variety of materials can be grown using this technique that are difficult to grow by other epitaxial methods. This makes MOCVD one of the most important fabrication methods in the opto-electronics area. The organometallic compounds used in MOCVD are generally liquids or solids at room temperature. They are transported as vapour phase species to the reaction chamber by bubbling a suitable carrier gas through the material as it is held in a container at room temperature. The reactants then begin to thermally decompose in the reaction chamber as they encounter the hot susceptor. The thermal decomposition depends on the flow rate and the reactor geometry.

While CVD and its variants are versatile as deposition techniques, there are some disadvantages. Due to the nature of the materials involved in the CVD process it can be hazardous as toxic, flammable, corrosive and even explosive materials may be required. If multicomponent films are deposited the stoichiometry of the material is difficult to control.

## **2.5 Thermal Oxidation**

In this case the substrate itself provides the source for the metal or semiconductor constituent of the oxide film. Oxygen is passed over the substrate to cause the oxidation. Although this is a limited technique, it is very important in silicon device development where high quality oxide films with a high quality interface are required. In this case high temperatures are necessary to oxidize a surface. This technique is routinely used to produce silicon dioxide by heating silicon to 1200°C in an oxygen atmosphere. For the devices produced here sol-gel techniques were used to produce the SiO<sub>2</sub> films. Since low temperatures are used, the technique has advantages over thermal oxidation.

## **2.6 Atomic layer epitaxy (ALE)**

Atomic layer epitaxy is a surface deposition process that involves the controlled growth of epitaxial layers. These layers can be used to fabricate molecular structures on the surface of substrates that can be designed to specific standards. One of the most important properties of atomic layer epitaxy is the ability to grow monatomic layers. These can be deposited in a given order or sequence to produce multicomponent materials. Since the film is deposited in this way the thickness of the film is easy to control to sub-nanometre values, since the number of reaction sequences can be counted. Since ALE has no gas phase reactions, a wider choice of reactants is available enabling a wide variety of films to be fabricated such as semiconductors, oxides, nitrates and metallic films<sup>47</sup>. ALE has good conformal coverage and provides good uniformity on complex substrate shapes. Because of its sequencing complex layer structures can be fabricated and the crystallinity of the materials tailored using this technique. Originally developed for the fabrication of amorphous and polycrystalline zinc sulphide and oxide thin films for thin film electroluminescent displays<sup>48</sup>, today the range of materials deposited has expanded. ALE has also been used to control growth and deposit 3-20nm thick layers of alternating dielectric materials to reduce leakage current.

## **2.7 Liquid Phase Chemical techniques**

The liquid phase coating methods include all methods where thin films are obtained from chemical reactions carried out in the liquid phase. This covers a large range of coating methods that include anodization, electroplating and mechanical methods.

### **2.7.1 Anodization**

In this type of coating method the substrate is immersed in a chemical bath. The anode (substrate) reacts with the electrolyte and an oxide is formed its surface.

### **2.7.2 Electroplating**

In this case the substrate is the cathode in the chemical bath. The electrolyte contains metal ions that are attracted to the cathode when a bias is applied. Thus the metal coating is applied to the substrate.

### **2.7.3 Mechanical Methods.**

This area includes all type of coating where the liquid media is removed from the substrate by mechanical means. These mechanical means include spraying, spinning, dipping, draining, flow coating and roller coating. The liquid residue then forms the thin film. This is the basis of the sol-gel coating method.

## **2.8 Selection of a coating method**

In choosing a deposition method for a specific thin film there are a variety of considerations. The nature of the deposited film can vary extensively depending on the deposition method chosen. The purity of the film and the thickness will initially limit the choice of deposition methods. When considering the manufacturability of a given film the yield is an important concern as well as the size of the substrate. When a vacuum system is needed, as in Sputtering and CVD methods, this adds to the cost of the product. Also understanding the dynamics of the system is fundamental to achieving a product with the correct constituents and uniformity. The dynamics in many of the processes described above are still not fully understood. Large-scale production of displays requires a technology that is capable of producing quality devices at low cost and in large sizes. Having an in-line process that can facilitate large substrates and has a high yield at a low cost that allows the same technology to be used to produce all the layers is the goal. It is for these reasons that the sol-gel process was chosen as the deposition method for this application.



## Chapter 3

### Sol-Gel Film Formation

#### 3.1 Introduction

Sol-gel technology enables the production of glasses, ceramics and thin films through chemical reactions at near ambient temperatures. It allows a variety of materials to be prepared in a variety of forms such as bulk powder, wire, thin film and aerogel with a wide variety of optical, structural, electroceramic, and biological applications.

In this chapter the history and the underlying physics and chemistry associated with the sol gel process itself and thin film formation is discussed in detail. Also the precautions and special conditions are considered.

#### 3.2 History of the sol-gel process

The sol-gel process was first observed and used in 1846 to form silicate glass by the hydrolysis and polycondensation of silicic acid<sup>49</sup>. Further development of SiO<sub>2</sub> layers took place in 1939<sup>50</sup> when it was shown that alkoxides could be used in the preparation of oxide films. Several other products consisting of SiO<sub>2</sub> and TiO<sub>2</sub> layers were also developed at this time<sup>51</sup>. This led to the development of rear view mirrors for cars going into production in 1953. Uses of the sol-gel process expanded to include anti-reflection (AR) coatings in 1964<sup>52</sup> and solar reflective coatings from 1969<sup>53</sup>.

A development of the chemical principles involved in the years 1969-1971 showed the importance of the reactions of several alkoxides in solution and the formation of metal-oxygen bonds<sup>54,55</sup>. This led to the production of multicomponent glasses and glass ceramics. Ceramic fibres produced from metalorganic precursors were also developed during this period<sup>56,57,58</sup>. Mineralogists also investigated the use of sols and gels to prepare homogenous powders<sup>59</sup>. The nuclear industry developed the area of sol-gel by using it to prepare small spheres of radioactive oxides for fuel rods<sup>60,61</sup>. The production of monoliths by special drying processes sparked a new interest in the sol-gel process in the late 1970's<sup>62,63,64</sup>. As a knowledge of the process and the

importance of the chemistry involved developed the areas of application expanded<sup>65 66 67</sup>

Sol-gel processing is widely used as a technology for preparing thin films, fibers, glasses, monoliths, ceramics, micro spheres and fine powders<sup>68</sup>

### **3.3 Basic Principles**

The objective of this process is to be able to manipulate molecular scale reactions to produce precursors with the desired structure and to maintain this structure through all stages of material formation and device fabrication. A summary of the material changes encountered is shown in Figure 2.1<sup>69</sup>. There are many parameters that can be varied resulting in materials with significantly different properties.

#### **3.3.1 Introduction**

The sol-gel process involves many stages to completion. Initially a precursor solution is formed from all the components required for the film in the form of soluble precursor compounds. Mixing can be considered to be at the molecular level at this stage. This precursor then undergoes hydrolysis, condensation and gelation between the homogenous or molecular phase and the heterogeneous or polymeric phase. Between these two, a transition state exists which can be described as a colloidal state. The molecular and colloidal states are defined as the 'sol' state. The polymerized multiphase state is defined as the 'gel' state. The transition from sol to gel can be achieved in three different ways<sup>70</sup>

- (i) Growth of polymeric molecules which crosslink randomly to form a three dimensional network
- (ii) Growth of individual particles, which grow together as they become larger
- (iii) The stabilization of colloids by surface charges by a change of the zeta potential followed by an interparticular condensation, which leads to gelation

Due to the large number of parameters numerous reaction paths exist. The main influencing parameters are

- (i) Precursor choice
- (ii) Reaction conditions- which include pH, solvents, catalysts and temperature considerations, and
- (iii) Mechanical parameters

This section will look at how each of these influences each stage of growth and the final product

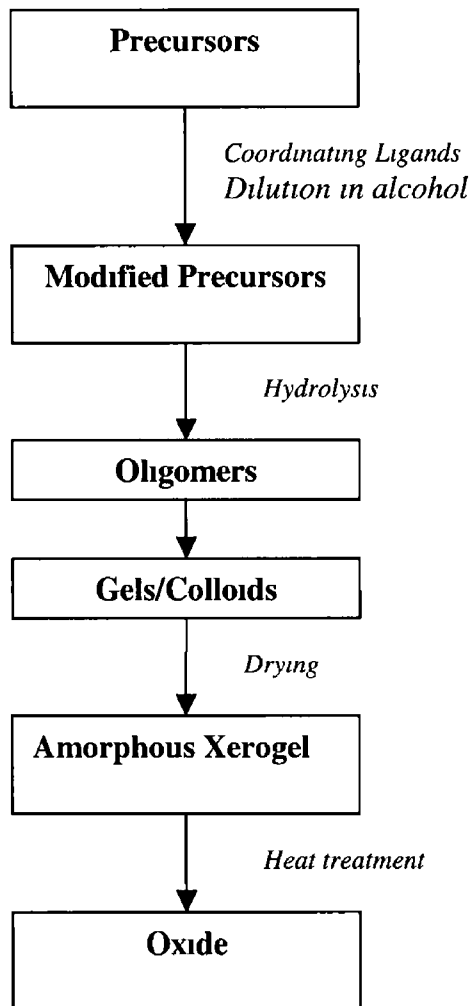


Figure 3 1 Various steps in the sol-gel process

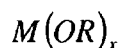
### 3.3.2 Precursor Choice

There are a number of different precursors materials used depending on the type of film required. All should be soluble in organic solvents and easily converted to the relevant oxide. Any solution of a suitable compound that can be hydrolysed can, in theory, be used. In practice, the reaction rate for the hydrolysis and condensation for the gel formation should be higher than the crystallization rate from the solution in order to obtain uniform coatings<sup>71</sup>. For this reason alkoxides are preferred. Ethanol is the preferred solvent because of its wettability of the substrate<sup>72</sup>. Depending on the

nature of the starting materials several preparative methods are available and the two common methods are described below

### 3.3.2.1 All Alkoxide Method

Metal alkoxides are probably the best starting materials for sol-gel preparations. All metal alkoxides have the following general form

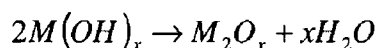
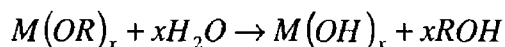


where M=metal,

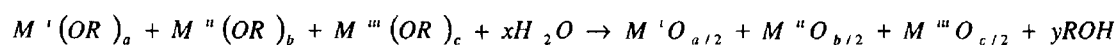
R=proton or alkyl group  $C_zH_{2z}$  and

x is the valence state of the metal

All, but two, alkoxides are readily hydrolysed to the corresponding hydroxide or oxide. The method of hydrolysis can be varied depending on the final product required. The overall reaction can be represented as follows



The by-product ROH is an aliphatic alcohol and is easily removed by volatilisation. The two exceptions to the above are silicon and phosphorus. An acid or base is required to catalyse hydrolysis in silicon alkoxides, and even with this the reaction rate is slow. Variations in the reaction rate can give rise to inhomogeneities in the final product. This can be avoided by carrying out the hydrolysis slowly<sup>73</sup>. The simplest preparation method for a multicomponent system is the mixing of all the components as alkoxide precursors in a suitable organic solvent and the reacting of the resultant solution with water to form the oxide mix. The reaction for a three-component system can be represented as follows<sup>74</sup>



### 3.3.2.2 Alkoxide Salt Method

When low solubility or unavailability of alkoxides of a metal is a problem alternative starting materials can include metal salts provided they can be readily converted to the oxide by thermal or oxidative methods. Salts of organic acids such as acetates are potential candidates

The preparation method is similar to the all alkoxide method. All alkoxide components are mixed together. The salts are added as solutions in alcohol or in the water that is to be used for further hydrolysis. Since all components are then uniformly dispersed the gelation should freeze all elements in a gel network. This preparation method has been used successfully for sol-gel preparation<sup>75</sup> although hydrolysis with only alkoxides is more readily achieved than the thermal or oxidative degradation required here.

Once the precursor has been successfully mixed and hydrolysis has taken place, then condensation takes place. The actual reaction involved is more than the simple hydrolysis shown above. Firstly, the hydrolysis of metal alkoxide groups is followed by the condensation of these groups with each other to form products containing M-O-M linkages<sup>76</sup>. The more alkoxides present in the original mixing, the more complex the polymerization can become. Ultimately the polymeric products become insoluble due to crosslinking and gelation or precipitation occurs.

### 3.3.3 Condensation

Polymerization can occur by either an alcohol producing or water producing reaction. For example in silicates a typical sequence of condensation is monomer, dimer, linear trimer, cyclic trimer and higher order rings. These then form the framework for the generation of discrete colloidal particles<sup>77</sup>. The identity of the precursor, pH, type of catalyst and solvent, water/alkoxide ratio, addition sequence, atmosphere above the reaction chamber, time of mixing, addition of drying control additives or templating agents control the final microstructure of the gel. The hydrolysis rate increases with

- (i) Increasing the polarity of the M-X bond
- (ii) Decreasing the concentration of catalysts (acids or bases)
- (iii) Temperature

Also varying the pH or the molar ratio of H<sub>2</sub>O/M can vary the structure of the inorganic polymer considerably.

A lower pH slows the condensation rate and the consequences of that is that,

- (i) Highly concentrated solutions can be prepared which are stable with respect to gelation and therefore can be used to produce thin films
- (ii) Linear polymers will tend to align due to the shear stress imposed during dipping or spinning which may result in anisotropic optical properties
- (iii) Evaporation of the solvent combined with shear allows the polymers to become highly compacted and aligned without initially causing gelation. Conversely, if the pH is increased, the consequences of increased condensation rates are,,
  - (i) Dilute solutions are required to avoid premature gelation, thus film thickness from a single application is limited
  - (ii) Growth in dilute solutions may occur by a process analogous to random particle aggregation<sup>78</sup>
  - (iii) During film deposition gelation occurs at an early stage of evaporation and subsequently during continued solvent removal, the modulus of the gelled film increases rapidly. Thus porosity is created at an early stage of the deposition process and the resulting pore volume is large giving a low refractive index.

As the pH is increased further, the pore volume is also increasing. By varying the pH of the solution in the case of SiO<sub>2</sub> a variety of refractive indices may be achieved in the range 1.25-2.30<sup>79</sup>. Work on silicates has shown the condensation results in a spectrum of structures varying from weakly branched polymers to highly condensed uniform particles.

The use of a catalyst influences the pH of the precursor and hence changes the hydrolysis and condensation rates, and the structure of the condensed product. The catalyst used can be an acid or a base. If an acid is used it will enhance the reaction kinetics. Since acid catalysed condensation is directed towards the ends rather than the center of the ligand chains, this results in more extended less highly branched polymers. Acid catalysts combined with a low water to alkoxide ratio can result in monolithic gels<sup>80,81</sup>. Base catalysed condensation and hydrolysis is directed towards the middle rather than the ends of the chains leading to a more compact highly branched species.

### 3.3.4 Gelation

Gelation occurs when the clusters grown by condensation of the polymers or aggregation of the particles collide and form links to produce a single cluster. The gel point occurs when the last link is formed between two large clusters to create a spanning cluster. At this point the viscosity will rise and the elastic response to stress appears<sup>82</sup>. The sudden change in rheological behavior can be used to roughly determine the gel point. The gel network still contains a continuous liquid phase, which allows relatively fast transport, and the reactions continue as the properties continue to evolve. During the aging process the gel continues to stiffen, coarsen and shrink.

### 3.3.5 Aging of gels

As the aging process progresses the properties and structure of the gel changes. The changes during aging after gelation are categorized as polymerization, coarsening and phase transformation.

During polymerization the connectivity of the network is increased by further condensation reactions. These reactions promote more hydrolysis and reesterification. Another consequence of condensation is syneresis, which is the contraction of the gel network resulting in the expulsion of liquid from the pores. These structural and phase transformations which take place during the aging process effect the drying process. The stiffer and stronger the gel the better it can withstand the capillary pressure and therefore it will be less susceptible to cracking.

Coarsening or ripening is a process of dissolution and reprecipitation, which causes growth of necks between particles increasing the strength and stiffness of the gel as shown in Figure 3.2. The rate of the coarsening is determined by the precursor conditions.

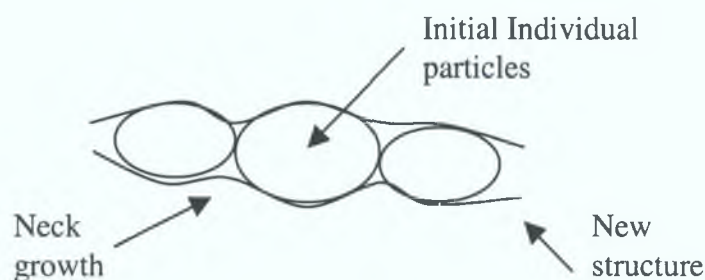


Figure 3.2 Coarsening of a gel showing the amalgamation of individual particles.

### 3.3.6 Drying of gels

There are several stages involved in the drying process. In the first stage called the constant rate period, the rate of evaporation per unit area of the drying surface is independent of time. Adsorption and capillary forces oppose exposure of a solid phase at the surface at this time so the liquid flows from the interior of the film to replace lost evaporated liquid. As the drying proceeds the network becomes increasingly stiff as the porosity decreases and the tension in the liquid rises correspondingly. Once the tension in the liquid cannot overcome further stiffening of the network the second stage begins as the critical point is reached.

Shrinkage stops at the critical point. Drying continues after the critical point and the gel expands slightly because the compressive forces exerted on the network are released as the liquid evaporates. Now the pressure in the liquid left is not uniform. Tension is greater in the liquid near the drying surface, which produces a differential strain and leads to cracking.

The next drying stages are referred to as the first and second falling rate periods. In the first falling rate period the evaporation drives the meniscus into the body of the film. Evaporation continues by fluid flow and via diffusion towards the exterior in the vapor phase. As drainage continues some pockets of small, still saturated pores become surrounded by regions of drained larger pores. These larger regions can scatter light and hence appear opaque during drying<sup>83</sup>. Drying under high vacuum can sometimes alleviate this. Once evaporation occurs by diffusion only the drying enters the second falling rate period. The drying rate slows down considerably and this in turn can lead to opacity<sup>84</sup>. The film expands slightly as the saturated region recedes



into the body and the stress on the network is relieved. Still strain between the receding saturated region and the dried area will cause cracking. Thus the thicker the film the more prone to cracking it is. Hence numerous dips rather than a single run achieve thin films.

## Chapter 4

### Sol-Gel Thin Film Deposition Techniques & Systems

#### 4.1 Introduction

Various methods are used to apply a thin film to a substrate using sol-gel methods. This chapter will look at the physics of the film formation in relation to the deposition parameters and how the apparatus is designed to optimise the film. Although sol-gel is a relatively simple, low temperature method of film formation, many parameters can be varied to produce materials with differing properties. In thin film formation the advantages of the sol-gel process outweigh the disadvantages, which can be minimized.

#### 4.2 Advantages of Sol-gel

The emergence and development of sol-gel processing has progressed to the point that the major chemistry in glass preparation is easily carried out at a low temperature in the laboratory<sup>85</sup>. Since the initial mixing is on a molecular level, a distinct advantage of the sol-gel process over conventional processes such as CVD and sputtering is the ability to tailor the pore volume, pore size and the surface area of the deposited film<sup>86</sup>. Other advantages include the improved homogeneity, lower impurity levels and the lower temperatures of formation. The ability to synthesise a large range of compositions and to mix biological and chemical materials is also an area where sol-gel excels<sup>87</sup>.

#### 4.3 Film Production Methods

##### 4.3.1 Dip Coating

The most prominent and widely used method of film deposition for sol-gel coatings is dip coating. With this method a high degree of uniformity and thickness control is achievable. Small thickness changes are easily detectable as the thickness range is

comparable to the wavelength of visible light. An additional advantage is the ability to produce multi-layer coatings permitting its use in this application.

The Dip coating process itself involves several stages. Firstly the substrate is immersed in the coating solution. The substrate is then withdrawn from the solution at a constant speed. The critical line is a region where vapour, liquid and solid co-exist as the flow advances. As the liquid film runs off the substrate it adheres to the surface and solidifies rapidly via evaporation. Evaporation of the alcohol continues as the sol gels to form the film during the drainage period. At this stage the chemical formation of the coating starts. Because of the evaporation and the draining taking place the fluid film terminates at a well defined drying line. When the receding drying line velocity equals the withdrawal velocity the process is in a steady state with respect to the liquid bath surface. A non-constant evaporation rate in the vicinity of the drying line results in a parabolic thickness profile<sup>88</sup>.

The thickness of the final film produced is governed by as many as six forces in the deposition region. The deposited film thickness is that which balances drag and gravity force when the liquid viscosity  $\eta$  and the substrate speed  $U$  are high enough to lower the curvature of the meniscus.

If drag  $D=\eta U/t$  and the gravity force is  $\rho gh$ <sup>89</sup>

Then

$$t = c_1 \left( \frac{\eta U}{\rho g} \right)^{1/2} \quad (4.1)$$

where  $c$  is a constant and  $c=0.8$  for Newtonian fluids<sup>90</sup>

Often in sol-gel deposition the substrate speed and viscosity are low and in this case the balance is modulated by the ratio of the viscous drag to the liquid-vapour surface tension  $\gamma_{LV}$  according to the following relationship<sup>91</sup>

$$t = \frac{0.94(\eta U)^{2/3}}{\gamma_{LV}^{1/6} (\rho g)^{1/2}} \quad (4.2)$$

This equation summarises the dependence of the thickness on the viscosity surface tension, speed of withdrawal from the solution and concentration of the solution. A further factor, that influences the thickness, is the angle of withdrawal, which is normally 90°. For all other angles the thickness will differ on either side of the

substrate. As the temperature of the solution and the substrate determines the process, the vapour pressure, temperature and relative humidity above the coating bath can have an effect on the film produced. Finally air velocity around the system needs to be controlled. Thickness variations depend on the gas flow through the solvent and are driven by changes in the location of the drying line. The mechanical compliance of the liquid surface is expected to be less for steady gas flow<sup>92</sup>. This has been found to change the speed of the process and hence the thickness.

### **4.3.2 Drain coating**

This method of applying a coating is a variation of the dip coating method. In this case the level of the bath solution can be lowered and the substrate to be coated remains stationary in the bath. The speed at which the liquid drains determined the thickness of the film. The atmosphere in the solution bath is variable. The method by which the vapour exits the container is very important. This can produce thickness variations in the film itself. The flow mechanism therefore is not the factor controlling the thickness of the films produced and therefore the quality of the films produced is not as predictable as the Dip method.

### **4.3.3 Spin Coating**

This process can be divided into four stages<sup>93</sup>. The first stage is the deposition stage. An excess of liquid is dispensed on to the centre of a substrate. The second stage is the spin-up where the substrate is rotated at speed. Driven by centrifugal forces, the liquid flows radially outwards. As this continues the liquid flows to the perimeter and then droplets develop at the edge of the substrate. This is the spin-off stage. As time progresses the rate of removal of the liquid slows down as the film thins. The resistance to flow increases because of the increased viscosity due to the higher concentration of non-volatile components. In the final stage evaporation controls the thinning process.

Due to a balance between the centrifugal and viscous forces the liquid forms a uniform layer during spin-off. If the viscosity is not shear dependent, and does not vary over the surface the film remains uniform<sup>94</sup>. If the liquid is shear thinning the lower shear rate near the centre causes the viscosity to be higher there and the film to be thicker there. A dispensing system, which meters out the liquid from a radially

moving arm can be used to overcome this problem. A spun film arrives at its final thickness by evaporation after the film becomes so thin and viscous that its flow stops.

Thus the thickness of an initially uniform film during spin-off is described as

$$x(t) = \frac{x_0}{\left(1 + \frac{4\rho\omega x_0^2 t}{3\eta}\right)} \quad (4.3)$$

which depends on the initial thickness  $x_0$ , time  $t$ , angular velocity  $\omega$ , viscosity  $\eta$  and the density of the liquid  $\rho$ . It can be seen that by increasing the speed the thickness is decreased and the refractive index may be affected<sup>95</sup>.

#### 4.3.4 Spray Pyrolysis

This method of applying sol-gel coatings is limited as thickness uniformity of the layers is difficult to achieve. Here the sol is sprayed on to the substrate<sup>96</sup>.

### 4.4 Film Deposition systems

When designing the system used for the film deposition there were several stages of development. When problems were encountered these were overcome in the next deposition system. This area shows how the system developed and the changes made to ensure repeatable film quality.

#### 4.4.1 Drain Coating

The initial system used for the deposition of the films was a Drain system as shown in Fig.4.1. The liquid is placed in a dropper unit. The substrate is lowered into the unit and the liquid is allowed to drain off. The film produced on the substrate is continuous over the area. There are various problems associated with this procedure.

1. Since the substrate is enclosed in a vapour environment the vapour itself has an effect on the film uniformity. The solution vapour atmosphere affected the vaporization rate of the ethanol from the substrate. The flow

mechanism is therefore not the factor controlling the thickness of the film  
It controls the rate at which the solution vapour recedes down the cavity  
and affects the thickness

- 2 The range of flow rates is limited by the size of the opening in the container so that in turn limits the upper film thickness producible
- 3 There is no direct correlation between flow rate and thickness other than a manual one, as the control on the unit cannot be mechanically controlled  
This leads to inconsistencies in the reproducibility of the thickness of the film in this case
- 4 The size of the container opening also limited the size of the substrate usable

Working within such a physically constrained environment means that the quality of the films is highly variable In order to eliminate these problems a new system was designed This system is based on the Dip coating method

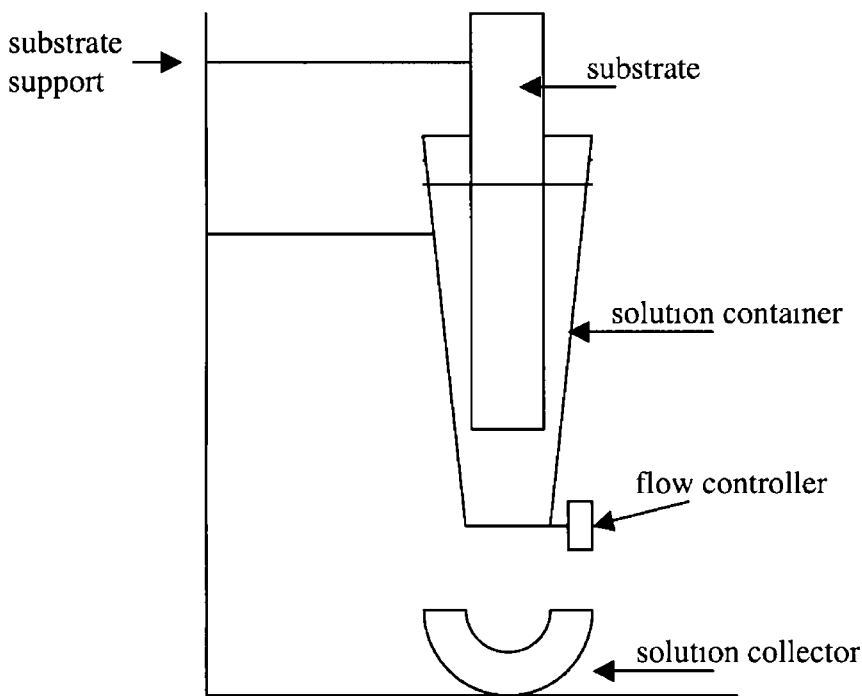


Figure 4 1 Drain coating system

### 4 4 2 Dip Coating Method

By withdrawing the substrate from the solution cavity, the vapour pressure in the confined area is no longer a control factor. Having a system activated by a variable d c motor accurate correlations between thickness and flow rate can be made. This activation method also extends the thickness range possible since it is limited only by the motor capabilities. It also opens up the possibility of automation accessible since the system may be computer driven. Once the correlation between thickness and voltage for a given viscosity is established, a desired thickness may be requested. The dipping apparatus is shown in Fig 4 2.

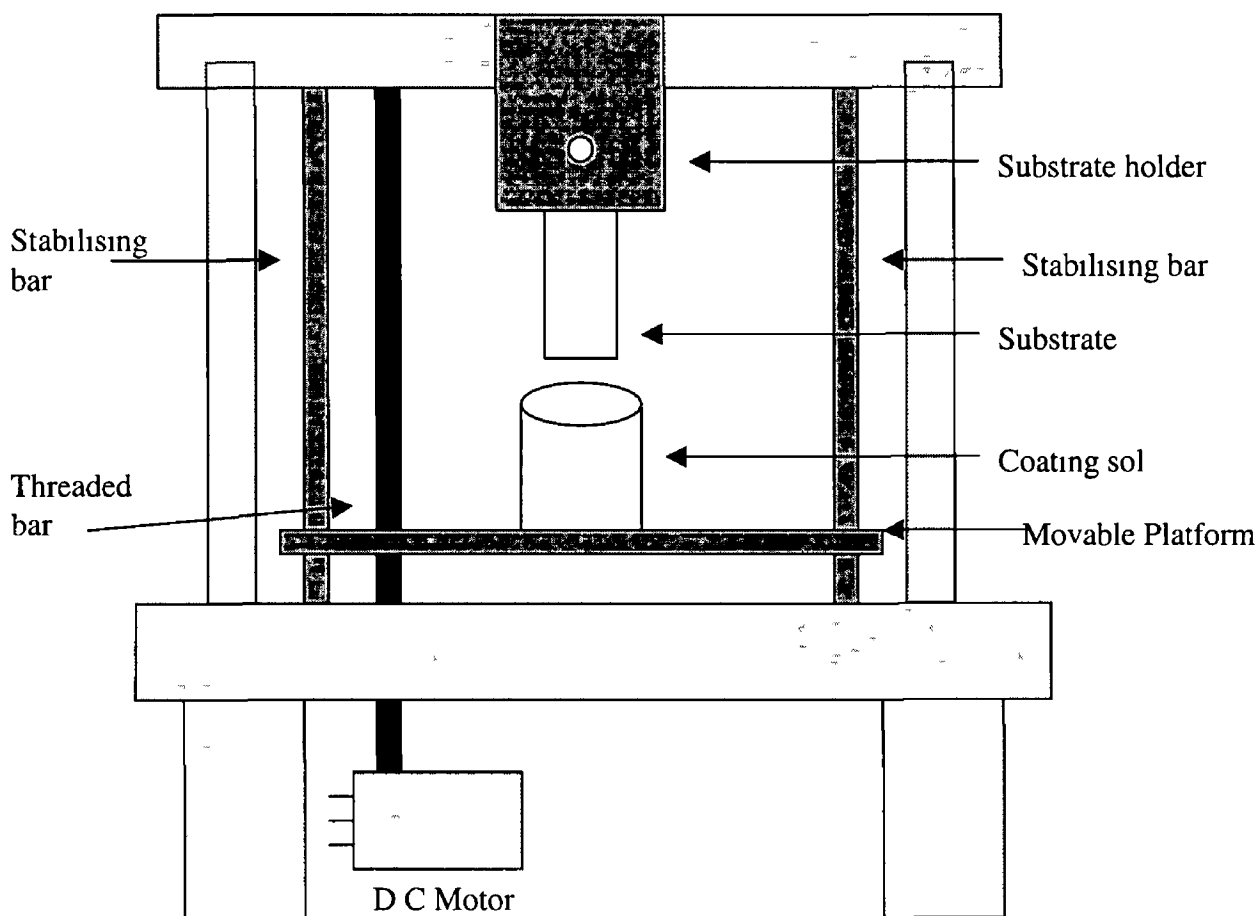


Figure 4 2 Dip coating system

It consists of a large frame on which the substrate is held on a movable platform connected to a d.c. motor via a threaded bar. The motor controls the threaded bar. As the bar turns the platform moves and hence the withdrawal speed can be controlled. It also lowers the substrate into the solution, which is placed on the platform. The substrate can be removed from the solution at a constant rate depositing a film having a thickness proportional to the withdrawal speed. The size of the solution container can be varied without affecting the process itself. This allows a variety of substrates to be used. The precision of the threaded bar and the d.c. motor controls the stability of the substrate and hence the quality of the films producible. Any variation in the stability of the substrate will produce variations in the thickness of the film. Therefore the threaded bar has a high specification and a good quality motor is used to ensure smooth movement. Stabilising bars are used to ensure smooth movement of the platform. The apparatus is placed in a convection free chamber closed to the environment. The chamber's function is to avoid any draughts, which would result in areas of uneven thickness in the film. Also the humidity in the chamber can be controlled so that the drying and thickness of the films can be consistent from film to film. This also limits the chances of the film not adhering to the substrate as it dries. The humidity also affects the transparency of the films in some cases and increased humidity results in cloudy films. As seen in Eq 4.3 the thickness of the film will vary if the viscosity of the liquid changes during the dipping process.

This system was chosen rather than a system where the liquid moves because the torque on the stand is minimized with this design. The upward drive motion of the system is smoother than the downward motion hence withdrawing the substrate from the solution rather than the solution being moved is the more stable option. The thickness of the film is determined by the withdrawal speed. The thickness of the film produced is dependent on the applied motor voltage. The voltage placed across it controls the motor speed. The faster the withdrawal the thicker the film produced.

## **4.5 Annealing systems**

After the dipping procedure is complete the films are then annealed in a furnace. For the oxide films this involves placing the films in a temperature-controlled furnace for the desired time. In order to produce the zinc sulphide films the zinc oxide must be



converted to zinc sulphide. This is achieved by annealing the zinc sulphide films in an atmosphere containing hydrogen sulphide and a hydrogen/nitrogen mix. The process itself is discussed in detail in the phosphor chapter. For the conversion of the oxide films to sulphide films, a special annealing system has been designed to control all the parameters and to contain the hydrogen sulphide.

#### 4.5.1 Sulphidation System Design

This system shown in Fig 4.3 consists of a heating tube contained in a specially designed vacuum system, which allows the hydrogen sulphide gas to be evacuated and the system to be placed under vacuum using an Edwards 2 Stage Rotary pump.

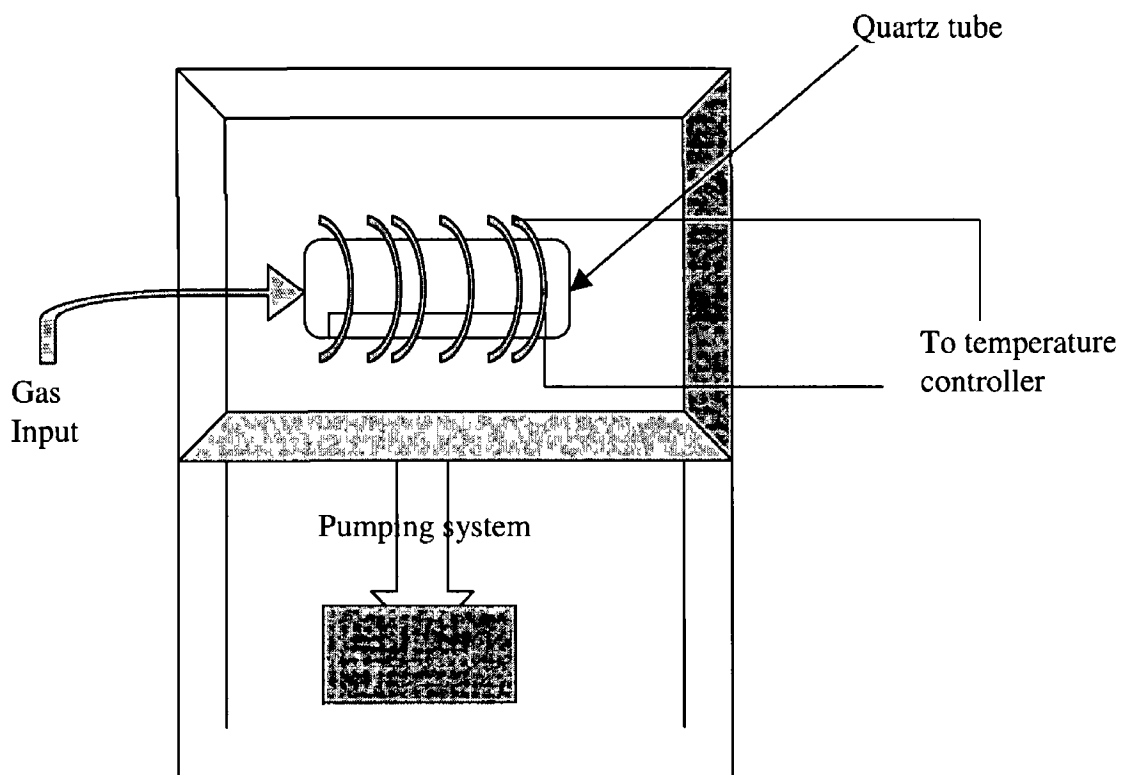
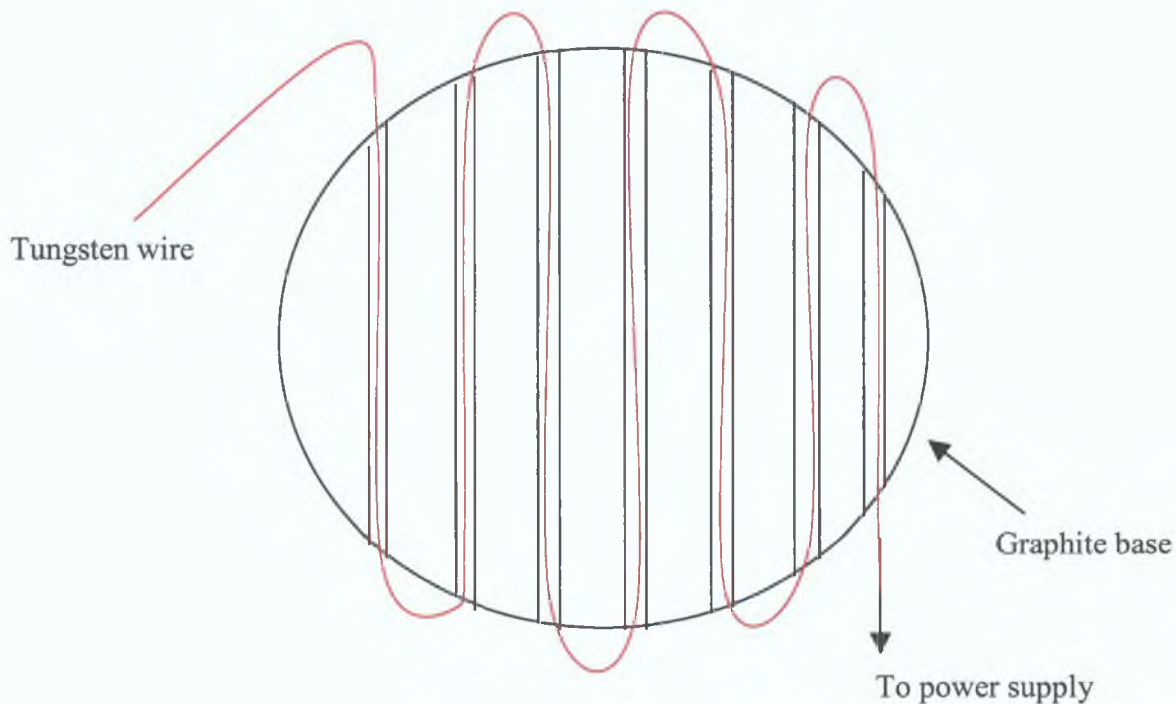


Figure 4.3 Annealing System design

#### 4.5.1.1 Heating System Design

The method of heating the substrate required three design iterations before film quality was assured. Initially a heating system based on Tungsten wire encapsulated in a graphite environment with a high current to produce a hot plate effect was used. This resistive method is shown in Fig. 4.4. The tungsten wire was placed in ceramic tubing, which was then placed in a graphite bed, which is then covered by a graphite plate. An Electrotherm that controls the temperature using a thermocouple placed in the graphite core controls heating of the graphite sandwich. The wire looping needed to be carefully checked so that the stress build up was limited. This system had to be placed in a vacuum, as the tungsten cannot be heated in an oxygen atmosphere. The graphite bed was insulated from the stainless steel base by ceramic spacers.



*Figure 4.4 Tungsten wire wound through a Graphite base*

By passing a current through the tungsten, it is heated, by resistive heating to the required temperature. The temperature was measured with a thermocouple attached to the silicon substrate placed on the heater itself. The main problem with this heating

system was the lifetime of the tungsten wire and the high temperatures required for this application. Also the high thermal mass limited this system. The maximum achievable temperature with this system was 400°C. The wire generally failed at a stress point when the temperature exceeded this or when the temperature was maintained for a long period. Tantalum wire was also used but again it failed at the turning points. The softening temperature of the metals limited the metal choice available. Outgassing and its effect on the films was also a consideration. The second design choice involved the use of lamps as heaters. This setup is shown in Fig 4.5. The lamps used were Phillips 500W lamps with built in reflectors. With this system the substrates are suspended above the source and the thermocouple is placed under the silicon so that the temperature being monitored is that of the silicon.

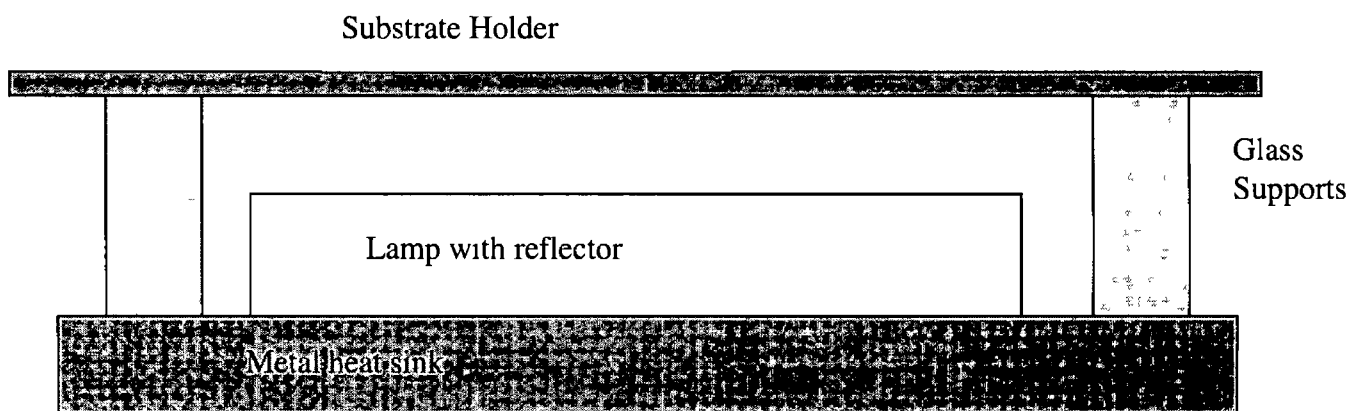
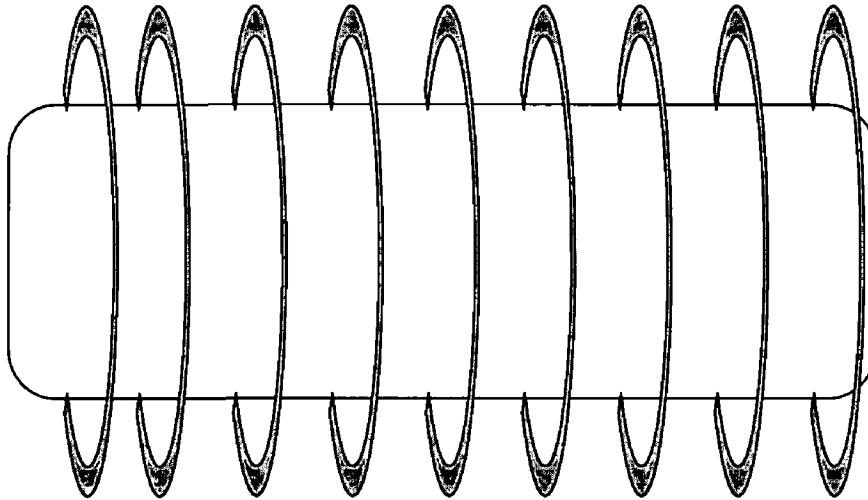


Figure 4.5 Lamp Heating System

The lamp is placed on a metal heat sink. The substrate is suspended above the lamp on metal grid using glass tubing. This system performed excellently up to temperatures of 520°C and short durations. Above that, the reliability was questionable and the system would not maintain temperature for long periods of time. This led to the development of the present heating system, which incorporates a quartz tube surrounded by a heating coil as shown in Fig 4.6. The coil is wrapped around the quartz container. It produces heat when a large current is passed through it. The substrates are placed in the tube and the thermocouple is placed in a silicon

sandwich in the tube also to ensure that the temperature given at any time is that of the silicon



*Figure 4 6 Present Heating system based on a quartz tube surrounded by a ceramic heating coil*

This system is accurate and reliable. It reached its equilibrium temperature quickly and it remained at this temperature for the times required. This system ensures that the temperature of the substrate is maintained at the required temperature for the correct times. It also has the flexibility of allowing the temperature range to be increased if required.

## Chapter 5

### The characterization of thin films

#### 5.1 Introduction

In order to ensure that the correct film has been achieved, the thin films must be characterized. The properties of thin films differ from the bulk material properties since the films have a large surface area to bulk volume ratio. Also depending on how the film is treated the morphology, structure, physical and chemical characteristics can vary from one film to another. In this chapter the characterization techniques used are explained. The physical and chemical parameters of the thin film which are investigated include

- i) Thickness measurements  
Interferometry  
Ellipsometry
  
- ii) Optical measurements  
Photoluminescence  
Refractive Index  
Spectral characterisation
  
- iii) Morphology  
X-ray diffraction  
SEM
  
- iv) Chemical Structure and composition  
FTIR  
Raman
  
- v) Electrical  
Resistivity  
Capacitance

## 5.2 Film Thickness Measurement

### 5.2.1 Interferometry

In this measurement, the phenomenon of interference is used to measure the thickness of the thin film. Interference occurs due to path differences between two coherent beams. When the path difference is integer multiples of  $\lambda$  bright fringes occur and when the path difference is  $\lambda/2$  dark fringes occur. Interference effects can be seen daily in oil slicks and soap films. These effects result from tiny thickness differences. In this case where optical thickness controls the interference and refractive index doesn't change, the fringes produced are referred to as *equal thickness fringes*. The surface of a thin film may be examined by placing it on an optical flat. The air space between the two surfaces generates a thin film interference pattern due to the path difference between light reflected from surface 1 and light reflected from surface 2. If the test surface is flat, a series of straight lines indicates a wedge shaped air film usually resulting from dust between the flats. Using a glass wedge will also show this effect. If a wedge has a step on it Fig 4.1 shows the resulting fringe pattern. If the top surfaces are parallel the fringes will again be equally spaced. When the separation of the fringes is  $b$  and the shift is  $a$  the height of the step  $t$  is given by

$$t = \frac{a \lambda_f}{b \cdot 2} \quad (5.1)$$

where  $\lambda_f$  is the wavelength of the light used.

When an optical flat is used as one surface and a thin film is the other surface the Fizeau fringes are contours of the surface under examination. To determine the thickness of a thin film it is coated with an opaque silver layer of about 70nm thick which accurately contours the under surface. A film thickness accuracy of about 2nm can be achieved using this technique.

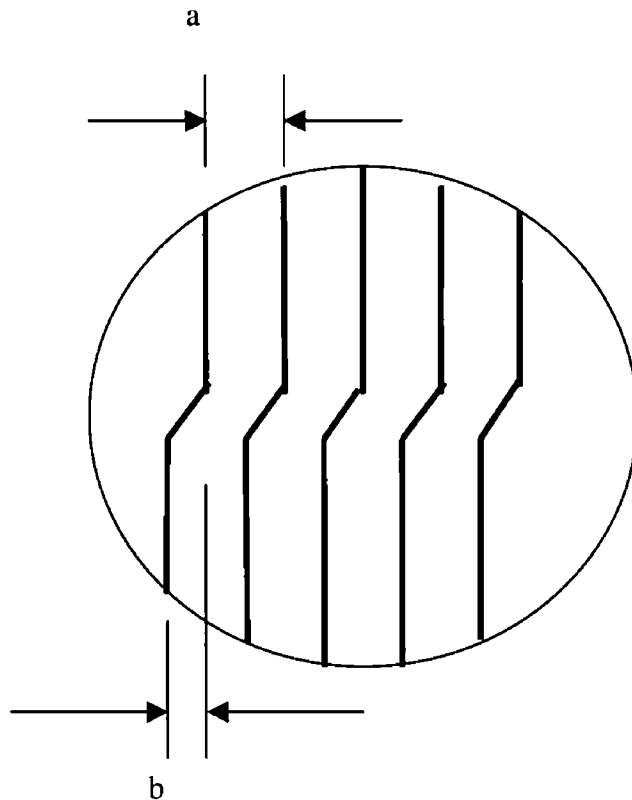


*Figure 5 1 Fringe pattern resulting from a glass wedge*

### **5.2.2 Ellipsometry**

In this technique the state of polarization of the film is analysed. From this data the parameters most frequently obtained are the thickness and the refractive index. Because the measurement uses the change in state of polarized light as it is reflected from the surface of the dielectric it is a non-destructive testing method.

When a plane polarized wave is incident at an angle to a film surface the reflected wave is elliptically polarized. Thus the lightwave consists of two orthogonal components, which are parallel (p) and perpendicular (s) to the film surface. For example given two component waves separated by a phase shift  $\delta$  as

$$\begin{aligned}
 E_x &= a_1 \cos \omega t \\
 E_y &= a_2 \cos(\omega t + \delta)
 \end{aligned}
 \tag{5.2, 5.3}$$

Thus eliminating  $t$ , the path traced out by the electric field is given by

$$\sin^2 \delta = \left( \frac{E_x}{a_1} \right)^2 + \left( \frac{E_y}{a_2} \right)^2 - \left( \frac{2E_x E_y}{a_1 a_2} \right) \cos \delta
 \tag{5.4}$$

This ellipse has a major axis making an angle  $\theta$  with the  $x$  axis where

$$\tan 2\theta = \left( \frac{2a_1 a_2}{a_1^2 - a_2^2} \right) \cos \delta
 \tag{5.5}$$

Precise values of  $a_1$ ,  $a_2$  and  $\delta$  are determined from Fresnel's equations. A comparison between experimental values and theoretically computed values will result in the determination of the optical constants of a film. A plane polarized wave incident on the film surface with its direction of polarization at  $45^\circ$  to the plane of incidence is the most common experimental arrangement as seen in Fig 5.2. Thus the polarization state and the amplitude of the incident wave are known.

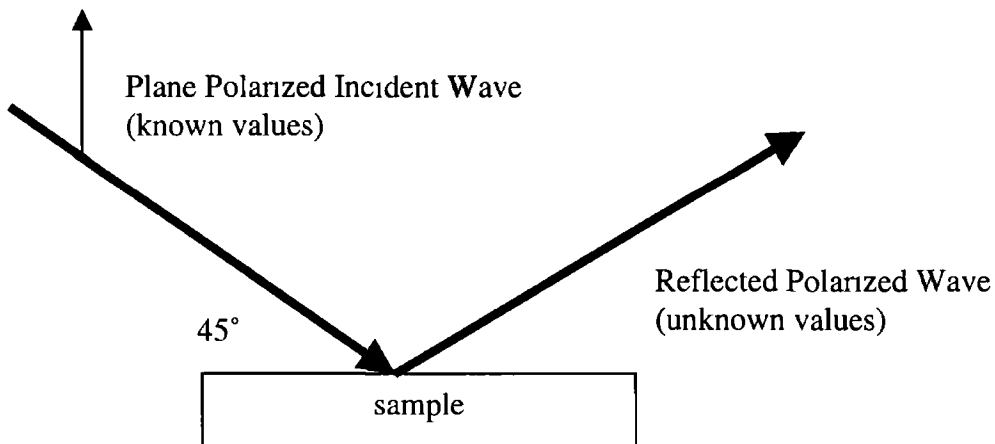


Figure 5.2 Ellipsometry Optical Arrangement



Fresnel equations are used to calculate the amplitudes and the phases of the reflected waves and hence determine the ellipticity of the wave. The complex reflection coefficient  $\rho$  is found from the complex amplitude reflection coefficient of the light polarized perpendicular and parallel to the plane of incidence as

$$\rho = \frac{r_p}{r_s} \quad (5.6)$$

This can also be represented by two angles  $\Psi$  and  $\Delta$  where,

$$\frac{r_p}{r_s} = \tan \psi \exp(j\Delta) \quad (5.7, 5.8)$$

where

$$\tan \psi = \frac{|r_p|}{|r_s|}$$

and

$$\Delta = \delta_{rp} - \delta_{rs} \quad (5.9)$$

By determining  $\Psi$  and  $\Delta$  the state of the reflected wave can be completely determined. It can be shown that, within a certain thickness range, each pair of thickness and refractive index values can be unambiguously and reversibly mapped to a pair of  $\Psi$  and  $\Delta$  values<sup>97</sup>

### 5.2.2.1 Instrumentation

There are two basic configurations, null ellipsometry and photometric ellipsometry<sup>98</sup>. In this case most of the measurements were made using a null ellipsometer.

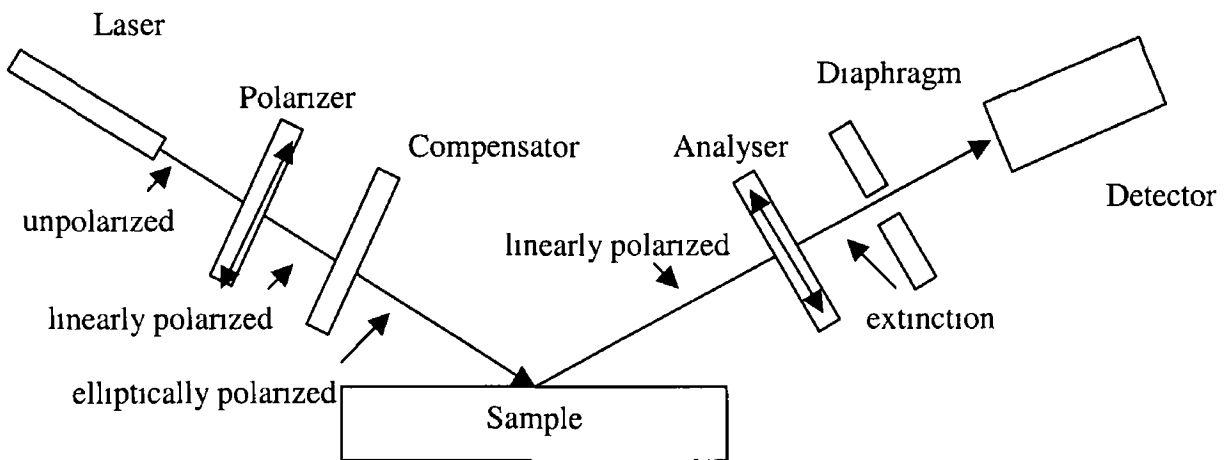


Figure 5.3 Null Ellipsometer

In a null ellipsometer as shown in Fig 5.3 the polarizer and the compensator are adjusted to produce elliptically polarized light, which is exactly cancelled from the film leaving plane polarized light to be extinguished by the analyser. This is called a Polarizer-Retarder-Sample-Analyser or PRSA configuration. Alternating the adjustments of the polarizer and analyser azimuths makes a measurement for minimum intensity<sup>99</sup>. It results in two independent sets of polarizer and analyser azimuths at which extinction occurs. The average value of  $\Psi$  and  $\Delta$  obtained from the compensator settings is known as the zone averaged value.

Generally there are five steps involved in an ellipsometric measurement

- a) the provision of a state of polarization for the incident light
- b) the interaction of the light with the thin film
- c) the measurement of the state of polarization of the reflected light
- d) calculation of  $\Psi$  and  $\Delta$
- e) determination of the physical properties from the measured values of  $\Psi$  and  $\Delta$

An Auto EL III Rudolf Research null ellipsometer having a HeNe (632.8 nm) laser was used to measure the refractive index and the thickness of films deposited on silicon substrates.

## 5.3 Electromagnetic wave interactions with matter

In this area various waves with different wavelengths or frequencies are used to analyse different properties of the thin film. Fourier Transform Infra-Red (FTIR) and Raman spectrometry are used to determine the bonding structure and composition of the films. UV-VIS studies involve band edge calculations and also show the transmission of the films in the visible region. Photoluminescence and cathodoluminescence are used to analyse the recombination methods that result in light emission. All of these techniques are based on exciting a film with an electromagnetic wave and analysing the interaction observed.

### 5.3.1 Vibrational Spectrometry

The characterisation of the molecules contained in a film is vital to the understanding of a large number of processes and interactions. Although many techniques can provide data on elemental composition, vibrational spectrometry is unsurpassed in obtaining detailed information on the nature of molecules<sup>100</sup>. When an electromagnetic wave interacts with a thin film it will excite certain vibrational modes. There are two types of molecular vibrations, stretching and bending. A stretching vibration involves the rhythmical movement along the bond axis so that the interatomic distance is increasing or decreasing. A bending vibration can result in a change of bond angle between the bonds with a common atom or the movement of a group of atoms in the group with respect to one another. Only those vibrations that result in a rhythmical change in the dipole moment are observed in the IR. The alternating electric field accompanying a vibration is produced by the changing charge distribution. This field couples the molecule vibration with the oscillating electric field of the EM radiation. To analyse vibrational modes FTIR or Raman spectrometry can be used. Infrared absorption arises when the IR interacts with a fluctuating dipole within the molecule. The raman effect depends on the polarisability of a vibrating group, its ability to interact and couple with the exciting radiation having a frequency that does not match that of the vibration itself. A given vibrational mode within a molecule may lead to fluctuations in the dipole making it infrared active. This may not lead to changes in the polarisability giving a

Raman active vibration Thus an infrared vibration may not be Raman active and visa versa This allows both methods to be used to gather complementary information about the vibrations

### 5.3.1.1 Fourier transform infrared spectrometry

Infrared radiation refers broadly to that part of the electromagnetic spectrum between visible and microwaves Generally the IR energy can be distinguished by its wavenumber in relation to visible waves as far IR or near IR Infra red spectra originate in transitions between two vibrational levels of the molecule in the electronic ground state and are usually observed as absorption spectra in the infrared region of the spectrum

Infrared spectrometry involves passing a beam of infrared radiation through a film and recording which frequencies are absorbed

Infrared radiation having wavenumbers less than  $100\text{cm}^{-1}$  is absorbed and converted into molecular rotation energy Radiation having wave numbers in the range  $1000\text{-}100\text{cm}^{-1}$  is absorbed and converted into vibrational energy This absorption is quantized but vibrational spectra appear as bands rather than lines because a single vibrational energy change is accompanied by several rotational energy changes

Band intensities can be expressed as either transmittance T or absorbance A

Transmittance is the ratio of radiant power transmitted by a sample to the radiant power incident on the sample Absorbance, A is defined as<sup>101</sup>

$$A = \log_{10} \left( \frac{1}{T} \right) \quad (5.10)$$

### 5.3.1.2 Raman Spectrometry

Raman spectrometry also excites the vibrational modes of the molecule While infrared spectrometry looks at the transmitted light, Raman spectrometry analyses the nature of the scattered light as shown in Fig 5.4

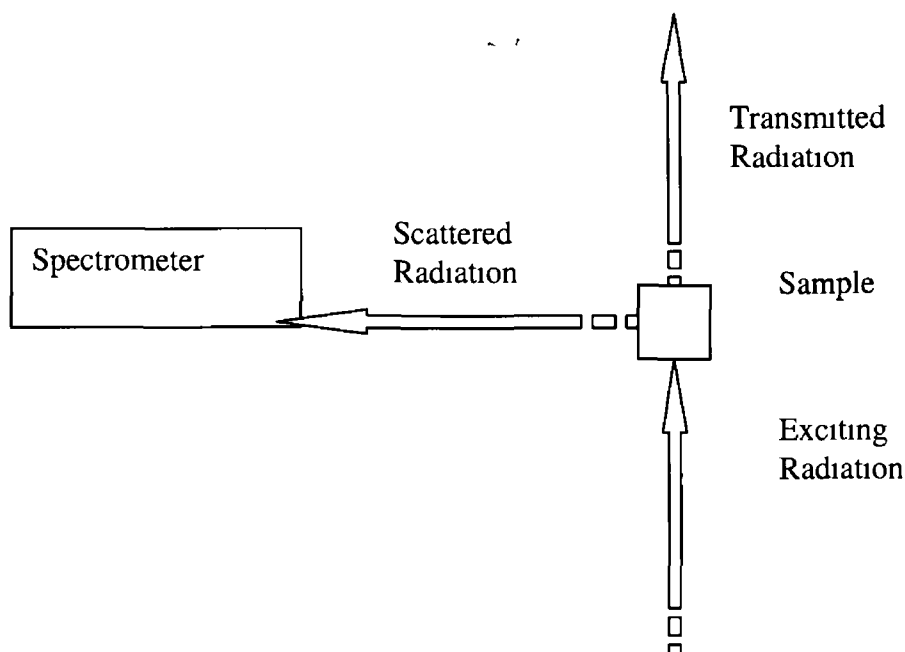


Figure 5 4 Raman system

Radiation scattered from a sample consists of the scattered incident radiation and additional frequencies<sup>102</sup> These additional frequencies are symmetrically arrayed above and below the frequency of the incident radiation or Rayleigh line<sup>103</sup> The difference in frequency between the incident and scattered radiation corresponds to frequencies in the mid-infrared region

These differences between Raman line frequencies and the Rayleigh line frequency correspond to the vibrational frequencies present in the molecule Thus by measuring these frequency differences as information about the vibrational frequencies within a molecule are obtained The magnitudes of the Raman shifts are independent of the excitation wavelength Therefore the same shift patterns for a given molecule will be obtained regardless of the source used Stokes lines are observed at wavenumbers lower than the Rayleigh line and Anti-Stokes lines are found at wavenumbers larger than the excitation line as shown in Fig 5 5 It can also be seen that the Anti-Stokes lines are of lower intensity than the Stokes lines and for this reason only the Stokes part of the spectrum is generally used Shifts towards lower energies are called Stokes shifts These are plotted without the negative sign and the general label of wavenumber,  $\text{cm}^{-1}$  is given rather than wavenumber shift

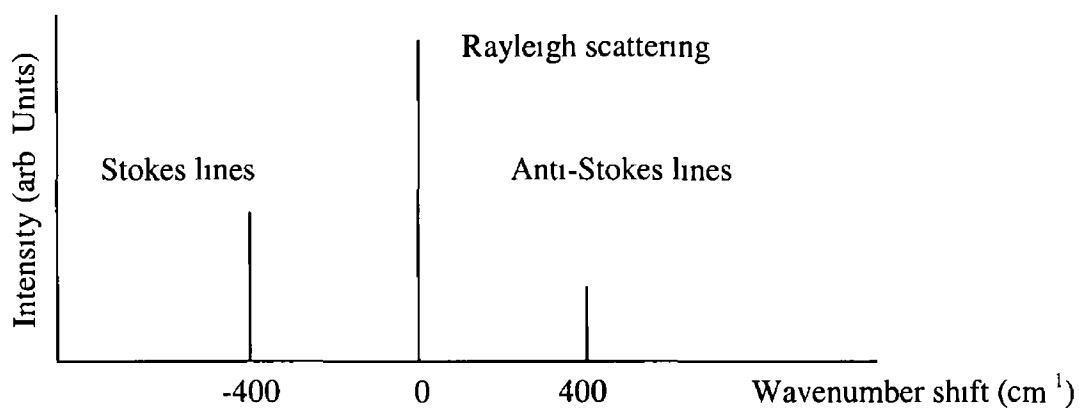


Figure 5.5 Typical components of a Raman spectrum

### 5.3.1.3 Instrumentation Vibrational Spectroscopy

The FTIR spectra were measured using a Perkin Elmer 983G. The resolution was  $2\text{cm}^{-1}$ . The range of the machine with a Potassium Bromide (KBr) window is  $400\text{cm}^{-1}$ - $4000\text{cm}^{-1}$ . This excludes the ZnS band of interest at  $240\text{cm}^{-1}$ . A Cesium Iodide (CsI) window was fitted to extend the range for this measurement.

Raman data was recorded using a Micro Raman Spectroscopy System Joban-Yvon HR-800 using a 325nm HeCd laser. The integration time used was 5s and 10 spectra were averaged for each measurement.

### 5.3.2 Ultraviolet-Visible Spectroscopy

For the qualitative and quantitative determination of film properties, absorption measurements based on ultraviolet and visible radiation have widespread applications.

The absorption of ultra violet or visible light by a molecular species is a two-step process involving excitation of the atom as the energy is absorbed and relaxation to its original state. The amount of thermal energy evolved by relaxation is usually not detectable. Therefore this absorption measurements cause minimal disturbance to the atom. The absorption results from the excitation of bonding electrons and therefore the wavelengths of the absorption peaks can be correlated to the type of bonds in the film. The characteristics of interest for a band are its position and its intensity. Its position indicates the energy required for an electronic transition. The intensity is dependent on two factors:

1. the probability of interaction between the radiation and the electronic system and
2. the energy difference between the ground and excited states.

Transitions of low probability are generally forbidden. The intensity of the absorption can be expressed in the form of transmittance and is given by

$$T = \frac{I}{I_o} \quad (5.11)$$

where  $I_o$  is the intensity of the radiant energy striking the film and  $I$  is the intensity of the emerging radiation.

All measurements were carried out on samples prepared on glass substrates on a Perkin Elmer UV/Vis spectrometer.

### 5.3.3 Photoluminescence

Photoluminescence measurements the quantitative measurement of a variety of important inorganic and organic species in trace amounts. One of its most attractive features is its inherent sensitivity. Its detection limits are one to three orders of magnitude lower than those encountered in absorption measurements. However luminescence methods are less applicable than absorption methods because only a limited number of systems exhibit luminescence. Since ZnS:Mn is the primary layer in the device it exhibits luminescence.

Photoluminescence is a two-step process. First the molecule is excited with the correct electromagnetic energy. An excited molecule can return to its ground state by a combination of several methods as discussed in Chapter 6. The favoured route is the one that minimizes the lifetime of the excited state. One of these methods is radiative emission. If deactivation is rapid compared to the radiationless process then radiative emission is observed. Since radiative emission may also take place via impurity states, photoluminescence is a standard technique for the investigation of impurity states, in semiconductors. Since photoluminescence is limited to a relatively small number of systems incorporating the required structural and environmental features, it can also be used to identify the presence of these molecules<sup>104</sup>. In photoluminescence measurements the sample is excited by a fixed wavelength while the emission intensity is recorded as a function of wavelength. Photoluminescence usually occurs at wavelengths longer than the excitation wavelength.

### 5.3.3.1 Instrumentation

All the photoluminescence measurements were taken at room temperature. The system used a He-Cd laser with a 1-metre focal length spectrometer in a Czerny-Turner configuration. The photomultiplier tube was a Hamamatsu Model R3310-02 with a spectral range from 300-1040nm and configured for photon counting.

### 5.3.4 Cathodoluminescence

Cathodoluminescence (CL) is the emission of light under electron bombardment. Three fundamental processes result in a CL emission. These are the generation, motion and recombination of electron-hole pairs. This method is used to investigate the luminescent properties of different materials. When the sample is excited using an electron beam light emission results from all the radiative recombination methods present in the sample. Since the electrons also possess momentum in addition to their energy, the non-equilibrium carriers appear in indirect bands and hence there are extra peaks in a cathodoluminescence spectrum compared to a photoluminescence spectrum. Three modes of recombination, which includes interband recombination,



surface recombination and recombination via localized states can be identified on the CL spectrum<sup>105</sup>

The SEM permits a measurement of the luminescence parameters over the sample surface to be made. A thin electron probe focused on a given point on the surface of the sample excites CL. The dimensions of the interaction region are in the order of  $1\mu\text{m}$  but depend on the energy of the incident electron and the mass of the scattering atom. High spatial resolution can be obtained due to the spot size. The spatial resolution of CL may be expressed as a geometrical sum of the<sup>106</sup>

- a) beam diameter at the sample
- b) lateral dimension of the energy dissipation volume which is the electron penetration depth  $R_e$
- c) minority charge carrier diffusion length  $L$

The electrons are collected from the sample by a mirror that collects as many emitted photons as possible. At this point there are two modes of operation of the CL system. In one case the detector collects the total or panchromatic CL signal by bypassing the monochromator. This allows the full luminescence from the sample to be observed. Here the electron beam is scanned over the sample area during the measurement. In the other case the photons are channeled via a monochromator to a photomultiplier tube for detection. In the near IR range solid-state photodetectors are used. In this case the electron beam is positioned at a definite fixed point on the sample surface and the monochromator is scanned over a given wavelength region. The detected photons then produce a CL radiation spectrum for that point. CL can also be used to detect the presence of structural defects in a sample. These usually reveal themselves as centers with higher nonradiative recombination rates. These can be observed in the panchromatic mode of operation<sup>107</sup>

#### **5.3.4.1 Instrumentation**

The CL measurements were taken using an SEM with the beam energy set at 15kV, with a CL system attached. For comparison purposes the probe current was maintained at 1nA and the slits were set at 1.5mm

## 5.4 X-ray Diffraction

X-rays are electromagnetic waves with a wavelength of the order of a fraction of a nanometre and are therefore suitable for interaction with crystal planes. When X-ray radiation interacts with the electrons in the matter through which it passes it is scattered. If x-rays are scattered by an ordered environment such as a crystal, interference takes place between the scattered rays producing a diffraction pattern. This occurs because the distances between the scattering centres are of the same order of magnitude as the wavelength of the x-rays.

### 5.4.1 Bragg's Law

When a narrow beam of radiation strikes a crystal surface at an incident angle  $\theta$  scattering occurs due to the interaction of the radiation with atoms located at O, P and R in Figure 5.6. If the distance

$$AP + PC = n\lambda \quad (5.12)$$

Where  $n$  is an integer, the scattered radiation will be in phase at O, C, and D and the crystal will appear to reflect the x-ray radiation. It can be seen that

$$AP = PC = d \sin \theta \quad (5.13)$$

when  $d$  is the interplanar distance of the crystal. Thus the condition for constructive interference at angle  $\theta$  is

$$n\lambda = d \sin \theta \quad (5.14)$$

which is known as the Bragg Equation<sup>108</sup>. X-rays will only appear reflected from the crystal if the angle of incidence satisfies the condition

$$\sin \theta = \frac{n\lambda}{2d} \quad (5.15)$$

At all other angles destructive interference occurs.

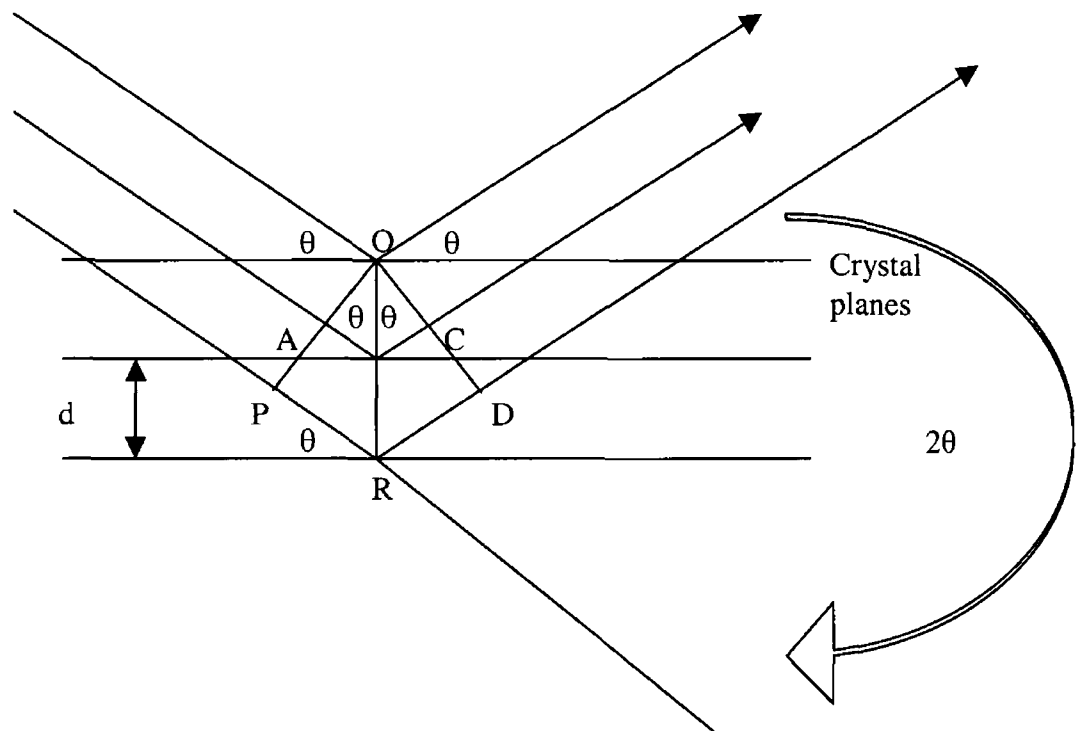


Figure 5 6 Diffraction of X-rays by a crystal

The x-ray diffractometer records the intensity of the radiation at the reflected angles, and by observing the diffraction pattern it is possible to identify the structure of the material. A large library of diffracted patterns from standard elements and compounds is available and it can be used to identify any unknown phases present in a sample.

The diffraction pattern produced can also determine the size of the crystal present as smaller crystals cause broadening of the diffracted beam. This is caused when the destructive interference is not complete. This means that somewhere in the crystal there is a plane scattering a ray and allowing diffraction to take place at angles that don't exactly satisfy the Bragg equation.

## 5.4.2 Instrumentation

All the x-ray spectra were obtained using a  $\text{CuK}\alpha$  line at either a  $10^\circ$  glancing angle or  $\theta$ - $2\theta$  configuration

## 5.5 Electron Microscopy

One of the most versatile tools available for the characterisation of materials is the electron microscope. By utilising a variety of attachments significant data about the construction, composition and luminescence of a sample can be obtained. The three methods using electron bombardment of the sample used here are scanning electron microscope (SEM), energy dispersive x-rays (EDX) and cathodoluminescence (CL). These will be looked at in detail.

### 5.5.1 Scanning Electron Microscope

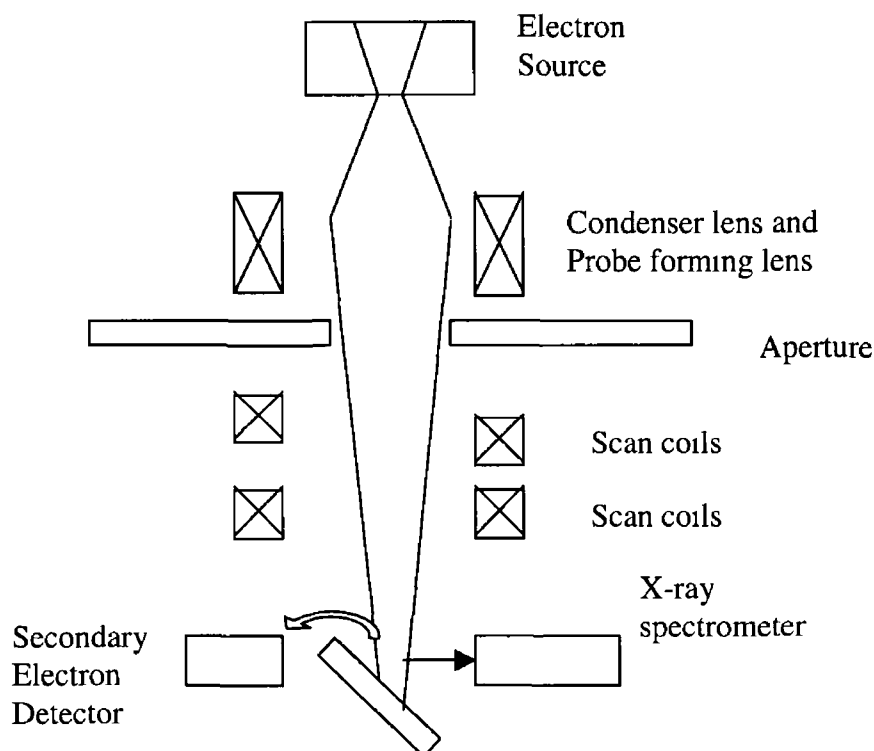


Figure 5.7 Schematic diagram of a Scanning Electron Microscope

The scanning electron microscope is like an ordinary microscope except that electrons rather than electromagnetic radiation are used to irradiate and study the sample. An electron having a momentum  $p$  behaves as a wave of wavelength  $\lambda$  where

$$\lambda = \frac{h}{p} \quad (5.16)$$

and  $h$  is Planck's constant

Electrons are used to increase the resolution of the microscope. Electric and magnetic fields are used to control the motion of the electrons and so focus the beam on a given area of a sample provided the electron beam divergence is successfully controlled.

The basic construction is shown in Fig. 5.7<sup>109</sup>

In a SEM the beam is focused on a fine spot on the surface of a sample.

Backscattered or secondary electrons from the surface are collected, as the incident beam is raster scanned over the surface of the sample to generate an image. The electron beam interacts with the solid via electrostatic forces with the excitation volume of the solid shown in Fig. 5.8, dependent on the atomic number of the elements involved. The shape of this area varies from a pear shape for a low atomic number ( $Z$ ) material to a spherical shape for  $15 < Z < 40$ <sup>110</sup>. For larger atomic numbers the interaction area becomes hemispherical. The actual escape depth of the electrons also depends on the beam energy. The process can result in a build up of charge on the surface of low conductivity materials, which can distort the final image. To overcome this, materials can be coated in a conductive material. Contrast in the SEM images arises from variations in the number of electrons reaching the detector from different regions of the spectrum. The spot size determines the resolution. This also depends on the probe current intensity since this determines the number of secondary electrons present. The number of secondary electrons reaching the detector depends on the angle between the incident beam and the surface at the point where the beam strikes therefore irregularities can be clearly seen.

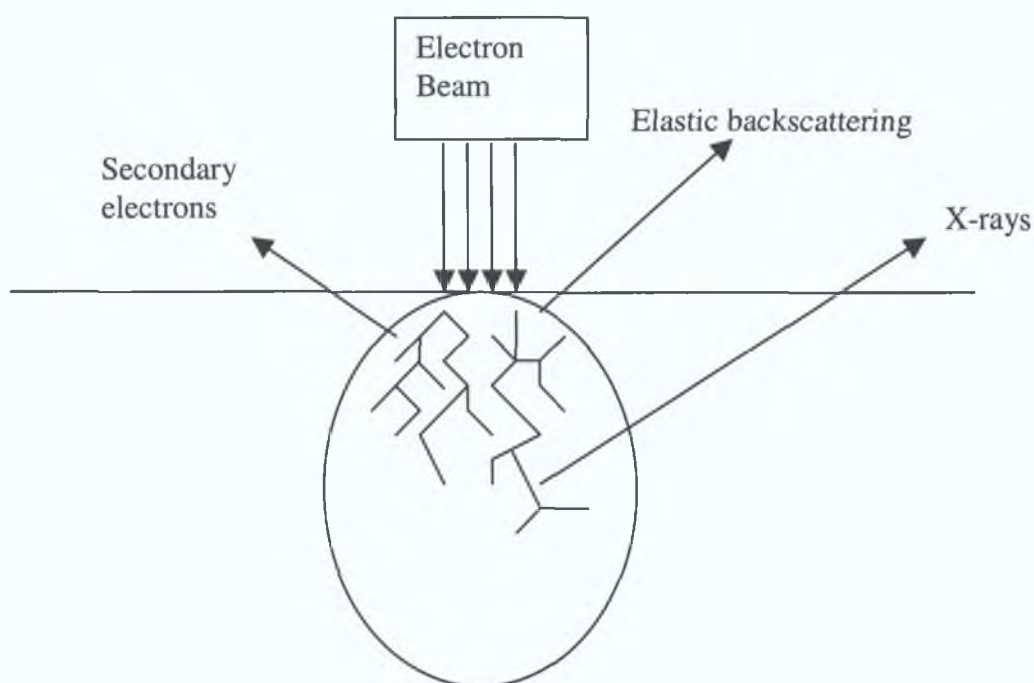


*Figure 5.8 Interaction between the incident electron beam and a sample in a pear shaped volume*

### 5.5.2 Energy Dispersive X-rays

When an electron beam hits a sample it can excite an electron from the inner shell of the atom leaving behind a hole that can be filled by an electron from another shell by the emission of x-rays or Auger electrons. These have energies characteristic of the atom emitting them. This gives an elemental microanalysis of the sample. The x-ray monitoring is carried out with energy dispersive spectrometers. The intensity of the x-rays is proportional to the atomic number of the atom. Thus different elements present in the material can be catalogued according to the energy of the x-rays they emit. Usually a Be window is used to cover the silicon detector. This will absorb low energy x-rays and so this technique is limited to elements having an atomic number greater than ten. The x-rays are generated deep in the pear shaped region shown in Figure 4.8 and so the resolution of this technique is limited.

## 5.6 Electrical Measurements

In characterizing a TFEL device the electrical parameters determine the response of the device. The measurements of film resistivity for the conducting and insulating layers and the capacitance of the insulator are fundamental to the device performance.

### 5.6.1 Thin Film Resistivity Measurement

The resistivity,  $\rho$  is defined as the proportionality constant between the electric field,  $E$  and the current density  $J$ <sup>11</sup>

$$E = \rho J \quad (5.17)$$

Its reciprocal value is the conductivity  $\sigma = 1/\rho$ , and

$$J = \sigma E \quad (5.18)$$

For semiconductors where both electrons and holes are carriers

$$\rho = \frac{1}{\sigma} = \frac{1}{q(\mu_n n + \mu_p p)} \quad (5.19)$$

where  $n$  and  $p$  are the free electron and hole concentrations and  $\mu_n$  and  $\mu_p$  are the electron and hole mobilities respectively. The resistivity may be calculated from this formula if both carrier concentrations and both mobilities are known. For extrinsic materials in which the majority carrier concentration is much higher than the minority carrier concentration the above formula is simplified to include just the majority concentration and mobility. The carrier concentration and mobility are generally not known therefore an alternate method must be used. Techniques for measuring the resistivity vary but are generally based on the link between resistance and resistivity. Since

$$\rho = \frac{RA}{l} \quad (5.20)$$

where  $A$  is the cross-sectional area and  $l$  is the length

This gives a general expression for the resistivity as

$$\rho = \frac{VA}{I\lambda} \quad (5.21)$$

A two point probe can be used to find the resistance of a film. The total resistance between the two probes is given as

$$R_T = \frac{V}{I} = 2R_C + 2R_{sp} + R_s \quad (5.22)$$

where  $R_C$  is the contact resistance at each probe-semiconductor contact,  $R_{sp}$  is the spreading resistance under each probe and  $R_s$  is the semiconductor resistance. The value of  $R_s$  cannot be accurately determined because the values of  $R_C$  and  $R_{sp}$  cannot be measured accurately.

A more general method for measuring the resistivity of a thin film is using a four-point probe. In this case two probes carry the current and two probes measure the voltage. Developed as a general Geophysics measurement technique, referred to as Wenner's Method<sup>112</sup>, it has found applications in the semiconductor area<sup>113,114</sup> and has become one of the most common methods for measuring resistivities. A small current from a constant current source is passed through the two outer probes and the floating voltage is measured between the two inner probes when the probes are set on a flat surface of the film to be measured as shown in Fig. 5.9.

For a four point probe having an equal spacing between the probes  $s$ , the resistivity is given by

$$\rho = 2\pi s \frac{V}{I} \quad (5.23)$$



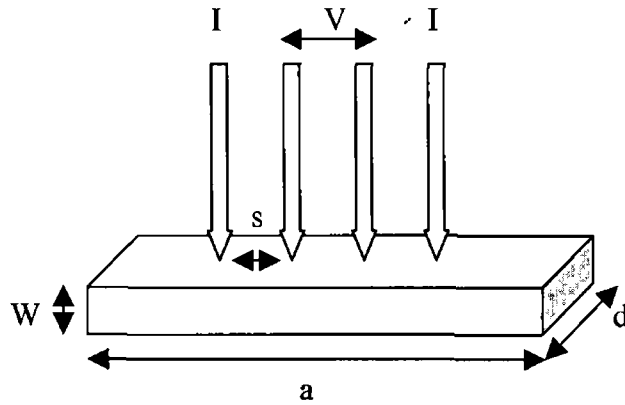


Figure 5 10 Four point Probe setup on a thin film surface

For a film of thickness  $W$  much smaller than either  $a$  or  $d$  the sheet resistance is given by

$$R = \frac{V}{I} F \quad \Omega/\text{square} \quad (5 24)$$

and the resistivity is given by

$$\rho = RW \quad \Omega\text{cm} \quad (5 25)$$

Thus, combining the above for a thin film, the resistivity is

$$\rho = 2\pi s F \frac{V}{I} \quad (5 26)$$

For sample thicknesses greater than the probe spacing this simple correction factor will not apply. For thicknesses less than the probe spacing  $s$  and in the limit when  $d \gg s$ , the correction factor becomes  $(\pi/\ln 2)$  and the equation becomes<sup>115</sup>

$$\rho = \frac{\pi}{\ln 2} W \frac{V}{I} = 4.5324 W \frac{V}{I} \quad (5 27)$$

The sheet resistance can also be used to characterise thin films or layers such as polycrystalline silicon

A collinear probe configuration is the most common four-point probe arrangement but other arrangements such as a square are also used

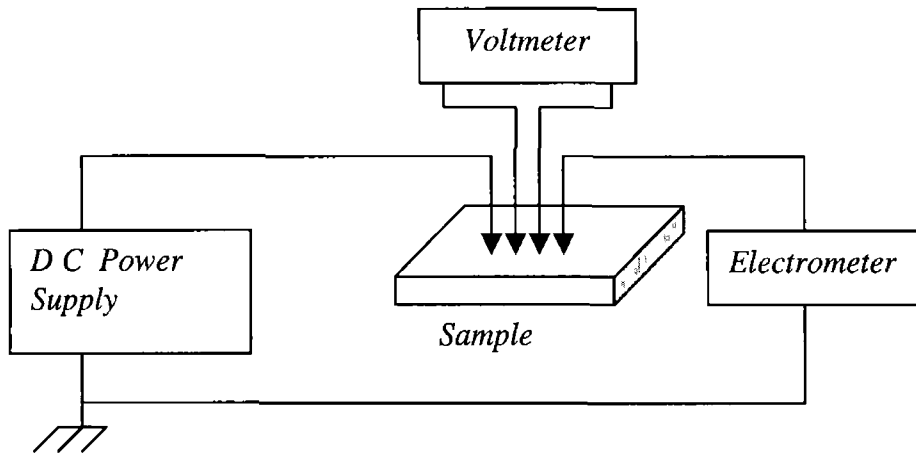


Figure 5 10 Resistivity Measurement Circuit

If the following conditions are met the resistivity of a flat sample of an arbitrary shape can be measured without knowing the current pattern<sup>116</sup>,

- i) the contacts are sufficiently small
- ii) the sample has a uniform thickness
- iii) the contacts are at the circumference of the sample
- iv) the surface on which the probes rest is flat with no surface leakage

The circuit shown in Fig 5 10 is used to measure the resistivity of the films

## 5.7 Electroluminescence Measurements

The display itself has to be characterised and the important considerations here are

- i) the light output of the device
- ii) the spectral region of the output
- iii) the electrical behaviour of the device
- iv) the relationship between the driving voltage and the light output

The first two measurements are purely optical and the second two measurements are both electrical and optoelectronic

## 5.7.1 Brightness Measurement

The quality and characteristics of an EL display are evaluated by measurement of the light output or brightness of the device. The system used to determine the brightness of the devices consists of an optical detector or optometer, an EL device driver and the device to be tested. The EL driver circuit consists of a generator and an amplifier that allows the regulation of the supply to the device. The generator produces a sine wave, triangular wave and a pulse wave whose duration can be modified. The output voltage can be varied from 0-300V. The UDT Model 380 dual channel optometer is used for the measurements. This is used in conjunction with a UDT detector head. The experimental set-up is shown in Figure 5.11. The main consideration when using the equipment is the coupling of the signal into the detector. When making the brightness measurement the following calculations were carried out. The  $\mu\text{W}$  are converted to Lumens by multiplying by the photopic factor found in the photopic curve. This is taken at 580nm since that is the peak wavelength for ZnS:Mn. This is 0.87, since

$$683 \text{ Lumens} = 1 \text{ Watt}$$

This is then converted to candela by dividing by the angular response in steradians. To convert to  $\text{candela}/\text{m}^2$  the candelas are divided by the area of the device in question<sup>117</sup>

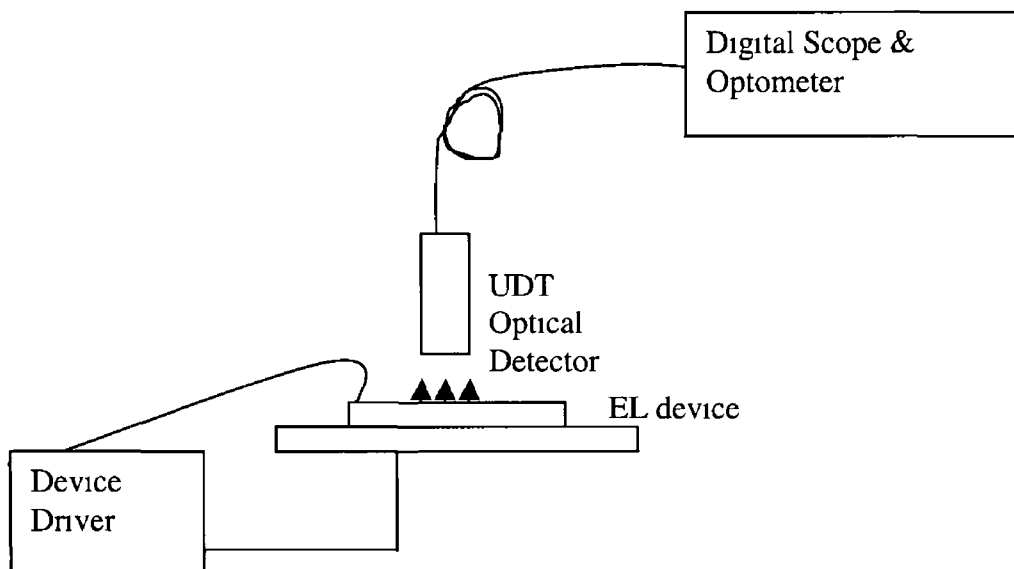


Figure 5.12 Brightness Measurement system for an EL device

Since the luminous output of a device can be given in a variety of different units a conversion table is given in Table 5.1 to facilitate conversion<sup>113</sup>.

	nit (nt)	stilb (sb)	apostilb (asb)	Lambert (L)	Milli-lambert (mL)	Foot-lambert (fL)	Candela per square foot (cd ft <sup>-1</sup> )
1 nit (cd m <sup>-2</sup> , or lm sr <sup>-1</sup> m <sup>-2</sup> ) (nt)	1	1x10 <sup>-4</sup>	3.1416	3.1416 x10 <sup>-4</sup>	0.31416	0.2919	0.0929
1 stilb (cd cm <sup>-2</sup> ) (sb)	1x10 <sup>-4</sup>	1	3.1416 x10 <sup>-4</sup>	3.1416	3141.6	2919	929
1 apostilb (π <sup>-1</sup> cdm <sup>-2</sup> ) (abs)	0.3183	3.183x10 <sup>-5</sup>	1	1x10 <sup>-4</sup>	0.1	0.0929	0.02957
1 lambert (π <sup>-1</sup> cdcm <sup>-1</sup> ) (L)	3183	0.3183	1x10 <sup>-4</sup>	1	1000	929	295.7
1 millilambert (mL)	3.183	3.183x10 <sup>-4</sup>	10	0.001	1	0.929	0.2957
1 footlambert (π <sup>-1</sup> cd ft <sup>-2</sup> ) (fL)	3.426	3.426x10 <sup>-4</sup>	10.764	0.0010764	1.0764	1	0.3183
1 candela per square foot (cd ft <sup>-2</sup> )	10.764	0.0010764	33.82	0.003382	3.382	3.1416	1

**Table 5.1 Conversion factors for commonly used luminance quantities.**

### 5.7.2 Electrical Device Characterisation

The system set-up shown in Figure 5.11 can also be used for the electrical characterisation of the EL device. The optometer and the device driver are connected to the oscilloscope in order to view the luminance as a function of the input waveform. The charge versus voltage measurements are carried out using the EL device as part of a Sawyer-Tower set-up and this is explained in detail in Chapter 9.

### 5.7.3 Spectral Output Measurement

The spectral output of the device is measured using a Spectrometer. The spectrometer consists of a PMT and a monochromator integrated with a computer to output the wavelength response of the device. The light from the device is coupled to the detector by a fibre optic link. The system used in the measurements is a SOFIE spectrophotometer with a spectral range of 200-900nm. The system set-up is shown in Fig 5.12.

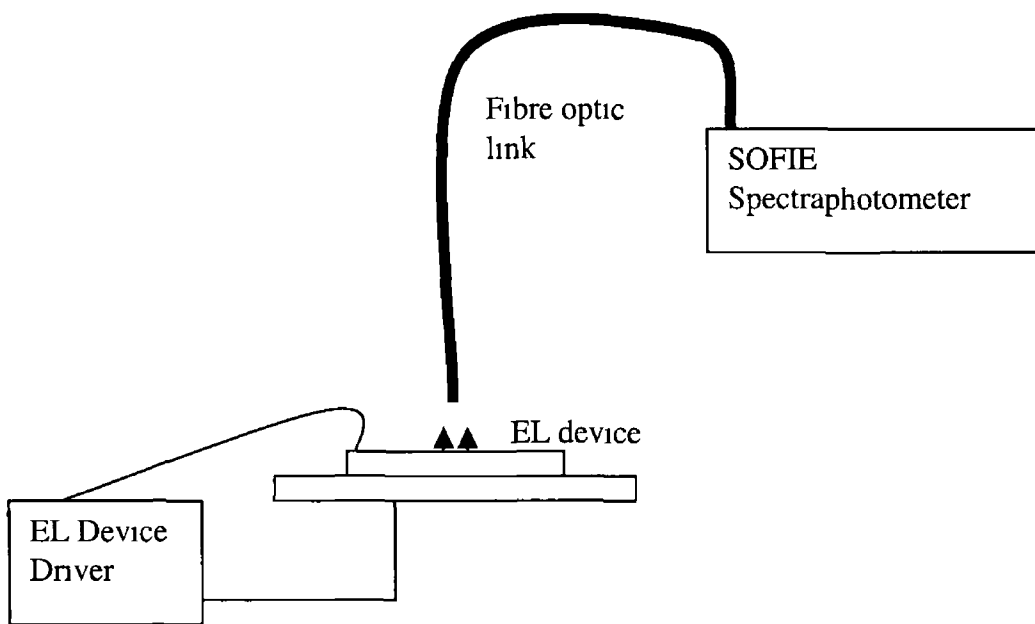


*Figure 5.12 Spectral output Measurement system*

This records the luminous intensity of the device at each wavelength between 400 and 700nm. The output is the spectral response of the device over the visible spectrum. This system can also be used to measure qualitatively the brightness of the devices as the spectral output can be seen to grow as the input voltage is increased.

## Chapter 6

### Phosphor Films

#### 6.1 Introduction

The luminescent material is of primary interest in any display. Generally a host material with a luminescent centre is required. The portion of the electromagnetic spectrum visible to the human eye is the 400-700nm region. The material chosen must produce luminescence in this region and therefore have a band gap of  $\sim 3$  eV. Many phosphors have been developed<sup>118 119 120 121</sup> for the CRT but most of these have proved unsuccessful when used for ac thin film electroluminescent applications<sup>122</sup>. For an electroluminescent device the material must luminesce when placed in an appropriate electric field. Due to the complex interaction between the host material and the luminescent centre both will be treated separately here. This chapter will detail the mechanisms for radiative and non-radiative decay and the fundamentals of the emission process. Several models are also discussed. Thin films have the advantage that they do not suffer from the diffuse reflectivity of powders and therefore the contrast achievable between lit and unlit pixels can be high. For marketable displays, brightness, efficiency and lifetime must also be high. In order to achieve these criteria the physics of the material and its interaction with other films in the display must be discussed.

#### 6.2 Theory

An accelerating charge, which impacts and excites an electron, causes luminescence. The important forms of luminescence are summarized in Table 6.1<sup>123</sup>

Luminescence Type	Typical Application	Luminous Efficiency
Black Body Radiation	Tungsten Filament Lamp	5%
Photoluminescence	Fluorescent Lamp	20%
Electroluminescence	LED Flat Panel Display	1-50%
Cathodoluminescence	Television Screen	10%

**Table 6 1 Comparison of luminescence types and their efficiencies**

It can be seen here that electroluminescent materials are capable of high efficiencies

### 6.2 1 Host Materials for Luminescence

In order to discuss the materials involved in the luminescence process it is necessary to first look at the physics of the process and see how the host material must achieve the following characteristics For successful and efficient electroluminescence to take place the host material must incorporate

- a) A sufficiently high band gap to minimize absorption
- b) Good high field transport properties
- c) A sufficiently high dielectric strength and,
- d) Have a high probability of radiative decay

This implies that the material should allow electron acceleration to a kinetic energy sufficient for impact excitation The choice of material is limited to wide-gap semiconductors of II-VI compounds, which include IIb-VIb such as ZnS and IIa-VIb compounds such as CaS and SrS ZnS has a band gap of 3.6-3.7 eV<sup>124 125</sup> thus allowing all visible light to pass but restricting the avalanche multiplication of electrons so that they are available for impact excitation Its properties and suitability as a host material are discussed later

## 6 2 2 Mechanisms of Luminescence

In order to produce luminescence there must be a transfer of energy from the accelerated charge to an electron having an energy  $E_1$  in order to promote it to a higher energy state having  $E_k$

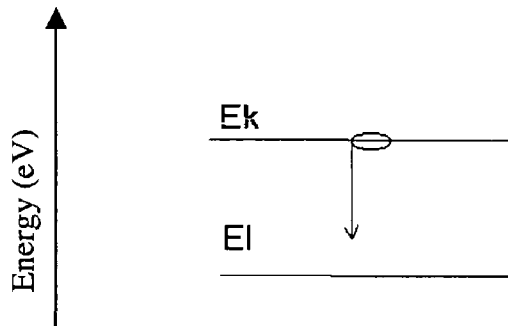


Figure 6 1 Energy level diagram showing the two states,  $E_k$  eV having a higher energy than  $E_1$  eV

Various selection rules govern the transfer of energy exchange between the accelerated particle and the electron at  $E_1$  eV

Once the particle has gained sufficient energy the next stage involves the return of the electron from state k to state l. This can be achieved by either spontaneous or stimulated field emission. This may be a radiative or a non-radiative process. If it is nonradiative the energy of the excited state k is used to excite the vibrations of the surrounding material and therefore heat is generated. The radiative transition is called luminescence and is seen in Fig 6 1. The emission is usually situated at a longer wavelength than the original excitation. This energy difference is called the Stokes Shift. The quantum efficiency  $\eta$  of the luminescence is the ratio of the number of photons emitted to the number of photons absorbed. If there are no competing non-radiative transitions  $\eta=1$  and when  $\eta=0$  there no emission. If there is a neighboring center the excited center may transfer its energy to it. This again may be followed by a radiative or non-radiative decay. Here the non-radiative decay is described as quenching. With materials of larger band gap the radiative transition probability decreases with the possibility of having unwanted non-radiative recombination.



centers in the gap increases. Such mechanisms can most easily be discussed with the aid of the configurational model.

### 6.3 The isolated luminescent centre

#### 6.3.1 Single Configurational Coordinate model

In this section the microscopic structure of the defects responsible for luminescence are investigated. In order to study the theoretical nature of the interaction an understanding of how the Stokes shift depends on the interaction between electronic states of the luminescent center and the vibrational states of the host lattice is needed. Looking at a simple model of the process<sup>126, 127</sup>, consider a dopant ion in a host lattice and assume it shows luminescence. The environment of the dopant ion is not static and only one vibrational mode, the breathing mode is considered. The surrounding ions vibrate about some average positions so the crystal field varies. In order to study the theoretical nature of the interaction an understanding of how the Stokes shift depends on the interaction between electronic states of the luminescent center and the vibrational states of the host lattice is needed.

The mode is assumed to be described by the harmonic oscillator model. The configurational coordinate ( $Q$ ) describes the vibration.  $Q$  represents the distance between the dopant ion and the surrounding ions, that is the  $Mn^{2+}-S^2$  distance. Plotting the energy vs  $Q$  gives the electronic states parabola (harmonic approximation) for the ground state  $g$  and one excited state  $e$  as shown in Figure 6.2.  $Q_0$  represents the equilibrium distance in the ground state and  $Q_0'$  that in the excited state. The parabola offset is given by  $\Delta Q$  and this represents the transition. After the absorption the excited state,  $e$  relaxes to its lowest vibrational level i.e. its equilibrium position giving up its excess energy as heat to the lattice. If the temperature is not low, higher vibrational states may be occupied thermally and broadening of the absorption and emission bands takes place.

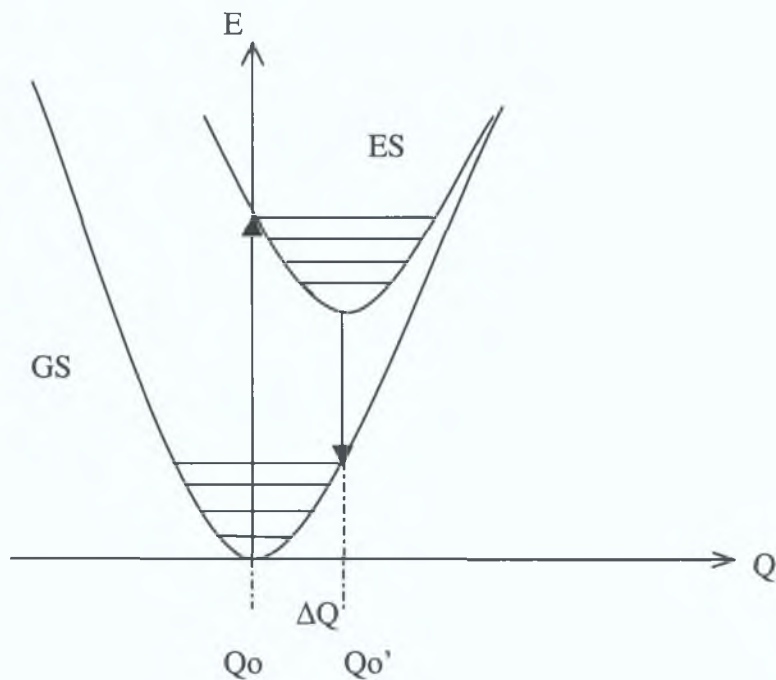


Figure 6.2 Energy diagram showing electronic states GS and ES containing vibrational energy levels that are represented by the horizontal lines. The arrows represent the excitation and emission transitions.

The emission transition takes place at a lower energy usually and is known as the Stokes Shift. Only the zero vibrational transition is expected to occur at the same energy in the absorption and emission spectra. The shape and widths of the bands and the difference between the emission and absorption frequencies is determined by the interaction between the electronic states of the luminescent center and the vibrational states of the host lattice.

In measuring an absorption or emission spectrum the properties of the lines or bands can be summarized as follows:

1. Their spectral position that is the energy at which the transition occurs
2. The shape i.e. line, band etc.
3. The intensity which is determined by in the electronic matrix element  $\langle v(Q)|r|u(Q)\rangle$  where  $r$  represents the electric dipole operator.

In the configurational coordinate model so far all decays from the excited state are assumed to be radiative implying a quantum efficiency (ratio of the number of emitted to absorbed photons) of 100%. Unfortunately nonradiative transitions severely limit this value

## 6.4 Non Radiative processes

Radiationless dissipation of excitation energy can occur by means of many mechanisms. These generally give rise to energy levels in the forbidden gap through which free electrons and holes can be affected with a high transition probability. Local imperfections can act as nonradiative recombination centers and Fig 6.3 shows how phonons can be generated.

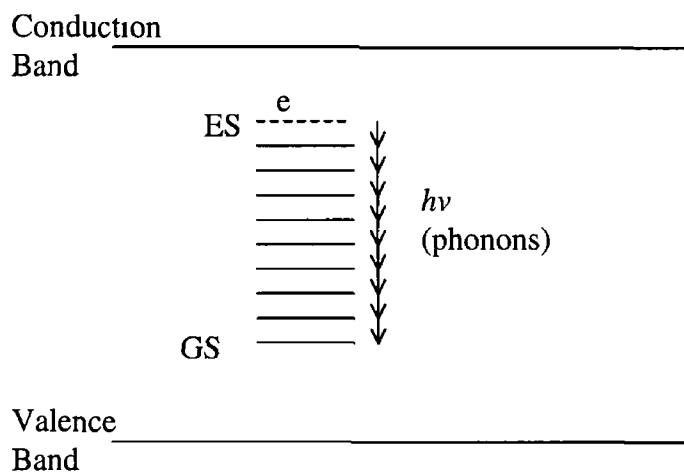


Figure 6.3 Energy band diagram showing how nonradiative decay from the excited state, ES to the ground state, EG can generate phonons

In order to understand how this process occurs the single configurational coordinate model is used to describe the states involved and in Fig 6.3a,b,c three cases are described

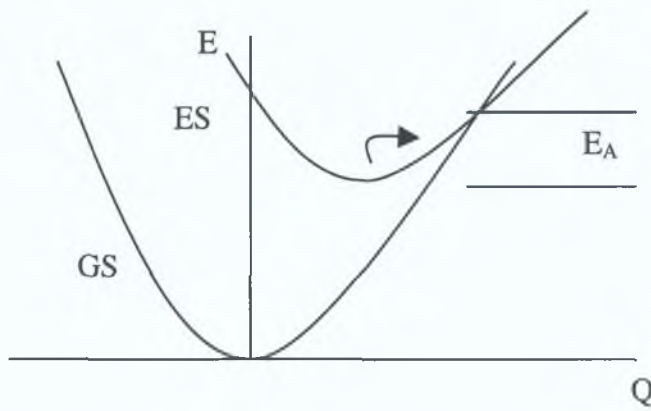


Figure 6.3a Non-radiative transitions in the configurational coordinate diagram for a strong coupling case between the ground state, GS and the excited state, ES of an atom.

Figure. 6.3a looks at the strong coupling case where the absorption and emission transitions are possible but if the relaxed-excited state overlaps with the ground state parabola it is possible to return to the ground state in a non-radiative transition. The excitation energy is given up as heat to the lattice. This is termed thermal quenching. The temperature dependence of the luminescence is governed by the activation energy  $E_A$  for the thermal release of holes to the valence band as shown in Fig. 6.3(a). Energy transport properties transfer the holes ionized by the luminescent centers to deep traps or surface states where radiationless transitions can occur. Defects of this kind are “killer” centers and can be Co, Ni, or Fe in ZnS.

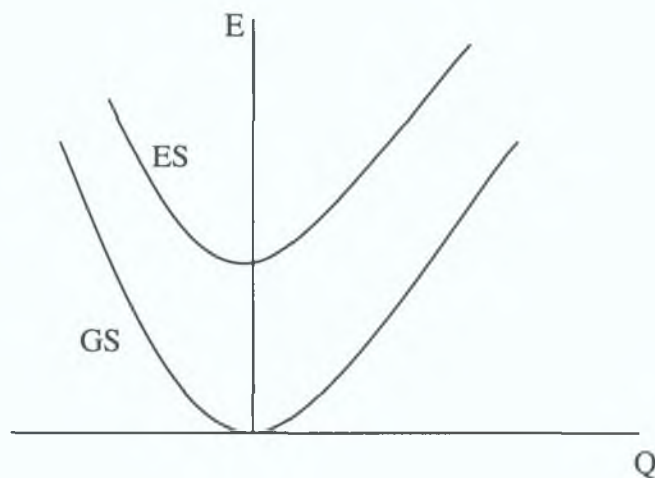
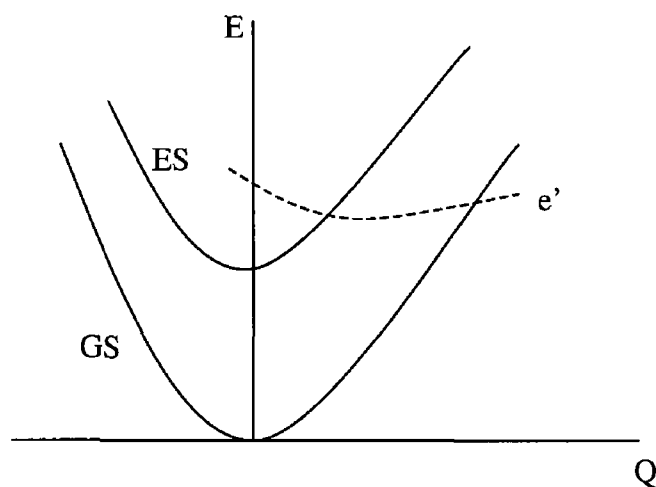


Figure 6.3b Non-radiative transitions in the configurational coordinate diagram for weak coupling

Figure 6 3b looks at the weak coupling case Here the two parabolas never cross but non-radiative transitions are possible if the energy difference  $\Delta E$  is equal to or less than 4-5 times the highest vibrational frequency

Normally this amount of energy can excite a few high-energy vibrations and the energy is lost from the radiative process This non-radiative process is termed multiphonon emission



*Figure 6 3c Nonradiative transitions in the configurational coordinate diagram for a combination of both*

Fig 6 3c is a combination situation where both processes are possible The parallel parabolas are connected by forbidden optical transitions only The third parabola originates from a different configuration and is probably connected to the ground state by an allowed transition Excitation occurs from the ground state to the highest parabola in the allowed transition The system relaxes to the excited state of the second parabola Non-radiative emission between the two upper parabolas happens A line emission now occurs from the second parabola The magnitude of the non-radiative rate is not well understood and cannot be easily calculated with accuracy except for the weak coupling case

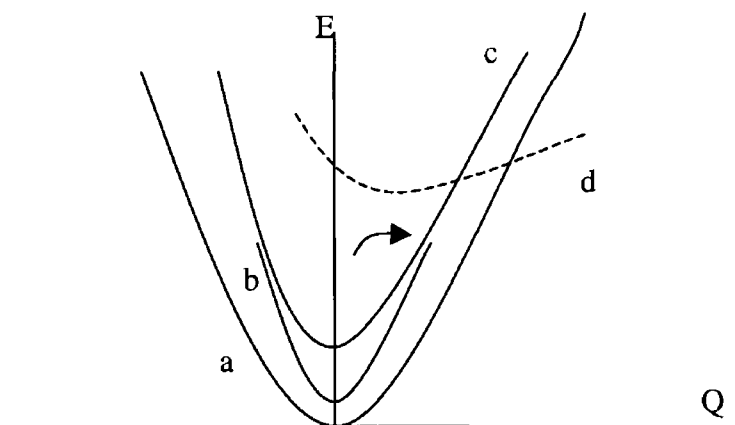


Figure 6.4 Configurational coordinate representation of luminescence quenching by electron transfer

Another method for non-radiative decay is quenching by electron transfer<sup>128</sup> Fig 6.4 shows the energy levels *a*, *b*, *c* of a species A and parabola *d* for species A+B-. The electron transfer from species A to species B obtains this state. The offset of *d* is large and its position is as a medium energy. Therefore from parabola *c* the ground state can be reached by non-radiative transition through *d*. This is mainly seen with ion pair situations<sup>129</sup>

## 6.5 Energy Transfer

If luminescent centers are in close proximity to each other energy may be transferred between the two. The transfer of energy from an excited center to an energy acceptor can be described as energy migration if the energy level structure of the donor and the acceptor match and is controlled by a diffusion process. If there is a mismatch in energy level structures the transfer is known as energy transport. Consider the energy transfer between a donor S and an acceptor or activator A. The process occurs if a suitable interaction exists between both systems exists and when the energy difference between the ground and the excited states of both S and A are equal. This resonance condition can be tested<sup>130</sup> by considering the spectral overlap of the S emission spectrum and the A absorption spectrum, a condition which is essential for transfer to occur. The interaction may be an exchange interaction if there is a wavefunction overlap. Otherwise it may be an electric or magnetic multipolar interaction. The

transfer mechanisms differ from one another in the dependence of the transfer rate on donor-acceptor distance. In the general case where the emission transition  $S^* \rightarrow S$  and the absorption transition  $A \rightarrow A^*$  have line functions  $g_S(E)$  and  $g_A(E)$  respectively. The transfer is brought about by an interaction Hamiltonian  $H_{SA}$  and there is a resulting transfer probability  $P_{SA}$ <sup>131</sup>

Not all of the excitation energy may be transferred. If only part is transferred this is called cross relaxation which is seen in Rare Earth systems and has been considered in detail elsewhere<sup>132</sup>

So far only one step processes have been considered. There could be many transfer steps that would bring the energy far from the original site where the original absorption took place. This is termed energy migration. If the excitation energy is then lost non-radiatively at a quenching site the luminescence efficiency will be low. This form of loss does not occur at low concentrations since the average distance between centers is so large that migration is hampered. Hence this type of loss is termed concentration quenching. Thus, in most cases doping concentrations are therefore limited to the order of 1%. To maintain good crystallinity at these high concentrations the dopant needs to have a high degree of both geometric and valence similarity to the host cation<sup>133</sup>

## 6.6 Luminescence production

Having looked at the various methods by which the luminous efficiency is reduced now methods of luminescence production are discussed here. Luminescence emission can be excited in many ways. Photoluminescence (PL) is excitation by photons, cathodoluminescence (CL) is excitation by cathode rays, electroluminescence (EL) the excitation by electric fields and thermoluminescence (TL) the excitation by the release of energy stored in previously excited solids. Various different processes produce luminescence in semiconductors and these are discussed here. Also the nature of the host and luminescent materials and their interaction are investigated

## 6.6 1 Excitons

When an electron is excited from the valence band to the conduction band an empty electron state is created in the valence band and this behaves like a particle with a positive charge. This 'hole' exerts an attractive force on the electron forming an exciton<sup>134</sup>. They are localized excited electronic states in a nonmetallic crystalline lattice. Two models can be applied to the exciton depending on the degree of localization of the excitation energy. If the energy is localized on one ion in the crystal the Frenkel exciton occurs<sup>135</sup>. In highly covalent materials where the excitation energy extends over several unit cells, the Wannier-Mott<sup>136</sup> exciton is found. This exciton can be regarded as an interacting electron-hole pair with a small binding energy. Excitons can also form complexes by bonding to defects such as donors, acceptors, or dislocations. Since the kinetic energy of the bound exciton complex is zero the optical transitions lead to sharp lines. A broadening of the lines indicates fluctuations originating from crystalline imperfections or impurities. Excitons have been shown to play a role in the excitation of ZnS:Mn<sup>137</sup>.

## 6.6.2 Donor- Acceptor pairs

Pairs of oppositely charged defects in II-VI compounds can provide effective radiative recombination centers for excitons. The system can be described as a ground state having an ionized donor and acceptor with an inter-impurity distance  $R$ , with photoexcitation resulting in a neutral pair in the excited state. These can be described as either

- a) An exciton bound to the ionized donor-acceptor core called fundamental activators or,
- b) A neutral donor and a neutral acceptor perturbed by the interaction with each other called characteristic activators.

These donor and acceptor defects give rise to localized levels near the conduction or valence bands respectively. The free electrons or holes with the opposite carrier trapped at these levels gives rise to the luminescence bands. Many of the known luminescence bands in ZnS can be attributed to association at near neighbour sites of the activator or co-activator impurities with zinc or sulfur vacancies. Four electron-hole recombination mechanisms are shown in Fig. 6.5



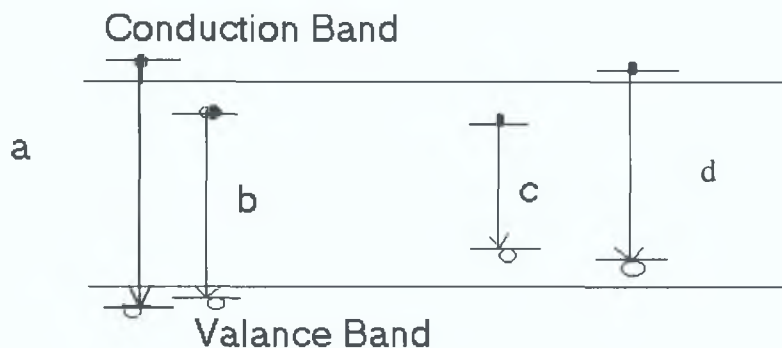


Figure 6.5 Diagram showing the four electron hole recombination mechanisms, a) band to band b) captured electron recombines with a hole in the valence band, i.e. donor site to valence band (Lambe-Klick model); c) donor state to acceptor site recombination (Prener-Apple-Williams model) and d) a conduction electron is captured by an empty center, i.e. conduction band to acceptor state (Schön-Klasens model)<sup>138</sup>

The positions of the recombination states depend on the electronic properties of the solid, which can be described quantum mechanically by Schrödinger's equations. However the optical transitions in the transition metals incorporated into the ZnS lattice are internal ones between the states of the  $3d^n$  configurations.

Since donors and acceptors occupy definite sites within the crystal lattice, lattice statistics can be used to determine the distribution of different pairs with distances  $R_i$ . The recombination transition can be described using effective mass theory as

$$h\nu = E_g - (E_D + E_A) + e^2/\epsilon R \quad (6.6)$$

where  $E_g$  is the bandgap and  $E_D$  and  $E_A$  are the ionization energy of the donor and the acceptor respectively,  $h\nu$  is the photon energy, and  $\epsilon$  is the relative permittivity/dielectric constant.

I	II	III	IV	V	VI	VII
		B	C	N	O	F
		Al	Si	P	S	Cl
Cu	Zn	Ga	Ge	As	Se	Br
Ag	Cd	In	Sn	Sb	Te	I
Au	Hg					

**Table 6.2** The periodic table is shown with the elements relevant to the II-VI compounds.

In Table 6.2 the portion of the periodic table with the elements relevant to the II-VI compounds is shown<sup>139</sup>. Pure stoichiometric ZnS does not itself luminesce. The introduction of lattice defects or the addition of other atoms, which then introduce a deviation from the stoichiometric Zn-S ratio and rearrange the lattice, can cause luminescence. The activator impurities Cu, Ag, and Au when substituted for Zn and Sb when substituted for S behave as acceptor sites and the coactivators Cl, Cr, I at anion sites or Al, Ga, In at cation sites behave as donors.

### 6.6.3 Deep Level Centres

Localized states, having greater depth than the hydrogenic levels in the compounds, can form in the fundamental band gap of semiconductors and are termed deep level centers. The radiative recombination of the electrons and holes at these sites gives rise to luminescence. They originate from intrinsic defects, impurities, or combinations of both. Both rare earth ions and transition metals, in low concentrations (so that they do not interact with each other) in crystals provide deep level luminescence sites. The atomic transitions are localized radiative events that occur between atomic states associated with the luminescent center but the host lattice material also influences them. In the case of the transition metals it is the  $3d^n$  levels,

which are involved in the luminescence. The combination of cation or Zn vacancies and impurities in II-VI compounds lead to the characteristic “self-activated” emission in ZnS and ZnSe. In order to understand the interactions and specifically how the local environment influences the transition energy, the atomic and crystal fields, the lattice symmetry and the ion spacing must be considered.

The study of the zero phonon line fine structure and the shape of phonon-assisted transitions are used to determine the vibration properties of the local ion environment. Broadening of the zero phonon lines is due to inhomogeneous and homogeneous effects. Inhomogeneous broadening is caused by broadband excitation since the activation sites are not identical due to dislocations, strains etc. When a dopant is considered in a solid the emission spectra will show inhomogeneous broadening. Homogeneous broadening is as a result of the finite lifetime of both the initial and final states of the transition.

#### 6.6.4 Host Materials

The structure and the properties of the host material are important in determining the interactions and the efficiency of the luminescence produced. In general the most efficient EL host materials are metal sulfides. Of these materials ZnS is the most commonly used host material.

ZnS can be prepared with either a cubic zincblende (sphalerite or  $\beta$ -ZnS) or hexagonal (wurtzite or  $\alpha$ -ZnS) structure. Both forms of ZnS have regular four-coordination of zinc and sulfur, but differ by the arrangement of the second nearest neighbour. The wurtzite configuration consists of two interpenetrating hexagonal close-packed lattices, one containing anions, and the other cations. Several natural occurring polymorphs are known. The sulfur atoms in zincblende are cubic close packed and those in wurtzite are hexagonal close packed, in both cases zinc occupied half the tetrahedral sites. Since the arrangement of nearest neighbors is nearly identical, and interatomic distances are comparable in both structures, the local environment and chemical bonding is nearly identical. The differences in the bands arise from the difference in the crystal field and from the difference in the Brillouin zones. The Brillouin zone of the fcc (zincblende) lattices and the wurtzite lattice are shown in Fig 6.6a & Fig 6.6b respectively.<sup>140 141</sup> The crystalline variations can be distinguished using optical microscopy with polarized light as the hexagonal crystals

are birefringent and the cubic crystals are not. The effect this has on the observed luminescence from the materials is that the emission peak of the cubic crystals is shifted to a slightly longer wavelength due to the smaller energy band-gap for this form.

ZnS has a dielectric breakdown strength of about  $1 \text{ MVcm}^{-1}$ , which allows the electrons to reach high enough energies to facilitate excitation of luminescent centers. Its bandgap ( $\sim 3.6 \text{ eV}$ ) makes it transparent to visible light so optical absorption in the visible spectrum is minimal. The density of interface states dictates the total current transported in the device. ZnS has a high density of interface states and these are sufficiently deep ( $1.0\text{--}1.3 \text{ eV}$ ) for the thermally assisted electron tunneling process. The band structure for hexagonal ZnS is shown in Fig. 6.7<sup>142, 143, 144</sup>. It is a direct gap semiconductor with both the conduction band bottom and the valence band top at  $\Gamma$  point and the energy gap is given by  $\Gamma_{15} - \Gamma_1$ . The outermost s-electron states of the metallic and the p-electron states of the nonmetallic constituent generate the upper valence band, while the lower valence band ( $L_1 - \Gamma_1 - X_1$ ) is attributed to the anion s-electron states. The level bands containing the representations  $\Gamma_{15}$  and  $\Gamma_{12}$  in the region of the valence band belong to the 3d electrons of Zn. The energy of the 3d electrons of the free Zn atom is about  $3.7 \text{ eV}$  higher than that of the free S atom.

### 6.6.5 Luminescent centres

Transition metal ions such as Mn (yellow-orange), and rare earth ions such as Tb (green), Sm (red), Eu (red), Ce (blue-green) and Pr (white) are suitable luminescence centers<sup>145</sup>. For transition metal ions, d-d intrashell transitions occur and in rare earth (lanthanide) ions both 4f-5d intershell and 4f-4f intrashell transitions produce luminescence. In the rare earth ions, the outer electrons in the 4f shell are screened by the  $5s^2 5p^6$  closed shells and therefore these ions in host materials are not greatly influenced by crystal fields. Consequently external fields can have a significant effect on their energy level position. To effectively dope a host the chemical properties and ionic radii between the cations of the host phosphor and the luminescent centers must be matched.

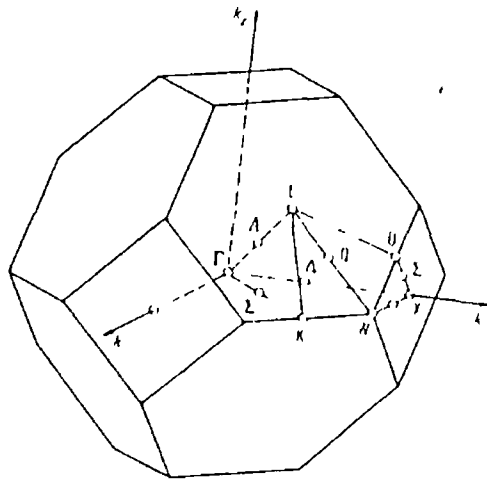


Figure 6 6a Brillouin zone of the f c c and zincblende lattice

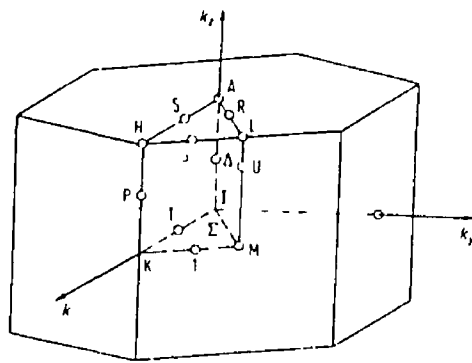


Figure 6 6b Brillouin zone of wurtzite lattice

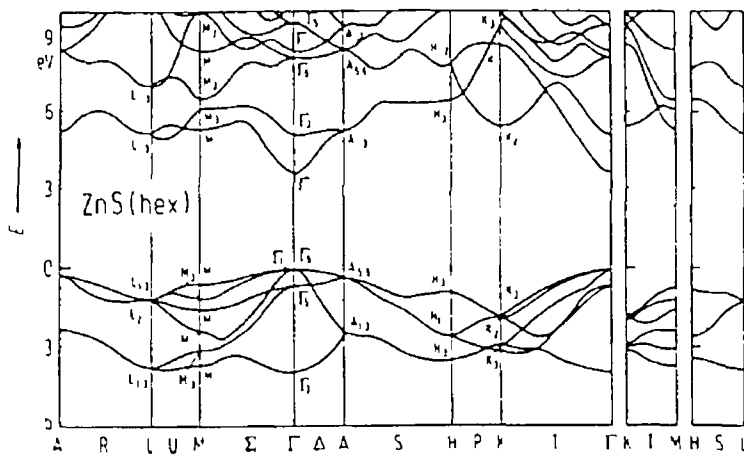


Figure 6 7 Band structure diagram of hexagonal ZnS

Ion	Radius (Å)	Ion	Radius (Å)	Ion	Radius (Å)
Zn <sup>2+</sup>	0.74	Ce <sup>3+</sup>	1.034	Gd <sup>3+</sup>	0.938
Ca <sup>2+</sup>	0.99	Pr <sup>3+</sup>	1.013	Tb <sup>3+</sup>	0.923
Sr <sup>2+</sup>	1.13	Nd <sup>3+</sup>	0.995	Dy <sup>3+</sup>	0.908
Mn <sup>2+</sup>	0.80	Sm <sup>3+</sup>	0.964	Ho <sup>3+</sup>	0.894
		Eu <sup>3+</sup>	0.950	Er <sup>3+</sup>	0.881
		Eu <sup>3+</sup>	1.09	Tm <sup>3+</sup>	0.869

**Table 6.3 Radii of common host and luminescent materials.**

The ionic radii and the electronic configurations of host materials and luminescent centers are shown in Table 6.3 and Table 6.4<sup>146,147</sup>. For ZnS as a host, Mn is an ideal center, as the rare earth ions have a valence of +3 and are larger than the Zn and therefore they are not easily incorporated into the ZnS lattice.

#### 6.6.5.1 Mn in ZnS.

ZnS:Mn, with a luminance of 300 cdm<sup>-2</sup> and an efficiency of 5 LW<sup>-1</sup><sup>148</sup> is the brightest and most efficient ACTFEL phosphor. When Mn is present in ZnS as an activator it directly substitutes an Mn<sup>2+</sup> for a Zn<sup>2+</sup><sup>149</sup>. It is clear from the electron configuration shown in Fig 6.4 that the 3d orbitals in the Mn<sup>2+</sup> ion are not shielded from the host lattice by any occupied orbitals.

Atom	Ion	Electron Configuration
Zinc (Zn)	Zn <sup>2+</sup>	1s <sup>2</sup> 2s <sup>2</sup> 2p <sup>6</sup> 3s <sup>2</sup> 3p <sup>6</sup> 3d <sup>10</sup> 4s <sup>2</sup>
Gallium (Ga)	Ga <sup>3+</sup>	1s <sup>2</sup> 2s <sup>2</sup> 2p <sup>6</sup> 3s <sup>2</sup> 3p <sup>6</sup> 3d <sup>10</sup> 4s <sup>2</sup> 4p <sup>1</sup>
Calcium (Ca)	Ca <sup>2+</sup>	1s <sup>2</sup> 2s <sup>2</sup> 2p <sup>6</sup> 3s <sup>2</sup> 3p <sup>6</sup> 4s <sup>2</sup>
Strontium (Sr)	Sr <sup>2+</sup>	1s <sup>2</sup> 2s <sup>2</sup> 2p <sup>6</sup> 3s <sup>2</sup> 3p <sup>6</sup> 3d <sup>10</sup> 4s <sup>2</sup> 4p <sup>6</sup> 5s <sup>2</sup>
Oxygen (O)	O <sup>2-</sup>	1s <sup>2</sup> 2s <sup>2</sup> 2p <sup>4</sup>
Sulfur (S)	S <sup>2-</sup>	1s <sup>2</sup> 2s <sup>2</sup> 2p <sup>6</sup> 3s <sup>2</sup> 3p <sup>4</sup>

Manganese (Mn)	Mn <sup>2+</sup>	1s <sup>2</sup> 2s <sup>2</sup> 2p <sup>6</sup> 3s <sup>2</sup> 3p <sup>6</sup> 3d <sup>5</sup> 4s <sup>2</sup>
Cerium (Ce)	Ce <sup>3+</sup>	1s <sup>2</sup> 2s <sup>2</sup> 2p <sup>6</sup> 3s <sup>2</sup> 3p <sup>6</sup> 3d <sup>10</sup> 4s <sup>2</sup> 4p <sup>6</sup> 4f <sup>2</sup> 5s <sup>2</sup> 5p <sup>6</sup> 6s <sup>2</sup>
Europium (Eu)	Eu <sup>2+</sup>	1s <sup>2</sup> 2s <sup>2</sup> 2p <sup>6</sup> 3s <sup>2</sup> 3p <sup>6</sup> 3d <sup>10</sup> 4s <sup>2</sup> 4p <sup>6</sup> 4f <sup>7</sup> 5s <sup>2</sup> 5p <sup>6</sup> 6s <sup>2</sup>
Terbium (Tb)	Tb <sup>3+</sup>	1s <sup>2</sup> 2s <sup>2</sup> 2p <sup>6</sup> 3s <sup>2</sup> 3p <sup>6</sup> 3d <sup>10</sup> 4s <sup>2</sup> 4p <sup>6</sup> 4f <sup>9</sup> 5s <sup>2</sup> 5p <sup>6</sup> 6s <sup>2</sup>

**Table 6.4 Electron configurations for common electroluminescent hosts and luminescent centers**

Mn possesses deep lying levels, which can be described approximately by the states of the free divalent ion. Surrounded by the host matrix, normal orbital distributions are perturbed and new energy states are produced. The orbital interactions create lower energy bonding states and higher energy anti-bonding states through hybridization.

Fig. 6.8 shows the energy levels for the free Mn<sup>2+</sup> (3d) ion and the Mn<sup>2+</sup> in the ZnS host lattice. The electron configuration of Mn in Table 6.4 shows that the 3d orbitals are not shielded from the host lattice by any occupied orbitals.

The host lattice can therefore be modified to change the energy difference between the ground and the excited states. The Mn<sup>2+</sup> ion 3d<sup>5</sup> configuration has a spherically symmetrical <sup>6</sup>S ground electronic state in which all the 3d electron spins are in parallel. The state configuration is shown in Fig. 6.9. In the low lying excited states one of the electron spins is reversed giving rise to the series of quartet levels <sup>4</sup>G, <sup>4</sup>P, <sup>4</sup>D, <sup>4</sup>F. The excited configuration 3d<sup>5</sup>4s lies 7eV above the ground configuration and is not involved in any of the observed absorption and emission bands<sup>150</sup>

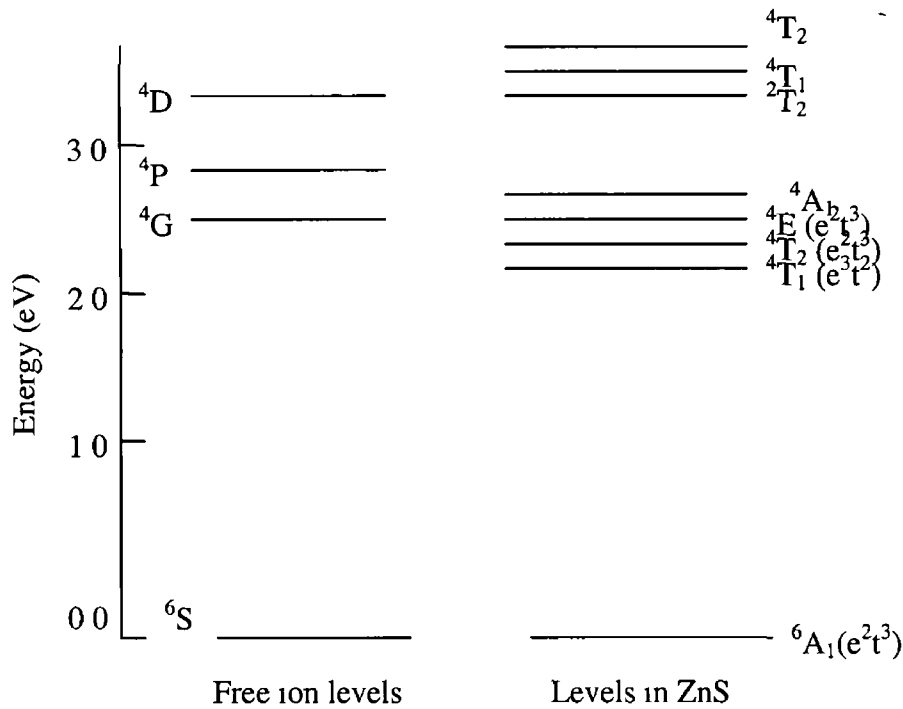


Figure 6.8 The energy levels for the free  $Mn^{2+}$  ( $3d$ ) ion and the  $Mn^{2+}$  in the ZnS host lattice

The transition responsible for the broad ZnS Mn emission involves states with the  $3d^5$  electronic configuration. The ground state is the  ${}^6S$  ( ${}^6A_1$ ) state, the excited state may be approximated by the  ${}^4G$  ( ${}^4T_1$ ) state although the significance of the angular momentum quantum number of the free ion is reduced due to coupling of the angular momentum of the free ion with the crystal field<sup>151</sup>. The Mn activator is excited by resonance interaction with other previously excited impurity systems. The luminescence transition fits well with the configurational model shown in Fig. 6.2. The excited state responsible for emission is only 2.12 eV above the ground state. The activator system in ZnS Mn is stable against field ionization in applied fields as great as  $10^7 \text{ V cm}^{-1}$ .



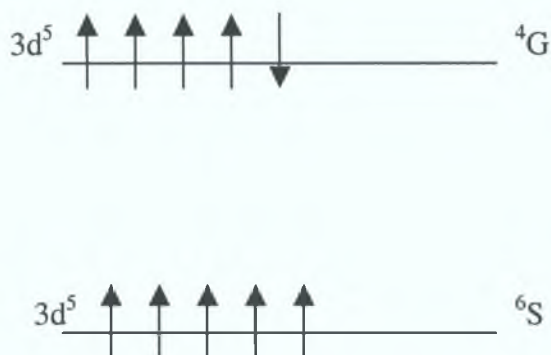


Figure 6.9 The transition state configurations for  ${}^4G$ - ${}^6S$  in the  $\text{Mn}^{2+}$  ion

$\text{Mn}^{2+}$  produces one characteristic broadband emission with the peak centered at  $\sim 585\text{nm}$ . Modes of excitation or the presence of coactivators have little effect on the emission spectrum of  $\text{Mn}^{2+}$  centers. This broad band is due to longitudinal (LO and LA) and transverse optical and acoustic (TO and TA) phonons, which are not resolvable at room temperature but can be detected at low temperatures. These phonon replicas arise because there is strong coupling between the Mn  $3d$  orbitals and the ZnS lattice. Mn is very soluble in ZnS but it does not change the electrical properties of the host lattice significantly even at several percent concentration because the Zn and the Mn ions are isovalent<sup>152</sup>. The quantum efficiency increases with increasing concentrations of Mn and then levels off at  $\sim 0.8\text{mol}\%$ <sup>153,154</sup>. With concentrations of Mn greater than  $1\text{mol}\%$  the luminescence decreases due to concentration quenching<sup>155</sup>. This saturation effect places limits on achieving high brightness. At high concentrations three additional emission bands have been observed<sup>156</sup>. Since the luminescence centers are in close proximity to each other the emission from the de-exciting centers is absorbed by those ions or “traps” in the ground state. However the decay time for this high concentration emission is greater than that expected for Mn-Mn pairs<sup>157</sup>. Energy migration may take place and the excited Mn center can lose its energy through a resonant non-radiative transfer process in the form of a red or infrared non-radiative center<sup>158</sup>. Mathematical models for the problem of concentration quenching have been setup and these are the diffusion model and the hopping model<sup>159,160,161</sup>. The diffusion model assumes that radiationless energy transfer takes place via Mn clusters or pairs that form. The

hopping model treats the energy transfer as a percolation. Therefore the energy loss is proportional to the probability of finding an energy sink near the excitation path. Studies have shown that the concentration can be increased to 3mol% if particular deposition techniques are used<sup>162</sup>. Also a  $Zn_{1-x}Mg_xS:Mn$  phosphor has been developed in which the Mn 3d levels, involved in the traditional emission, are caused to move farther apart which increases transition energy and has resulted in a peak shift to 550nm<sup>163</sup>. Incorporating CdS(Se) with ZnS and Mn in the form ZnS-CdS(Se):Mn produces emission in the range 600-680nm<sup>164</sup>.

## 6.7 Production of zinc sulphide thin films

ZnS:Mn is used as a luminescent material in a variety of devices<sup>165</sup>. It can be deposited using various deposition methods including sputtering<sup>166,167,168</sup>, electron beam evaporation<sup>169,170</sup>, multi-source deposition<sup>171</sup>, metal-organic deposition<sup>172</sup> and atomic layer epitaxy<sup>173</sup>. The doped zinc sulphide thin films are produced in this study from sol-gel produced doped zinc oxide films that are sulphidised in an atmosphere containing hydrogen sulphide ( $H_2S$ ). The conversion of zinc oxide into zinc sulphide is diffusion controlled rather than rate controlled. The mathematics of the process is discussed and the diffusion coefficient for the conversion calculated. The procedure involved in the production of both doped and undoped zinc sulphide from sol-gel produced zinc oxide thin films is also described.

### 6.7.1 Diffusion Process

Diffusion can be defined as the migration of an atomic or molecular species within a given matrix under the influence of a concentration gradient<sup>174</sup>.

From an atomic perspective diffusion is a migration from lattice site to an adjacent lattice site. In order for diffusion to take place two conditions must be fulfilled:

- i) the adjacent site must be vacant and
- ii) the atom must have sufficient vibrational energy to move.

This movement involves the breaking of the existing bonds and the distortion of the lattice during the movement. At low temperatures some of the atoms have sufficient energy by virtue of their vibrational energies. As the temperature is increased this

fraction increases and the extent of the observable diffusion effects depends on the diffusion coefficient  $D$ .  $D$  increases exponentially with temperature, according to the Maxwell-Boltzmann relation

$$D = D_0 \exp\left(\frac{-E_D}{RT}\right) \quad (6.7)$$

where  $D_0$  is a constant and  $E_D$  is the activation energy. There are three broad types of diffusion which are now considered separately.

### 6.7.1.1 Vacancy Diffusion

At equilibrium a crystal will contain a certain number of vacancies. Vacancy diffusion involves the movement of an atom from one lattice site to an adjacent one that is vacant. It necessitates the presence of vacancies and this is a function of the number of defects present. The higher the temperature the larger the fraction of defects and vacancies present.

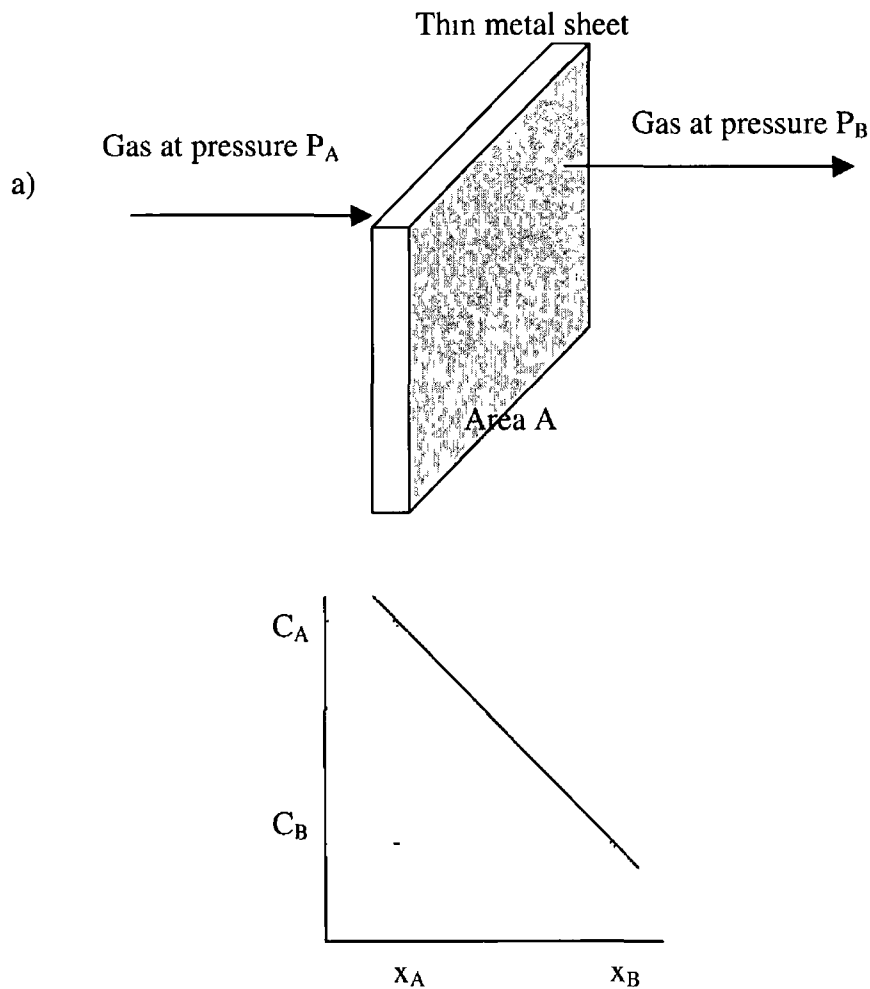
### 6.7.1.2 Interstitial Diffusion

In this process atoms migrate from one interstitial position to a neighbouring vacant interstitial site. Generally the atom needs to be small enough to fit into the interstitial positions. In a dilute interstitial solution empty interstitial sites normally surround a diffusing atom so it does not have to wait for a vacancy. Since there is less room at an interstitial site it is favoured by small atoms in open lattices. Therefore this mechanism can be found in the diffusion of impurities such as hydrogen, carbon, nitrogen and oxygen.

If the atom is not very small then diffusion is more likely to occur in a two-step process. Therefore generally this type of diffusion can take place in a crystal region where there is one more atom than lattice site. In this situation where an extra atom in one row compared to the adjacent rows in a crystal structure or 'crowdion' exists its movement in the lattice is similar to that of an edge dislocation.

### 6 7 1 3 Steady State Diffusion

Diffusion is a time dependent process This leads to determining the rate of mass transfer as the diffusion flux,  $J$



b)

*Figure 6 10 Diagram showing a) a thin metal plate having the pressure of the diffusing species on both surfaces held constant and b) the associated concentration profile*

It is defined as the mass,  $M$  diffusing through and perpendicular to a unit cross-sectional area of solid per unit time

$$J = \frac{M}{At} \quad (6.8)$$

or in differential form

$$J = \frac{1}{A} \frac{dM}{dT} \quad (6.9)$$

A steady state condition exists if the diffusion flux does not change with time. Consider an example of gas atoms diffusing through a metal plate for which the concentration of the diffusing species on both surfaces of the plate is held constant as shown in Fig 6.10.

When the concentration (C) is plotted against position or distance within the solid (x), the resulting curve is called a concentration profile and the slope of the curve is the concentration gradient. If this is assumed to be linear then

$$\frac{\Delta C}{\Delta x} = \frac{C_A - C_B}{x_A - x_B} \quad (6.10)$$

This gives a flux that is proportional to the gradient. This can be summarized as Fick's First Law. Here

$$J = -D \frac{dC}{dx} \quad (6.11)$$

where the mass flux (J), is a function of the variation of the concentration (C), with distance (x) and dependent on the diffusion coefficient (D).

#### 6.7.1.4 Non steady state Diffusion

In most cases the diffusion is not steady state. Fick's first law is still valid but its form needs to be altered. There is normally a flux or concentration gradient at some point in the solid that varies with time. This results in a net accumulation or depletion of the diffusing species. This concentration gradient over time is equal to the flux gradient. Thus, if D is not a function of position,

$$\frac{\partial C}{\partial t} = \frac{\partial \left( \frac{D \partial C}{\partial x} \right)}{\partial x} \quad (6.11)$$

and this gives

$$\frac{\partial C}{\partial t} = D \frac{\partial^2 C}{\partial x^2} \quad (6.12)$$

which is known as Fick's Second Law. In three dimensions using vector notation gives

$$\frac{\partial C}{\partial t} = -\nabla J \quad (6.13)$$

This equation is known as the continuity equation. Solutions to these equations are possible where physically meaningful boundary conditions are specified<sup>175</sup>. This is the basis for most of the diffusion measurements in solids in general. When the diffusion distance is short compared to the relative dimensions of the initial inhomogeneity, the concentration term can be most simply expressed in terms of the error function. One such solution can be defined for the case of a species diffusing in a thin film.

#### 6.7.1.5 Thin Film Solution

Consider the indiffusion of a solute into an initially undoped film with the surface concentration kept at  $C_0$  as shown in Fig. 6.11. Outdiffusion from an initially homogeneously doped sample can also be dealt with in the same way. Assuming that a solution to Fick's law exists, the concentration is a product of two functions, one that is time dependent only and one that depends only on distance giving<sup>176</sup>

$$C = X(x) \cdot T(t) \quad (6.14)$$

As complete homogenisation is approached  $C(x,t)$  can be represented by the first few terms of an infinite trigonometric series<sup>177</sup>.

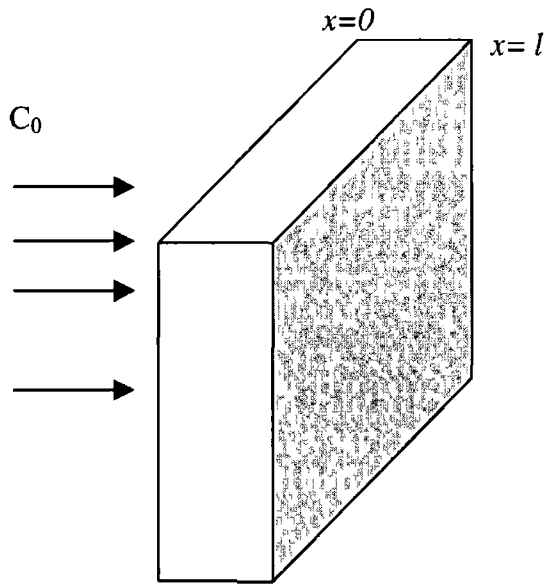


Figure 6 11 Thin film showing the surface concentration of the diffusant set at  $C_0$  throughout the time period for a film thickness  $l$

In the case of a thin film diffusion takes place from one side of the thin specimen. In this case the diffusing material enters only at the face  $x=0$  and can only penetrate a distance  $x=l$ . As the film is initially undoped the surface concentration is the initial concentration  $C=0$ . The concentration of the diffusant is maintained at  $C=C_0$  throughout the annealing time period.

The problem of indiffusion is defined by the following conditions

$$C = C_0 \text{ at } x=0 \text{ and } x = l \text{ for } t > 0$$

$$C = 0 \text{ in the range } 0 < x < l \text{ at } t = 0$$

The concentration of the solute at a time  $t$  will be given by

$$C(x,t) = \frac{lc_0}{2\sqrt{\pi Dt}} \exp\left(\frac{-x^2}{4Dt}\right) \quad (6 15)$$

in regions where  $\sqrt{Dt} > l$  since extra terms need to be applied if this criteria is not met<sup>178</sup>

$$J = -D \frac{\partial C}{\partial x} = 0 \text{ at } x=l \quad (6 16)$$

This from of the equation works well in situations where the source of the diffusant can be described as having a Fermi-Dirac delta distribution<sup>179</sup> However normally it is not possible to obtain a Dirac delta function to describe the diffusant distribution Therefore when the initial diffusant has a thickness h, that is of the order of the diffusion distance ( $\sqrt{Dt}$ ), the initial source conditions can be given as follows

$$C = C_0 \text{ for } t = 0 \text{ and } h \geq x \geq 0$$

and

$$C = 0 \text{ for } x > h$$

For  $t > 0$

the boundary condition is

$$\frac{\partial C}{\partial x}(0,t) = 0 \tag{6 17}$$

This gives the solution of for the variation of concentration with time as<sup>180</sup>

$$C(x,t) = \frac{C_0}{2} \left[ \operatorname{erf} \left( \frac{h-x}{2\sqrt{Dt}} \right) - \operatorname{erf} \left( \frac{h+x}{2\sqrt{Dt}} \right) \right] \tag{6 18}$$

If a diffusion couple is formed where  $C_0$  and  $C_1$  are the initial uniform concentrations or the diffusing species the boundary conditions for the initial conditions at the interface when  $x = 0$  and  $t = 0$  are

$$C(x,0) = C_1 \text{ for } x < 0 \text{ and}$$

$$C(x,0) = C_0 \text{ for } x > 0$$

The solution to the above equation 6 18 is then given by

$$\left( \frac{C(x,t) - C_0}{C_1 - C_0} \right) = \frac{1}{2} \left[ \operatorname{erf} \left( \frac{x}{2\sqrt{Dt}} \right) \right] \tag{6 19}$$

The solution to Eq 6 19 is based on a constant D In a situation where the diffusion coefficient varies with concentration,  $D(C)$  it is difficult to find a solution<sup>181</sup>



Boltzmann<sup>182</sup> developed this procedure for cases where D is a function of C only. Then C may be expressed in terms of a variable,  $\eta = x/2t^{1/2}$ . In order to determine D at a known composition, Boltzmann- Matano<sup>183</sup> analysis is used<sup>184, 185</sup>. In the situation where the source of the diffusant is infinite, the concentration at the surface immediately achieves the solubility  $C_0$  and remains at this value throughout the experiment. Considering that the material also being infinite, extending from  $x = 0$  to  $x = \infty$ , the solution to equation 6.19 is

$$C(x,t) = C_0 \operatorname{erfc} \frac{x}{2\sqrt{Dt}} \quad (6.20)$$

This can be used to calculate the total mass of the diffusant<sup>186</sup>. Also, rearranging

$$\frac{C(x,t)}{C_0} = \operatorname{erfc} \left( \frac{x}{2\sqrt{Dt}} \right) \quad (6.21)$$

If

$$\frac{C(x,t)}{C_0} = 0.5 \quad (6.22)$$

then, plotting the experimental profile points on probability paper as  $(C/C_0 \times 50)$  against  $(x/t)^{1/2}$  produces a straight line, the diffusion coefficient is assumed to be constant. This is plotted on probability paper to minimize errors that arise. Probability paper is graph paper that produces a straight line when the error function is plotted on it. Thus the profile is an error function complement. At each end of the plot the error in the calculated  $D(C)$  is at a maximum since this is where  $C/C_0$  approached one or zero. Then combining Equations 6.21 and 6.22 gives

$$\frac{x}{\sqrt{Dt}} = 0.96 \quad (6.23)$$

and therefore

$$D = \left( \frac{x^2}{t} \right) 1.08 \quad (6.24)$$

Thus, from Eq 6.24,  $D$  can be calculated from the graph of  $x^2$  vs  $t$

### 6.7.2 Conversion of zinc oxide thin films

Zinc oxide films were prepared using a dip coating method. Dissolving 6 wt % zinc acetate 2-hydrate in anhydrous ethanol by heating to 80°C while stirring and refluxing produced the ZnO precursor solution. The solution was cooled quickly to prevent the zinc acetate from crystallising out of the solution. The precursor was hydrolysed using two mols H<sub>2</sub>O per mol zinc acetate. This was achieved by forming a 10 vol% H<sub>2</sub>O solution in ethanol and adding the correct amount dropwise to the precursor. Lactic acid was added to the solution from a 5 vol% in ethanol solution. The solution was clear and colourless thereby ensuring that the zinc acetate had dissolved in the ethanol.

The substrates used were both glass slides and silicon wafers. The coating procedure was then carried out at a dipping speed of 0.2 cm s<sup>-1</sup>. After coating the substrate was dried in normal atmosphere at a temperature of 240°C for 10 minutes. The substrate was then recoated to obtain thicker coatings. Final annealing took place when the desired thickness was achieved. The film shrinks during the heating process. This had to be taken into account when the number of coating runs was estimating the thickness. The ZnO films were annealed at 700°C. Poor adhesion may result if the deposited film is too thick. In order to produce ZnS films, the ZnO films were heated by infrared radiation in a sulphidising atmosphere containing a gas mix of N<sub>2</sub>, H<sub>2</sub>, H<sub>2</sub>S of 9 : 1 : 10 at a pressure of 930 Pa at temperatures up to 560°C to promote exchange between the oxygen and sulphur atoms.

Elemental depth analysis was carried out by secondary neutral mass spectrometry (SNMS).

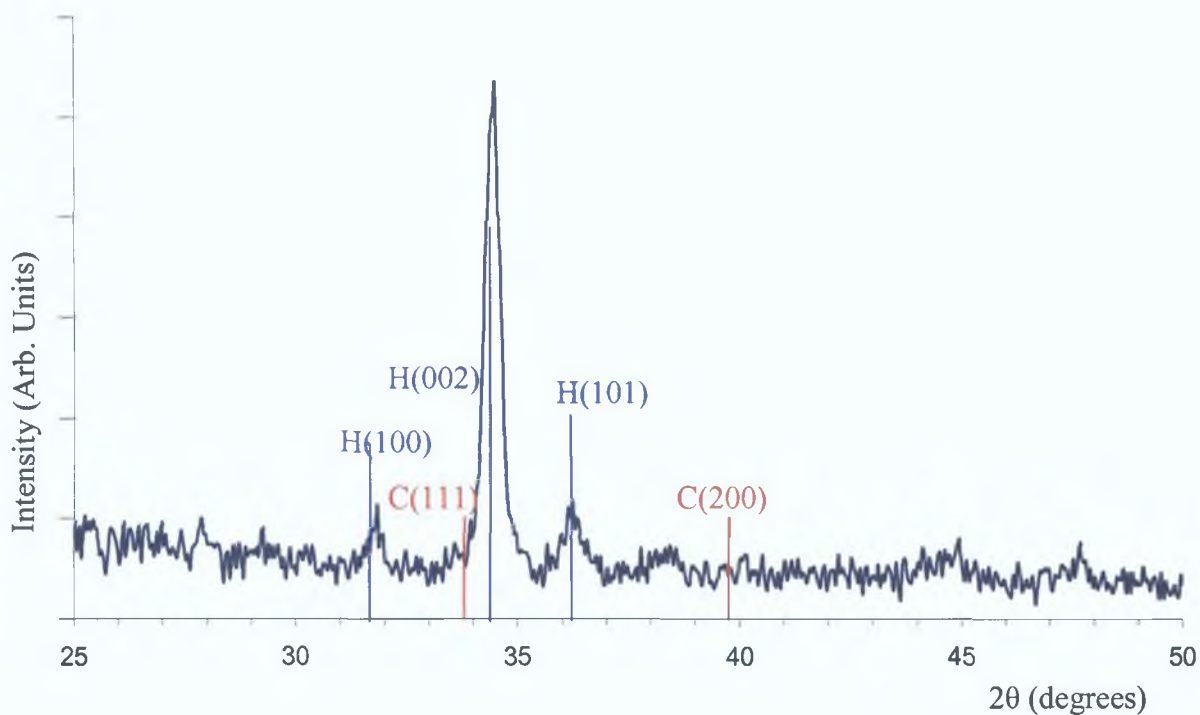


Figure 6.12 XRD profile of sol-gel deposited ZnO film including the corresponding positions for the hexagonal peaks in blue and the cubic peaks in red<sup>187</sup>.

The film thickness of ZnO obtained after one dip coating and annealing was 40nm. Thicker films were obtained *pro rata*. XRD of the zinc oxide films shows that the as deposited films are amorphous, however, after annealing at 700°C in air the films become crystalline with the hexagonal structure. The presence of three peaks at  $2\theta=31.75$  (100), 34.44 (002) and 36.25 (101) shows that the ZnO films have a hexagonal structure<sup>187</sup> as shown in Fig. 6.12.

From the relative intensities it can be seen that there is a strong preferential orientation with the c-axis perpendicular to the substrate surface. The normal stable state of ZnO is the cubic, zincblende structure, however here the metastable hexagonal structure is obtained. This form is obtained whether bare or oxidized silicon is used as the substrate, therefore it is not caused by the influence of the silicon lattice.

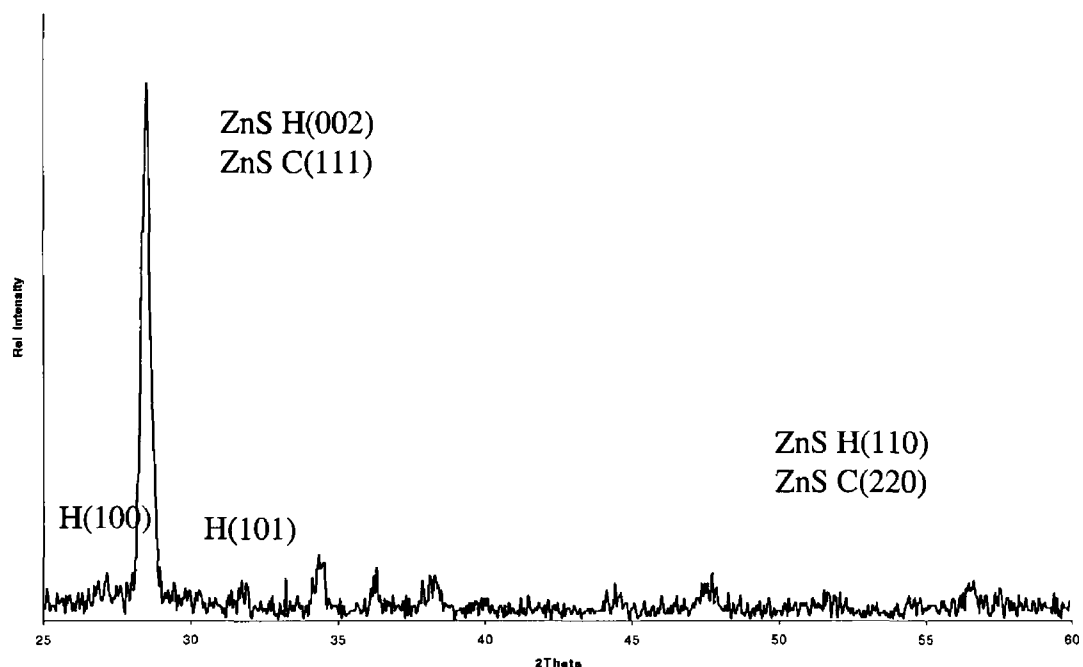


Figure 6 13 XRD profile of ZnS

The XRD structure of ZnS is shown in Fig 6 13. The presence of the two peaks at  $2\theta = 28^\circ$  and  $47^\circ$  shows that the ZnS and ZnS Mn films have overlapping contribution from the cubic phase having planes (111) at  $28.56^\circ$  and (220) at  $47.51^\circ$ <sup>188</sup>, and the hexagonal phase having planes (002) at  $28.49^\circ$  and (110) at  $47.54^\circ$  respectively. The additional peaks due to hexagonal ZnS for planes (100) and (101) are found at  $26.9^\circ$  and  $30.5^\circ$ <sup>189</sup>. After annealing in an atmosphere containing hydrogen sulphide, the XRD measurements as shown in Fig 6 14, show that the oxide is gradually converted to sulphide as the anneal time is increased. It can be seen that almost total conversion to ZnS takes place over longer annealing times.

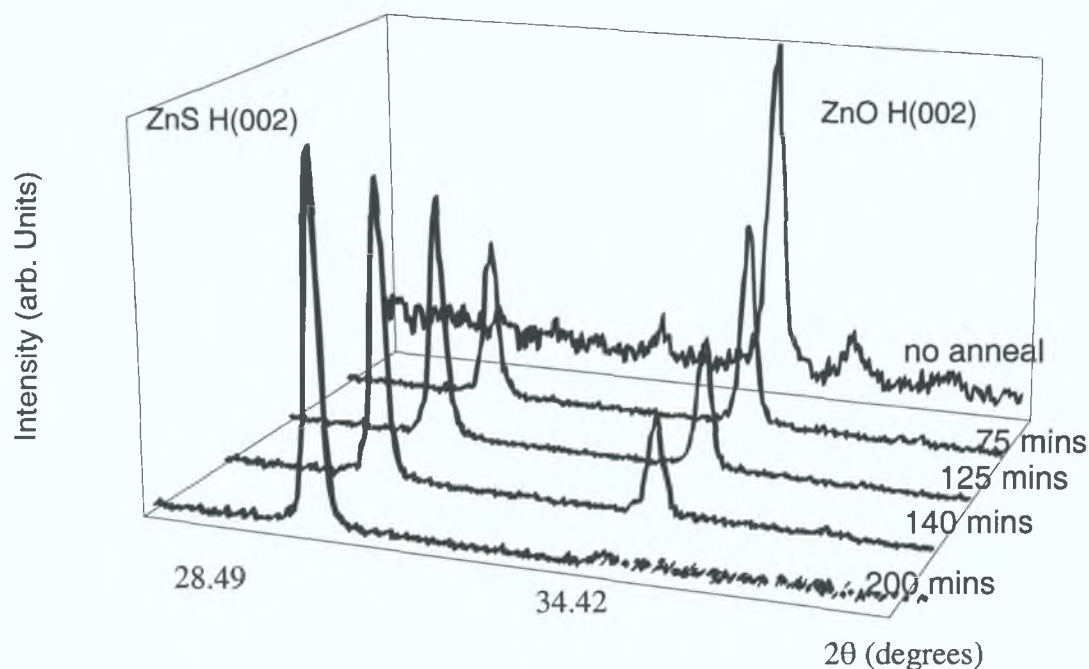


Figure 6.14 Normalized XRD spectra from the films at different stages of the sulphidation process.

In order to obtain the optimum sulphidation conditions the kinetics of the transformation between oxide and sulphide was studied. This was done in two ways: (i) the oxygen and sulphur content of the films was measured by SNMS profiling and (ii) the overall ZnO/ZnS ratio was estimated by measuring the relative peak heights of the XRD diffraction from each lattice. The depth to which the sulphur penetrated at a given temperature was approximated from the XRD spectra assuming that the depth of the point of transition from oxide to sulphide could be estimated from the relative heights of the ZnO and ZnS peaks and the total film thickness. Each method gave similar results. According to the SNMS profiles, the sum of the O and S contents was constant giving overall stoichiometry for the  $ZnS_xO_{1-x}$  material. The depth to which the sulphur penetrated at a given temperature was approximated by the point at which the O and S contents were equal, i.e. if the sulphur concentration was greater than the oxygen concentration, the material was assumed to be ZnS and if  $S < O$  it was assumed

to be ZnO. The surface concentration of sulphur should be constant therefore the sulphur profile should be described by a complementary error function

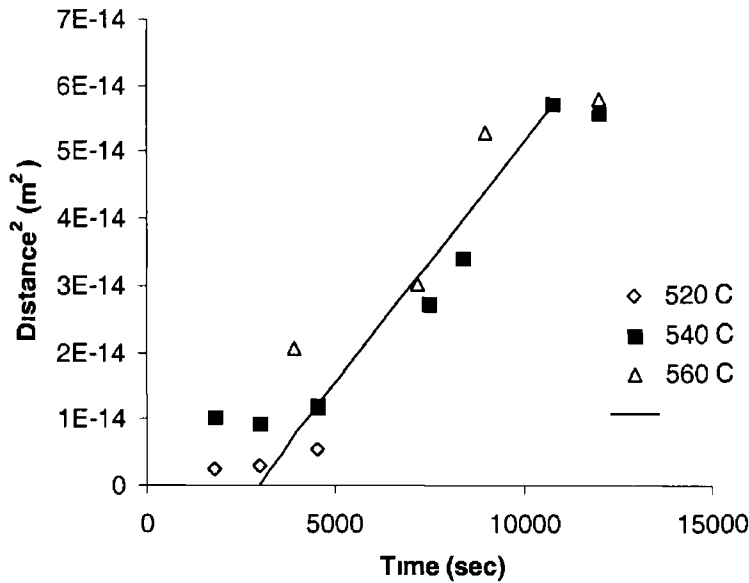


Figure 6.15 Graph of (diffusion depth)<sup>2</sup> vs time for 520 °C, 540 °C and 560 °C sulphidation temperature. The solid line shows an approximation of the linear section of the 540 °C curve.

Therefore if the point at which the bulk concentration is a fixed fraction i.e. 50% of the surface concentration is taken as the point to which indiffusion of sulphur has progressed, a plot of (diffusion depth)<sup>2</sup> vs annealing time,  $t$ , at a fixed temperature, should give a straight line from whose slope the diffusion coefficient can be calculated from Eq. 6.24, if the diffusion coefficient is constant. If the process is diffusion limited the depth is proportional to  $\sqrt{t}$  and if the process is reaction limited the depth is proportional to  $t$ . Fig. 6.15 shows such a plot for three different temperatures. It can be seen that the diffusion coefficient is not constant with time. There is an initial period where the diffusion coefficient is low followed, after a lag time of around 4000s by an approximately linear region of higher constant diffusion coefficient. This delay time suggests a two-step process. The conversion from zinc oxide to zinc sulphide requires (i) the indiffusion of sulphur, (ii) the interchange of

sulphur and oxygen at the appropriate site and (iii) the outdiffusion of oxygen. To decide which is the rate limiting step in this process it is necessary to consider the details of the conversion process. This delay could be caused by having an initial reaction rate that is small compared to the rate of diffusion and in this region the overall rate of reaction is determined by the chemical reaction rate at the surface. When the reaction rate is equal to the diffusion rate the process passes into the region where the reaction is controlled by the diffusion rate. This type of reaction can be observed in catalytic reactors<sup>190</sup>. Here the depth is proportional to  $\sqrt{t}$  and therefore the process is controlled by diffusion. From this linear portion, the diffusion coefficient can be calculated to be  $7.8 \times 10^{-18} \text{ m}^2 \text{ s}^{-1}$  at  $540^\circ\text{C}$ .

Looking at the conversion process, Fig 6.16 shows the concentration versus depth data taken from the SNMS profile of one film annealed at  $540^\circ\text{C}$  for 75 mins. These have been plotted on a probability scale. It can be seen that the line is reasonably linear although there is some deviation at low concentrations, indicating a slightly higher diffusion coefficient at low concentration. There is a small reduction in diffusion coefficient with an increase of concentration. Fig 6.16 shows that the depth of diffusion follows a parabolic law, which is typical of a diffusion limited rather than a reaction rate limited process. The reasons for the change in effective diffusion coefficient with time are not clear. The question of whether the indiffusion of sulphur or the outdiffusion of oxygen is the limiting diffusion step is harder to decide. The SNMS profile for a film annealed at  $540^\circ\text{C}$  for 125 mins is shown in Fig 6.17. This shows the depth profile for the Zn, S, O and also shows the silicon substrate. The decrease in zinc content at depth  $> 170 \text{ nm}$  is due to the analysis profile crossing the interface into the silicon substrate. The S is seen to diffuse into the ZnO. At the S/ZnO interface the exchange of oxygen and sulphur requires (i) the indiffusion of sulphur, (ii) the interchange of sulphur and oxygen at the appropriate site and (iii) the outdiffusion of oxygen. In order to understand the reaction and its properties a plot of  $(\text{S}+\text{O})/\text{Zn}$  concentration for a film annealed at  $540^\circ\text{C}$  for 125 mins is shown in Fig 6.18.

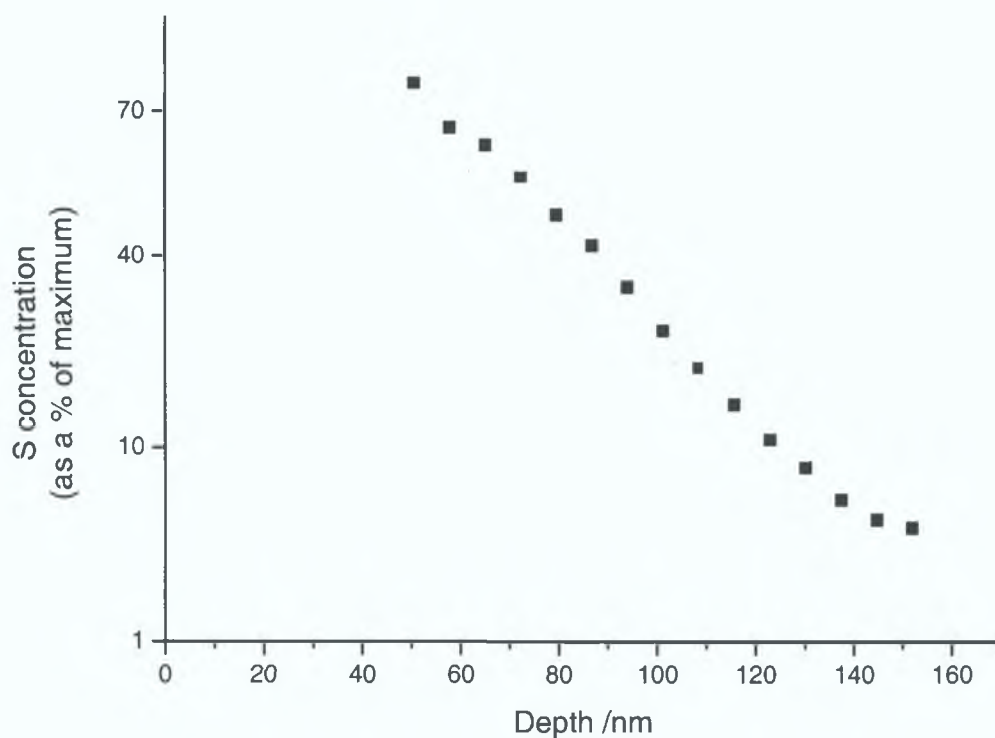


Figure 6.16 Plot of sulphur concentration (as a percentage of the maximum) vs. depth for a film annealed at 540 °C for 75 mins.

This shows that the overall chalcogenide/zinc stoichiometry is constant throughout the film within the accuracy of the SNMS measurement. This suggests that the diffusion coefficients for oxygen and sulphur are the same otherwise there would be a variation in overall stoichiometry within the film. This is understandable if the diffusion process is strongly vacancy-driven. It is to be expected that the diffusion coefficient of oxygen will be higher than that of sulphur due to the smaller size of the atom therefore outdiffusion of oxygen will take place faster than indiffusion of sulphur. However, this would give rise to a greater concentration of oxygen vacancies, which would consequently increase the sulphur diffusion coefficient. Therefore, the overall effect would be that the oxygen and sulphur diffusion coefficients would be the same. Sensitive measurements of vacancy concentration might confirm this mechanism, however, the accuracy of the SNMS measurement is not high enough to detect the change in vacancy concentration, which would result from this process. The effect of grain boundaries on the diffusion process is not clear.



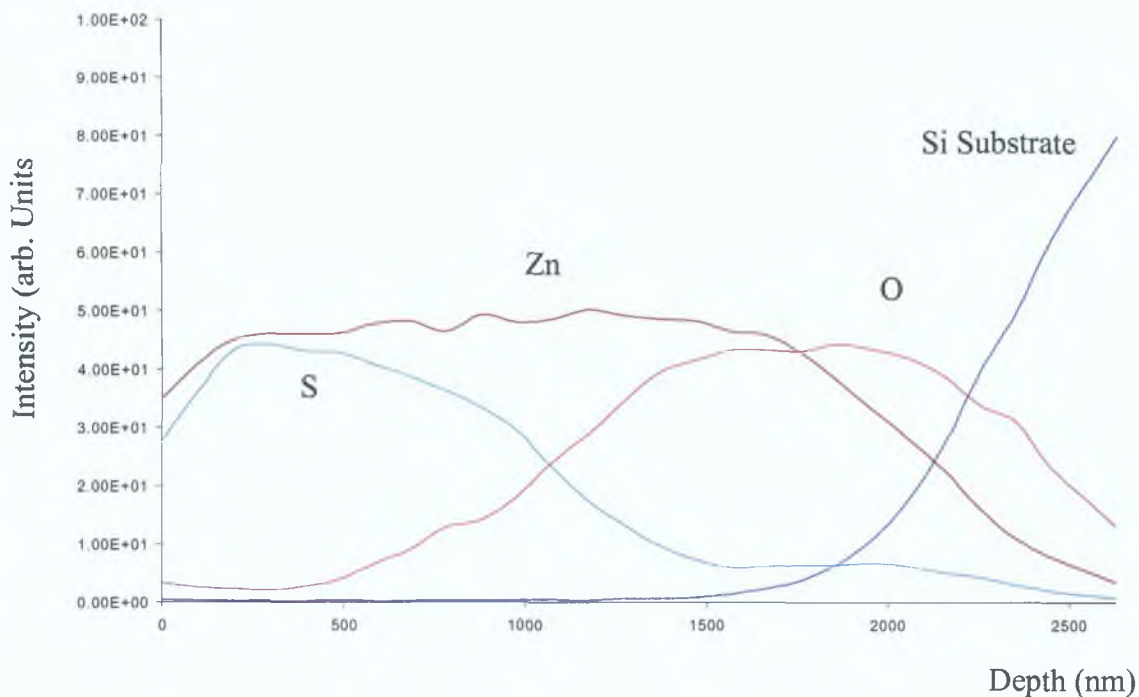


Figure 6.17 SNMS plot of S, O, Zn concentration for a film annealed at 540 °C for 125 mins.

It should be possible to extract an activation energy for the diffusion coefficient from the values of the diffusion coefficient obtained at different temperatures. However, as seen in Fig. 6.12, the scatter in the data was too large to obtain an accurate value since the temperature range is rather small. The SNMS curves, as seen in Fig. 6.17 and Fig 6.18, show a constant stoichiometry of the  $ZnS_xO_{1-x}$  (within the limits of resolution) therefore it appears likely that the process occurs due to minor non-stoichiometries due to oxygen vacancies or sulphur interstitials. The effect of grain boundaries on the diffusion process is not clear.

SEM studies were also carried out on the ZnO as it was converted to ZnS and the results are shown in Fig 6.19. The ZnO films annealed for 30 mins are particulate in nature. When annealed for 50mins and above the films develop a columnar structure as the densification increases. This structure is preferable in TFEL devices<sup>191</sup>. It can be seen that the average grain size increases with the anneal time as the concentration of sulphur is increased. The increase in the grain size decreases the number of grain boundaries and therefore also decreases the conductivity. The surface roughness decreases with increasing anneal time and this will enhance the adhesion of the top

insulating material but in some cases it has been seen to lower the luminescence efficiency<sup>192</sup>.

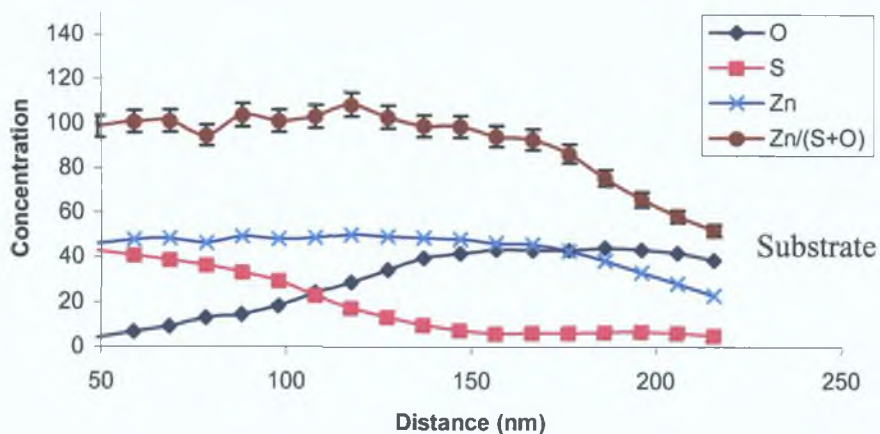
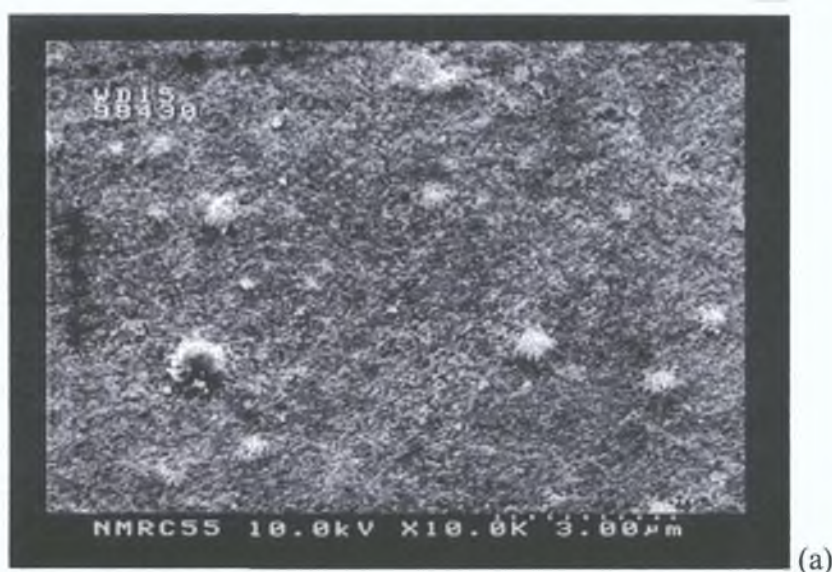
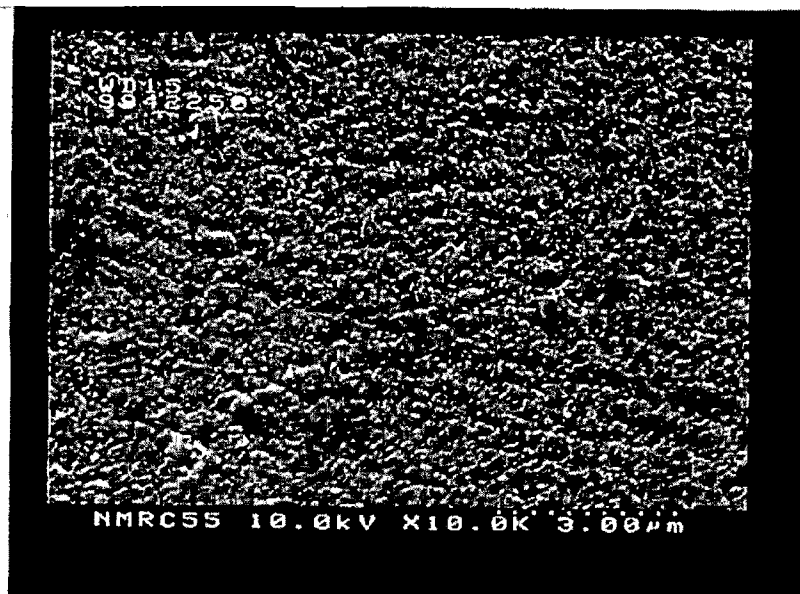
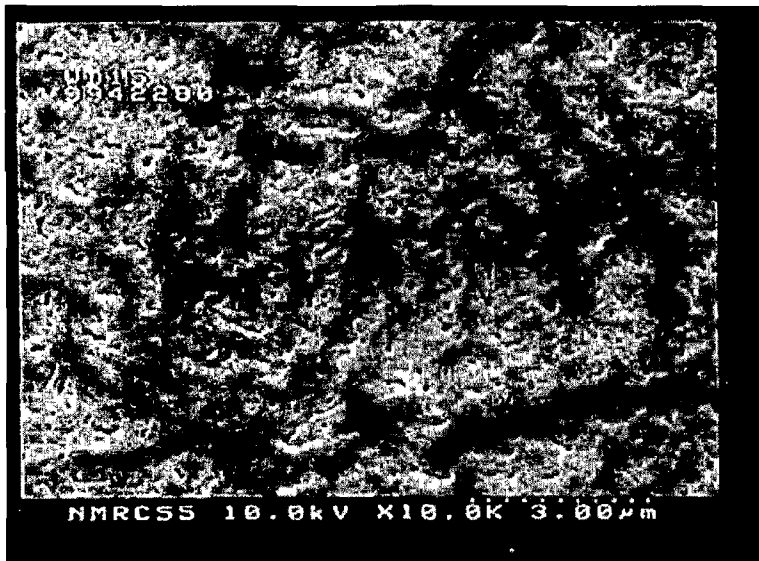


Figure 6.18 SNMS plot of S, O, Zn and Zn/(S+O) concentration for a film annealed at 540°C for 125 mins.

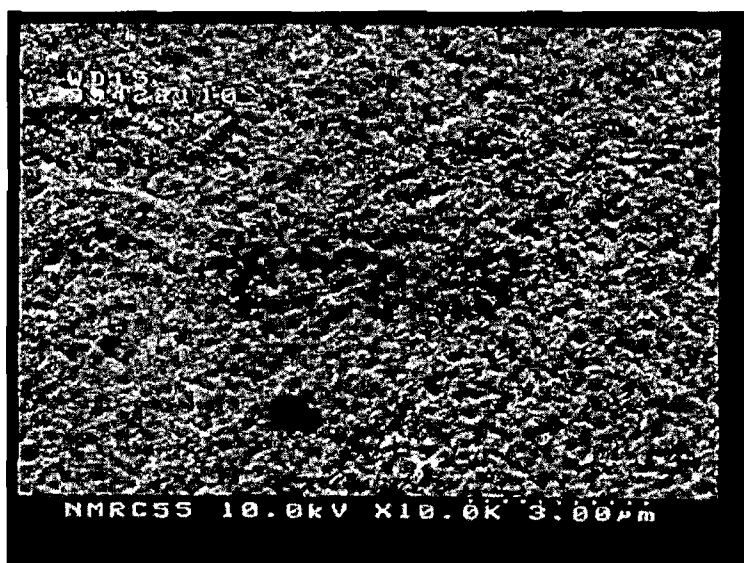




(b)



(c)



(d)

Figure 6 19 SEM scans of ZnO films annealed for (a) 30mins, (b) 50 mins, (c) 80mins and (d) 110 mins in a hydrogen sulphide atmosphere

Raman studies were also carried out on ZnS:Mn using a 325nm He-Cd laser since the energy of the excitation source is near the band gap energy of ZnS. The Raman spectrum shown in Fig 6.20 has three Raman lines at  $\sim 350$ , 700 and  $1050\text{cm}^{-1}$ . These are identified as the resonant Raman lines for ZnS. The three longitudinal-optical phonon lines in the ZnS spectrum are reported as R1LO at a shift of  $354\text{cm}^{-1}$ , R2LO at  $699\text{cm}^{-1}$  and R3LO at  $1045\text{cm}^{-1}$  and the results here correspond favorably with these<sup>193</sup>, showing that ZnS is present. The shoulders present on R1LO at  $\sim 280\text{cm}^{-1}$  could correspond to the TO phonon mode of ZnS<sup>194</sup>. Also there are no contributions present from ZnO.

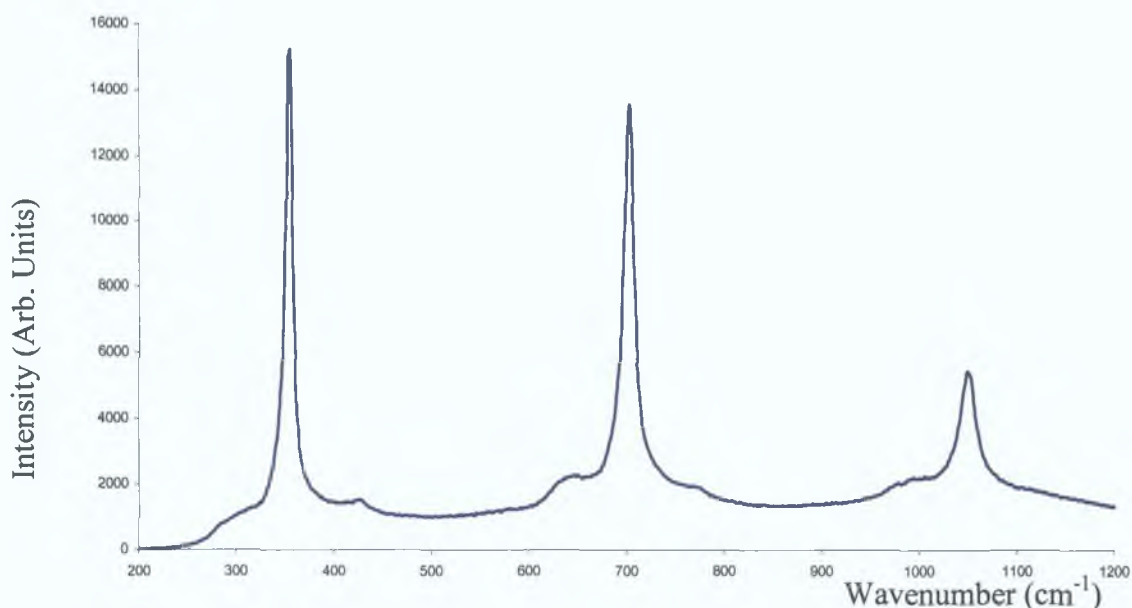


Figure 6.20 Raman spectrum for a 550nm ZnS:Mn film annealed for 4 hours at  $560^{\circ}\text{C}$ .

### Conclusions

Hexagonal ZnO films have been deposited on Si and  $\text{SiO}_2$  surfaces using a sol-gel process. When exposed to a sulphidising atmosphere total conversion from ZnO to ZnS takes place and the material remains in the hexagonal modification. The replacement of oxygen by sulphur in the ZnO occurs with a “two step” process. Initial slow diffusion is followed by a certain length of time with a higher diffusion coefficient of  $7.8 \times 10^{-18}\text{m}^2\text{s}^{-1}$ .

## Chapter 7

### Electroluminescence

#### 7.1 Introduction

Destriau first discovered the effect known as electroluminescence in 1936<sup>195</sup> when he observed light emitted from a ZnS compound when a large electric field was applied to it. Since then interest in the phenomena and research into this area has produced two distinct fields. The first involves the light emitting diode field in which electron-hole pairs recombining near a p-n junction generate light. In the second field the light is generated by the impact excitation by high-energy electrons and subsequent relaxation of a light-emitting centre. The behaviour of these electrons determines the device physics and is the main focus of this section.

The high energy gained by the electrons is due to the electric field, which is in the order of  $10^8 \text{Vm}^{-1}$ . Four types of high field electroluminescent devices have been developed and they are categorised according to the drive voltage waveform and the phosphor configuration. They are ac thin film electroluminescence, ac powder electroluminescence, dc thin film electroluminescence and dc powder luminescence. Powder electroluminescence, both ac and dc, has been investigated since Destriau first experimented with a phosphor. It was thought in the early 1950's that it could replace the CRT or the light bulb and therefore the research intensified. II-VI materials, in particular ZnS with its variety of available dopants became the focus. However, because of the poor lifetimes observed, after 1963 research was curtailed<sup>196</sup>. AC powder luminescent devices are generally now used as backlighting in LCD's and plasma panels while DC devices have been used in car dashboards and laptop computers.

The development and streamlining of thin film processes brought about a new avenue of research for electroluminescence.

#### 7.2 Thin Film Electroluminescence Devices

In the area of thin film electroluminescent devices there are currently three design areas. These are dc, ac and the growing area of organic thin film electroluminescent

devices. The merits of each of these device structures are discussed here. In all cases the phosphor type governs the emission colour characteristics of the display and the different activators used as summarized in Table 7.1<sup>197 198</sup>.

Phosphor	Activator	Colour
ZnS	Mn	Orange
ZnS	Tb	Green
ZnS	Sm	Red
ZnS	Cu, Cl	Green
ZnS	Mn, Cl	Yellow
ZnSe	Cu, Cl	Yellow
ZnSSe	Cu, Cl	Yellow
CaS	Ce, K, Eu	White

**Table 7.1 Phosphor and activator choice available.**

### 7.2.1 D.C. TF Electroluminescence

DC thin film electroluminescence was the first avenue of development in TFEL devices. It has the simplest structure consisting of a thin film phosphor layer (ZnS:Mn, ZnS:Cu,Cl, ZnS:Mn,Cu) sandwiched between two electrodes. The problem with this structure is that it is prone to catastrophic failure due to the lack of current limiting. Incorporation of a current limiting layer improves the device characteristics and research in this area is ongoing<sup>199</sup>.

### 7.2.2 Organic TF Electroluminescence

This type of device incorporates an organic element as the light-generating layer. The mechanism responsible for the light generation differs from the inorganic devices. The inorganic devices rely on high field transport to accelerate the electrons that impact the luminous centres and radiatively decay. In organic devices a multiplayer diode structure is employed in which the recombination of electrons and holes leads to light emission. Therefore for organic devices the requirements are high currents and low voltages while inorganic EL requires high fields and low currents. This advantage of having low operating voltages has the disadvantage of requiring constant

current driving and this leads to severe ohmic losses in the electrodes. This limits the total display area to small sizes if passive-matrix driving is applied. Large area devices require an active matrix technology allowing current switching and therefore active matrix driving. Also the lifetime of the displays produced so far does not meet the requirements for stability. Thus the reported device performances for the organic EL devices are inferior to the inorganic semiconductor devices<sup>200</sup>.

The types of displays produced using organic elements are all LED based. Two avenues of development have been identified and these are the Alq devices and the polymer devices.

### 7.2.2.1 Alq Devices

Since the first reported devices in the late 1980s<sup>201</sup> the development of this type of device has continued. The Alq devices contain aluminium tris 8-hydroxyquinoline (Alq) with quinacridone molecules (Qd)<sup>202</sup>. Having a broad emission extending from 450nm to 700nm Alq can be tailored to emit each of the primary colours required<sup>203</sup> using microcavity effects.

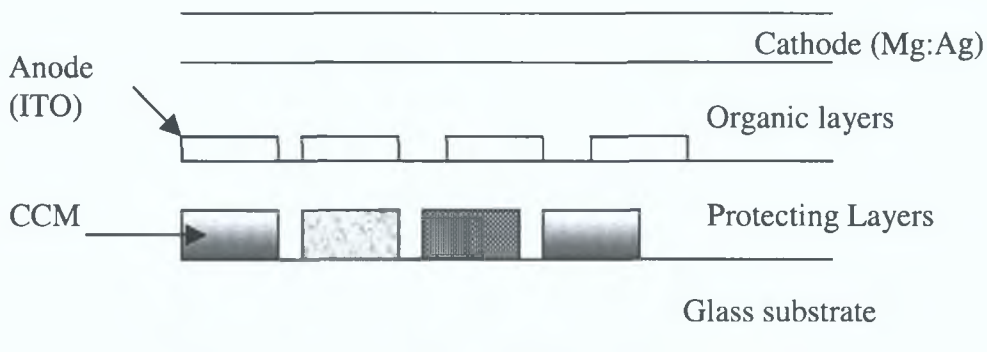


Figure 7.1 Experimental Structure for an Alq based RGB device. The CCM or colour changing media is used to generate the R, G and B

However a display not requiring structuring of the diode array allows a simpler approach to be adopted. An experimental organic RGB display structure is shown in Fig. 7.1<sup>204</sup>. Here the different colours are selected using filtering rather than tailoring the LED structure using Fabry-Perot cavities.

## 7.2.2 Polymer Devices

This area of organic displays has only been developed since 1990<sup>205</sup>. These organic EL devices are based on conjugated polymers, polypropylenevinylene or PPV. This system allows for the formation of the conjugated polymer by heat treatment or by UV exposure. Different emission colours can be formed by chemical modification of the PPV material. Again stability is a problem.

A hybrid mix of organic and inorganic displays are being developed that use the best features from each area. Incorporating non-volatile organic groupings with a metal backbone has led to materials such as organically modified ceramics and silicates<sup>206</sup>. These displays incorporate organoaluminosilicate deposited using sol-gel techniques<sup>207</sup>.

## 7.2.3 AC TF Electroluminescence

The structure of ACTFEL devices has developed significantly since 1974<sup>208</sup>. Despite having different layer types and properties, two different approaches have emerged. One involves a conventional approach and the other is an inverted device structure. The conventional device is a metal-insulator-semiconductor-insulator-metal or MISIM structure deposited on a glass substrate (Corning 7059). The metal electrodes are then deposited and the phosphor layer is sandwiched between two insulators before the final electrodes are deposited.

M	Reflecting Electrode (Al)
I	Top insulator
S	Electroluminescent Phosphor
I	Bottom Insulator
M	Transparent Electrode (ITO)
	Glass Substrate

Figure 7.2 Conventional ACTFEL device structure

An example of this structure is given in Fig. 7.2. The phosphor layer may incorporate several colours or may involve only one colour. The electrodes on the glass are



transparent and are generally ITO. The insulators are transparent and can be SiO<sub>2</sub> or TiO<sub>2</sub>. This five-layer structure is a development of the original three/four layer approach and has several advantages<sup>209</sup>. The double insulating layer prevents the direct flow of electrons from the electrode to the phosphor while trapping electrons at the phosphor/insulator interface and thus increasing the effective electric field. The phosphor layer is protected from outside impurities by the double insulating layer ensuring an increase in luminous efficiency.

The inverted device structure is used in active matrix electroluminescence (AMEL) and in thick film dielectric hybrid electroluminescence (TDEL) displays. The general structure is shown in Fig. 7.3.

M	Transparent Electrode (ITO)
I	Top insulator
S	Electroluminescent Phosphor
I	Bottom Insulator
M	Reflecting Electrode (Al)
	Opaque Substrate

Figure 7.3 Inverted structure of an ACTFEL device

It was found that the annealing temperatures on the conventional device were limited since the resistance of the ITO layer increases enormously and the general substrate used has a softening temperature of 598°C. Using fused silica as a substrate eliminated the substrate problem but this is expensive. Therefore the blackening after annealing, of the ITO layer when incorporated into a structure is the limiting factor. This is due to a change in the structure of the ITO, where X-Ray photo-electron spectroscopy (XPS) studies have shown a shift in the energy states of indium to lower binding energy resulting in increased resistance<sup>210</sup>. This structure allows the device to be annealed at high temperatures before the final ITO layer is added. If silicon is used as the substrate it doubles as an electrode and eliminates the problem of oxidation of

the first electrode layer. Also it allows the drive electronics to be incorporated on to the substrate. High performance AMEL displays have been developed with this technology<sup>211</sup>. TDEL devices use an alumina ceramic substrate with a screen printed high dielectric constant ferroelectric thick film as one of the insulating layers. Alumina's high temperature properties make it an ideal candidate for this purpose but it also limits the resolution obtainable due to surface roughness. This problem has been overcome in some recent devices where sol-gel films were used to planarize the surface of the thick film<sup>212</sup>.

Whichever structure is used, the basic function of each layer is the same. The outer electrodes are the electrical contacts to the drive circuitry. The phosphor or semiconductor is sandwiched between two insulators, which are current limiting layers that prolong the lifetime of the device.

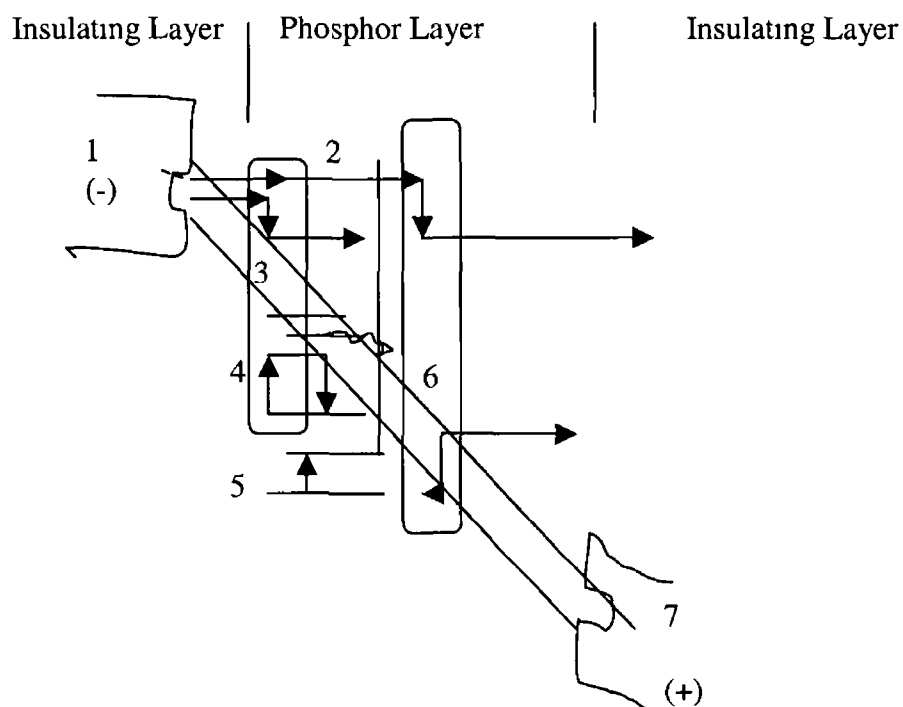


Figure 7.4 Energy Band Diagram For EL Mechanism

The phosphor layer is the central layer where electrons are injected from the phosphor/ insulator interface<sup>213</sup> and accelerate through the phosphor layer when a large electric field is induced across the layer. These “hot” electrons impact and excite the luminescent centres, which subsequently generate light. The EL emission process is summarised in Fig 7.4<sup>214</sup>

The process shown above includes

- 1 Above the threshold voltage electrons from interface states between the insulator and the phosphor layers are injected into the phosphor layer by high-field assisted tunnelling
- 2 Ballistic acceleration takes place and the electrons gain the necessary kinetic energy to
- 3 impact excite a luminescent centre and result in
- 4 radiative transitions to the ground state or
- 5 nonradiative de-excitation of the Mn centre or
- 6 carrier multiplication by lattice impact can also take place
- 7 The electrons can be trapped by interface states on the anode side, causing polarisation

When the polarity of the ac voltage is reversed, the same process takes place in the opposite direction

For the ZnS/Mn system this is recognised as the accepted mechanism. However in other II-VI systems (CaS or SrS) an additional process takes place. This is characterised by a field-induced ionisation of luminescent centres and the subsequent trapping of low energy electrons, resulting in EL emission<sup>215</sup>

How the electroluminescence process takes place and how to optimise it involves looking at the device physics. A device needs efficient conversion of the electrical input into the kinetic energy of the charge carriers. Without a large fraction of these carriers being swept through the active material, possessing energies above the excitation energy of the centres, only low efficiency will be obtained.

### 7.3 Device Physics

Electroluminescence is neither a simple or single phenomena. Even for the same material the local field conditions produced by impurity defects and electrode contacts to the material may produce quite different EL mechanisms. Having both covalent and ionic properties ZnS is a particularly complex II-VI compound. It is

approximately 62% Ionic in character<sup>216</sup>. It has a complex energy level structure due to self-compensation and a large number of impurities can be incorporated into the lattice.

Looking at Fig. 7.4, tunnel emission of electrons, acceleration of these electrons, impact ionisation or excitation and successful radiative recombination are the main points to concentrate on.

### 7.3.1 Tunnel Emission

Two mechanisms are responsible for the emission of electrons from the interface states, shown in Fig. 7.5, and these are thermionic emission and field emission or tunnelling.

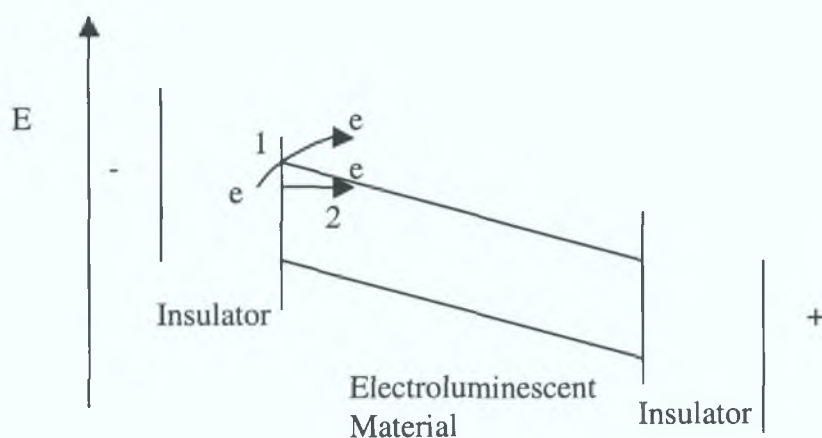


Figure 7.5 Energy band diagram showing 1) thermionic and 2) field emission or tunnelling as two possible electron emission mechanisms

When the voltage in the device is above the threshold the electrons are emitted from the interface states at the insulator/phosphor junction and accelerated to the anode where they are again trapped at the phosphor/insulator interface states to be emitted again when the polarity is reversed. This is the accepted theory on the carrier injection in most EL phosphors<sup>217</sup>. When different top and bottom insulators are used the threshold voltage varies for opposite polarities, showing that the tunnelling mechanism is thermally assisted<sup>218</sup>. Since the electrical properties only depend weakly on temperature a strict thermionic emission process is ruled out<sup>219</sup>. On the rising pulse of the ac voltage, it has been proposed that direct tunnelling dominates,

while at the trailing edge, phonon assisted tunnelling alters the interface electron distribution ensuring that high fields are required to access them<sup>220</sup>.

ACTFEL devices are usually driven by a 60Hz ac voltage supply. The voltage driving the ACTFEL rises and the energy bands begin to bend under the induced field until the threshold voltage is reached. At this point the bands are bent enough so that the electrons can tunnel through into the phosphor band from the interface states. The depth of the interface states determines the effectiveness of the emission. If the states are too shallow, the electrons emitted will not be accelerated enough to cause impact excitation, too deep and no electrons will be emitted. Electron state depths of 1.0-1.3 eV have proven optimum<sup>221</sup>. The density of these states controls the current injected into the device. The density of the interface states (Ds) is dependent on the bonding properties of the semiconductor. The more covalent the semiconductor the higher the density of interface states but these semiconductors with covalent properties generally have a small bandgap which makes them unsuitable for EL devices. In order to increase the density of interface states and the number of electrons tunnelling into the phosphor layer many devices have been proposed which incorporate an extra layer between the insulator and the semiconductor<sup>222,223,224</sup>.

### 7.3.2 Electron Acceleration

Under the influence of the electric field the electrons are accelerated once they are injected into the semiconductor. Below the threshold voltage the whole device can be considered as a loss free capacitor as the semiconductor is highly resistive. Above threshold the voltage partition changes by increasing over the insulator films and remaining constant over the phosphor film. Rearranging Maxwell's Equations for series capacitors the electric field in the phosphor layer ( $E_p$ ) may be calculated as

$$E_p = V_{tot} \frac{\epsilon_i}{(\epsilon d_p + \epsilon(2)d_i)} \quad (7.1)$$

where  $\epsilon$  is the dielectric constant,  $d$  is the layer thickness and the subscripts  $i$  and  $p$  represent the insulator and the phosphor respectively. Using the values of 300nm(x2) for the insulator thickness and 20 for its dielectric constant, 500nm for the phosphor thickness and dielectric constant of 13 and a total voltage of 180-200V, the phosphor field ranges from 2.0-2.5MVcm<sup>-1</sup>. These field strengths ensure that the electron is

accelerated quickly. The electron energy distribution is a function of high field scattering mechanisms that depend on the energy band properties of the host. Initial vacuum experiments showed a high availability of “hot” electrons<sup>225</sup>. Since the electrons loose their energy by several mechanisms electron high field transport simulations have been set up.

Numerical Monte Carlo simulations consider the carrier dynamics and the carrier kinetics by simulating the trajectories of individual carriers as they move through the device. The carrier kinetics are controlled by the scattering rates and the carrier kinetics are controlled by the scattering rates due to inter valley scattering, polar optical phonon scattering, acoustic phonon scattering and ionised impurity scattering as shown in Fig. 7.6<sup>226</sup>. Taking these into account the electron energy distribution can be calculated and by estimating the impact excitation cross-section as a function of energy the quantum yields of the devices can be approximated.

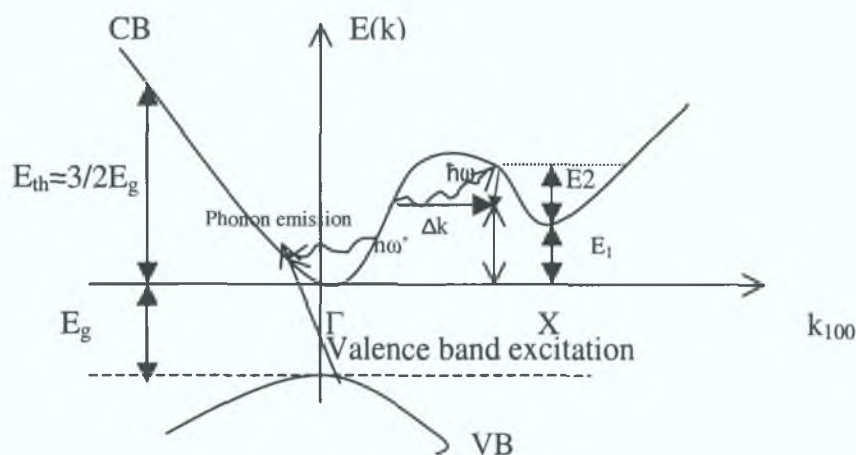


Figure 7.6 Electron scattering mechanisms in a semiconductor with sidebands (ZnS)

Simulations based on a nonparabolic multi-valley model, have indicated that the polar optical phonon and intervalley scattering to be the dominant transport methods in bulk ZnS and that the tail of the hot electron distribution occurs below 4eV so that that band to band excitation would seem precluded since this is below the 4.3eV threshold for impact ionisation<sup>227</sup>. In further studies, which used a nonlocal empirical

pseudopotential method (EPM) to obtain a full band structure, the impact excitation yield was also found to be sensitive to the optical deformation potential<sup>228</sup>. However, modelling the device using impact ionisation as the current gain mechanism in a nonparabolic four-valley model of the first and second conduction bands, the simulations show that impact ionisation is indeed responsible for the high current gains<sup>229</sup>.

Another model used for analysing the electron transport in the semiconductor is the Lucky Drift Model, which is a more simplistic analytical model. There are two basic transport modes considered by the Lucky Drift model. Firstly the ballistic or collision free mode that is spatially defined by the optical-phonon mean free path  $\lambda$  and temporally by the electron-phonon collision rate  $1/\tau_m$ . Secondly the drift mode, after the electron has suffered one collision, which is characterised by the energy relaxation length  $\lambda_E$  and the energy relaxation rate  $1/\tau_E$ <sup>230, 231</sup>. Both models have contributed significantly to the understanding of the high field electron transport phenomena in ACTFEL devices<sup>232</sup>.

### 7.3.3 Impact excitation/ ionisation

Once the electron has been accelerated to energies exceeding the threshold it can interact with a luminescent centre and promote one of the luminescent centre's ground state electrons. The electron can undergo either impact excitation where it is promoted into a higher atomic state of the luminescent centre or impact ionisation where it is promoted into the conduction band of the host material as seen in Fig 7.7. Also, excitation can be caused by avalanching followed by the recombination of the resulting electrons and holes at an impurity centre.

Since the threshold for electron-hole production is between  $E_g$  and  $3/2E_g$  and therefore much larger than that required for impact excitation it is not considered a major contributor to the luminescence<sup>233</sup>. When the centre is impact excited it can relax back to its ground state either radiatively or non-radiatively.

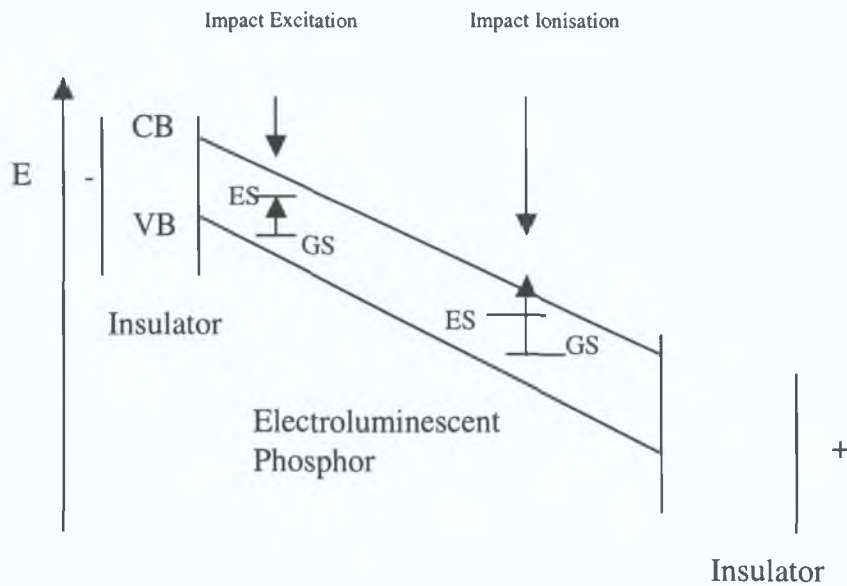


Figure 7.7 Demonstration of impact excitation and impact ionization mechanisms. CB and VB are the conduction and valence band, respectively and GS and ES refer to the ground state and the excited state of the luminescent center, respectively.

### 7.3.3.1 Impact Excitation

In impact excitation the electrons energy is transferred directly to the impurity. This is the simplest of all the processes discussed here and it requires the least amount of energy. When looking at the power efficiency the impact cross-section, concentration quenching and the loss of energy of hot electrons to the lattice are important factors. The power efficiency  $\eta_{power}$  of a device is directly proportional to the cross-section of the luminescent centre and is expressed by the following equation<sup>234</sup>

$$\eta_{power} = \frac{h\nu\sigma N}{eE} \quad (7.2)$$

where the average cross-section is  $\sigma$  with an optimum concentration of luminescent centres  $N$ , the emission photon has energy  $h\nu$  and the electric field strength is  $E$ .

When a hot electron travels a distance  $(\sigma N)^{-1}$  there is on average one impact resulting in the emission of energy  $h\nu$ . For a 2.0eV photon to be emitted in the presence of a



field strength of  $10^6 \text{Vcm}^{-1}$  and given a cross-section of  $10^{-16} \text{cm}^2$  for a luminescent centre<sup>235</sup> concentration of  $10^{20} \text{cm}^{-3}$  the power efficiency works out at 2%

The quantum efficiency also depends on the cross-section and the field strength and is given by

$$\eta_{qu} = WN\sigma f(E) \quad (7.3)$$

where  $W$  = depletion region width and  $f(E)$  is the fraction of electrons which have energy greater than the threshold as a function of the applied field  $E$ . In studies on impact excitation in ZnS:Mn Schottky diodes, the quantum efficiency has been found to drop off at fields greater than  $5 \times 10^5 \text{V/cm}$ <sup>236</sup>. Looking at the band structure of ZnS:Mn can give a possible explanation for this drop. The threshold energy for impact excitation is 2.1 eV and therefore only applies to electrons in the  $X_3$  minimum or higher. At high fields the electrons tend to congregate near band minima where the group velocity is small and the effective mass is large. As the fields increase these electrons could then transfer to states higher up in the conduction band accounting for the saturation in the quantum efficiency and the drop off. These electrons having a greater group velocity will spend less time in the depletion layer and hence may be slightly less efficient in exciting manganese luminescence than electrons near the  $X_3$  minimum. Also these electrons may have enough energy to cause current multiplication either by impact ionisation or by direct band-to-band ionisation. In order to increase the cross-section without introducing threshold effects it is important to distinguish between the direct processes where the incident particle retains its identity after a scattering event and the exchange processes where the incident particle changes places with a particle during the scatter. For direct processes, slow incident electrons and a small change in crystal momentum is desired. Exchange processes, which are short-range effects, slow electrons with long interaction times are required and this explains why these dominate at energies just above threshold.

### 7.3.3.2 Impact Ionisation

Two types of impact ionisation can take place and these are classified as band-to-band impact ionisation and impact ionisation

### 7.3.3.2.1 Band-to-Band Impact Ionisation

Here electrons and holes are created which can recombine radiatively through some centre. Only a few electrons in the tail of the energy distribution of the accelerated particles contribute to ionisation. In materials with an ionic component in their bonding there can be long-term damage due to the rapid increase in the current with the applied voltage.

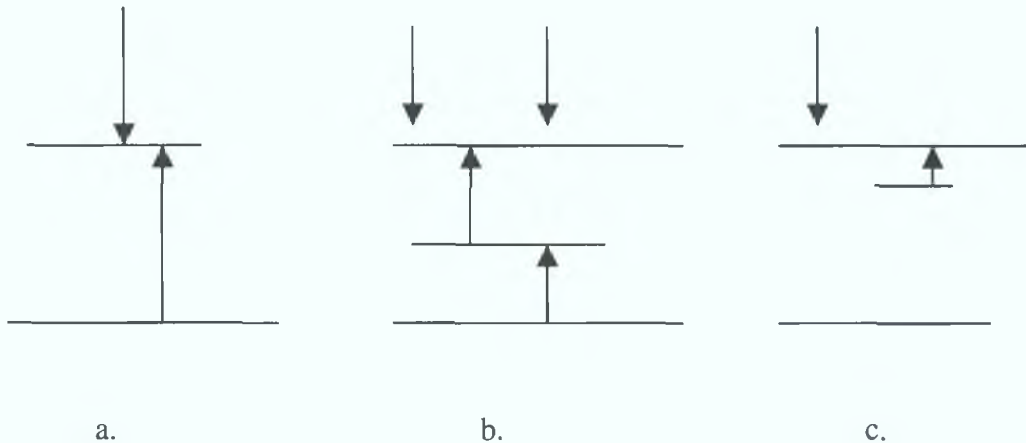


Figure 7.8 Impact processes in a solid. a) band-to-band ionisation b) two step band-to-band ionisation c) impact ionisation.

A modification of this is the two-step band-to-band ionisation. This two step process involves the incident hot carrier ionising a deep level by an electronic transition to the conduction band and a second hot carrier raises an electron from the valence band to the deep level as shown in Figure 7.8(b). This process tends to occur at lower field strengths than that required for band-to-band ionisation and it tends to saturate at high fields rather than accelerate.

### 7.3.3.2.2 Impact Ionisation

This effect can be neglected at fields less than 1MV/cm. As seen in Fig.7.8c) the hot carrier promotes an electron into the conduction band of the solid and it is accelerated towards the anode by the electric field. The result is electron multiplication and avalanche breakdown<sup>237</sup>.

Of the processes discussed two-step band-to-band ionisation and impact excitation dominate the impact processes in thin film electroluminescent displays. It has been

shown that band-to-band impact ionisation is the main method of luminescence generation in ZnS Mn devices<sup>238</sup>

### 7.3 4 ElectroLuminescence

Before looking at the specific luminescence, recapping on the types of levels in the luminescent material is important. In general a level that is normally empty near the conduction band behaves as an electron trap and an occupied level that is near the valence band behaves as an electron trap. Thus a level that is approximately midway between the bands acts as either a radiative or a non-radiative recombination centre. The luminescence produced by the applied field can therefore be divided into two categories

- i) Pure or intrinsic electroluminescence that is the result of the sole action of the electric field as found in electroluminescent cells or panels
- ii) Electroluminescence due to charge carrier injection

The second type of luminescence is concentrated on here

Here the current actually passes through the phosphor through contact with the electrodes and the intensity is proportional to the current, in contrast to the intrinsic luminescence where the phosphor need not be in contact with the electrodes and no net current passes through the phosphor. But since the TFEL is a capacitive load, a significant amount of the load current is displacement current<sup>239</sup>. After the electron has been sufficiently accelerated by one of the methods described and excitation has taken place the light emission results from the radiative decay of the centre.

Maximizing the efficiency of the display involves ensuring the electrons are available and this depends on the other constituent layers of the device. The properties necessary for the additional films are discussed in the next chapter. The properties of the display and the parameters involved in maximising the luminous output are then discussed.

## 7.4 Luminescence Studies.

The behaviour of the luminescent material in a variety of devices has been studied. This behaviour of the material gives a very important insight into the process governing the luminous output in the devices.

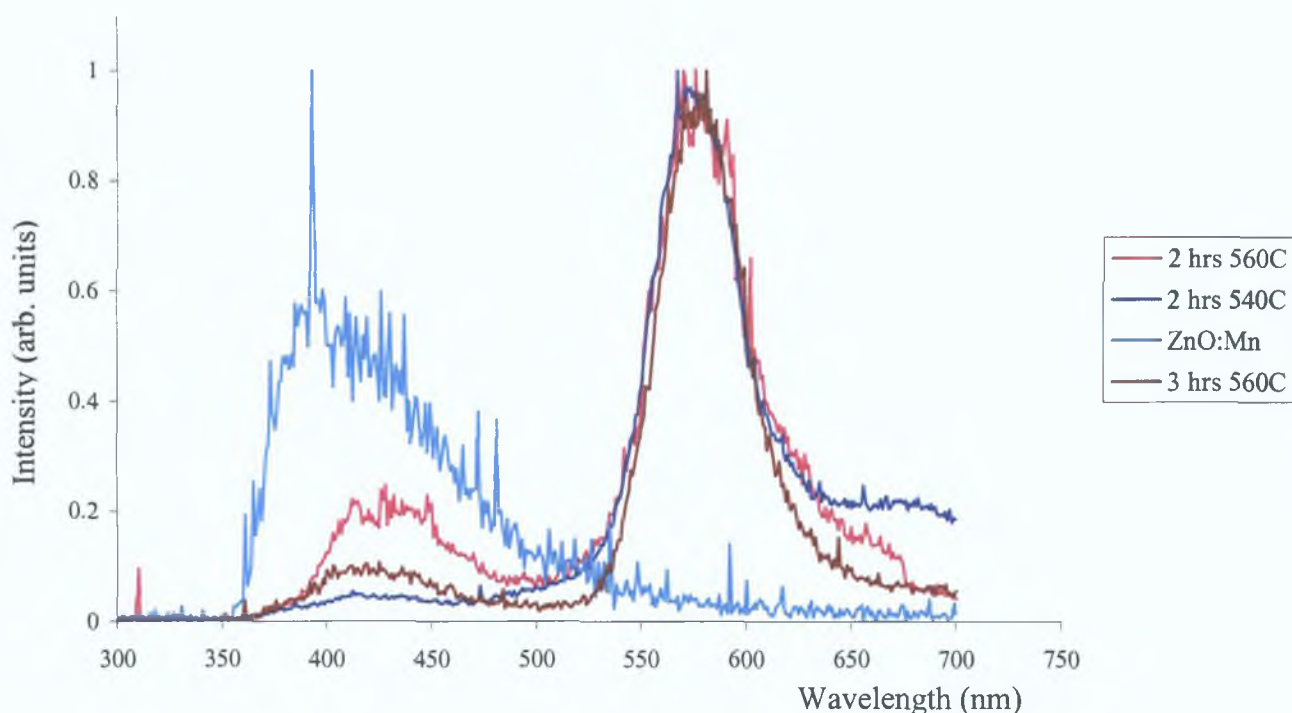


Figure 7.9 PL studies showing the transition from ZnO:Mn to ZnS:Mn as the anneal time in  $H_2S$  is increased.

Photoluminescence results from the direct excitation of the Mn centres and hence can be used to look at the expected luminescence from a given device. The output is independent of nonradiative recombination paths and if no EL is seen from the device subsequently this may be due to point defects<sup>240</sup>. The processes that are discussed here led to the light output but predicting the output from a given combination of films requires looking at the various excitation methods and identifying any possible traps that may be present in the material to prevent luminescence in a given device. Cathodoluminescence (CL) and photoluminescence (PL) are used to look at the Mn doped zinc sulphide, which has a strong orange emission due to the  $Mn^{2+} {}^4T_1({}^4G) \rightarrow {}^6A_1({}^6S)$  transitions.

The spectra obtained using CL, PL and AC electroluminescence have been compared and have shown that the electroluminescence produced is dependent on the ZnS Mn structure

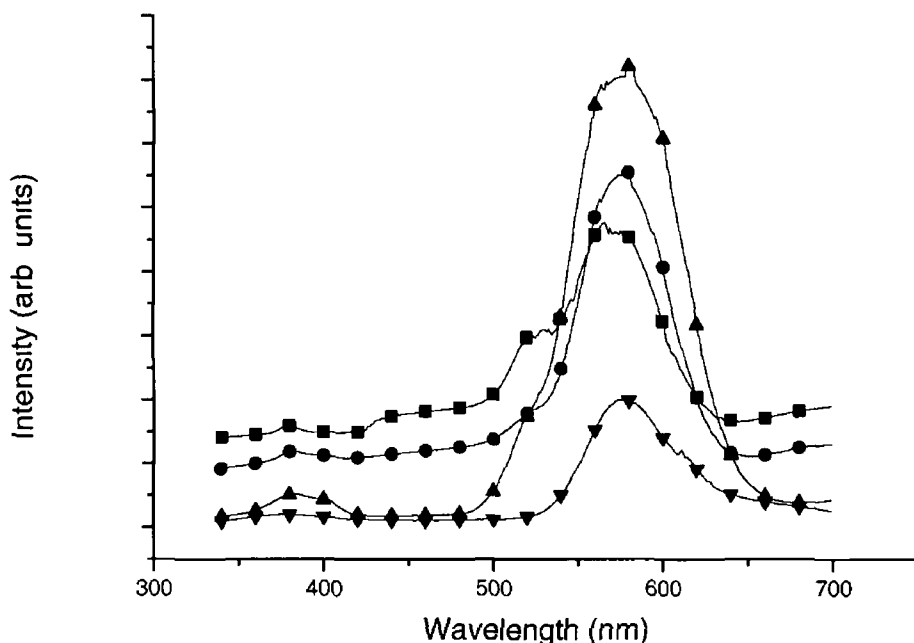


Figure 7.10 CL Spectra showing growth of ZnS Mn with anneal time ■ 2hrs 540 °C, ● 2hrs 560 °C, ▲ 3hrs 560 °C, ▼ 4 hrs 560 °C

PL data, shown in Fig 7.9, obtained during the anneal process show the growth of the ~580nm peak and the decline of the band edge ~380nm peak as the anneal time is increased. The peaks present in the spectra compare favourably to those found in the literature<sup>241</sup>. The 580nm peak is the characteristic peak of ZnS Mn due to the  ${}^4T_1 \rightarrow {}^6A_1$  transitions and shows that the structure of the films is hexagonal as the cubic ZnS Mn electroluminescence peak is found at 585nm. The ZnO Mn curve shows only the band edge emission at ~380nm and no peak is seen at 510nm due to vacancies. As the anneal time is increased this shifts towards the ~420nm region in the ZnS Mn and this is due to a self activated centre formed by a zinc vacancy<sup>242</sup>. In the 2hrs at 540°C spectrum an extra peak is seen in the red region centred at ~660nm. This is due to that sample having a higher concentration of manganese and this can also

result in concentration quenching<sup>243</sup> Since the  $3d^5$  electrons of  $Mn^{2+}$  are fully exposed to interacting fields this emission may be due to the perturbation of the energy levels The  $^4G$  state splits into four levels as shown in Fig 6 7 The  $^4T_1$  level shifts to lower energy at stronger interacting fields due to the increased concentration of  $Mn^{2+}$  ions<sup>244</sup>

CL studies confirm the transition from ZnO Mn to ZnS Mn Fig 7 10 shows the growth of the  $\sim 580nm$  peak as the anneal time is increased A very weak band edge emission is also apparent in all the spectra At short low temperature anneal times the main spectrum is made up from three overlapping spectra centred at  $\sim 460nm$ ,  $\sim 525nm$  and the  $Mn^{2+}$  characteristic band at  $\sim 580nm$  The excitation band at  $\sim 460nm$  is due to the  $Mn^{2+}$  self activated direct transition, which has widely distributed d energy levels<sup>245 246</sup> The  $\sim 525nm$  band is seen in the CL spectra for the lower anneal times and can be attributed to a hybrid emission due to the presence of sulphur in ZnO<sup>247</sup> This luminescence peak has also been seen in photoluminescence studies of hot luminescence due to vibronic transitions from the vibrational states of the excited  $Mn^{2+}$  to its ground state, but this is unlikely here as this luminescence has a relatively short decay time<sup>248</sup> As the anneal time is increased the contributions from the smaller bands diminish and the spectrum only shows the characteristic 580nm band It has been seen that films that display this 580nm peak under CL and EL also exhibit EL when placed in a device This is a quick way to ensure that the luminescent material is functioning before completing the display itself Any problems with the luminescence can be easily identified here In some cases impurities and unwanted interactions can cause other peaks which can be seen in the luminescence curves and these limit and quench the electroluminescence present in the devices Some of these problems have been encountered and these are discussed in detail in Chapter 9

## Chapter 8

### Insulating and Transparent Conducting Thin Films

#### 8.1 Introduction

The insulating layer in the display is there to protect the phosphor from electric breakdown in electric fields of more than  $2 \times 10^8$  V/m thereby preventing catastrophic breakdown. In order to accomplish this, the insulating layer must be free from significant defects over areas in excess of  $200 \text{cm}^2$ . Secondly, they must satisfy mechanical requirements in terms of stress and adhesion over the various processing temperatures. From an electrical viewpoint the film must prevent metal-ion diffusion into the phosphor layer and provide interface states from which the electrons can be ejected into the conduction band of the phosphor via tunnelling when the applied field is larger than the threshold electric field. Also from an optical engineering aspect the film must minimize the reflectance of the light and thus improve readability of the image. This section will look at insulating films in terms of the properties requirements for an efficient film and the material choice available.

#### 8.2 Film Properties

##### 8.2.1 High dielectric constant.

The primary role of the insulator is electrical breakdown protection and the minimum voltage drop across the dielectric layers is desired. The thin film electroluminescent device operates as an ideal capacitor at below threshold electric fields. Its operation is governed by Maxwell's equations that give the following boundary conditions at the interface between the individual film layers

$$\epsilon_0 \epsilon_I E_I = \epsilon_0 \epsilon_{EL} E_{EL} \quad (8.1)$$

where  $E_I$  and  $E_{EL}$  are the electric field strengths of the insulator and the electroluminescent layers respectively and  $\epsilon_I$  and  $\epsilon_{EL}$  are the relative dielectric constants.

If the applied voltage  $V_A$  is given as

$$V_A = E_I d + E_{EL} d \quad (8.2)$$

then the voltage across the phosphor layer can be calculated as

$$V_{EL} = E_{EL} d_{EL} \quad (8.3)$$

which is therefore

$$V_{EL} = \left( \frac{\epsilon_I d_{EL}}{\epsilon_I d_{EL} + \epsilon_{EL} d_I} \right) \quad (8.4)$$

Making  $\epsilon_I$  as large as possible and the thickness of the insulating layer as small as possible maximises the efficiency of the device. Also this can lead to a lowering of the operating voltage. However, a limitation exists on the film thickness as the device reliability decreases because pinholes in the film cause localised high field regions, which result in breakdown.

### 8.2.2 Dielectric breakdown strength

The threshold field strength for a ZnS:Mn device is  $1.5 \times 10^8$  V/m approx<sup>249</sup>. Thus an insulating film must be able to stand a field given by

$$E = \frac{\epsilon_{EL} E_{EL}}{\epsilon_I} \quad (8.5)$$

therefore the higher the dielectric constant of the insulating layer the greater the reliability due to the operation at lower field levels. One of the accepted figures of merit for the selection of an insulator is the charge density of the electric displacement at the breakdown. This is the product of the dielectric constant  $\epsilon_I$  and the breakdown electric field  $E$ . The classical value is at least three times that of the active zinc sulphide layer, thus values in excess of  $3 \mu\text{C}/\text{cm}$  must be achieved<sup>250</sup>.

### 8.2.3 Film Breakdown Characteristics

Insulating layers in thin film electroluminescent devices exhibit two distinct breakdown modes



### **8.2.3.1 Propagating breakdown**

All thin films have some microscopic defects and these can become the centre of a breakdown. In this case a propagating arc destructively grows in size until there is significant microscopic damage resulting in a short circuit in the device. Dielectric films with large dielectric constants that are not fully oxidised tend to have this problem. Insulating films that exhibit this type of breakdown have proved unsuitable for electroluminescent devices. Titanium dioxide is an example of this type of film and therefore needs to be combined with other dielectrics to be converted to self-healing mode in order to be used in a device.

### **8.2.3.2 Self-Healing breakdown**

In this case the film defect is cleared by a self-healing localised discharge that causes a microscopic open circuit to occur around the breakdown site. Since all thin films will have some microscopic defects it is necessary that the insulating material have a self-healing breakdown. Insulating films that show this self-healing breakdown mechanism include  $\text{Al}_2\text{O}_3$ ,  $\text{Si}_2\text{N}_4$ ,  $\text{TiO}_2$ ,  $\text{BaTa}_2\text{O}_6$  and  $\text{Ta}_2\text{O}_5$ <sup>251</sup>.

## **8.2.4 General Properties**

As well as having a low pinhole density the insulating film should have a high resistivity, good barrier properties and moisture resistance. Good layer adhesion and the ability to self heal to passivate the device will enhance the performance of the device. From a mechanical viewpoint the film should be able to withstand thermal and mechanical stress during the device operation. Good heat conduction for the rear insulator and good optical transparency on the front insulator also help the device. Other criteria for selection can include requirements for the insulator-semiconductor interface (ISI) and these are thermal expansion matching, the amount of charge stored at the interface and low leakage of the bound charge under low applied voltages.

## **8.2.5 Driving voltage**

There is always a need to reduce the driving voltage of the EL device in order to reduce the power consumption and to minimize stress on the device. Various methods have been tried to accomplish this. The external voltage can be reduced and the field across the active layer maintained by choosing a material with a high

dielectric constant but high-k materials have a lower breakdown strength therefore thicker layers are required. High-k dielectrics have a significant density of slow carrier traps in their bandgap and the number of these traps increases proportionally to the thickness of the film. This thick dielectric EL or TDEL<sup>252</sup> device can be used but the processing is costly, extra buffer films are needed, and high optical absorption result in low device efficiency.

## 8.2.6 Stability

The ACTFEL device needs to have a stable operating lifetime in the region of 10,000h. The major sources of device failure are insulator failure and degradation of the interfaces. The insulator failures have two classifications:

- i) those due to internal dielectric problems – pinholes, dielectric electrical breakdown, thermo-electrical breakdown
- ii) those due to external or degradation of interfaces between the insulator and other layers – ion migration, moisture penetration

Both types of failure accumulate with time.

The ACTFEL device needs to be able to function in a range of different environments, that include high humidity environments. Therefore moisture resistant dielectrics with good barrier properties against ion diffusion ensure reliable device operation. Use of insulators with a stable stoichiometry is important to minimize  $\alpha$ -aging where

$$\alpha = \frac{C_i}{C_i + C_s} \quad (8.6)$$

and  $C_i$  and  $C_s$  are the capacitances of the insulator and the semiconductor respectively. Aging of the device can sometimes lead to the formation of zinc-oxi-sulphide in the ZnS/Mn-insulator and the insertion of an interlayer of stable stoichiometry can improve the aging characteristics<sup>253</sup>

## 8.2.7 Insulator- Electrode Interfaces

The interface between the electrodes and the insulating material influences the reliability of the display. Generally aluminium is used as a metal contact on the devices. In some insulating materials an intermixing layer can be formed.  $Ta_2O_5$ ,  $Al_2O_3$ <sup>254</sup> and also  $SiO_2$ <sup>255</sup> have shown process-controlled states near the  $SiO_2$ /metal surface. These may affect the field distribution in the structure due to trapped charge. Due to inherent inhomogeneities in the insulating layers such as pinholes or cracks the top electrode needs to favour non-shorting breakdowns. It must be so thin that it will evaporate or melt back quickly beyond the edge of a dielectric crater. If the top electrode is too thick and remains in contact with the edge of the dielectric, a second or continuing breakdown may occur through the weakened area at the edge of the crater.

## 8.2.8 Thermal Conductivity

The current flow in the device results in an appreciable amount of heat. Most of this heat is generated due to the charge transfer through the active layer with the rest of the heat generated by leakage current. Some hot spots can be generated due to slight thickness variation in the film and this heat needs to be dissipated by conduction. Insulators with high thermal conductivities are preferable. The thermal conductivity of thin films with sub-micron thicknesses can be up to two orders of magnitude lower than the corresponding bulk material<sup>256</sup>.

## 8.2.9 Insulator-semiconductor Interface

This is one of the most important areas of the device. The ideal interface must provide a high number of efficient electrons and be mechanically and chemically stable.

### 8.2.9.1 Bottom insulator and active layer

The structure of the bottom insulating layer influences the growth of the active layer. Grains with different crystallographic orientations have different surface and interface energies. If the active layer is grown on an amorphous surface the surface and interface energies will depend only on the grain orientation relative to the normal of

the plane of the film. The active layer grown on a polycrystalline film will be influenced by the grain orientation. Thus there can be poor crystallinity at the interface and a “dead layer” can be formed<sup>257</sup>. The lower insulating layer also prevents undesirable field deviation and current crowding<sup>258</sup>.

### 8.2.9.2 Nature of Insulator-semiconductor Interface states

In ZnS/Mn the insulator-semiconductor interface (ISI) states are the major carrier injection source. To ensure high efficiency the interface should provide a sufficient number of the electron states with the appropriate energy distribution. The interface can also be a source of carrier traps and this can affect the threshold of the device and its charge-to-breakdown characteristics. The nature of the interface states can also influence the operation of the device. The number of interface states generated for a particular insulator/semiconductor combination is dependent on the preparation conditions, the quality of the insulating film and the distribution of carrier traps. Not only the number of electrons participating in charge transfer but also their energy distribution at the interface is crucial for efficient device operation<sup>259</sup>. There is a continuous distribution of states in the bandgap of ZnS near the interface and these can be explained by superimposing several sets of states originating from interface stress and/or dopant presence on the original states characteristic for a given interface<sup>260</sup>. Due to these states, direct tunnelling takes place on the leading edge of the electric pulse and phonon assisted tunnelling at the trailing edge. An estimation of the total number of interface states participating in tunnelling can be found from measurement of the conduction current above threshold voltages<sup>261</sup>.

## 8.3 Material Choice

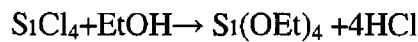
In selecting the material for the insulating layer it is important to consider the properties required for a given display. The advantages and disadvantages of a variety of insulators are shown in Table 8.1<sup>262</sup>. As it can be seen there is no one ideal insulating material and this makes the choice a hard one. The two insulating materials focussed on in this device are Ta<sub>2</sub>O<sub>5</sub> and SiO<sub>2</sub> and the properties of each film are discussed here.

Material	Advantages	Problems
BaTiO <sub>3</sub>	Excellent dielectric properties Moderate dielectric constant at submicron thicknesses Stable operation Excellent interface with ZnS Mn High brightness level	Crystallisation during annealing Interaction with ITO
Al <sub>2</sub> O <sub>3</sub>	Very stable Good self-healing properties High resistivity	Poor brightness characteristics Discoloration when adjacent to ITO
Ta <sub>2</sub> O <sub>5</sub>	Suitable dielectric constant High luminance level Low dissipation High charge storage capacity High resistivity	Poor breakdown characteristics Interaction with ITO Alteration of properties during annealing Poor adhesion to ZnS Interlayer formation when adjacent to Al
SiO <sub>2</sub>	High dielectric constant Moderate dielectric breakdown strength	Stability problems Severe charge trapping at the SiO <sub>2</sub> /metal interface
SiON	High dielectric breakdown strength Good barrier properties Good self-healing properties	Poor adhesion characteristics Image retention

**Table 8.1 Comparison of some different insulating materials**

### 8 3.1 Silicon Dioxide Thin Films

Silicon dioxide ( $\text{SiO}_2$ ) thin films are used in many industrial applications including microelectronics, optoelectronics and protective coatings. Both doped and undoped  $\text{SiO}_2$  films are frequently used in silicon integrated circuits as insulators between metals and as passivating layers<sup>263</sup>.  $\text{SiO}_2$  films have also found applications in areas such as sensors<sup>264</sup>, anti-reflective coatings<sup>265</sup> and high-speed logic circuits<sup>266</sup>. Since it has a wide area of application silicon dioxide thin films have been studied extensively. Various deposition methods have been used to form silicon dioxide films and these include oxidation<sup>267</sup>, CVD<sup>268</sup>, and sol-gel<sup>269-270</sup> processes. Interest in the sol-gel deposition of silicon dioxide has progressed since it was first developed over fifteen years ago<sup>271</sup>. The most common precursors used in the formation of silicon dioxide film are tetraalkoxysilanes, the most common of which are tetraethoxysilane (TEOS) and tetramethoxysilane (TMOS). TEOS is the preferred choice for this reaction. TEOS is formed when anhydrous ethanol is reacted with tetrachlorosilane as follows<sup>272</sup>



Solutions containing varying amounts of TEOS, ethanol and water were prepared with a small amount of 1M HCl to promote hydrolysis. It has developed into a general formulation for the formation of different film types having specific properties

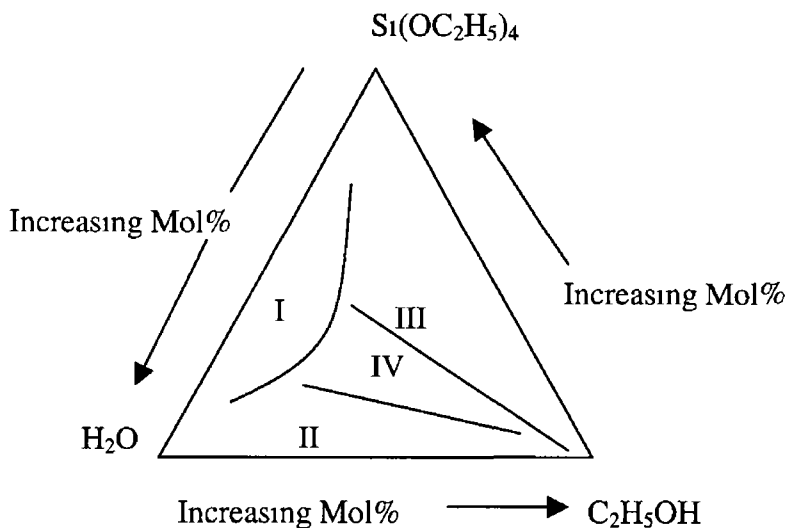
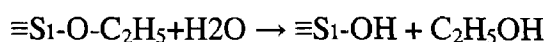


Figure 8 1 Triangular diagram showing the relationship between TEOS water and ethanol in a silicon dioxide thin film

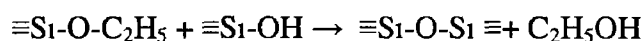
The structure of the sol can vary extensively depending on the conditions during the hydrolysis and condensation reactions. The relationship between the water, TEOS and the ethanol content allow the film properties to be tailored. The mixing possibilities are summarized in Fig 8 1<sup>273</sup>

The triangle can be divided into four areas. Area I represents the region where the components are not miscible with each other due to the low ethanol content. Area II the H<sub>2</sub>O/Si(OC<sub>2</sub>H<sub>5</sub>)<sub>4</sub> ratio, *R* is over 5 thus producing a solution that becomes elastic just before solidification making it unsuitable. In area III, *R* is less than 1.5 and thus the time required for the solution to become viscous and solidify is too long. Area IV is the area in which *R* ranges from 1.5 to 4. This is the ideal area for producing suitable thin films. The size of the sol particles and the density are primarily dependent on the pH and the *R* value. Generally an *R* value greater than 2 is required to complete hydrolysis and condensation<sup>274</sup>

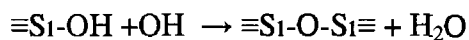
The chemical reactions can be classified as hydrolysis and esterification and are summarized as follows



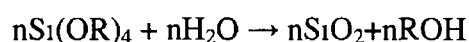
Followed by alcohol condensation



water condensation and hydrolysis



Thus the complete reaction can be summarized as



For the thin films used in the devices an *R* = 4 mix was used. The procedure is summarized in Fig 8 2. The silica sol was prepared by adding a TEOS to a solution containing ethanol and pH1 water, keeping the molar ratio of the water to TEOS equal to four. A molar ratio of 6-8 of ethanol/TEOS is used. This ratio determines the thickness of the films produced per dip. The films are deposited on silicon and glass substrates by dipping the substrates in the solution and withdrawing them at a rate of 1 cm/sec to produce a film thickness of approximately 50nm per dip. The humidity needs to be maintained at ~50% to ensure clear films. The deposited films are annealed at 260C between dipping and are post annealed for 1 hour at 700C

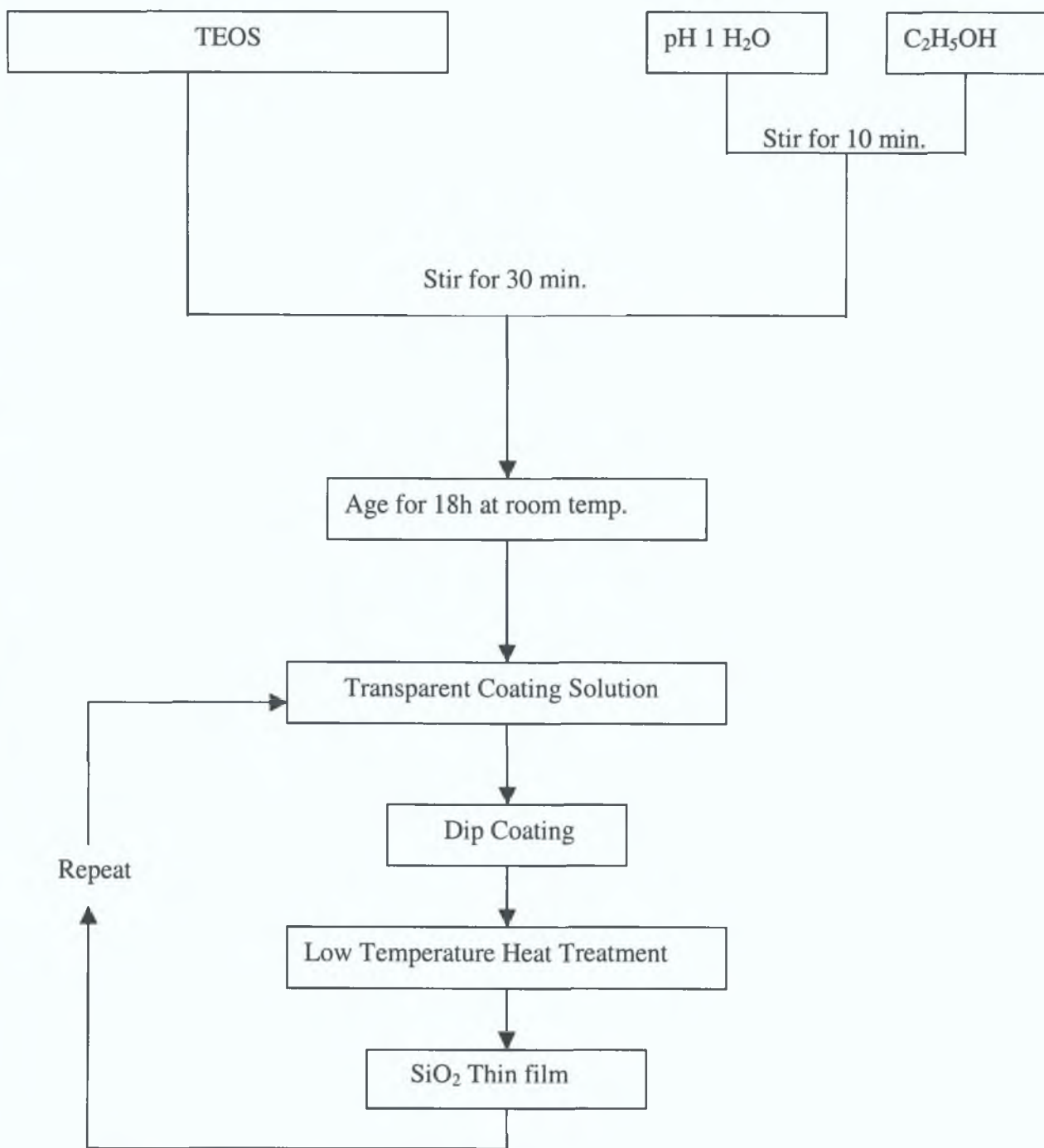


Figure 8.2 Outline of the sol-gel process for the production of  $\text{SiO}_2$  thin films.



The presence of SiO<sub>2</sub> was confirmed using FTIR as shown in Fig 8.3. The IR bands observed were the ~430, ~800, ~1080, and ~1220cm<sup>-1</sup> bands. The ~1080 and ~1220cm<sup>-1</sup> bands are the LO and TO Si-O-Si asymmetric stretching bands respectively.

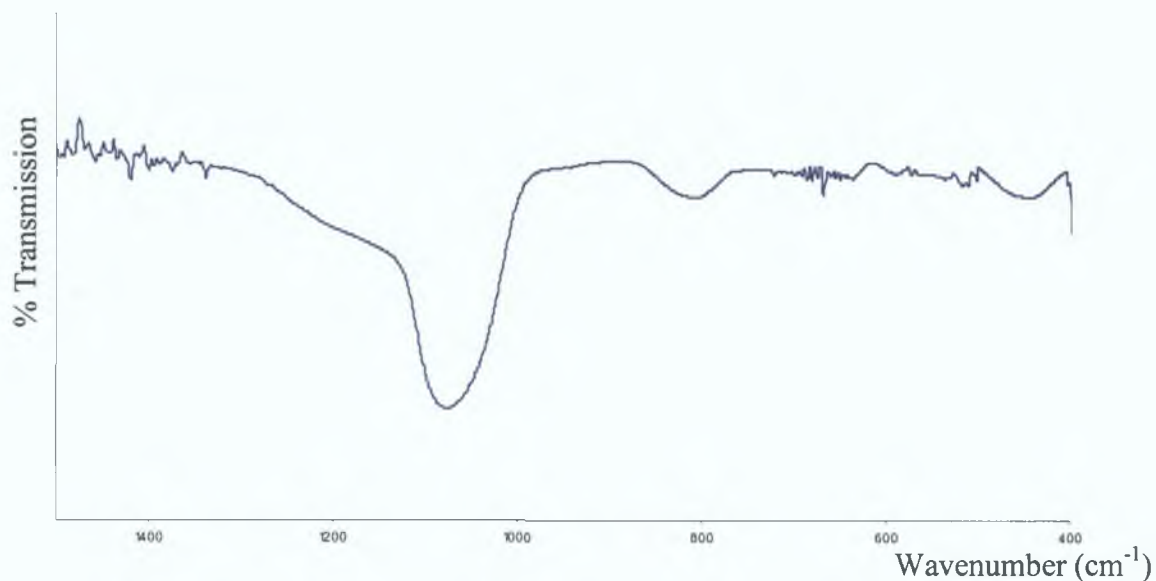


Figure 8.3 FTIR spectra of sol-gel produced SiO<sub>2</sub> thin film.

The ~800cm<sup>-1</sup> band is due to the symmetric Si-O-Si stretching or vibrational modes of the ring structures and the ~460cm<sup>-1</sup> band is due to the Si-O-Si bending mode. The refractive index was found to be 1.43.

### 8.3.2 Tantalum Pentoxide Thin Films

Tantalum pentoxide coatings have been used extensively in many optical and electronic applications. Because of their wide area of application<sup>275,276,277,278</sup> they have been studied both experimentally and theoretically over the past three decades. The scaling down of silicon integrated circuits has pushed conventional dielectric thin films to their physical limit and led to the study of insulators with high dielectric permittivity to enable an increase in the packing density of devices without a reduction in the insulator thickness<sup>279</sup>.

Tantalum pentoxide can be deposited using a variety of methods<sup>280</sup> including thermal oxidation of tantalum layers<sup>281</sup>, sputtering<sup>282,283</sup>, atomic layer epitaxy<sup>284</sup>, CVD<sup>285</sup> and sol-gel<sup>286,287, 288</sup> methods.

A problem associated with the growth of  $Ta_2O_5$  on silicon is the formation of a thin silicon dioxide layer at the  $Ta_2O_5/Si$  substrate interface as a result of the oxidation of the silicon. The thin oxide will reduce the dielectric constant of the system since the permittivity of  $SiO_2$  is equal to 3.9, which is 6 times less than that for amorphous  $Ta_2O_5$ . The growth of this layer is dependent on the deposition method and subsequent annealing processes. A high temperature oxidising atmosphere enhances it.



**Figure 8.4** SEM image of 60nm  $Ta_2O_5$  deposited by sol-gel method and annealed in  $O_2$  at 700C for 1 hr showing the polycrystalline structure with highly elongated,  $\sim 0.1\mu m$  wide, several  $\mu m$  long,  $Ta_2O_5$  crystals.

Ta<sub>2</sub>O<sub>5</sub> has two crystalline phases<sup>289</sup>, an orthorhombic phase and a hexagonal phase. The orthorhombic form can be divided into two forms, a high temperature form and a low temperature form called *L*-Ta<sub>2</sub>O<sub>5</sub>, with a reversible transition occurring at 1360C. Fig 8 4 shows a scanning electron microscope (SEM) image of an annealed Ta<sub>2</sub>O<sub>5</sub> film showing a polycrystalline structure. The deposition procedure and annealing process controls the structure of the Ta<sub>2</sub>O<sub>5</sub>. In electronic materials the dielectric material should have an amorphous structure, as in polycrystalline materials the electrical properties are poor due to the presence of grain boundaries. The sol-gel method allows for low temperature processing with high homogeneity in the deposited films. The layers are generally porous and contain amounts of CH-based groups that can be removed by thermal treatments. Control of the process allows for the formation of transparent pinhole free layers rather the opaque films with or without pinholes and cracks. The UV-Vis spectrum obtained for a 120nm Ta<sub>2</sub>O<sub>5</sub> thin film on glass is shown in Figure 8 5. This has a greater than 90% transmission in the visible region.

The following sol-gel method was used to obtain the films used in the devices<sup>290</sup>. The solution is prepared by reacting tantalum ethoxide (Ta(OC<sub>2</sub>H<sub>5</sub>)<sub>5</sub>) with ethanol. This was achieved using the sequence shown in Figure 8 6. Two solutions are prepared

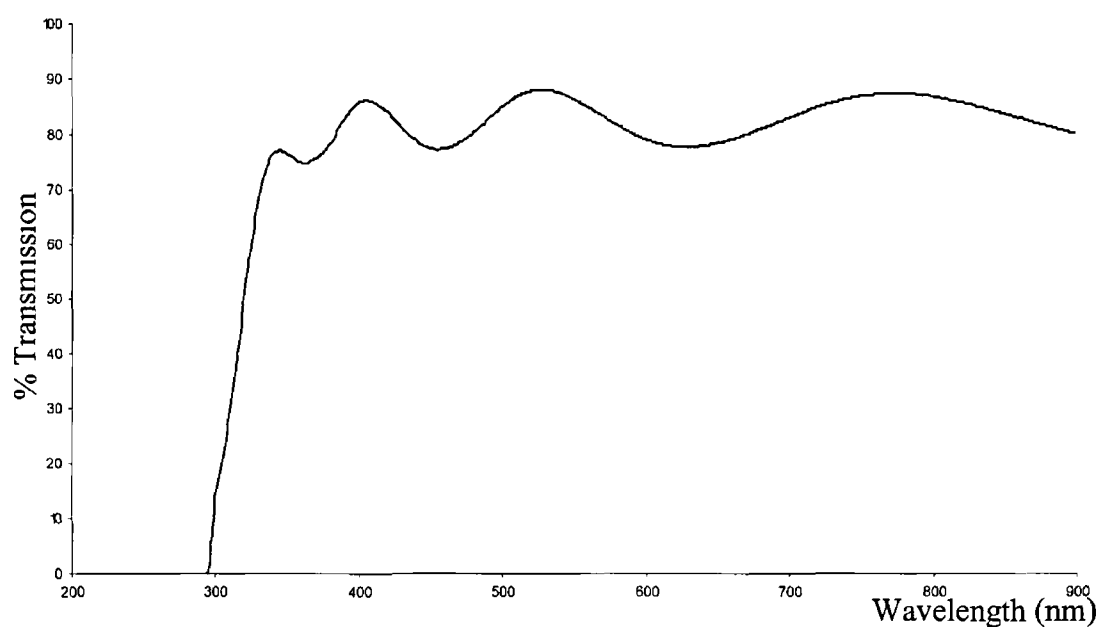


Figure 8 5 UV-Vis Spectrum of 120nm Ta<sub>2</sub>O<sub>5</sub> deposited on a glass slide

The first involved mixing  $\text{Ta}(\text{OC}_2\text{H}_5)_5$  with ethanol and acetic acid while stirring for 30 minutes and the other involved Ethanol and acetic acid stirred for 10 minutes. These solutions are then mixed and stirred for 18 hours to produce a clear coating solution.

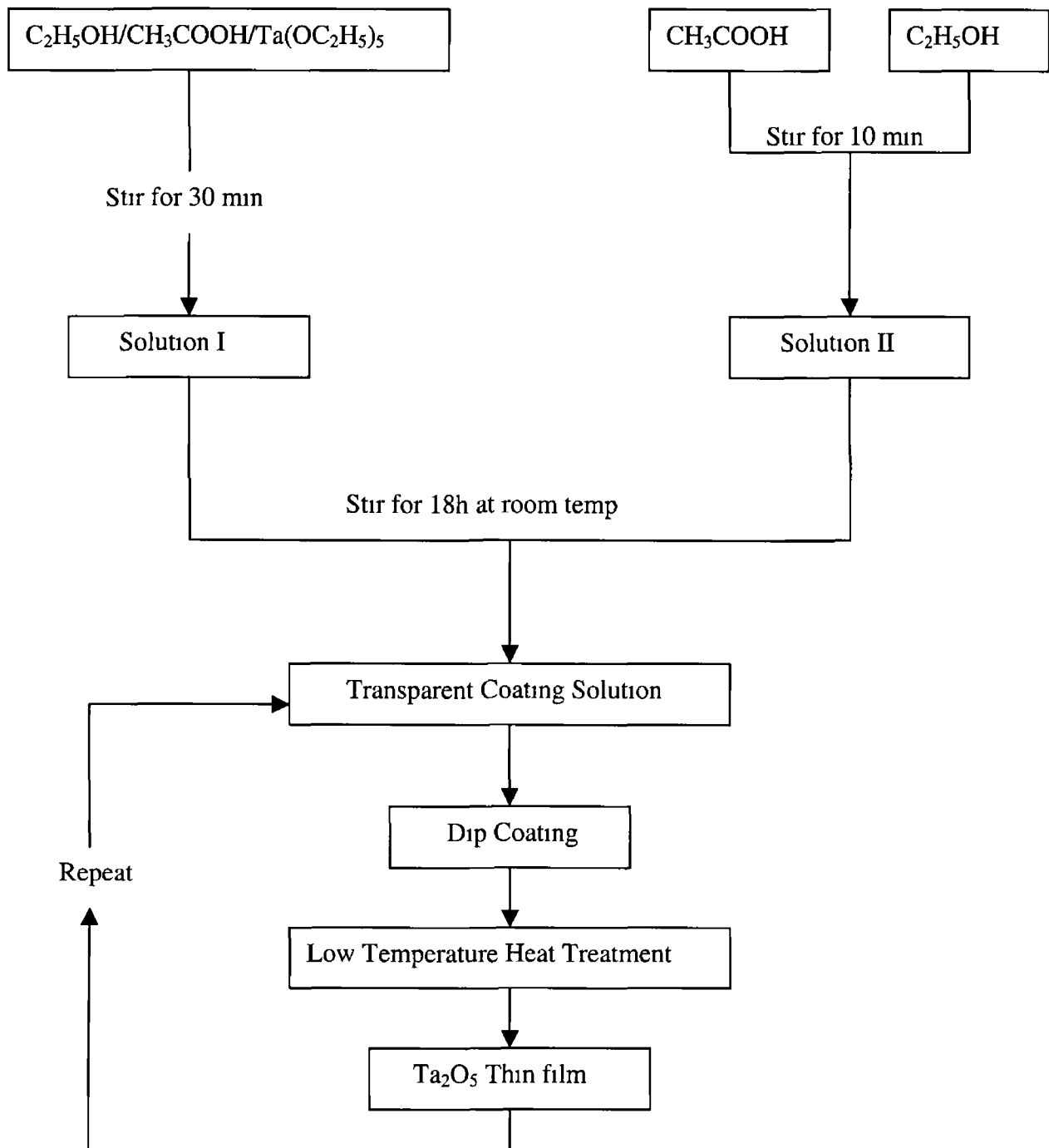


Figure 8.6 Sol-gel Process for  $\text{Ta}_2\text{O}_5$  films

The tantalum oxide films are obtained by dipping the substrates in the solution and withdrawing them at a rate of 1.2 cm/sec to produce a film thickness of approximately 60nm. The humidity needs to be maintained at 45% to ensure clear films. These are heat treated at 260C in between dips and thicker films may be obtained by repeat dipping. The films are then annealed in an oxygen atmosphere for 1 hour at 700C. The presence of tantalum oxides was confirmed using FTIR spectrometry as shown in Fig. 8.7. The dominant feature is the 650cm<sup>-1</sup> absorbance band associated with the Ta-O-Ta and Ta-O stretching vibrational modes. This band is present in the 600°C spectrum. The shift of the absorbance peak to 530cm<sup>-1</sup> in the 700°C spectrum is indicative of the crystallisation of the tantalum oxide as confirmed by XRD as described below. There is evidence of suboxides in the absorption band present in the range 800-1000cm<sup>-1</sup> due to TaO and TaO<sub>2</sub><sup>291</sup>. There are no C-H bands present at 1400-2900cm<sup>-1</sup> as these have been removed by the heat treatment.

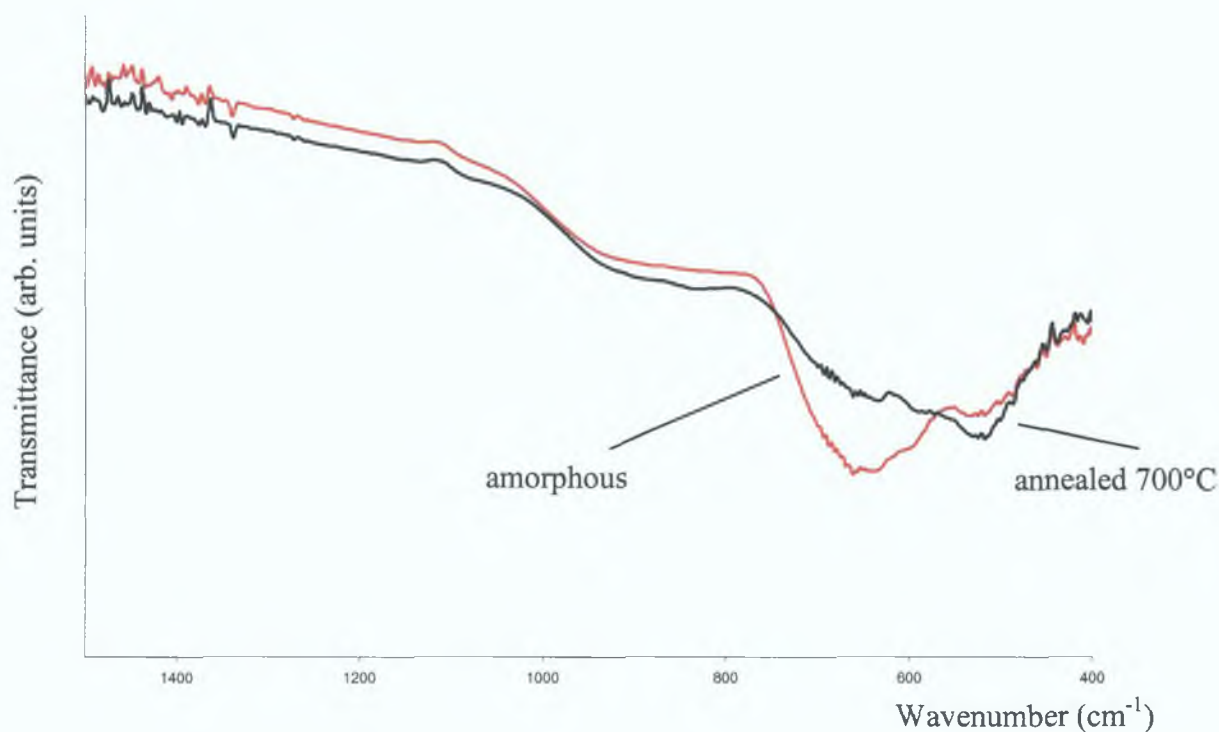


Figure 8.7 FTIR of amorphous and crystalline Ta<sub>2</sub>O<sub>5</sub> films on a silicon substrate

There is also no absorbance at  $1070\text{ cm}^{-1}$  showing that no interstitial layer of  $\text{SiO}_2$  between the silicon substrate and the  $\text{Ta}_2\text{O}_5$  has been formed. These layers, which can form when  $\text{Ta}_2\text{O}_5$  is deposited on silicon substrates, have been shown to significantly reduce the effective dielectric constant of the insulator<sup>292</sup>.

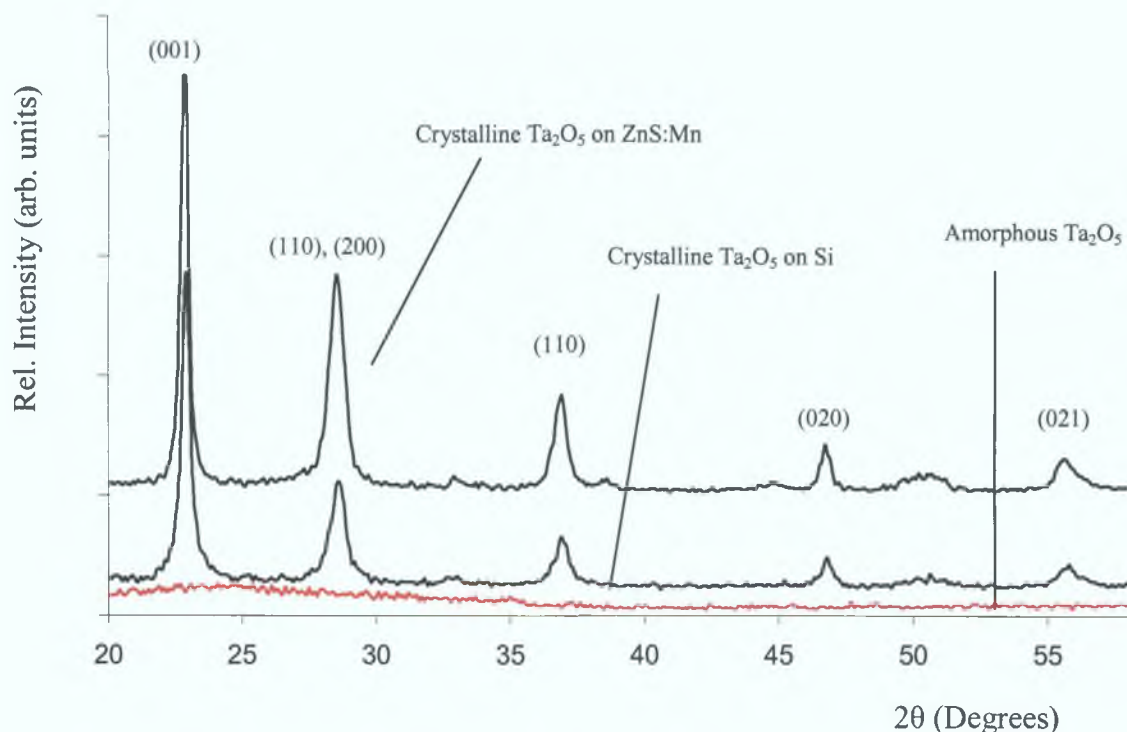


Figure 8.8 XRD spectra from  $\text{Ta}_2\text{O}_5$  films showing the amorphous state when annealed at  $600^\circ\text{C}$  and the crystalline state when annealed at  $700^\circ\text{C}$

The crystalline state of the tantalum oxide was examined using XRD measurements.  $\text{Ta}_2\text{O}_5$  has two crystalline phases<sup>293</sup>, an orthorhombic phase and a hexagonal phase. The orthorhombic form can be divided into two forms, a high temperature form and a low temperature form called  $L\text{-Ta}_2\text{O}_5$ , with a reversible transition occurring at  $1360^\circ\text{C}$ . Fig. 8.8 shows the difference between the XRD patterns for the  $\text{Ta}_2\text{O}_5$  annealed at  $600^\circ\text{C}$  and  $700^\circ\text{C}$  for one hour on oxygen at atmospheric pressure. The  $\text{Ta}_2\text{O}_5$  annealed at  $600^\circ\text{C}$  (and below) has an amorphous structure and the  $\text{Ta}_2\text{O}_5$  annealed at  $700^\circ\text{C}$  has a randomly oriented polycrystalline structure. The presence of peaks at  $2\theta = 22.84^\circ$  (001),  $28.29^\circ$  (110),  $28.77^\circ$  (200),  $36.66^\circ$  (111),  $46.66^\circ$  (002),  $47.78^\circ$  (020) and  $55.47^\circ$  (021) confirm the orthorhombic structure of the film (Card

No 89-2843 JCPDS) The main insulator properties that need to be considered for the efficient functioning of the device are its dielectric constant and its dielectric breakdown strength. A high dielectric constant will reduce the driving voltage required for the display but will also reduce the breakdown strength. The  $Ta_2O_5$  had a dielectric constant of approximately 20 when deposited and this increased with anneal temperature as shown in Fig. 8.9 up to a maximum of 50 when annealed at 700°C.

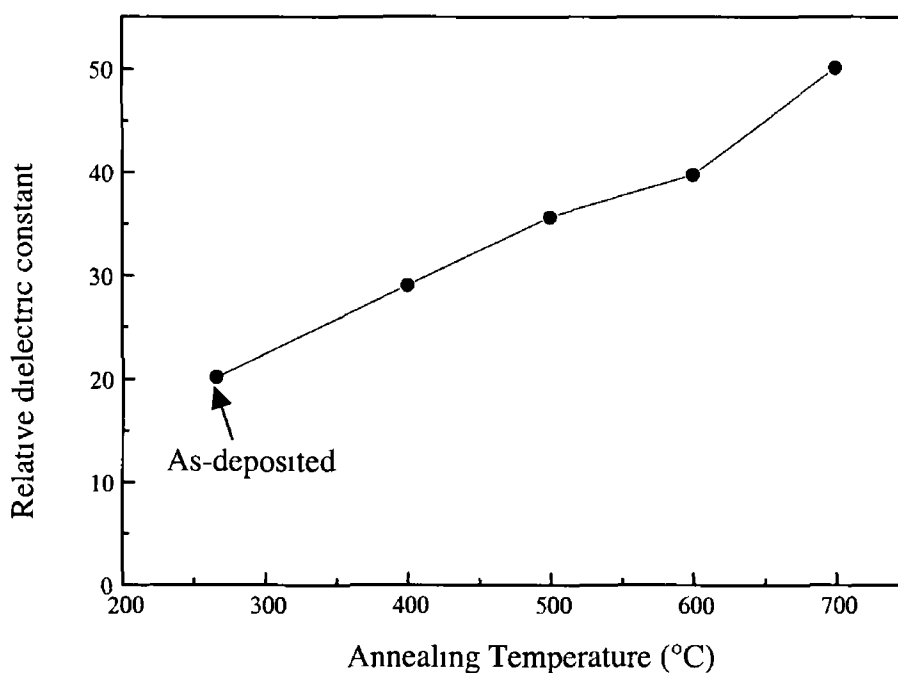


Figure 8.9 Variation of the relative dielectric constant of  $Ta_2O_5$  as a function of annealing temperature in oxygen<sup>292</sup>

The resistivity of the films also increased with increasing anneal temperature as shown in Fig. 8.10. The resistivities, which were measured at a field of  $1 MV cm^{-1}$ , show an as-deposited resistivity of  $1.3 \times 10^{11} \Omega\text{-cm}$  that increased to a maximum value of  $1.39 \times 10^{12} \Omega\text{-cm}$  when annealed at 700°C.

## 8.4 Conducting Thin Films.

### 8.4.1 Introduction

The large interest in transparent conductive thin films for optoelectronic devices such as solar cells<sup>294</sup>, liquid crystal displays, transducers<sup>295</sup>, sensors<sup>296</sup>, heat mirrors and

multiplayer photo-thermal conversion systems has led to the optimisation of the electro-optical properties of these films

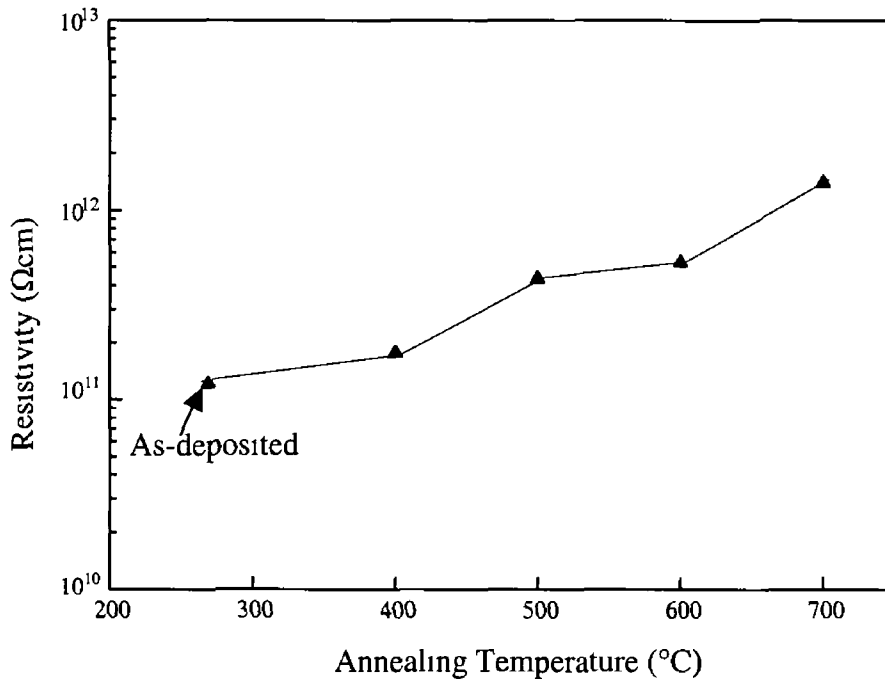


Figure 8 10 Variation of the resistivity of  $Ta_2O_5$  films as a function of annealing temperature, measured at a field of  $1 MVcm^{-1}$ <sup>297</sup>

#### 8.4.2 Zinc Oxide and doped Zinc Oxide thin films

Zinc oxide (ZnO) has attracted interest as a transparent conductive coating material because the film

- i) consist of abundant and cheap non-toxic elements
- ii) is readily producible as large scale coatings and
- iii) allows tailoring of the UV absorption
- iv) has a high electrochemical stability and
- v) a large bandgap

Also the resistivity of ZnO can be modified by the addition of impurities<sup>298</sup> Non-stoichiometry of the films resulting from the presence of oxygen vacancies and interstitial zinc determine the properties exhibited by ZnO<sup>299</sup> The electrical behaviour of the films can be improved by replacing  $Zn^{2+}$  atoms with elements having



a higher valance number such as Group III atoms including  $\text{In}^{3+}$ ,  $\text{Al}^{3+}$  and  $\text{Ga}^{3+}$ . The choice of the impurity also has to take into account the size of the ionic radius to avoid lattice distortions. The electro-optical properties are generally dependent on the deposition and annealing conditions because these change significantly with the absorption and desorption of oxygen that occurs during these procedures. There are many methods of depositing ZnO and doped ZnO thin films and these include sputtering<sup>300,301,302</sup>, evaporation, chemical vapour deposition<sup>303,304,305</sup>, spray pyrolysis<sup>306,307</sup>, molecular beam epitaxy<sup>308</sup> and sol-gel<sup>309</sup> deposition.

The following sol-gel method was used to obtain the films used in the devices. A solution of ZnO precursor was made by dissolving 6wt % zinc acetate 2-hydrate in anhydrous ethanol by heating to 80°C while stirring and refluxing. The solution is cooled quickly to prevent the zinc acetate from crystallising out of the solution. Ethanol was chosen over methanol due to its increased surface wettability. To achieve aluminium doping aluminium chloride ( $\text{AlCl}_3$ ) or aluminium nitrate ( $\text{Al}(\text{NO}_3)_3 \cdot 9\text{H}_2\text{O}$ ) is added to the solution. Previous studies have shown that 0.8 at % Al Zn produces films with high conductivity<sup>310</sup>. The precursor is hydrolysed using two mols  $\text{H}_2\text{O}$  per mol zinc acetate. This is achieved by forming a 10vol%  $\text{H}_2\text{O}$  solution in ethanol and adding the correct amount dropwise to the precursor. Lactic acid is added to the solution from a 5vol% in ethanol solution. The solution should be clear and colourless. Adding extra concentrated acid can eliminate precipitation. Another method of hydrolysing zinc acetate was investigated. Since zinc acetate dissolves easily in water, these were combined first, keeping the molar ratio correct. The ethanol was added to the solution in a 3:1 vol ratio. Lactic acid was added from a 5 vol% ethanol solution, since the addition of concentrated acid quickened the gelation time to a matter of 7-10 minutes. The coating procedure was then carried out at a dipping speed of 1.2  $\text{cm s}^{-1}$ . There is a strong coordination of  $\text{Zn}^{2+}$  ions in aqueous solution therefore the surface interaction is weak in this case<sup>311</sup>. The coatings obtained had adhesion and crazing problems therefore the former method was chosen as a primary method for producing the coating solution.

The substrates used were both glass slides and silicon wafers. The glass slides were cleaned in deionized water and dried in nitrogen. The silicon dioxide layer was removed using a buffered hydrofluoric acid (BHF) solution<sup>312</sup> and they were dried in nitrogen. The coating procedure is then carried out. After coating the substrate is

dried at a low temperature of 260°C for 10 minutes. The temperature is increased at a ramp rate of 10°C/min in each case. The substrate may then be recoated to obtain thicker coatings. The coating procedure is summarised in Fig 8.11. Final annealing takes place when the desired thickness is achieved. The film will shrink during the heating process. This must be taken into account when the thickness is being estimated by the number of runs. Cracking and crazing may take place if the deposited film is too thick.

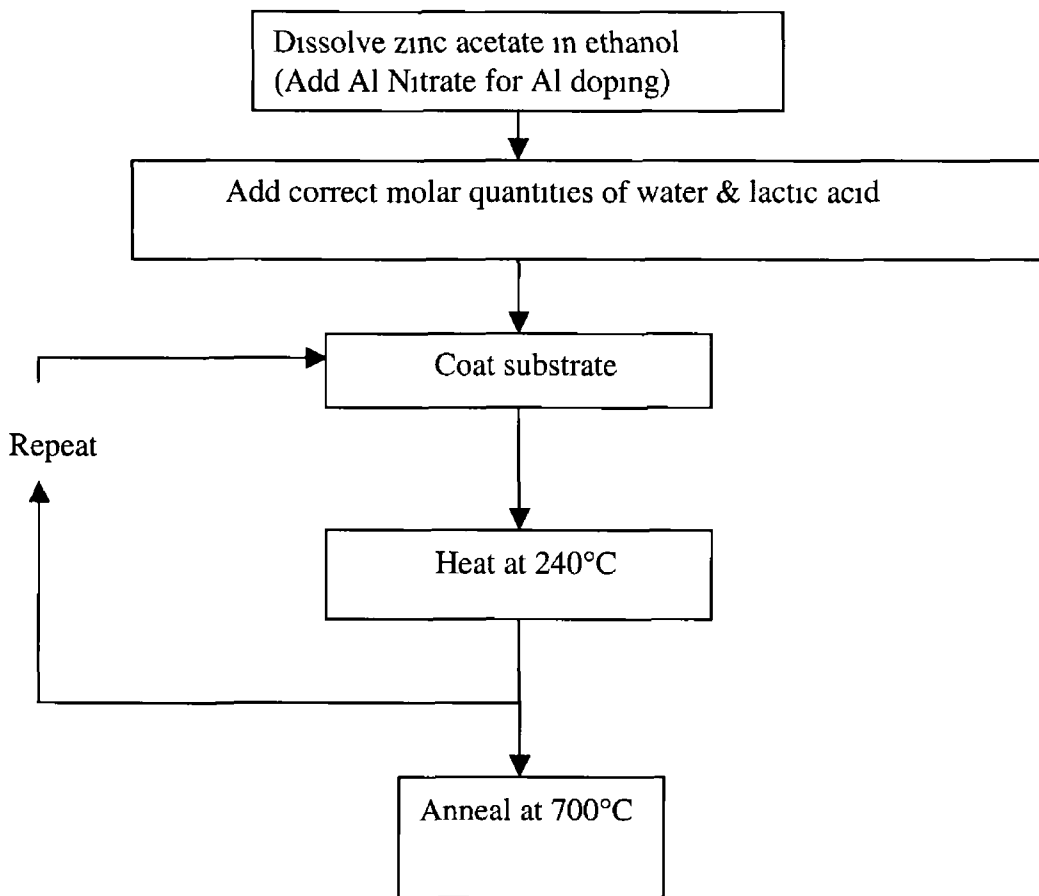


Figure 8.11 Flow diagram of sol-gel deposition process for ZnO & ZnO:Al thin films

The presence of Zinc oxide was verified using IR spectroscopy. The bonding structure of the films on silicon substrates were studied using IR spectroscopy which was carried out on a Perkin-Elmer 983G spectrometer in the transmittance mode in the range  $400\text{-}4000\text{ cm}^{-1}$ , using a bare silicon substrate as the reference. Zinc Oxide has a strong absorption band centred on  $420\text{ cm}^{-1}$ . This was located in films that had been annealed at  $500^\circ\text{C}$  as shown by the spectrum for an  $180\text{ nm}$  thick sample in Figure 8.12.

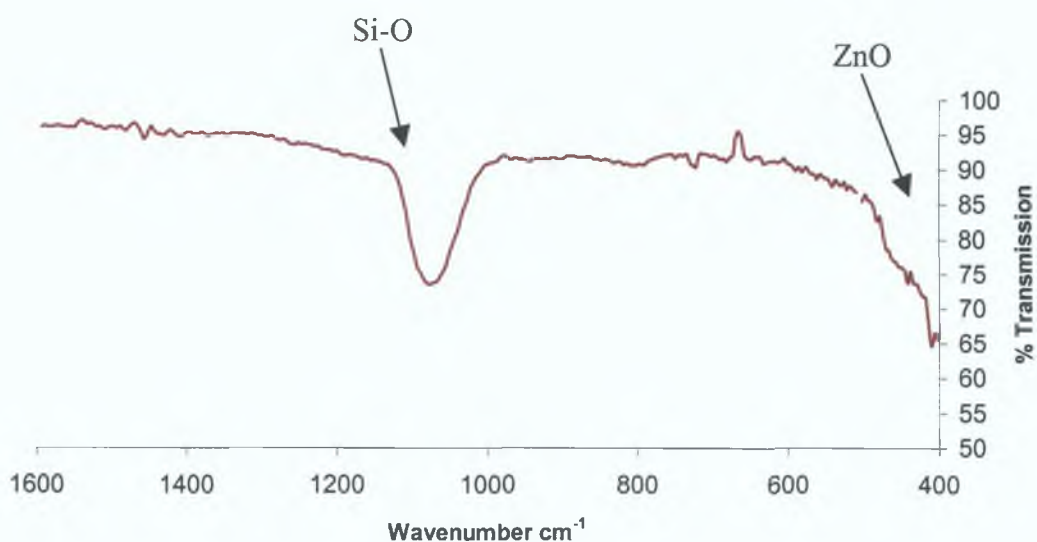


Figure 8.12 FTIR spectrum for an  $80\text{ nm}$  ZnO thin film annealed at  $500\text{ C}$  on  $\text{SiO}_2$

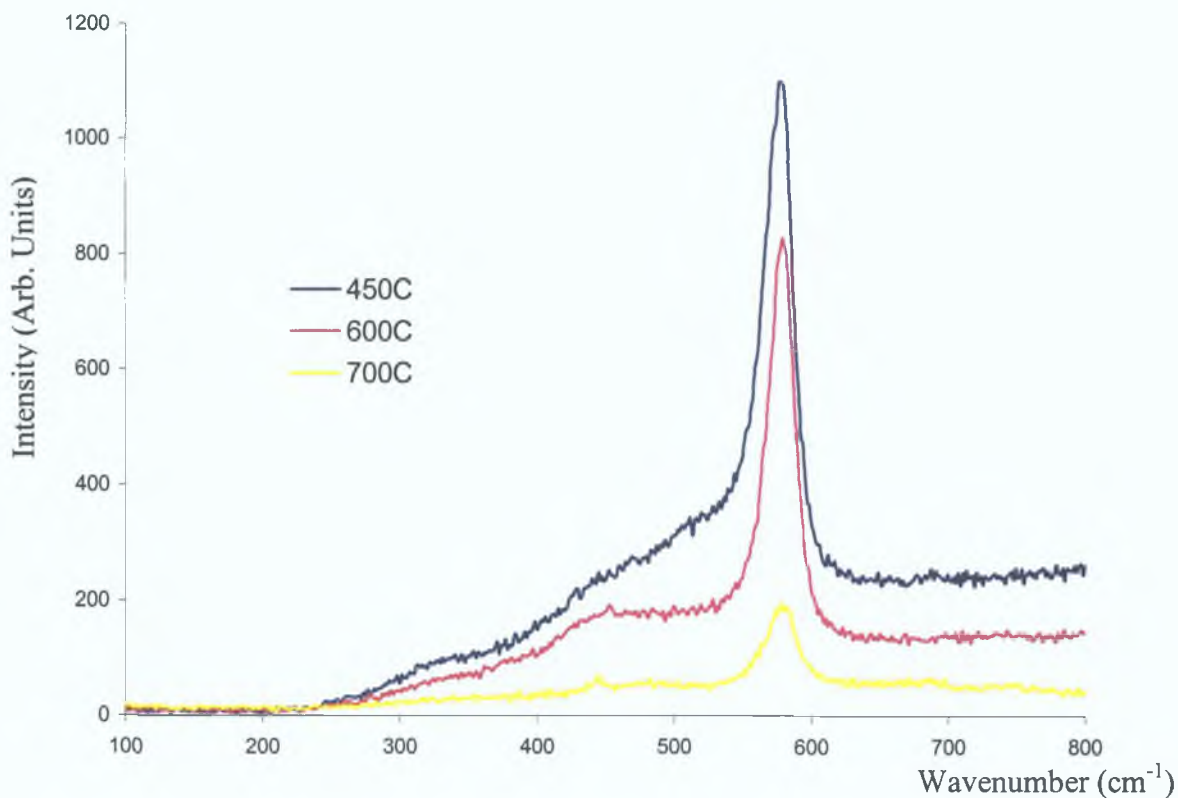


Figure 8.13 Raman studies of ZnO:Al annealed in air at different temperatures.

Raman studies on the ZnO:Al also showed the longitudinal optical (LO)  $E_1$  mode at  $583\text{cm}^{-1}$ . This peak decreased in intensity as the anneal time of the films was increased as shown in Fig 8.13. This peak is due to excess zinc and an oxygen deficiency and its intensity decreases as the zinc is oxidized at the higher temperatures<sup>313</sup>.

Crystalline properties were investigated by X-ray diffraction using Cu  $K\alpha$  line at either a  $10^\circ$  glancing angle or  $\theta$ - $2\theta$  configuration. Patterns taken on samples exhibited a high degree of orientation even on glass substrates. The presence of the three peaks at  $2\theta=31.75$  (100),  $34.44$  (002) and  $36.25$  (101) shows that the ZnO films have a hexagonal structure. From the relative intensities it can be seen that there is a strong preferential orientation with the c-axis perpendicular to the substrate surface. The normal stable state of ZnO is the cubic, zincblende structure, however here the metastable hexagonal structure is obtained. This form is obtained whether bare or oxidised silicon is used as the substrate, therefore it is not caused by the influence of the silicon lattice. Fig. 8.14, a typical  $\theta$ - $2\theta$  diffractogram shows peaks characteristic

of hexagonal ZnO. The degree of orientation depends on the amount of water added and the temperature of the heat treatment.

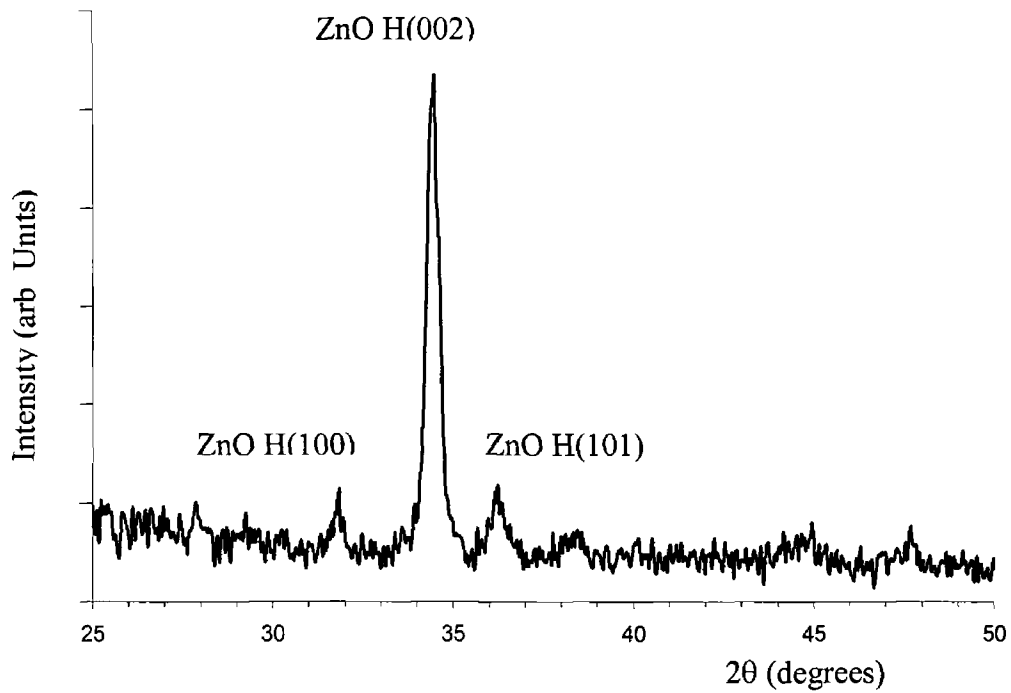
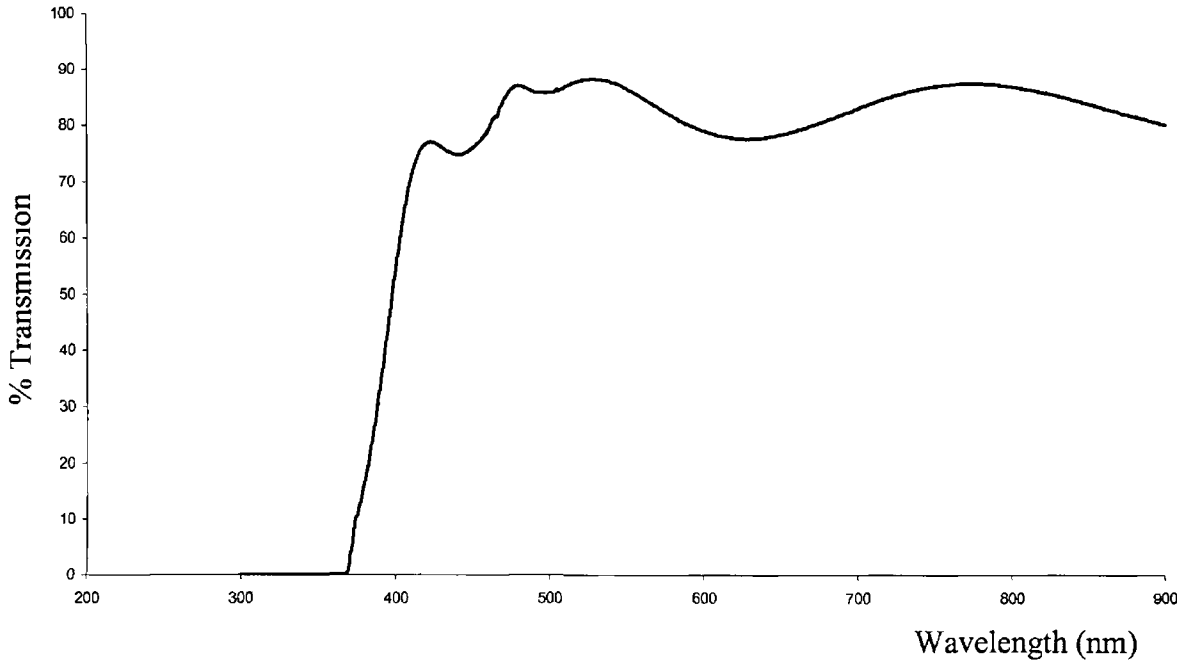


Figure 8 14 XRD pattern for ZnO Al thin film annealed at 700C for 1 hour

#### 8 4 2 1 Optical properties

A UV-visible scan on the samples shows a featureless, greater than 85% transmission in the visible with a strong absorption slope towards the UV. The band edge is seen to move towards the UV region when annealing in a vacuum takes place as seen in a typical scan of a 200nm thick ZnO Al film annealed at 450°C is shown in Figure 8 15



*Figure 8 15 UV-Vis spectral scan of a ZnO Al thin film on a glass slide substrate*

## 8.5 Conclusions

In this chapter the importance of the choice of the insulating and the conducting films has been discussed. It is important that the films chosen are compatible with the application. In this case this leads to the necessity of the films having the following properties:

In the case of the insulating materials they must

- 1 be transparent
- 2 have a self-healing repair mechanism
- 3 adhere to the other films in the stack
- 4 enhance the EL process
- 5 have a high dielectric strength

The reaction of the insulating film to the electric field and the generation of interface states for the electrons are also key qualities. Two films that meet these criteria are  $\text{SiO}_2$  and  $\text{Ta}_2\text{O}_5$  and these have been selected for use in the ACTFEL devices tested.

For the conducting films, they must

- 1 be transparent

- 2 have a low resistivity
- 3 adhere to the other films in the stack

In this case ZnO Al has been chosen as it meets these criteria In some of the test devices semi-transparent aluminium is used as the top electrode but this would be unsuitable for the final device, as it does not meet criterion 1

## Chapter 9

### Display Characteristics

#### 9.1 Introduction

The thin film electroluminescent device needs characterisation in several different areas. The primary areas of interest are the electrical and electro-optical behaviour of the device but the material properties as well as the structure needs to be addressed. This interaction and the possible material consequences have been discussed in the previous chapter.

In this chapter an overview of the different areas of characterisation specific to the operation of the display are given and this is followed by a description of the devices manufactured and the results obtained for the devices. The results obtained include the material and electrical considerations discussed in Chapter 2.

#### 9.2 Electro-optical Properties

A variety of models have been proposed for an ACTFEL device. Before discussing the electrical and optical properties of the device it is important to simulate how an ideal device works and the parameters that need to be measured and optimised.

##### 9.2.1 Ideal Model

This model treats the insulating layers of the device as perfect capacitors. The first and second insulating layers can be incorporated into one effective insulating layer with the effective capacitance per unit area  $C_1$  given by

$$C_1 = \left( \frac{C_{i_1} C_{i_2}}{C_{i_1} + C_{i_2}} \right) \quad (9.1)$$

where  $C_{i_1}$  and  $C_{i_2}$  are the capacitances per unit area of insulator one and insulator 2 as shown in Fig 9.1 and the equivalent circuit is shown in Fig 9.2.



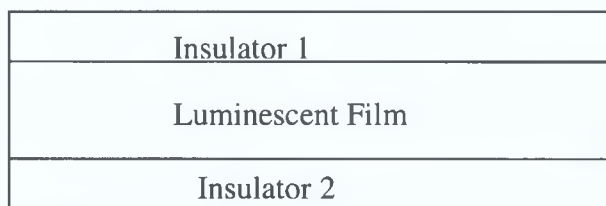


Figure 9.1 Simplified Thin Film Electroluminescent display

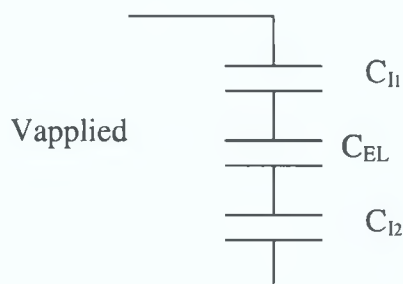


Figure 9.2 Equivalent circuit for an electroluminescent display below threshold

The electroluminescent layer also has a capacitance given by  $C_{EL}$  when the device is below the threshold voltage  $V_{TH}$ . Above this threshold voltage the device becomes conductive and a dissipative current flows giving rise to light emission. Therefore this film can be simulated by a capacitor in parallel with a non-linear resistor as shown in Fig. 9.3<sup>314</sup>. Above the threshold voltage the resistive branch turns on and current flows to discharge the voltage across the phosphor capacitor back to the threshold level while also supplying current to charge up the insulating layer capacitor by an equal voltage increment to maintain a constant voltage across the device. The luminance of the device is proportional to the power consumed in this resistive branch. Thus the proportionality constant is the experimentally determined luminous efficiency  $\eta$ , in units of lumens/watt (lm/W). Analysis of this model shows the dependence of the device performance on structure parameters such as layer thickness, dielectric constant, dielectric breakdown strength, threshold field and luminous efficiency<sup>315</sup>. In the ideal case this nonlinear resistor can be replaced by two back-to-back zener diodes. This will give the I-V characteristics shown in Fig 9.4.

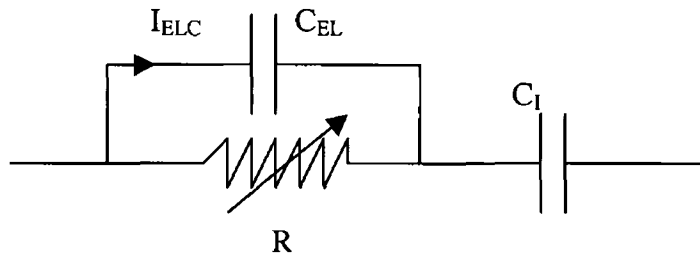


Figure 9 3 *Ideal circuit for a Thin film Electroluminescent Display*

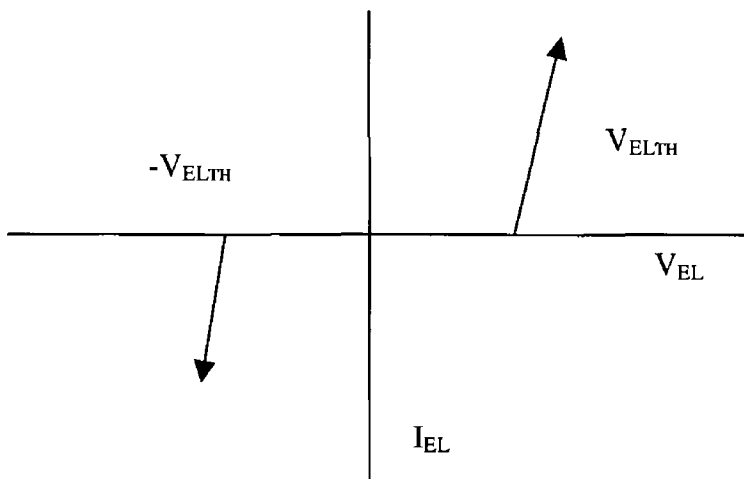


Figure 9 4 *I-V Characteristics for an ideal Electroluminescent Display*

Real devices will also include influences from the interfaces, which control the release of primary carriers and these are dealt with separately

The basic ACTFEL device can be modelled as a simple circuit where the insulators are represented by perfect capacitors and the phosphor layer is represented by a capacitor below threshold and by a pair of back-to-back diodes above threshold<sup>316</sup>

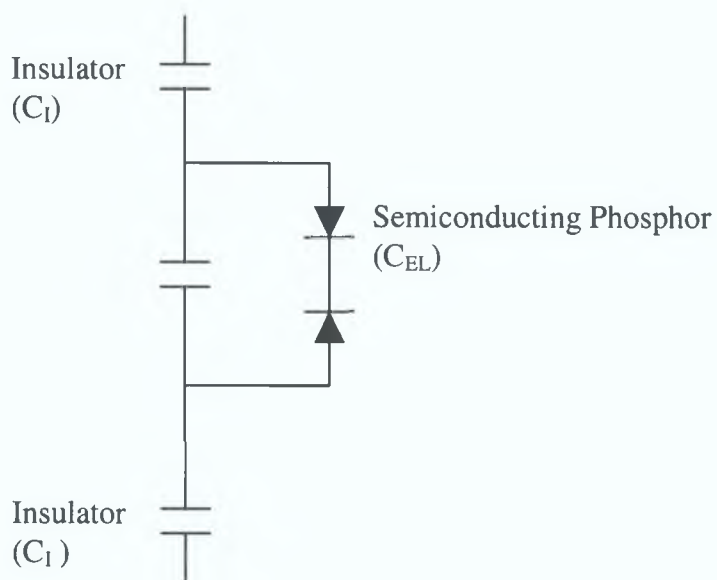


Figure 9.5 Equivalent Circuit Diagram for an ACTFEL Device.  $C_I$  and  $C_{EL}$  are the insulator and phosphor capacitance respectively.

The device below threshold is a three series capacitor circuit where the voltage drop across each layer is proportional to the dielectric constant and the layer thickness. Assuming a loss free capacitance at low applied voltages, a constant displacement current flows and no EL emission takes place. For light emission to take place the power converted into light must be deposited to the phosphor layer by a dissipative current. At threshold, the electrons are injected by tunnelling into the phosphor layer and, the phosphor layer experiences a Zener breakdown. This produces a real current, represented by the back-to-back Zener diodes in the diagram, which is transported across the phosphor layer. Above threshold the estimated capacitance is the total capacitance of the insulating layers in series, with the phosphor layer being shunted. The electrons in the interface states between the phosphor layer and the insulating layer are injected into the conduction band through a tunnelling effect. This indicates that the phosphor layer loses its insulating characteristics. Also, the electric field of the phosphor is kept at a constant value or clamped above threshold<sup>317 318</sup>. This indicates that the excess voltage is placed across the insulating layers, highlighting the importance of the insulating layers against the dielectric breakdown of the EL device. EL emission is due to this electron flow, therefore the current and the transferred charge are important parameters in the analysis of the EL emission mechanism.

## 9.2.2 Polarization Characteristics

The light emission from a device is strongly dependent on the polarity of the preceding pulse<sup>319</sup>. If the polarity of the preceding pulse is the same the light output is low and if it is inverted the light output is high. This is due to the polarization of the electrons at the interface of the phosphor/insulator. The voltage pulse creates a strong field that accelerates the electrons within the phosphor layer. After travelling across the phosphor layer and exciting the Mn luminescent centres they accumulate in the interface states between the phosphor and the insulator. They remain for a long time after the pulse is removed. Thus if the polarity of the next pulse is the same as the last pulse the inner electric field across the phosphor is lowered. In some circumstances this can lead to a second light pulse at the trailing edge of the electrical pulse<sup>320</sup>. When the polarity of the next pulse differs from the first pulse the inner electric field is enhanced due to the additive polarization. Thus the devices are driven with an alternating voltage supply.

## 9.2.3 Charge v Voltage Characteristic

In characterising the device the charge-voltage diagram (Q-V) allows the process to be viewed from an electrical viewpoint. This can be measured using a measuring circuit based on a Sawyer-Tower circuit as shown in Fig.9.6. The circuit is set up where the charge density Q is given as

$$Q = \frac{C V_s}{A} \quad (9.2)$$

where  $V_s$  is the partial voltage drop across the sense capacitor and A is the test area of the EL device.

Initially there is no stored polarization charge so that at zero volts there is zero charge. Since below the threshold voltage the EL device can be considered as a series of capacitors, the Sawyer-Tower circuit acts as a simple capacitive voltage divider<sup>321</sup>.

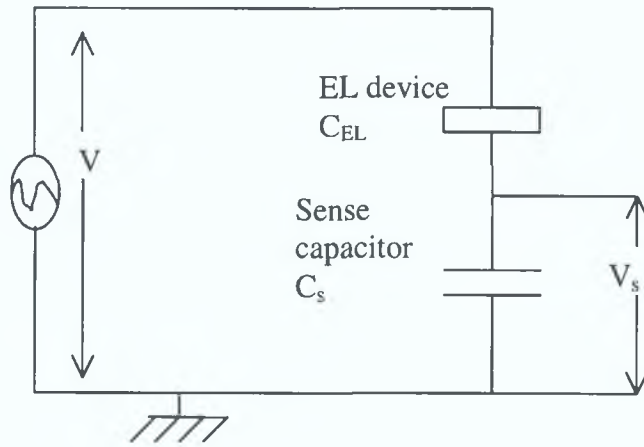


Figure 9.6 Charge-Density versus Voltage (Q-V) Characteristic measuring circuit.

The Q-V diagram is given by the straight line passing through the origin with a slope  $C_i$  given by

$$Q = C_i V \quad (9.3)$$

The slope of the curve ( $dQ/dV$ ) is equal to the total capacitance of the insulators and the phosphor layer. At the threshold voltage the phosphor breaks down and the slope of the Q-V diagram increases sharply. The new slope is equal to the series capacitances only. Above the threshold voltage, when the voltage is cycled through an entire a.c. loop a hysteresis loop is formed and the Q-V diagram is represented by a parallelogram as shown in Fig. 9.7<sup>322</sup>. At sub-threshold voltages ellipses can also be obtained. The parallelogram spreads out equally from the  $Q = C_i V$  line as the voltage is increased from  $V_{th}$ .

$C_{EL}$  is given by the slope of the sides crossing the ordinate and the slope of the remaining sides in the high voltage region is given by  $C_i$ , the capacitance per unit area of the insulators taken alone. The threshold voltage  $V_{th}$  and the threshold charge density can be determined from the point of intersection of two straight lines: the

$Q=C_{EL}V$  straight line below threshold and the straight line in the high-voltage part of the Q-V parallelogram

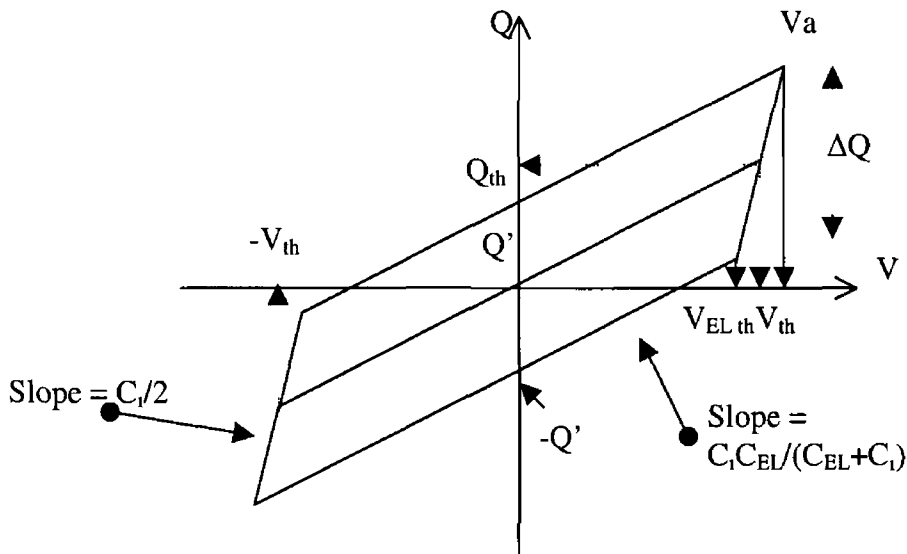


Figure 9.7 Charge density versus voltage (Q-V) characteristic diagram with definitions of physical quantities

The equation of the straight line in the high voltage part of the Q-V parallelogram in the first quadrant, is given by

$$Q - Q_{th} = C_1(V - V_{th}) \quad (9.4)$$

where

$$Q_{th} = C_1 V_{th} \quad (9.5)$$

thus

$$Q = C_1(V - V_{ELth}) \quad (9.6)$$

and

$$V_{ELth} = \frac{C_1}{C_1 + C_{EL}} V_{th} \quad (9.7)$$

The energy density delivered to the EL pixel per cycle,  $E_{in}$ , ie the input power density per cycle, is given by the device area encompassed within the Q-V diagram. The input power delivered to the test area,  $P_{in}$  is just the drive frequency times  $E_{in}$ . Assuming a parallelogram form for Q-V diagram,  $E_{in}$  and  $P_{in}$  are given by<sup>323</sup>

$$E_{in} = 2V_{ELth} \Delta Q = 4V_{th} Q' \quad (9.8, 9.9)$$

$$P_{in} = fE_{in} = 4fV_{th} Q'$$

Thus, the power as a function of the applied voltage,  $V_a$  is

$$P_{in} = 4fC_i (V_a - V_{th}) V_{ELth} \quad (9.10)$$

and hence the luminance is

$$L = \frac{1}{\pi} \eta P_{in} = \frac{4}{\pi} \eta f C_i (V_a - V_{th}) V_{ELth} \quad (9.11)$$

The  $\pi$  factor is due to the assumption that the surface of the EL device is a perfectly diffuse surface. The assumptions made to simplify the above equation are

- 1) that the luminous efficiency  $\eta$  is assumed to be independent of the electric field and the phosphor thickness and
- 11) that all the charge is transferred at  $V_{ELth}$  and not at higher voltages

The following simulation of Q-V shown in Fig 9.8 and Fig 9.9 was found using the circuit as shown in Fig 9.5 and the measuring system used in Fig 9.6

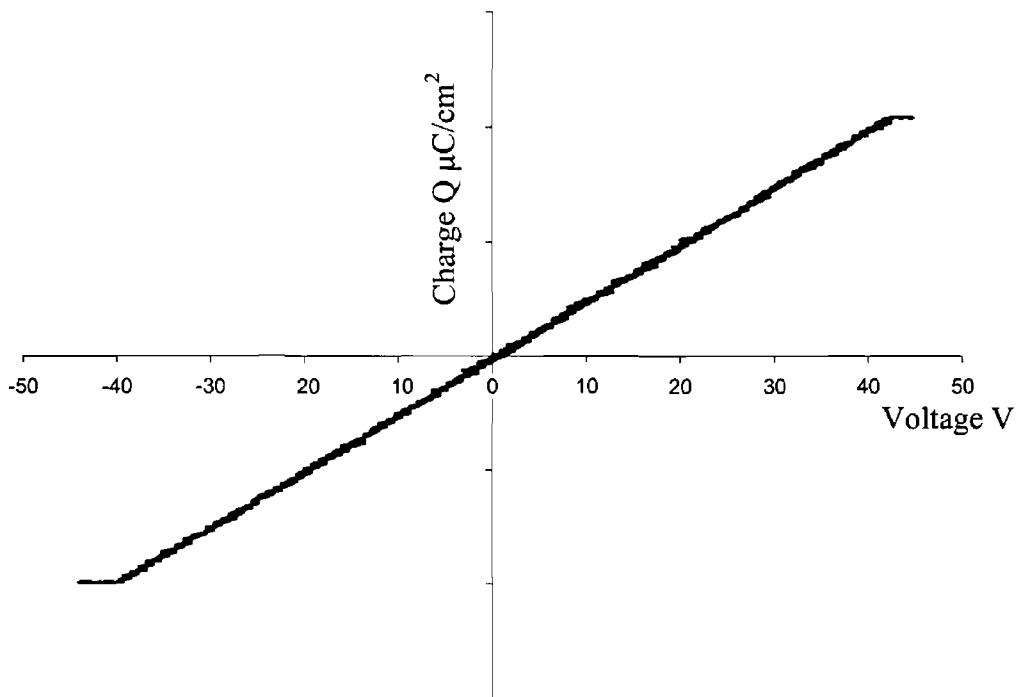


Figure 9.8 The Q-V response of the capacitive section of the device below threshold

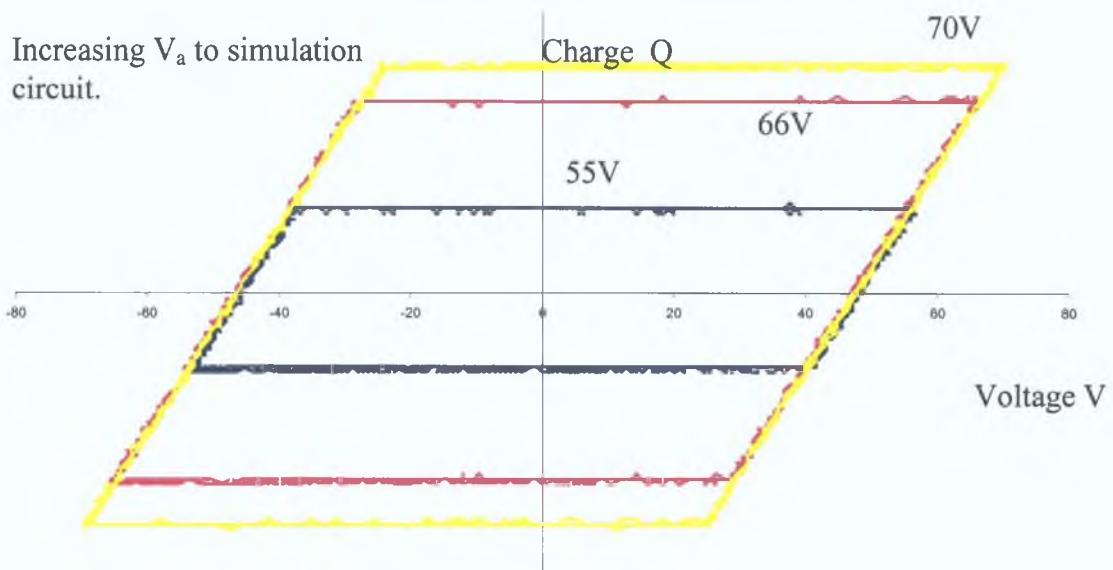


Figure 9.9 The  $Q$ - $V$  above threshold response characteristic for an ideal circuit.

The values for the sense capacitor was 33nF and the diodes used were 47V zeners and the insulator capacitor values were both 16nF. The below threshold response of the simulated circuit shown in Fig. 9.5 is shown in Fig. 9.8. It is a straight line due to the pure capacitive nature of the circuit. The three graphs shown in Fig 9.9 give the response of the circuit in Fig. 9.5 to increasing voltages as the voltage is increased above the threshold, to a maximum in the last curve. The zener diodes act as clamps on the voltage at 47V thereby limiting the field. The charge, in this case does not change until the device is functioning above the threshold voltage unlike the ideal response curve shown in Fig. 9.7 where the charge varies as the voltage changes and this clamping is not achieved. This test setup can now be applied to the devices. In fact the ideal back-to-back model is not precisely equivalent to the real devices. Other models have been developed to take into account the charge movement with time<sup>324,325</sup>.

Often in real devices a 'saturation' is observed mainly due to the depletion of electrons in the interface states<sup>326</sup>. This means that the voltage must be increased to supply the electrons and this affects the response curve of the device making it non-uniform.



## 9.2.4 Luminance Measurements

Since ultimately it is the optical response to an electrical signal that is important, characteristics such as the luminance versus voltage (L-V) and the transferred charge ( $\Delta Q$ ) versus luminance (L- $\Delta Q$ ) are important. From analysis of the ideal model, given that

$$C_i = \frac{\epsilon_o \epsilon_i}{d_i} \quad (9.12)$$

and

$$V_{ELth} = E_{ELth} d_{ELth} \quad (9.13)$$

from Eq. 9.11 the luminance is found to be

$$L = \frac{4}{\pi} \eta f \epsilon_o \left( \frac{d_{EL}}{d_i} \right) E_{ELth} (V_a - V_{th}) \quad (9.14)$$

Thus, showing that to optimise the luminance with a constant modulation voltage ( $V_a - V_{th}$ ) the relative thickness of the phosphor layer to the insulating layer thickness should be maximized and the insulating layer should have a high dielectric constant. The luminance of the device is proportional to the product of the drive frequency and the transferred charge density over a wide range<sup>327</sup>. Therefore in order to increase luminescence the transferred charge density within the phosphor must be increased. Also the excitation probability of the luminescent centers by hot electrons, which is a product of the electric field and mean free path, needs to be maximized. The electric field is limited due to the clamp field and the mean free path is dependent on the crystallinity of the phosphor. The concentration of the Mn atoms in the phosphor also plays a role in the mean free path of the electrons and it has been shown that at concentrations of Mn greater than 1% the luminance decreases due to the scattering of hot electrons by the Mn centers and the decrease in crystallinity in the phosphor layer<sup>328</sup>.

## 9.3 Device Results

### 9.3.1 Introduction

In this section the properties and results of the specific types of displays produced are presented. The general information that applies to all the devices is given in Appendix

And then the comparison of the optoelectronic data for each device structure is presented and discussed. Device 1 is omitted as its results have already been discussed previously.<sup>329</sup>

### 9.3.2 Structural Properties

In all the tested devices the ZnS/Mn layer is similar. It has a hexagonal structure and its production and optimization has been discussed in Chapter 6. The layer thickness of the ZnS/Mn is 500nm in each case. This is the minimum thickness for maximizing brightness.<sup>328</sup>

The SiO<sub>2</sub> insulating layers have an amorphous structure and are annealed at 700°C for densification and to minimize stress when the ZnS/Mn layer is added. If the SiO<sub>2</sub> is annealed at a lower temperature the formation of an interstitial ZnO layer limits the function of the device. The ZnO layer does not undergo electroluminescence but a 510nm peak is seen in photoluminescence studies of the devices. This applies to device types 2 and 3 where an SiO<sub>2</sub> film is deposited on top of ZnS/Mn. Thus it is important that the top SiO<sub>2</sub> film is annealed at a temperature of at least 700°C in both these device types.

When Ta<sub>2</sub>O<sub>5</sub> is used as the insulating material and its structure is also important. If the Ta<sub>2</sub>O<sub>5</sub> is annealed at a temperature less than 700°C the structure is amorphous. When the Ta<sub>2</sub>O<sub>5</sub> is annealed at 700°C or above the structure is orthorhombic. As the Ta<sub>2</sub>O<sub>5</sub> is used as the lower insulator in device types 4,5 and 6 it is important that it is crystalline as the ZnS/Mn has adhesion problems when placed on top of the amorphous Ta<sub>2</sub>O<sub>5</sub>. This makes it unsuitable as a lower insulator in the device. The ZnS/Mn had no adhesion problems when deposited on the crystalline Ta<sub>2</sub>O<sub>5</sub>. For the top electrode, crystalline Ta<sub>2</sub>O<sub>5</sub> also had to be used with a top ZnO/Al transparent conductor to ensure good adhesion in device type 6. When deposited on top of ZnS/Mn and annealed at 700°C, the Ta<sub>2</sub>O<sub>5</sub> had a similar orientation to the Ta<sub>2</sub>O<sub>5</sub> film deposited directly on silicon.

### 9.3.3 Electronic Properties.

#### 9.3.3.1 Threshold Voltage

All the tested devices emit a bright orange light under AC voltages in excess of the threshold voltage. The threshold voltage in the case of devices 1,2 and 3 is 56V. This is reduced in the devices that use  $Ta_2O_5$  as the insulating material. In devices using  $Ta_2O_5$  the voltage is as low as 36V. This is due to the increased dielectric constant of the material.

#### 9.3.3.2 Charge vs. Voltage

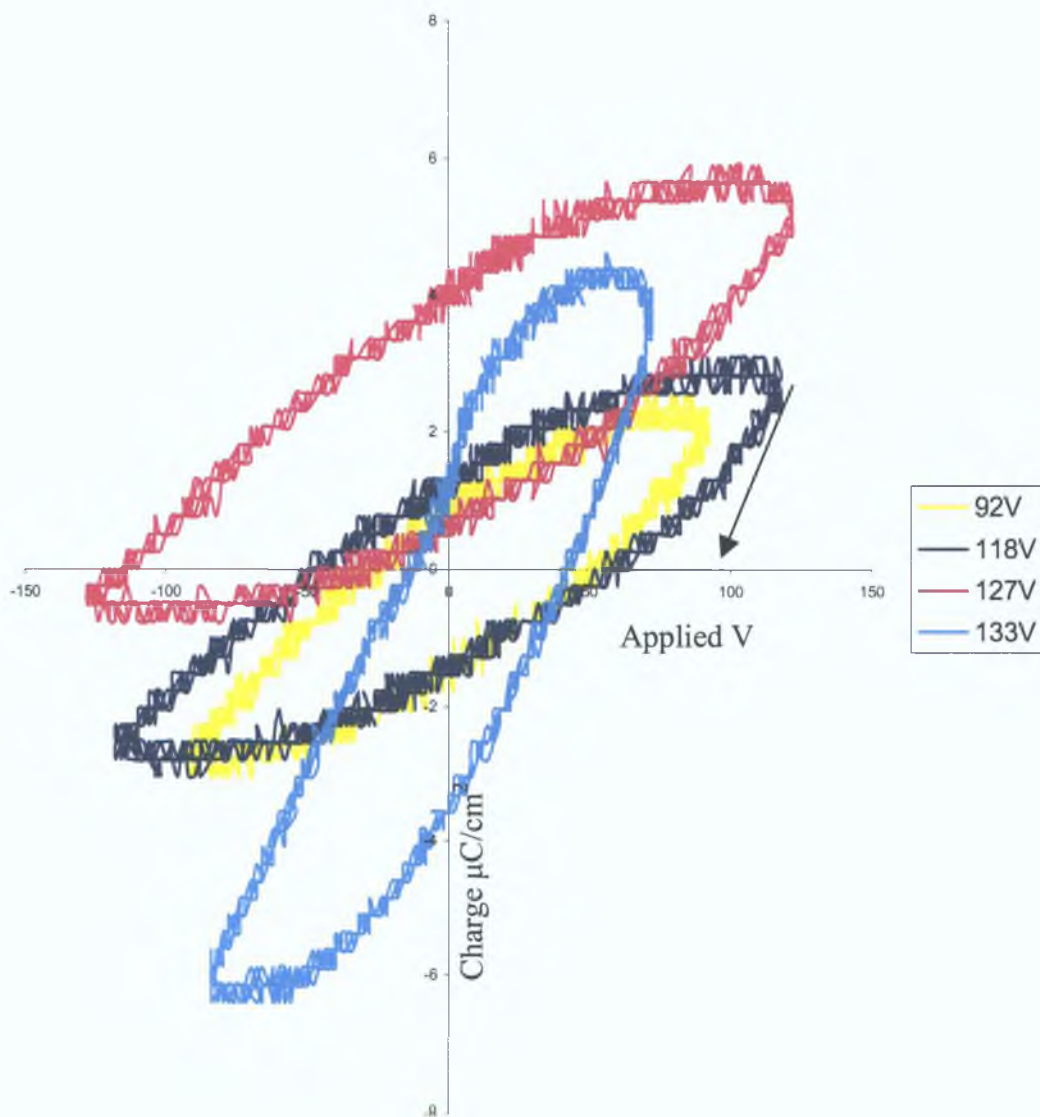


Figure 9.10 charge versus voltage curve for a typical Device type 3 ( $SiO_2-ZnS:Mn-SiO_2-ZnO:Al$ ). The legend shows the peak-to-peak applied voltage.

In characterising the device the charge-voltage diagram (Q-V) allows the process to be viewed from an electrical viewpoint. This can be measured using a measuring circuit based on a Sawyer-Tower circuit as shown in Fig 9.6. A 100nF sense capacitor is used in this case. The Q values are obtained using Eq 9.2. Results have been obtained from the various devices and their performance can be seen here.

#### *Devices using SiO<sub>2</sub> insulators*

For some of the devices especially device type 4,5,6 light is emitted below threshold and therefore the response is a straight line. For device 2 and 3 results are shown for a typical device in Fig 9.10. It can be seen from these curves that the device starts to become unstable at voltages above 118V and the response begins to wander and above 133V the device failed.

In quantifying the response of the device the values are taken from the V=118V response curve. It can be seen from this response curve that the threshold voltage is 48V. This is lower for the 92V having a value of about 37V and this is consistent with the 127V response also.

The capacitance of the insulator from the graph is 16.54nF/m<sup>2</sup> at 118V. The capacitances for the 92V and 127V are 11.14nF/m<sup>2</sup> and 8.27nF/m<sup>2</sup> respectively and this explains the similarity of their responses. These values compare favorably with those found for the insulator on its own and also with those in the literature<sup>330</sup>. The capacitance increases just before the device fails in the 133V response to 28.49nF/m<sup>2</sup>.

Calculating the capacitance for the phosphor gives an average value of 9.7nF/m<sup>2</sup> that again agrees with results found for the phosphor on its own. The threshold voltage for electroluminescence V<sub>ELTH</sub> calculated from Eq 9.7 is 38V in all cases showing that this is independent of the applied voltage. This results in a low power consumption of an average of 3W/m<sup>2</sup> for the device. Substituting these values into Eq 9.11 and assuming an efficiency of 2.5lm/W gives a luminance of ~1cd/m<sup>2</sup>. This is a very low value for a device and therefore this construction using the SiO<sub>2</sub> insulators is not very efficient.

### Devices using $Ta_2O_5$ insulators

In the device types 4,5 and 6,  $Ta_2O_5$  is used as the insulating material. Here the Q-V results for a  $Ta_2O_5$  device type 5 are presented and compared to the  $SiO_2$  devices.

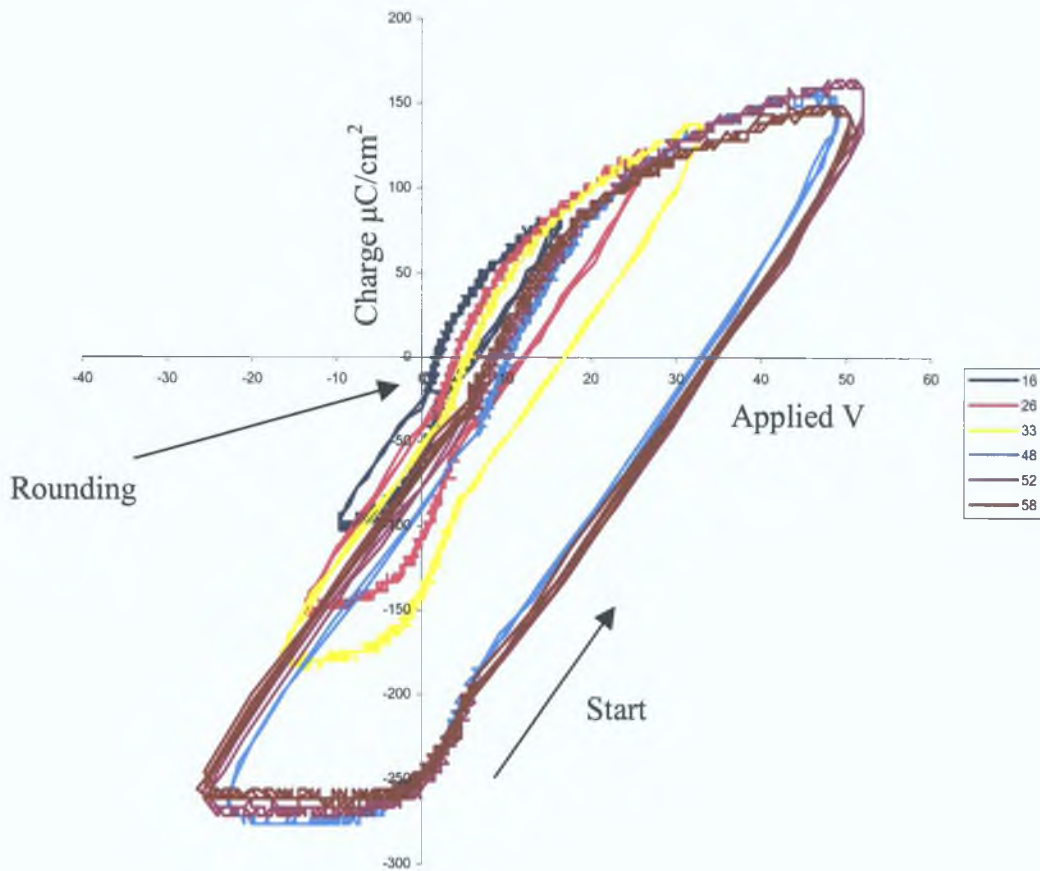


Figure 9.11 Q-V response for a Type 5 device having  $Ta_2O_5$  insulators

For device 5 and 6 results are shown for a typical device in Fig 9.11. The voltage of the phosphor layer increases with applied voltage at the lower voltages. Rounding of the Q-V curves is found near zero volts in the lower voltages. This is due to the anodic or polarization, electric field increasing enough for charge injection from the interface or ionization of the bulk traps to occur. Clamping of the voltage and electric field can be seen in the response curves for the higher voltages when the electric field is high enough to accelerate the electrons. Clamping of the voltage in the phosphor layer is caused by the counter electric field originating from electrons trapped in the

opposite interface between the phosphor and the insulating layers. Its value is affected by the crystallinity of the ZnS:Mn layer<sup>331</sup>. It can be seen that at the lower voltages luminance is due to leakage current generated in the insulating layers. The shape of the curves shows that the insulating material is only efficient in one direction. That means that one of the insulating materials, although it is working is not working efficiently. This is the top insulator since it has adhesion problems when placed on ZnS:Mn in an amorphous state as the lower insulating material is crystalline.

In quantifying the response of the device the values are taken from the clamped region rather than the unstable lower voltages that exhibit some charge collapse that diminishes as the voltage is increased. Measurements from the 52V response curve produce a threshold voltage of ~37V. This is much lower in the lower voltage curves.

The capacitance of the insulator from the graph is  $1\mu\text{F}/\text{m}^2$  at 48V. The capacitances for the 52V and 58V are both  $490\text{nF}/\text{m}^2$  respectively and this explains the similarity of their responses. The values are much higher than the  $\text{SiO}_2$  value but this is to be expected as the dielectric constant is also higher.

Calculating the capacitance for the phosphor gives an average value of  $10\mu\text{F}/\text{m}^2$  and this is quite high. The threshold voltage for electroluminescence  $V_{\text{ELTH}}$  calculated from Eq. 9.7 is 36V in all cases showing that this is independent of the applied voltage. This results in a power consumption of an average of  $40\text{W}/\text{m}^2$  for the device. Substituting these values into Eq. 9.11 and assuming an efficiency of 2.5lm/W gives a luminance of  $\sim 8\text{cd}/\text{m}^2$ . This is a low value for a device and shows that there are some inefficiencies in the device.

### 9.3.4 Optical Properties.

#### 9.3.4.1 Electroluminescence

Manganese-doped zinc sulphide has a strong orange emission due to the  $\text{Mn}^{2+}$   $T_1(^4G) \rightarrow ^6A_1(^6S)$  transitions. The orange light output is due to the  $\text{Mn}^{2+}$  luminescent center excited by hot electrons in the ZnS. Display structures using this material

show a typical high intensity around 580nm due to this transition. Similar spectral responses were recorded for each of the display types (1-6) and a typical response is shown in Fig 9.12. The output has only one peak present due to the  $Mn^{2+}$ . There is no peak towards the red end of the spectrum indicating that the Mn concentration is correct and not too high.

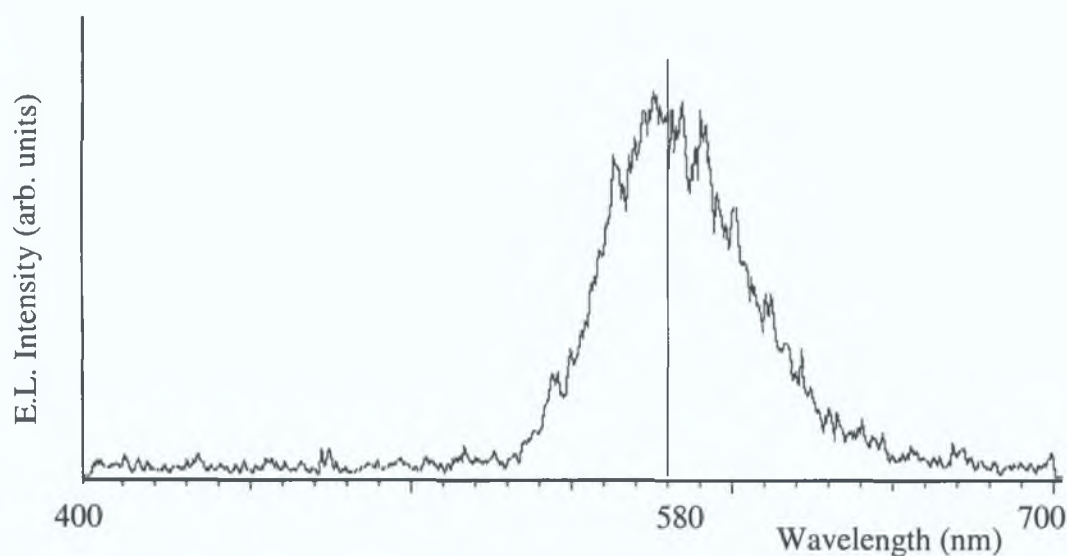


*Figure 9.12 Electroluminescence Spectrum for sol-gel deposited ZnS:Mn device*

In device types 2 and 3 some problems were encountered with the electroluminescence process. After deposition of the top  $SiO_2$  insulating layer and the Al electrode there was a variation in behavior of the devices; some showed the EL from the  $Mn^{2+}$  transition while others showed no EL.

There is a correlation between the position and the intensity of the peaks measured by PL, CL and EL which helps to explain why this is so. Fig. 9.13 shows the PL spectra for two test devices of device type 2. Test piece 1, having the top insulator annealed at  $700^{\circ}C$ , showed a luminescence peak at  $\sim 580nm$  and did show electroluminescence. Test piece 2, having a top insulator annealed at  $500^{\circ}C$  did not show any EL. This spectrum is dominated by broadband luminescence centered at  $\sim 510nm$  and small

band centered at ~580nm. The films only show this 510 nm peak after the second insulator is added on top of the active layer.

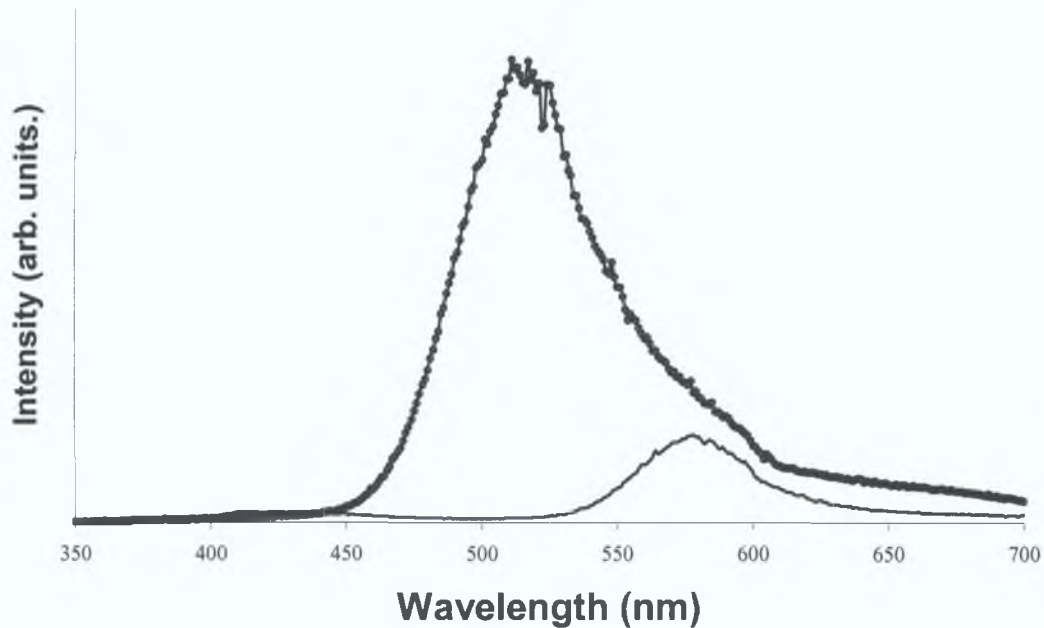


*Figure 9.13 PL Spectrum for nonluminescent films (o) and luminescent films (-). The luminescent film has the expected ~580nm peak and the non-luminescent film also has a large peak at ~510nm.*

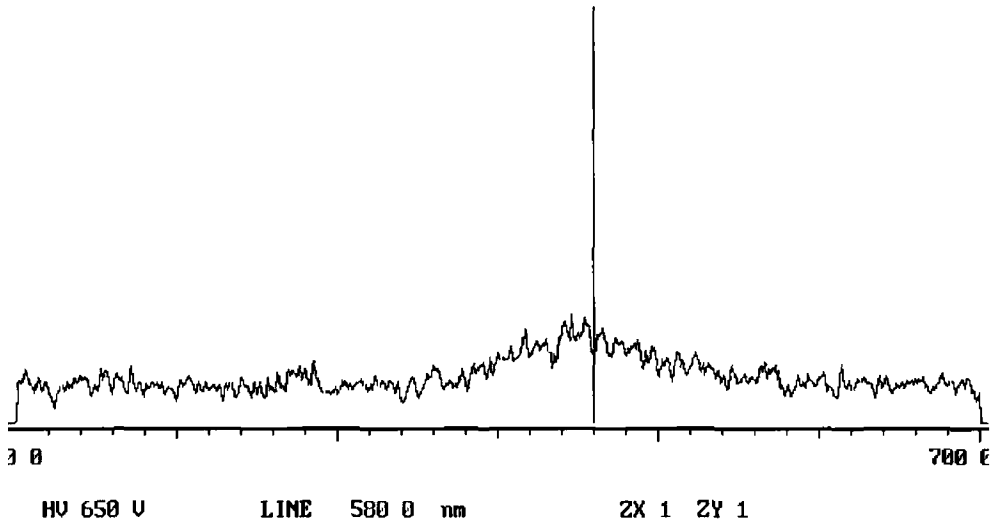
The 510 nm peak corresponds to paramagnetic isolated oxygen vacancies that occur in ZnO thin films<sup>332</sup>. It is clear therefore that the interface structure between the ZnS and top SiO<sub>2</sub> which gives rise to these vacancy states also kills the electroluminescence. Moreover, the intensity of this peak in ZnO films has been observed to be dependent on the free-carrier concentration<sup>333</sup>. The peak intensity has been found to be maximum at concentrations of around mid-10<sup>18</sup> cm<sup>-3</sup> with reductions of many orders of magnitude at lower and higher concentrations. The presence of these vacancy states constitutes an alternative recombination pathway in the ZnS EL devices, which competes with the Mn<sup>2+</sup> transition. The physical reason for these states is probably due to an interdiffusion between the SiO<sub>2</sub> and the ZnS at the top interface whose properties vary with the annealing temperature. It cannot be due purely to the presence of the interdiffused region since annealing at lower temperature (500°C)



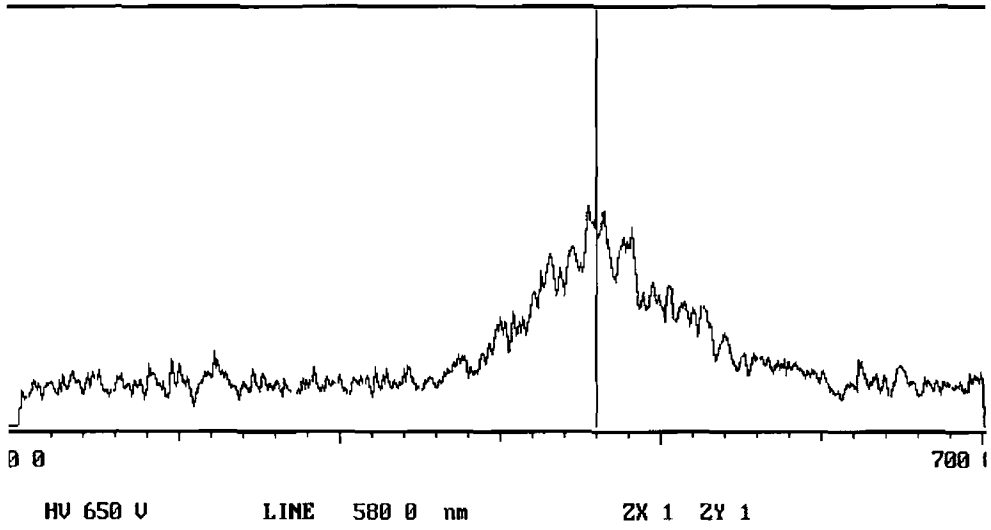
would be expected to give less interdiffusion than annealing at higher temperature (700°C) The behaviour of the luminescence produced by these states with carrier concentration may help to explain this At 500°C, the carrier concentration at the interface due to a balance between doping and trapping effects gives a net carrier density in the range, which can give rise to significant (photo)luminescence which prevents Mn<sup>2+</sup> EL On annealing to higher temperature it is likely that both doping and trap density will change by a significant amount such that this mechanism is no longer efficient and EL will occur as expected It should be noted that there is no observation of this 510 nm luminescence from the bottom ZnS-SiO<sub>2</sub> interface and therefore device type 1 does not exhibit this problem This limits the use of SiO<sub>2</sub> as an insulating material for the low temperature devices, as the problem can only be overcome by annealing the SiO<sub>2</sub> at 700°C thus 'sealing' the ZnS as the vacancies are reduced at this temperature as seen in the raman spectrum of ZnO Al in Fig 8 13

#### **9.3.4 2 Luminescence**

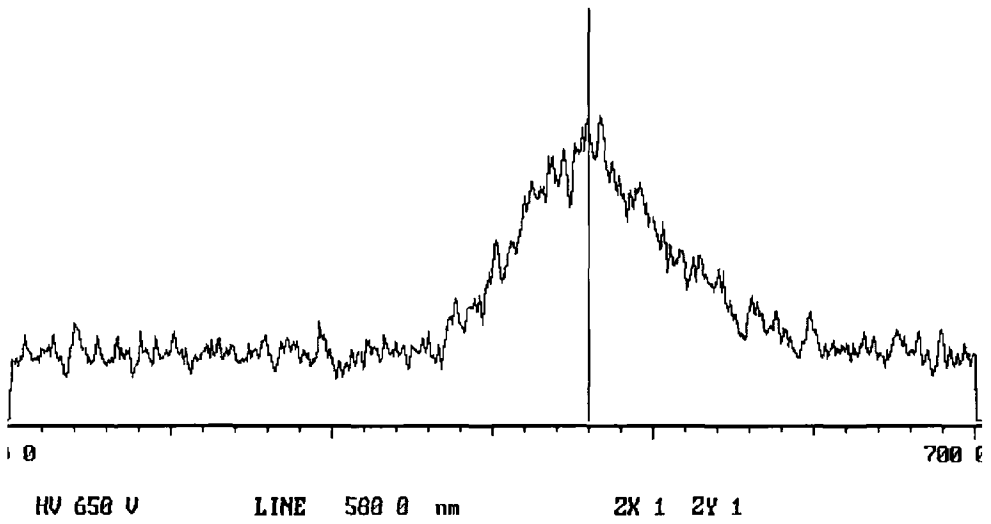
The luminance measurements were carried out on the different device types In the display the luminescence caused by electroluminescence starts at the threshold voltage and increases in intensity as the voltage is increased This can be seen more clearly in the family of electroluminescent spectra taken from a type 5 device having amorphous Ta<sub>2</sub>O<sub>5</sub> as the insulating material shown in Fig 9 14 The luminous intensity grows as the voltage is increased from 40V to 70V As it can be seen the spectral position of the luminance does not change with applied voltage



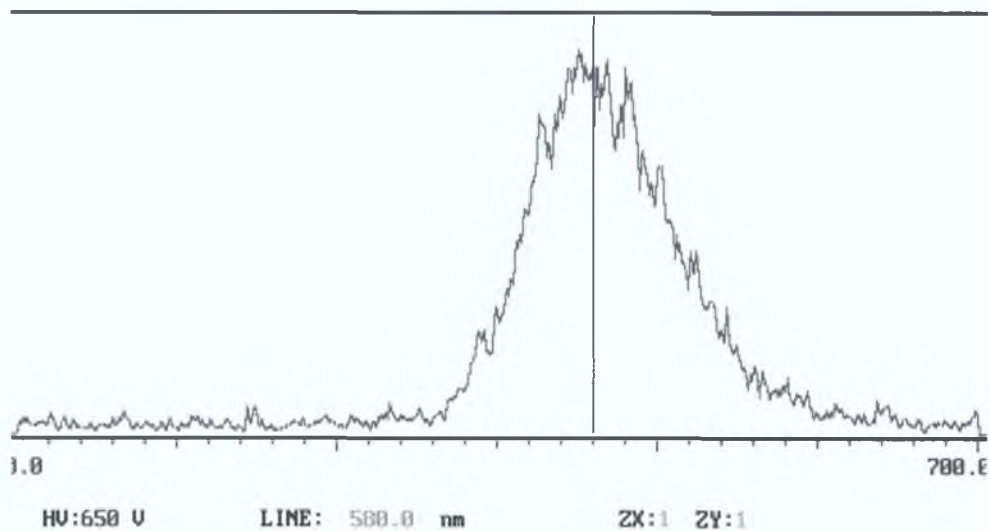
40V Ta-ZnS-Ta response



50V Ta-ZnS-Ta response



60V Ta-ZnS-Ta response



70V Ta-ZnS-Ta response

Figure 9.14 Series of electroluminescent spectra showing the growth of luminance with applied peak voltage. The marker is placed at 580nm.

### 9.3.4.3 Brightness

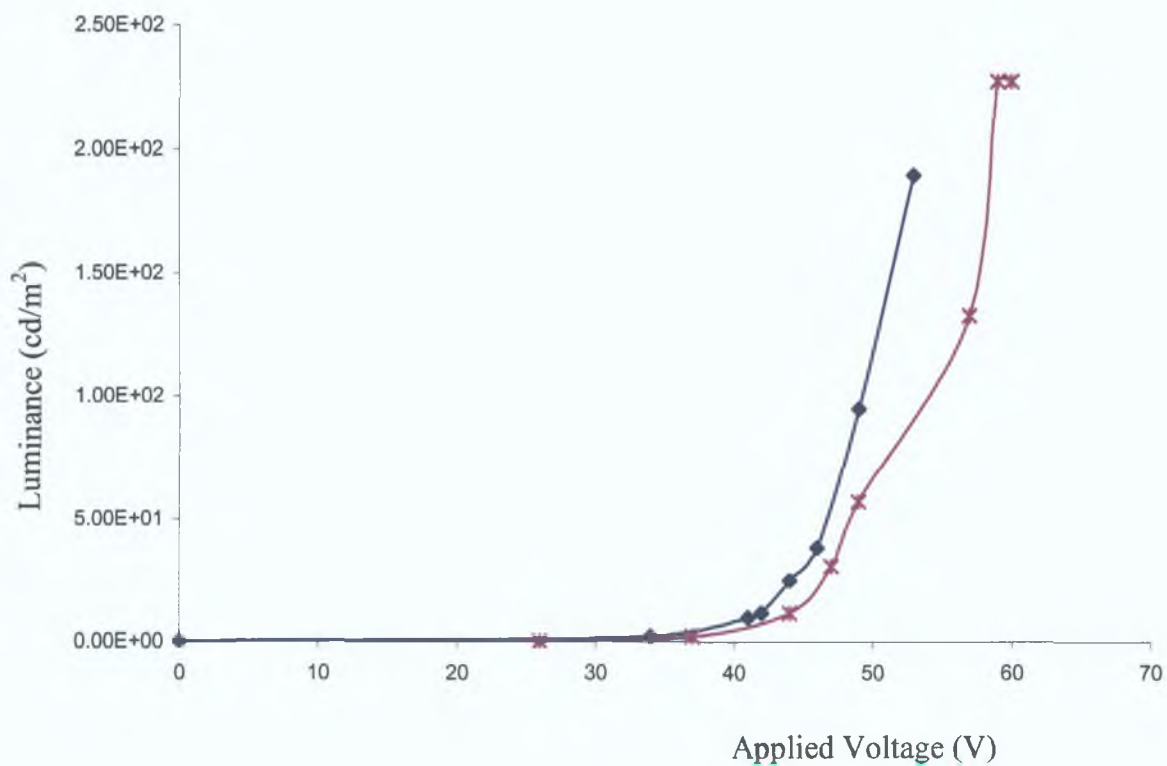


Figure 9.15 Brightness versus voltage response for two devices with SiO<sub>2</sub> insulating material

This property of the device is very dependent on the insulator and its uniformity and structure. The greater the dielectric strength the lower the threshold voltage of the device and so insulating materials with higher dielectric constants are favored.

For  $\text{SiO}_2$  devices the response is similar for the three types and a typical response for two devices are shown in Fig. 9.15. The response starts at a voltage of 35V in both devices and tends to saturate at higher voltages in device 2. Device 1 shows no saturation but the voltage level is lower. The stability of the  $\text{SiO}_2$  as an insulating material is questionable and most devices failed before saturation was reached.

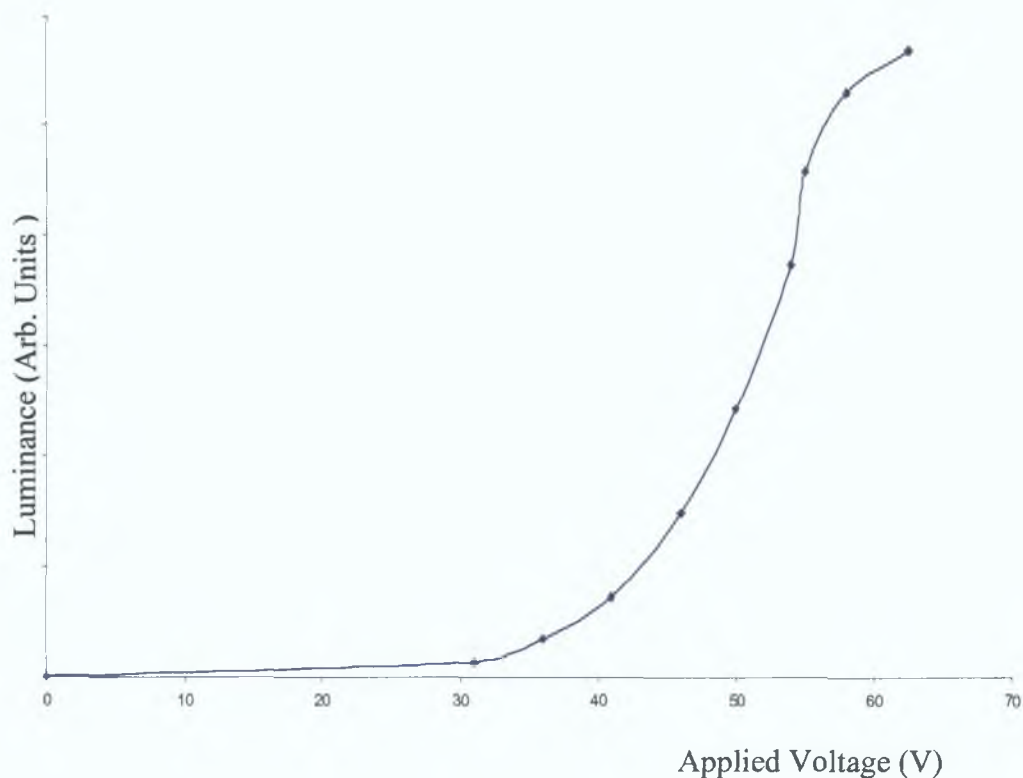


Figure 9.16 Brightness versus voltage response for a device with  $\text{Ta}_2\text{O}_5$  insulating material

For the devices containing  $\text{Ta}_2\text{O}_5$  the response is again similar for the three device types and a typical response is shown in Fig. 9.16. The response is seen to begin at 40V and again it as the voltage increased the luminance tends to saturate due to the depletion of electrons in the interface states above a drive voltage of 70V. This means that the voltage must be increased to supply the electrons and this affects the response

curve of the device making it non-uniform. This response was observed in all the  $Ta_2O_5$  devices regardless of the crystalline state of the  $Ta_2O_5$ .

Looking specifically at the response of the  $Ta_2O_5$  device and comparing the optical and electrical responses of the device shows how the  $Ta_2O_5$  device behaves differently to the  $SiO_2$  device. The luminance response for both insulating materials is shown in Fig. 9.17. It can be seen here that the  $Ta_2O_5$  devices have a lower threshold voltage than the  $SiO_2$  devices due to its larger dielectric constant. The response of the  $SiO_2$  device saturates before the  $Ta_2O_5$  device as it is limited in its capabilities. However the  $SiO_2$  device shows greater linearity in its response suggesting that the hot electron generation and recombination is more efficient in this type of device.

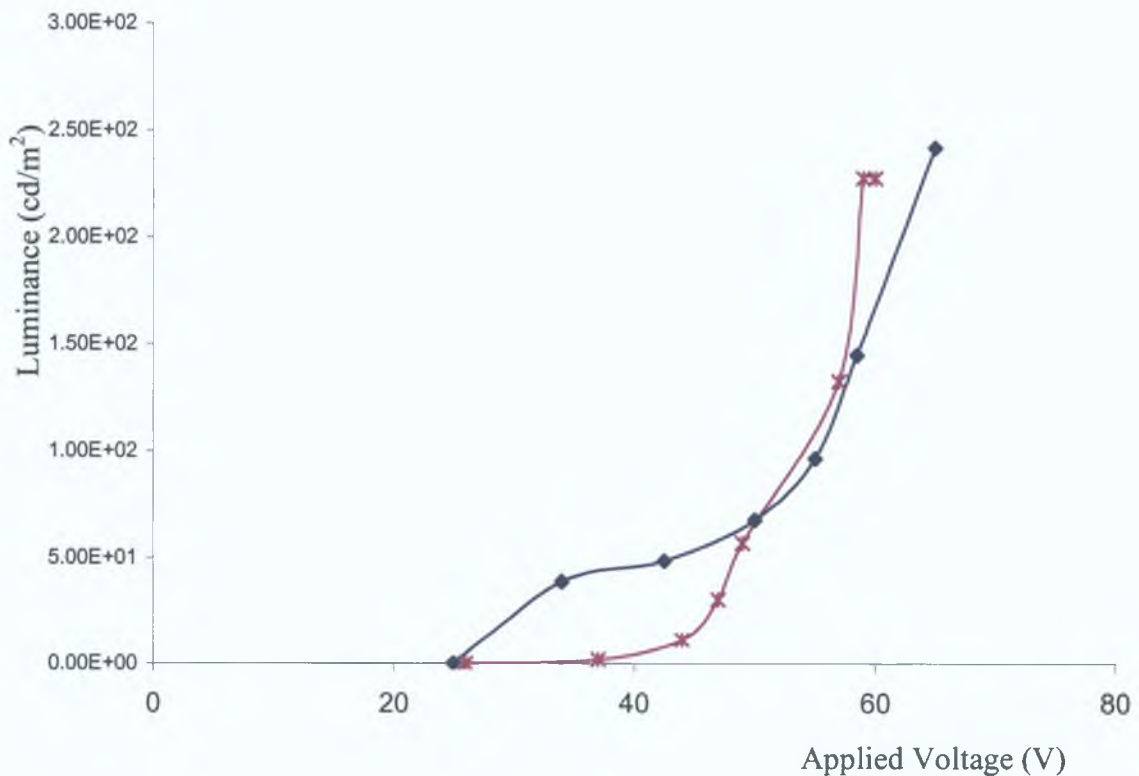


Figure 9.17 This is the luminance response curves of devices using  $SiO_2$  (\*) and  $Ta_2O_5$  (♦) insulating materials.

The  $Ta_2O_5$  response also shows an area of low luminescence followed by a steep rise in the light output. This is due to space charge in the device, which can be seen in the

Q-V curves, shown in Fig 9.18 also. This results in high current densities within the phosphor and due to this they tend to be bright, unstable and fail quickly.

#### *Tantalum pentoxide device response*

In looking at the response of devices with  $Ta_2O_5$  insulating materials it is interesting to look at the luminance versus applied voltage and the charge versus voltage results together.

In Fig 9.18 the charge versus voltage results for a type 5 Device with  $Ta_2O_5$  insulators is given. In this chart it can be seen that the response of the device changes as the applied voltage is increased from 47V to 54V. The response actually shifts to a smaller area.

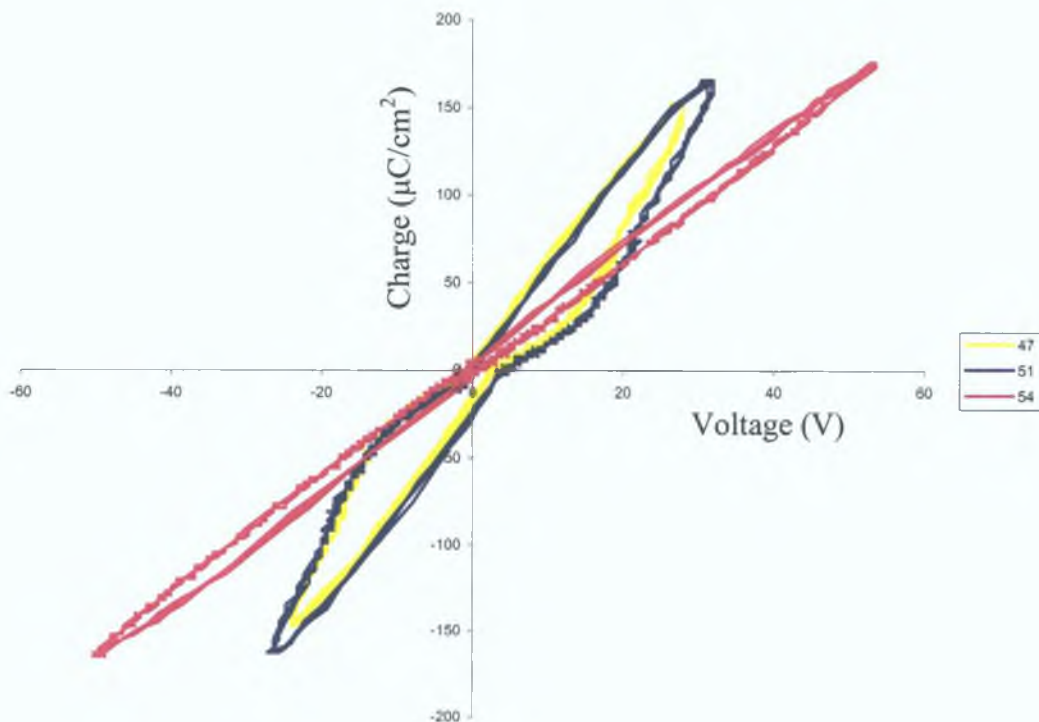


*Figure 9.18 Electrical response of a device with  $Ta_2O_5$  insulators*

The voltage range shown is chosen as the device is actually lighting and Fig. 9.19 shows the corresponding luminance values. Rounding can be seen at zero volts due to the leakage charge. As the applied voltage reaches its maximum the phosphor field

also should reach a maximum and the charge begins to transfer across the phosphor and the voltage does not increase

In contrast the luminance versus voltage results taken for this device are shown in Fig 9 19 and show the luminance of the device growing during this phase after turning on at 25V approximately The luminance in the region discussed shows steady growth despite the changes occurring in the charge within the device This shows that the Ta<sub>2</sub>O<sub>5</sub> device will show a light output even in less than ideal circumstances

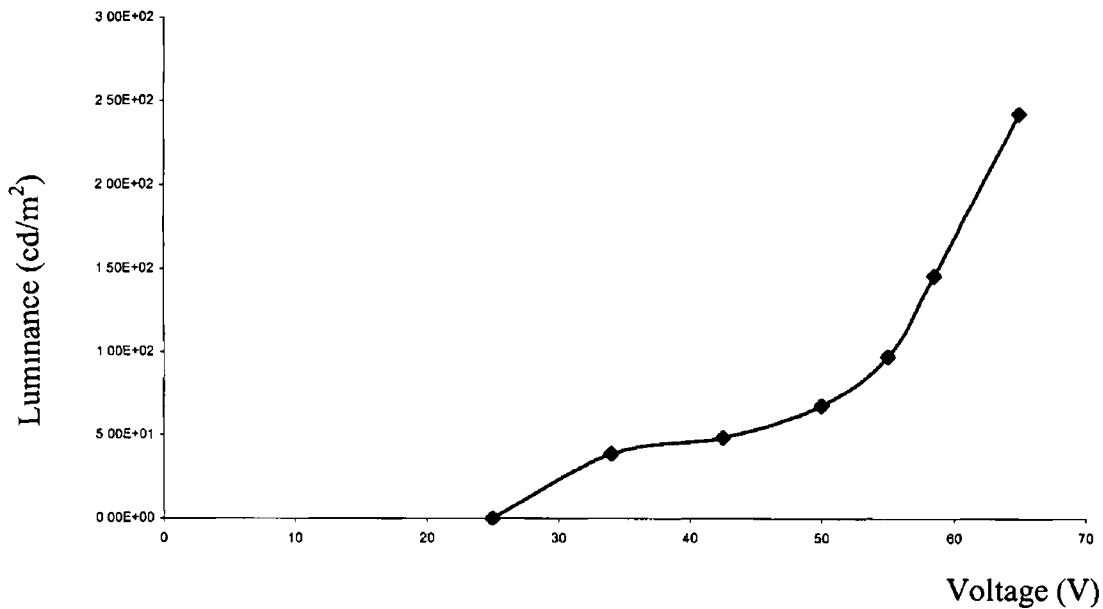


Figure 9 19 Luminance response of Ta<sub>2</sub>O<sub>5</sub> device

The variation of the luminance at the peak voltage of 65V was also investigated as a function of frequency and it was found that the output did not change over a 1kHz range

Calculating the values from the Q-V curve in Fig 9 18, as shown in Table 9 1, and comparing them to the values for L in Fig 9 18 it can be seen that the values are close and therefore the values for the capacitances found are correct

Voltage	47V	51V	54V
Capacitance of Insulator ( $\mu\text{F}/\text{m}^2$ )	21	18	7
Capacitance of Phosphor ( $\mu\text{F}/\text{m}^2$ )	7.78	8.52	5.89
$V_{\text{ELth}}$ (V)	51	61	183
Power ( $\text{W}/\text{m}^2$ )	278	316	389
Luminance ( $\text{cd}/\text{m}^2$ )	221	252	310

**Table 9.1** Values for type 5 Device calculated from Q-V curves in Fig.9.17.

The values found for the capacitances here are also similar to those found from Fig 9.11. It can be seen from the above table 9.1 and the response curve 9.17 that the calculated luminance response gives slightly higher luminance values than the experimental results suggesting that the efficiency, taken as  $2.5 \text{ Lm}/\text{W}$  is just a little too high.

#### 9.3.4.4 Stability and Reliability

From analyzing the different types of devices it is apparent that each of the devices has its limitations. The stability and reliability of the device depends on a number of factors. Firstly, the luminescent material must be stable and the crystallinity of the material must be uniform throughout to reduce any stress or strain that could produce nonradiative traps in the material. The material must also be compatible with and adhere to the other component films. This is one area where the structure of the underlying insulating film is important. In the case of  $\text{SiO}_2$ , the  $\text{ZnS Mn}$  adheres easily to the amorphous surface. In the case of  $\text{Ta}_2\text{O}_5$ , the  $\text{ZnS Mn}$  had adhesion problems with the amorphous material but not with the crystalline material. This limits the range of materials that can be used in the device.

Another factor that affects the stability and the lifetime of the device is the nature of the insulating material. If the material is a self-healing insulator then the failure of any part of the device is limited to the one area. However if the material is not self



healing then catastrophic failure will result and the device will fail completely Both  $\text{SiO}_2$  and  $\text{Ta}_2\text{O}_5$  are self-healing materials but  $\text{Ta}_2\text{O}_5$  appears to better limit the damage caused to the device than  $\text{SiO}_2$

# Chapter 10

## Conclusions and Future work

### 10.1 Introduction

The prototype devices that show the possibilities of the application of sol-gel technology to the thin film displays area have been demonstrated. In this section the progress, problems and future steps are looked at. The next stage involves developing the device to incorporate the full colour gamut and looking at the addressing issues. This section details the improvements made and suggests further steps in producing a large-scale full colour sol-gel inorganic thin film electroluminescent device.

### 10.2 Conclusions

A TFEL device incorporating ZnS:Mn has been produced using sol-gel methods in conjunction with sulphidation. The device has an inverted structure, using a silicon substrate and can use both tantalum pentoxide and silicon dioxide as possible insulating materials. Both insulating materials have been prepared using sol-gel methods. The top electrode used in the device is ZnO:Al also prepared using sol-gel. The electrical contact is made using vacuum deposited aluminium.

The process of converting the sol-gel deposited ZnO:Mn into ZnS:Mn has been investigated in detail. The process is diffusion controlled having a diffusion coefficient of  $7.8 \times 10^{-18} \text{m}^2 \text{s}^{-1}$ . The diffusion process itself is a two-step process, having an initial phase where little or no diffusion takes place followed by the conversion phase. The films are produced from hexagonal ZnO:Mn and have a wurtzite structure. For full conversion to take place the films are annealed in a  $\text{H}_2\text{S}$  atmosphere for 3hrs at  $560^\circ\text{C}$ . This optimises the films produced.

Initially  $\text{SiO}_2$  was used as the insulating material. It is an efficient insulating material and produced a luminance of  $228 \text{cd/m}^2$  at 60V. However the  $\text{SiO}_2$  needed to be optimised as it was found that if the annealing temperature of the sol-gel deposited  $\text{SiO}_2$  was too low the film formed an interstitial layer of ZnO in the stack when ZnS:Mn was added. This provided traps for the hot electrons and therefore quenched

the electroluminescence. Studies of the cathodoluminescence and photoluminescence of samples not exhibiting electroluminescence show a peak at ~510nm due to the presence of ZnO at the interface. This peak is due to oxygen vacancies in a ZnO layer formed at the interface between the ZnS active layer and the SiO<sub>2</sub> top insulator and its effectiveness as an EL killer depends on its efficiency as an alternative recombination pathway, which relates to the trap density and carrier concentration at the interface. The ~580nm peak characteristic of Mn<sup>2+</sup> is still visible in these scans but its intensity is greatly reduced. This peak at 510nm was removed by annealing the films at 700C. This peak is due to oxygen vacancies in a ZnO layer formed at the interface between the ZnS active layer and the SiO<sub>2</sub> top insulator and its effectiveness as an EL killer depends on its efficiency as an alternative recombination pathway, which relates to the trap density and carrier concentration at the interface. PL and CL measurements easily detect the presence of this transition and are, therefore, useful in determining quickly whether the fabrication process will result in a working device.

Tantalum pentoxide has also been used as an insulating material in the device. Its properties have been investigated and optimised. It has been shown that Ta<sub>2</sub>O<sub>5</sub> with the orthorhombic structure can be produced with a high dielectric constant of 50 and resistivity >10<sup>12</sup>Ωcm when annealed at 700°C in oxygen. When used as an insulator in a sol-gel TFEL structure the adhesion between the Ta<sub>2</sub>O<sub>5</sub> and the adjacent layers is poor for amorphous Ta<sub>2</sub>O<sub>5</sub> but good if it is crystalline. The device performance has been optimised using tantalum pentoxide as the insulating material. Since this is a transparent display it can also be used in the conventional structure using a glass substrate.

The optimum film structure for a TFEL inverted device is

Ta<sub>2</sub>O<sub>5</sub>/ZnS Mn/Ta<sub>2</sub>O<sub>5</sub>/ZnO Al. Devices constructed using this film stack have shown a luminance of 250cd/m<sup>2</sup> at 54V. This compares favourably with results attained in devices using ZnS Mn<sup>334</sup>. Multilayer devices incorporating ZnS produced using other coating technologies have also produced luminance in the order of 130-225cd/m<sup>2</sup> <sup>335</sup>

### 10.3 Future Work

The main concerns in the production of a large TFEL using sol-gel procedures involve the up-scaling of the dipping process. It has been demonstrated that this is not a problem as the only impediment to the size of the display is the size of the sol container. Different shapes and sizes up to 8cm x 2cm pieces have been dipped and have worked in all areas except the below the dry line of the gel. Thus there will be a wastage area at the ends of the samples. Also, the wider the sample, the easier it is to coat and less problems are encountered due to side drying. Once the environment of the chamber is controlled a display of any size or shape can be produced without any changes to the dipping rig itself. This offers an added versatility not shared with any other coating technology.

The device demonstrated here is ZnS:Mn. This has the characteristic orange colour that has a peak at 580nm. For a full colour display both the blue and green end of the spectrum needs to be addressed and this can be accomplished by doping the ZnS with other elements such as terbium for the blue region. Thus a full colour display is possible incorporating a large colour gamut.

A high luminous output from the device is also required for any application. The luminous output of the devices described here is in the region of 250cd/m<sup>2</sup> when tested with the aluminium dots. This needs to be addressed further by ensuring that the top insulating material is optimised. Other insulating materials could be used instead of Ta<sub>2</sub>O<sub>5</sub> and SiO<sub>2</sub> and these and their properties are shown in Table 8.1. Ta<sub>2</sub>O<sub>5</sub> was chosen in this case for its properties and SiO<sub>2</sub> was chosen because of its versatility and its producibility.

ZnO:Al has been used as the top electrode in this device. This is an efficient transparent conductor but currently has patterning difficulties when used in this device. Other low resistivity transparent films such as Indium Tin Oxide (ITO) could be used but as previously discussed in Chapter 8 blackening can sometimes occur. The properties of the insulator/conductor choice could be investigated and other combinations utilised in the device.

✓

The device developed here is an inverted structure. This device could also be prepared with a traditional structure as shown in Fig 7.2. This involves depositing the films on a high-temperature glass substrate starting with the conductor ZnO:Al. This is followed by the insulating film of Ta<sub>2</sub>O<sub>5</sub>. The ZnS:Mn is then deposited followed by the insulator and conductor. Initial studies have shown that the films are compatible and do form a transparent (30%) device. This then needs to have the top electrode patterned and electrical contacts attached.

Matrix addressing the luminescent material is another area that has to be developed in future work. It has been demonstrated here that ZnO:Al is a suitable candidate for the conductor in the device. The next issue is patterning the ZnO:Al to allow it to be addressed with an electrical pulse. This has been tried using photoresist but has not been successful to date. If the thin-film transistor technology could be applied here to each pixel it would enhance the performance as it has in the LCD area. Some research has been carried out in this area with ZnS:Mn<sup>336</sup> and this could be developed

# Appendix 1

## Introduction

This appendix lists the types and the properties of the specific types of displays produced. The general information that applies to all the devices is given here and the specific optoelectronic data for each device structure is presented and discussed in Chapter 9.

## Device 1

The first device is the single insulating structure using  $\text{SiO}_2$  as the insulator as shown in Fig 1. It has a three layer inverted structure deposited on silicon. The silicon also acts as the lower electrode for the device.

This device consists of a single lower insulating layer formed using an R=4 mix for the  $\text{SiO}_2$  thin films and deposited using the sol-gel process on to a silicon substrate. The silicon also serves as the lower electrode. This is followed by the deposition of an active layer formed by the conversion of sol-gel deposited  $\text{ZnO:Mn}$  films by annealing it for 4 hours in a  $\text{H}_2\text{S}$  atmosphere. The top Al electrode is deposited by evaporation.

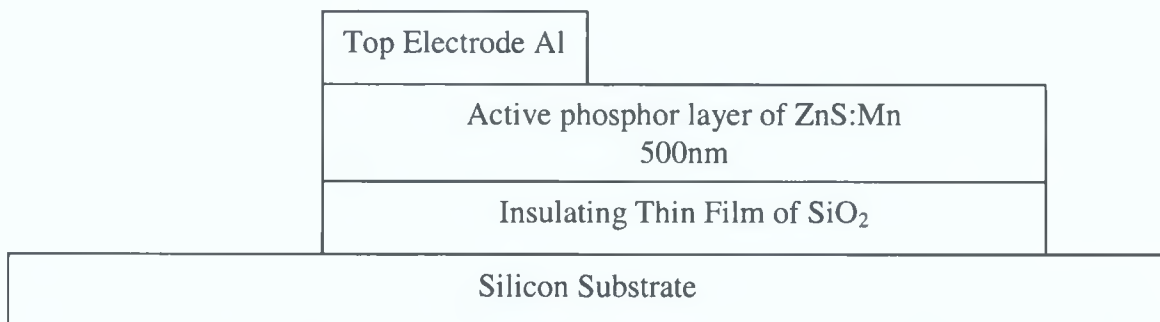


*Figure 1* Test device 1 showing a single insulating layer followed by an active layer and the top Al electrode on a silicon substrate.

This is the basic test device using the  $\text{SiO}_2$  insulating material. This was proved as a working device previously and all data on this device can be found in Ref [Tangs Thesis]

### Device 2

The first device studied in this discussion incorporates a double insulating inverted structure as shown in Fig 2

The insulating layers are formed using an R=4 mix for the  $\text{SiO}_2$  thin films that are then deposited using the sol-gel process on to a silicon substrate. The active layer is formed by the conversion of sol-gel deposited ZnO Mn films by annealing it for 4 hours in a  $\text{H}_2\text{S}$  atmosphere

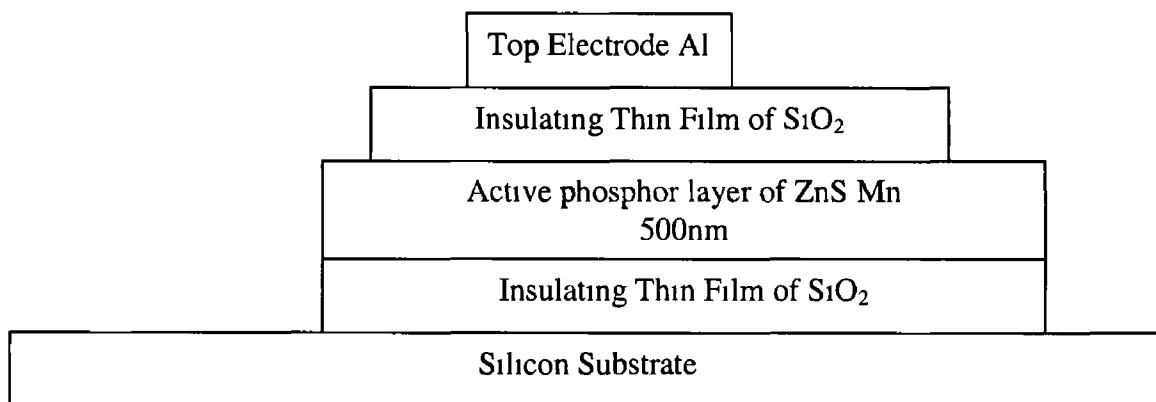


Figure 2 Schematic cross-section of Device 2 incorporating  $\text{SiO}_2$  as the insulating material

The layer thickness of the insulating layer is 80nm approximately. The active layer of ZnS Mn has a thickness of 500nm approximately. The top aluminum electrode is deposited using evaporation and the thickness of the film is 20-40nm. This semi-transparent film allows the light from the device to be collected.

### Device 3

The third device structure studied incorporates a double insulating inverted structure similar to Device 2. In this case the top electrode is ZnO Al and is produced using sol-gel methods. Here, evaporated Al is also deposited for electrical contact. The complete structure is shown in Fig. 3.

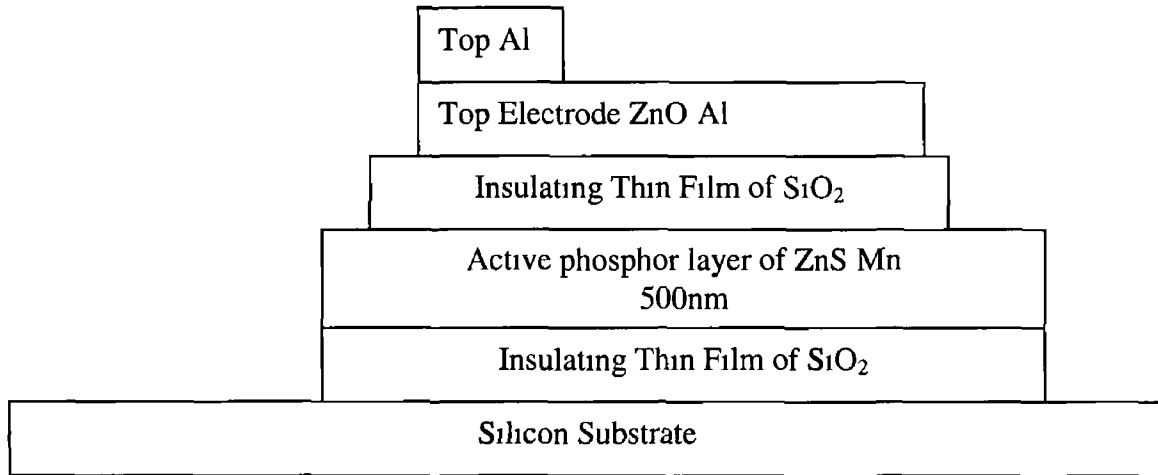


Figure 3 Structure of Device 3, the all sol-gel device using SiO<sub>2</sub> insulators

### Device 4

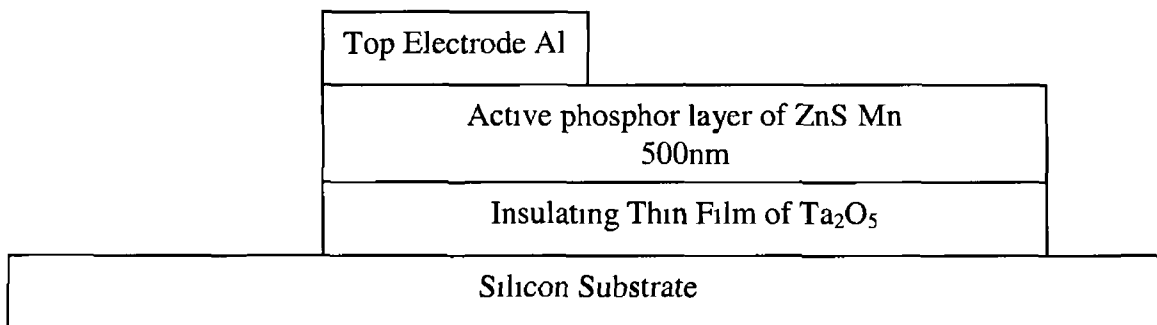


Figure 4 Test device 4 showing a single insulating layer of Ta<sub>2</sub>O<sub>5</sub> followed by an active layer and the top Al electrode on a silicon substrate



This device uses tantalum pentoxide as the insulating layer in a three layer inverted structure deposited on silicon. The  $Ta_2O_5$  is deposited using the sol-gel method described earlier in Chapter 8. This is followed by the active  $ZnS:Mn$  layer. The top electrode is evaporated Al. This structure is similar to device 1 and is shown in shown in Fig. 4.

### Device 5

In this case the tantalum pentoxide is used in a double insulating structure and the top electrode is Al. The 120nm insulating film of  $Ta_2O_5$  is deposited using the sol-gel method described earlier in Chapter X. This is followed by the active  $ZnS:Mn$  layer. The final insulating layer of  $Ta_2O_5$  is then applied to the device. The top electrode is evaporated Al. The structure of the device is shown in Fig. 5. This device has been manufactured with both amorphous and crystalline  $Ta_2O_5$ .

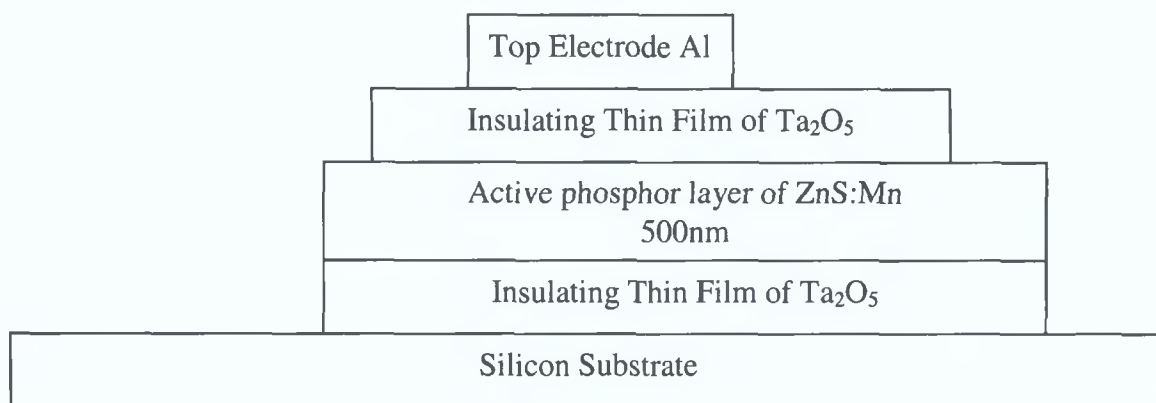


*Figure 5 Schematic cross-section of Device 5 incorporating  $Ta_2O_5$  in a 5 layer structure.*

### Device 6

Here the all sol-gel device is fabricated with the tantalum pentoxide as the insulator. The 120nm insulating film of  $Ta_2O_5$  is deposited using the sol-gel method described earlier in Chapter 8. This is followed by the active  $ZnS:Mn$  layer and the top

insulating film of  $Ta_2O_5$ . The transparent conductor used is ZnO:Al having a thickness of 250nm. Evaporated Al is used for electrical contact in this case. This complete structure is shown in Fig. 6.

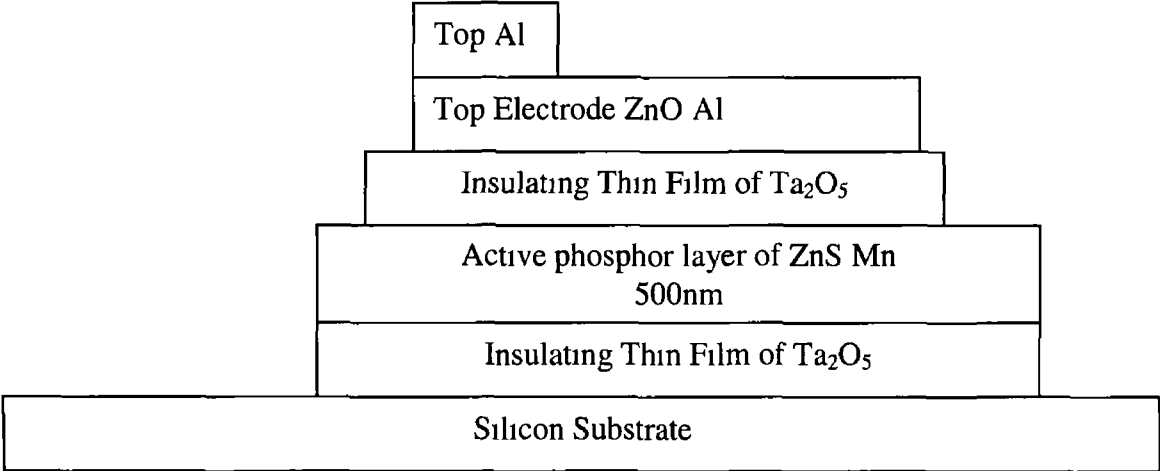


Figure 6 Inverted five layer structure using tantalum pentoxide with a sol-gel deposited transparent conductor of ZnO:Al

## References

- <sup>1</sup> P. Hill, *Displays Europe* 4 (2002) 11
- <sup>2</sup> E. Schlam, *SID Seminar Notes 1991 Vol 2 F-1/2* (1991)
- <sup>3</sup> S. Sherr, *Electronic Displays*, John Wiley, New York, (1979) Chapter 2
- <sup>4</sup> W. Hardin, *OE Magazine*, 12 (2001) 18
- <sup>5</sup> S. Hough, *Europhotonics*, 1 (2003) 32
- <sup>6</sup> O. Graydon, *Opto& Laser Europe*, 4 (2003) 5
- <sup>7</sup> S. Tanaka, H. Yoshiyama, J. Nishiura et al, *SID Intl. Digest Tech Papers*, (1998) 296
- <sup>8</sup> R.H. Mauch, *J. of SID* 5/3 (1997) 173
- <sup>9</sup> P. Hill, *Displays Europe*, 4 (2002) 9
- <sup>10</sup> F. Reinitzer, *Monatsh. Chem.* 9 (1888) 421
- <sup>11</sup> O. Lehmann, *Z. Kristallogr. Mineral.*, 18 (1890) 464
- <sup>12</sup> M. Schadt, W. Helfrich, *Appl. Phys. Lett.* 18 (1971) 127
- <sup>13</sup> S. Naemura, *Displays* (2001) 1
- <sup>14</sup> H. Oyama, N. Shiramatsu. *Displays* 23 (2002) 31
- <sup>15</sup> G C. Williams, *Displays Europe* 4 (2002) 19
- <sup>16</sup> C. Williams, *Displays Europe*, 4 (2002) 18
- <sup>17</sup> K. M. Johnson, D. J. Mcknight, I. Underwood, *IEEE J. Quant. Electron.* 29 (1993) 699
- <sup>18</sup> R.L. Melcher, *Displays* 23,3 (2002) 1
- <sup>19</sup> M. Schuck, D. Mcknight, K. M. Johnson, *SID 97 Digest*, 28 (1997) 293
- <sup>20</sup> M. L. Jepsen, M. J. Ammer, et al *Displays* 23 (2002) 109
- <sup>21</sup> P. Hill, *Displays Europe*, May (2002)
- <sup>22</sup> P. Bonhote, E. Gogniat, F. Campus L. Walder, M. Gratzel, *Displays* 20 (1999) 137
- <sup>23</sup> P.M.S. Monk, R.J. Mortimer, D.R. Rossenisky, "Electrochromism", VCH, Weinheim, 1995
- <sup>24</sup> P. R. Somani, S. Radhakrishnan, *Materials Chemistry and Physics* 77 (2002) 117
- <sup>25</sup> A. Poor, *Information Display* 17(10) (2001) 18
- <sup>26</sup> M.O. M. Edwards, T. Gruszecki, H. Pettersson, G. Thuraisingham, and A. Hagfeldt, *Electrochemistry Communication*, 4 (2002) 963

- 
- <sup>27</sup> Ch Poynton, A Technical Introduction to Digital Video, Wiley Chichester, UK, (1996) 85
- <sup>28</sup> C W Tang, SID '97 Seminar F4, (1997)
- <sup>29</sup> T Inoguchi, M, Takeda, Y Kakihara, N Nakata and M Yoshida, Digest of 1974 SID International Symp (1974) 84
- <sup>30</sup> P D Rack, A Naman, P H Holloway, S -S Sun, R T Tuenge, MRS Bulletin 21 (1996) 49
- <sup>31</sup> R Khormaei, et al, SID '94 Digest, (1994) 137
- <sup>32</sup> O Prache, Displays 22 (2001) 49
- <sup>33</sup> R H Mauch, SID Journal 5/3 (1997) 176
- <sup>34</sup> R W G Hunt, Measuring Colour, 2<sup>nd</sup> Edition, Ellis Horwood, Chichester England & Prentice-Hall New York, (1991)
- <sup>35</sup> R F Bunshah, Deposition technologies for films and coatings Developments and Applications, Noyes Publications New Jersey (1982), 83
- <sup>36</sup> A Fuh, R P Gallinger and O Caporaletti, Can Journal of Physics 65 (1987) 1060
- <sup>37</sup> A C Gossard in Treatise on Material Science and Technology, Vol 24, K N Tu editor, Academic Press, New York, (1982) 13
- <sup>38</sup> P H Singer, Semiconductor International, Vol 6 (10) 73
- <sup>39</sup> E H Parker, editor, The Technology and Physics of Molecular Beam Epitaxy, Plenum Press, New York (1985)
- <sup>40</sup> W R Grove, Philos Trans Faraday Soc, 87 (1852)
- <sup>41</sup> B Chapman, S Mangano, Handbook of thin Film Deposition Processes and Techniques, edited by K K Schuegraf Noyes Publications, New York (1988) 291
- <sup>42</sup> J L Vossen and J J O'Neill RCA Review Vol 29, (1968) 566
- <sup>43</sup> S Higuchi, M Ushio, Y Nakanishi, and K Takahashi, Appl Surface Sc , 33/34 (1988) 667
- <sup>44</sup> S M Ojha, Physics of Thin Films, Vol 12, G Hass, M H Francome and J L Vossen editors, Academic Press, New York, (1982) 237
- <sup>45</sup> H Yasuda, Chapter IV-2 in Thin Film Processes, J L Vossen and W Kern editors Academic Press New York (1978) 361
- <sup>46</sup> W Kern and K K Schuegraf, Chapter 1 in Handbook of thin Film Deposition Processes and Techniques, edited by K K Schuegraf Noyes Publications, New York (1988) 1

- 
- <sup>47</sup> K L Choy, *Progress in Material Science*, 48 (2003) 57
- <sup>48</sup> T Suntola, J Anston, *J Soc Inform Display Dig* , (1980) 108
- <sup>49</sup> Ebelmen, *Annales de Chemie et de Physique*, Ser 3 Bd 57, (1846) 319
- <sup>50</sup> W Geffcken E Berger, *Deutsches Reichspatent* 736,411 May 6 (1939) assigned to Jenaer Glaswerk Schott and Gen , Jena
- <sup>51</sup> Prospect Glaser mit Oberflächenschichten Schott Glaswerke, Mainz, FRG (1981)
- <sup>52</sup> Prospect Glasohne ohne Reflexe Deutsche Spezialglas AG Grunenplan FRG
- <sup>53</sup> Prospect Carolex ® Das absolut farbneutrale Sonnenreflexionsglas von Schott Glaswerke Mainz FRG (1983)
- <sup>54</sup> H Dislich, P Hintz & R Kaufmann FRG Patent 1,941,191 Aug 1969 assigned to Jenaer Glaswerk Schott and Gen , Mainz FRG
- <sup>55</sup> H Dislich, *Angewandte Chemie International Edition* 10, 6 (1971) 363
- <sup>56</sup> E Wainer, *German Patent* 1,249,832 (April 11 1968)
- <sup>57</sup> H G Snowman, *U S Patent* 3,795,324 (March 5 1974)
- <sup>58</sup> S Horikuri, K Tsuji, Y Abe, Y Fukui, E Ichiki, *Japanese Patent* 49-108325 (Oct 15 1974)
- <sup>59</sup> R Roy, *J Amer Ceram Soc* , 39 (4) (1956) 145
- <sup>60</sup> R M Dell, in *Reactivity of Solids*, eds J S Anderson, M W Roberts & F S Stone Chapman & Hall N Y (1972) 553
- <sup>61</sup> J L Woodhead, *Silicates Ind* , 37 (1972) 191
- <sup>62</sup> B E Yoldas, *J Mater Sc* , 10 (1975) 1856
- <sup>63</sup> B E Yoldas, *J Mater Sc* , 12 (1977) 1203
- <sup>64</sup> M Yamane, A Shinji & T Sakano, *J Mater Sc* , 13 (1978) 865
- <sup>65</sup> H Pentinghaus, *J Non- Cryst Solids*, 63(1984) 193
- <sup>66</sup> L C Klein, *Glass Industry*, 63 No 5 (1982) 27
- <sup>67</sup> C J Brinker, D E Clark, D R Ulrich, (eds) *Mat Res Soc Sym Proc* 32 (1984) New York, Elsevier Science Publishing Co
- <sup>68</sup> L Klein "Sol-Gel Technology for Thin Films, fibers, preforms, electronics and speciality shapes" ed L Klein (1988) Noyes publications
- <sup>69</sup> R C Methora, F Babonneau, C Sanchez & J Livage *J Non-Cryst Solids*, 106 (1988) 170
- <sup>70</sup> H Schmidt, *Sol-Gel Science and Technology Proceedings of the Winter School on glasses and ceramics from gels*, (14-19 Aug) (1989) 61

- 
- <sup>71</sup> H Schroder, in *Physics of Thin films*, Vol 5, G. Hass ed. Academic Press NY (1969) 87
- <sup>72</sup> H. Dislich in "Sol-Gel Technology for Thin Films, fibers, preforms, electronics and speciality shapes" ed L. Klein (1988) Noyes publications, 50
- <sup>73</sup> I. Thomas, in "Sol-Gel Technology for Thin Films, fibers, preforms, electronics and speciality shapes" ed L. Klein (1988) Noyes publications, 5
- <sup>74</sup> H. Schroder & G. Gliemerth, US Patent 3597252 Aug 3 1971 assigned to J. G. Schott & Gen.
- <sup>75</sup> R. Roy, *J. Amer. Cer. Soc.*, 6 (1969) 344
- <sup>76</sup> I. Thomas, "Sol-Gel Technology for Thin Films, fibers, preforms, electronics and speciality shapes" ed L. Klein (1988) Noyes publications 2
- <sup>77</sup> R. K. Iker *The Chemistry of Silica*, Wiley NY (1979)
- <sup>78</sup> T. Witten, L. M. Sanders, *Phys Rev. Lett.*, 47 (1981) 1400
- <sup>79</sup> R. B. Pettit et al "Sol-Gel Technology for Thin Films, fibers, preforms, electronics and speciality shapes" ed L. Klein (1988) Noyes publications, 91
- <sup>80</sup> M. Prassas, L. L Hench, in *Ultra Structure Processing of Ceramics, Glasses and Composites* eds Hench L.L. & Ulrich D. R. Wiley NY (1984)
- <sup>81</sup> B.E. Yoldas, *J. Mater. Sc.*, 21 (1986) 1087
- <sup>82</sup> B. Gauthur-Manuel et al *J Phys.*, 48 5 (1987) 869
- <sup>83</sup> C.J. Brinker, G.W. Scherer, *Sol-gel Science: The Physics and Chemistry of Sol-gel Processing*, Academic Press San Diego (1990)
- <sup>84</sup> Shaw T.M. *Phys Rev. Lett.*, 59 15 (1987) 1671
- <sup>85</sup> A. Newport, C. Gibbons, J. Silver and A. Vecht, *IEE Proc.-Circuits Devices Syst.*, 145 5 (1998) 364
- <sup>86</sup> C.J. Brinker, G.W. Scherer, *J Non-Cryst. Solids*, 70 (1985) 301
- <sup>87</sup> C. Perry, *Institute of Electrical Engineers*, (1998) 2/1
- <sup>88</sup> A. J. Hurd, in H. Bergna (ed.), *The Colloidal Chemistry of Silica*, (ACS Adv. In Chem. Series)
- <sup>89</sup> L. E. Scriven in C. J. Brinker, D. E. Clark and D. R. Ulrich eds., *Better Ceramics Through Chemistry III*, Materials Research Society Pittsburgh PA, (1988) 717
- <sup>90</sup> R. P. Spiers, C. V. Subaram & W. L. Wilkinson, *Chem. Eng. Sci.*, 29 (1974) 389
- <sup>91</sup> D. L. Landau & B. G. Levich, *Acta. Physiochim. U.R.S.S.*, 17 (1942) 42
- <sup>92</sup> M. L Parodi, et al, *SID 94 Digest* (1994) 933

- 
- <sup>93</sup> D E Bornside, C W Macosko and L E Scriven, *J Imaging Tech* , 13 (1987) 122
- <sup>94</sup> B Higgins, *Phys Fluids* 29 (1986) 3522
- <sup>95</sup> G Pantano, R K Brow and L A Carman in "Sol-Gel Technology for Thin Films, fibers, preforms, electronics and speciality shapes" ed L Klein Noyes Publications (1988) 110
- <sup>96</sup> J L Vossen, W Kern (eds), *Thin Film Processes* Academic Press New York (1978) 1
- <sup>97</sup> K Reidling, *Industrial Applications of Ellipsometry*, Springer-Verlag Wien, New York (1988) 6
- <sup>98</sup> R M A , Azzam N M Bashara, *Ellipsometry and Polarized Light*, Amsterdam North Holland (1977)
- <sup>99</sup> H G Tompkins, *A Users Guide to Ellipsometry*, Academic Press Inc , San Diego (1993)
- <sup>100</sup> P Griffith, J DeHaseth, *Fourier Transform Infrared Spectrometry*, Wiley Interscience (1986)
- <sup>101</sup> R M Silverstein, G C Bassler, T C Morrill, *Spectroscopic identification of organic compounds (fifth Ed)* J Wiley & Sons (1991) 290
- <sup>102</sup> N B Coltnup, L H Daly, S E Wiberley, *Introduction to Infrared and Raman Spectroscopy 3<sup>rd</sup> Ed* , Academic Press NY (1990)
- <sup>103</sup> P Hendra, C Jones, G Wanws, *Fourier Transform Raman Spectroscopy Instrumental and Chemical Applications* Prentice-Hall, Englewood Cliffs, NJ 1991
- <sup>104</sup> D Kouyate, J C Ronfard-Haret, P Valat, et al *J Luminescence*, 46 (1990) 329
- <sup>105</sup> V I Petrov, *Physics-Uspekhi*, 39(8) (1996) 807
- <sup>106</sup> P L Washington, H C Ong, Y J Dai, & R P H Chang, *Appl Phys Lett* , 74 (1999) 1114
- <sup>107</sup> B G Yacobi, D B Holt, *Cathodoluminescence Spectroscopy of Inorganic Solids* New York Plenum Press (1990)
- <sup>108</sup> W L Bragg, *The Crystalline State, Vol I A General Survey*, George Bell, London, (1933)
- <sup>109</sup> T E Jenkins, *Semiconductor Science, Growth and Characterization Techniques*, Prentice Hall (1995) 369
- <sup>110</sup> K Kanaya, S Okayama, *J Phys D Appl Phys* , 5 (1972) 43
- <sup>111</sup> S M Sze, "Physics of Semiconductor Devices", Wiley & Sons Inc (1981) 31
- <sup>112</sup> F Wenner, "Bulletin of the Bureau of Standards", 12 (1915) 469

- 
- <sup>113</sup> L. B. Valdes, "Proc. IRE", 40 Nov (1952) 1429
- <sup>114</sup> F.M. Smits, "Bell Syst. Tech. J.", 37 (1958) 711
- <sup>115</sup> L. B. Valdes, "Proc. IRE", 42 Feb (1954) 420
- <sup>116</sup> L.J. Van de Pauw, "Phil. Res. Rep", 13 (1958) 1
- <sup>117</sup> RCA Corporation, RCA Electro-Optics Handbook, RCA, (1974)
- <sup>118</sup> J.K. Berkowitz, J. A. Olsen, J. Luminescence, 50 (1991) 111
- <sup>119</sup> P. M. Jaffe, J. Electrochem. Soc., 108 (1961) 711
- <sup>120</sup> W. A. Thornton, Bull. Am. Phys., 3 (1958) 233
- <sup>121</sup> L. H. Zhang, L. Wang, W. Tong, Y.-B. Xin, "Luminescent Materials", Materials Research Soc., Symposium Proceedings Vol. 560 ed. J. McKittrick, B. Di Bartolo, K. Mishra, Materials Research Society, Warrendale Pennsylvania, (1999)
- <sup>122</sup> P. Rack, P. Holloway, Materials Science And Engineering, R21 (1998) 194
- <sup>123</sup> A.H. Kitai (ed), Solid State Luminescence Theory, Materials and Devices, Chapman & Hall (1993)
- <sup>124</sup> U. Rössler, H. Landolt, R. E. Bornstein, Semiconductors: Intrinsic Properties of Group IV Elements and III-V, II-V and I-VII Compounds, Berlin, New York, Springer Verlag, (1987) 167
- <sup>125</sup> R.H. Bube, Proc. I.R.E. 43 (1955) 1836
- <sup>126</sup> D. Curie, "Optical Properties of Ions in Solids," B. DiBartolo (ed.), Plenum Press New York (1975) 71
- <sup>127</sup> G. F. Imbusch, Chapter 1 "Luminescence Spectroscopy", Academic Press New York (1978)
- <sup>128</sup> V. Balzani, F. Bolleta, et al., J. Chem. Physics, 78 (1983), 5317
- <sup>129</sup> A. H. Kitai (ed.), Solid State Luminescence, Theory, Materials and Devices Chapter 2. Chapman and Hall 1993
- <sup>130</sup> M. Inokuti, F. Hirayama, "Influence of energy transfer by the exchange mechanism on donor Luminescence", J. Chem. Phys. 43, (1965) 1978-1989
- <sup>131</sup> B. DiBartolo, (ed.) Energy transfer processes in Condensed matter. Plenum, New York (1984)
- <sup>132</sup> G. Blasse, Prog. Solid St. Chem. 18 (1988) 79-171
- <sup>133</sup> S. Tanaka, V. Shanker, M. Shiiki, H. Deguchi and H. Kobayashi, Digest of 1985 SID International Symposium, (1985) 218
- <sup>134</sup> K.K. Bajaj, Materials Science and Engineering, R34 (2001) 59



- 
- <sup>135</sup> J I Frenkel, *Phys Z Sowjet Union* 9 (1936) 158
- <sup>136</sup> G H Wannier, *Phys Rev* 52 (1937) 191
- <sup>137</sup> P Jaszczyn-Kopec, B Canny, *J Luminescence* 28 (1983) 319-326
- <sup>138</sup> D Curie, *Luminescence in Crystals*, Wiley, New York, (1962) 129
- <sup>139</sup> D Come, J S Prener, *Physics and Chemistry of II-VI compounds*, M Aven, J Prener (eds ), North Holland Publ Comp Amsterdam, Chapter 9, (1967)
- <sup>140</sup> O Modelung, M Schulz, W Von der Osten, U Rossler, H Landolt, R E Bornstein, *Semiconductors Intrinsic Properties of Group IV Elements and III-V, II-V and I-VII Compounds*, Berlin, New York, Spring Verlag, (1987) 319
- <sup>141</sup> B Segall, D T F Marple, *Physics and Chemistry of II-VI compounds*, M Aven, J Prener (eds ), North Holland Publ Comp Amsterdam, Chapter 1, (1967)
- <sup>142</sup> Y R Yang, C B Duke, *Phys Rev B* 36 (1987) 2763
- <sup>143</sup> P Eckelt, *Phys Stat Sol* , 23 (1967) 307
- <sup>144</sup> K H Hellwege, O Modelung, M Schulz, H Weiss, I Broser, H Landolt, R E Bornstein, *Semiconductors Intrinsic Properties of Group IV Elements and III-V, II-V and I-VII Compounds*, Berlin, New York, Spring Verlag, (1987) 359-361
- <sup>145</sup> M Aozasa, H Chen, *Thin Solid Films*, 199 (1991) 129
- <sup>146</sup> P Rack & P Holloway, *Materials Science And Engineering*, R21 (1998) 171
- <sup>147</sup> Y A Ono, in *Encyclopaedia of Applied Physics*, ed G L Trigg, VCH Publishers Inc American Institute of Physics, Weinheim and New York, 5 (1993)
- <sup>148</sup> S Kobayashi, S Tanaka, *SID Journal* 4(3) (1996) 157
- <sup>149</sup> Y Charreine, *J Electrochem Soc* 140 (1993) 7
- <sup>150</sup> D Come, J S Prener, *Physics and Chemistry of II-VI compounds*, M Aven, J Prener (eds ), North Holland Publ Comp Amsterdam, (1967) 473
- <sup>151</sup> H E Gumlich, *J Luminescence* 23 (1981) 73
- <sup>152</sup> A Kumar Arora, A Mansingh, *J Phys D Appl Phys* , 24 (1991) 1462
- <sup>153</sup> S Gupta, J A McClure V P Singh, *Thin Solid Films*, 299 (1997) 33
- <sup>154</sup> A J Warren, C B Thomas, H S Reehal and P R C Stevens, *J Luminescence*, 28 (1983) 147
- <sup>155</sup> M B Bhise et al, *J Appl Phys* , 67 (1990) 1492
- <sup>156</sup> C Benecke, W Busse H E Gumlich and H -J Moros *J Luminescence* 40&41 (1988) 627
- <sup>157</sup> N E Rigby, J W Allen *J Luminescence*, 42 (1988) 143

- 
- <sup>158</sup> M. Katiyar, A. H. Kitai, *J. Luminescence*, 52 (1992) 309
- <sup>159</sup> M. Katiyar, A. H. Kitai, *J. Luminescence*, 46 (1990) 227
- <sup>160</sup> W. Lehmann, *Electroluminescence proceedings of the Sixth International Workshop on Electroluminescence*, Cinto Punto Press, El Paso, (1992) 65
- <sup>161</sup> P. De Visschere, K. Neyts, *J. Luminescence*, 52 (1992) 313
- <sup>162</sup> S. Schön, M. Chaichimansour, W. Park, T. Yang, B. K. Wagner and C. J. Summers, *J. Crystal Growth*, 175/176 (1997) 598
- <sup>163</sup> A. Mikami, I. Yashima, F. Kajikawa, *Electroluminescence proceedings of the Eight International Workshop on Electroluminescence*, Cinto Punto Press, El Paso, (1996) 369
- <sup>164</sup> T. Kiichi et al. *Electroluminescence proceedings of the Eight International Workshop on Electroluminescence*, Cinto Punto Press, El Paso, (1996) 61
- <sup>165</sup> A. Zeinert, P. Benalloui, J. Benoit, C. Barthou, J. Dreyhsig, H.E. Gumlich, *J. Appl. Phys.* 71 (6) (1992) 2855
- <sup>166</sup> J. Mita, M. Koisumi, H. Kanno, T. Hayashi, Y. Seikido, I. Abiko, K. Nihei, *Jpn. J. Appl. Phys.* 26 (1987) 558
- <sup>167</sup> M. Aozasa, K. Kato, T. Nakayama, K. Ando, *Jpn. J. Appl. Phys.* 29 (1990) 1997
- <sup>168</sup> C.T. Hsu, J.W. Liu, Y.K. Su, T.S. Wu, Y. Yokoyama, *Jpn. J. Appl. Phys.* 71 (1992) 1509
- <sup>169</sup> K. Ohmi, S. Tanaka, Y. Yamano, K. Fujimoto, H. Hobayashi, R.H. Mauch, K.O. Velthaus, H.W. Schock, *Jpn. Display S19-4* (1992) 725
- <sup>170</sup> Y.H. Lee, D.H. Kim, B.K. Ju, M.H. Song, T.S. Choh, M.H. Oh, *J. Appl. Phys.* 78 (1995) 4253
- <sup>171</sup> T. Nire, A. Matumoto, A. Miyakoshi, K. Ohmi, *Jpn. J. Appl. Phys.* 33 (1994) 2605
- <sup>172</sup> K. Hirabayashi, H. Kozawaguch, *Jpn. J. Appl. Phys.* 28 (1989) 814
- <sup>173</sup> S. Sinh, P.D. Keir, J.F. Wagner, *J. Appl. Phys.* 78 (1995) 5775
- <sup>174</sup> M. Ohring "The Material Sc. of Thin Films" 2<sup>nd</sup> Edition, Academic Press, 2001
- <sup>175</sup> H. S. Carslaw, J.C. Jaeger, "Conduction of Heat in Solids", Oxford University Press, (1959)
- <sup>176</sup> B. Tuck, "Introduction to Diffusion in Semiconductors", Institute of Electrical Engineers, Peter Peregrinus Ltd., Stevenage, England, (1974)
- <sup>177</sup> H.S. Carslaw, J.C. Jaeger, *Conduction of Heat in Solids* Oxford Univ. Press, 1959
- <sup>178</sup> W.A. Johnson, *Trans AIME* 147 (1942) 331

- 
- <sup>179</sup> G E Murch, A S Norwick, 'Diffusion in crystalline Solids', Academic Press (1984)
- <sup>180</sup> D Gupta, P S Ho, 'Diffusion Phenomena in Thin Films and Microelectronic Materials' Noyes Publications (1988)
- <sup>181</sup> B Tuck, J Phys D9 (1976) 1559
- <sup>182</sup> L Boltzmann, Annln Phys , 53 (1894) 959
- <sup>183</sup> C Matano, Japan Phys , 8 (1933) 109
- <sup>184</sup> P G Shewmon, 'Diffusion in Solids', New York McGraw-Hill (1963)
- <sup>185</sup> R Ghez 'A Primer of Diffusion Problems' Wiley Interscience, J Wiley & Sons, New York (1988)
- <sup>186</sup> J Crank, "The Mathematics of Diffusion", Second addition, Oxford Science Publications, London (1975)
- <sup>187</sup> Joint Committee on Powder Diffraction Standards, Card No 05-664
- <sup>188</sup> Joint Committee on Powder Diffraction Standards, Card No 05-0566
- <sup>189</sup> Joint Committee on Powder Diffraction Standards, Card No 05-0492
- <sup>190</sup> J W Fulton, Chemical Engineering 2 (1986) 118
- <sup>191</sup> N Romeo, S Cozzi, R Tedeschi, A Bosio, V Canevari, M A Tagliente, M Penza, Thin Solid Films, 348 (1999) 49
- <sup>192</sup> T Kawasima, H Taniguchi, H, Kato, F Yokoama, K Shibata, Electroluminescence proceedings of the Sixth International Workshop on Electroluminescence, Cinto Punto Press, El Paso, (1992), 299
- <sup>193</sup> Y-M Yu, S Nam, B O , K-S Lee, Y D Choi, M-Y Yoon, P Y Yu, Materials Chemistry and Physics, 78(2002) 149
- <sup>194</sup> C Lan, K Hong, W Wang, G Wang, Solid State Communications, 125 (2003) 455
- <sup>195</sup> G Destriau, J de Chimie Physique, 33 (1936) 587
- <sup>196</sup> S S Chadha, Chapter 6 "Solid State Luminescence", ed by A H Kitai, Chapman & Hall (1993) 159
- <sup>197</sup> W A Barrow, R E Coovert, C N Krug, M J Zruchkovski, SID 88 Digest, (1988) 284
- <sup>198</sup> K Okibayashi, T Ogura, K Terada, K Taniguchi, T Samashita, M Yosheda, S Nakajima, SID 91 Digest, (1991) 275

- 
- <sup>199</sup> S Kobayashi, Y Oaki, T Yoshii, T Anzakı, K Enjoı, Digest of 1991 SID International Symposium, (1991) 84
- <sup>200</sup> N E J Hunt, E F Schubert, R A Logan & G J Zydzyk, Appl Phys Lett 61 (1992) 2287
- <sup>201</sup> C W Tang & S Van Slyke, Appl Phys Lett 51 (1987) 913
- <sup>202</sup> H Nakada & T Tohma in "Inorganic and Organic Electroluminescence", R H Mauch & H-E Gumlich eds , W&T Verlag, Berlin (1996) 385
- <sup>203</sup> A Dodabalapur, L J Rothberg, T M Miller, Electronic Lett , 30/12 (1994) 1000
- <sup>204</sup> M Matsuura, H Tokailın, et al Proc of Asia Display '95 (1995) 269
- <sup>205</sup> J H Burroughes, D D C Bradley, A R Brown et al , Nature 347(1990) 539
- <sup>206</sup> H K Schmidt, SPIE Critical Reviews, CR68 (1997) 192
- <sup>207</sup> M A Fardad, M Fallahı, Electronic Lett , 34 (1998) 20
- <sup>208</sup> T Inoguchi, T Takeda, Y Kakihara, Y Nakata, M Yoshida, Digest of 1974 SID International Symposium, (1974) 84
- <sup>209</sup> G O Muller, R Mach, Journal of Luminescence, 40&41 (1988) 92
- <sup>210</sup> D Wauters et al, Journal of Crystal Growth, 204(1999) 97
- <sup>211</sup> C N King, Electroluminescence proceedings of the Eight International Workshop on Electroluminescence, Cinto Punto Press, El Paso, (1996) 375
- <sup>212</sup> X Wu, Electroluminescence proceedings of the Eight International Workshop on Electroluminescence, Cinto Punto Press, El Paso, (1996) 285
- <sup>213</sup> K Netys, et al, Electroluminescence proceedings of the Eight International Workshop on Electroluminescence, Cinto Punto Press, El Paso, (1996) 43
- <sup>214</sup> E Schlam, SID Seminar Lecture Notes 1991 SID International Symposium, (1991) F-1/22
- <sup>215</sup> H Yoshiyama et al, Electroluminescence proceedings of the Tenth International Workshop on Electroluminescence, Cinto Punto Press, El Paso, (1998) 48
- <sup>216</sup> S S Chadha, Solid State Luminescence, ed by A H Kitai, Chapman & Hall (1993) 198
- <sup>217</sup> G O Muller, Solid State Luminescence, ed by A H Kitai, Chapman & Hall (1993) 139
- <sup>218</sup> S Kobayashi, Electroluminescence proceedings of the Sixth International Workshop on Electroluminescence, Cinto Punto Press, El Paso, (1992) 179

- 
- <sup>219</sup> A. Aguilera, V. Singh, D.C. Morton, Digest of 1994 SID International Symposium, (1994) 565
- <sup>220</sup> S. Bhaskaran, V. P. Singh, J. C. McClure, D.C. Morton Digest of 1994 SID International Symposium, (1994) 133
- <sup>221</sup> S. Kobayashi, et al., Electroluminescence proceedings of the Sixth International Workshop on Electroluminescence, Cinto Punto Press, El Paso, (1992) 234
- <sup>222</sup> Y. Nakanishi, et al., Electroluminescence proceedings of the Eight International Workshop on Electroluminescence, Cinto Punto Press, El Paso, (1996) 395
- <sup>223</sup> B. K. Wagner, W. Tong and C. J. Summers, Electroluminescence proceedings of the Eight International Workshop on Electroluminescence, Cinto Punto Press, El Paso, (1996) 403
- <sup>224</sup> P. Rack & P. Holloway, Materials Science And Engineering, R21 (1998) 184
- <sup>225</sup> R. Mach, Electroluminescence proceedings of the Sixth International Workshop on Electroluminescence, Cinto Punto Press, El Paso, (1992) 31
- <sup>226</sup> H. J. Fitting, T. Hingst Electroluminescence proceedings of the Eight International Workshop on Electroluminescence, Cinto Punto Press, El Paso, (1996) 25
- <sup>227</sup> K. Bhattacharyya, S. M. Goodnick, J. F. Wagner, Electroluminescence proceedings of the Sixth International Workshop on Electroluminescence, Cinto Punto Press, El Paso, (1992) 55
- <sup>228</sup> S. M. Goodnick, M. Dür, S. Pennathur, Electroluminescence proceedings of the Eight International Workshop on Electroluminescence, Cinto Punto Press, El Paso, (1996) 13
- <sup>229</sup> J. Fogarty, W. Kong, R. Solanki, Digest of 1994 SID International Symposium, (1994) 569
- <sup>230</sup> E. Bringuier, Electroluminescence proceedings of the Sixth International Workshop on Electroluminescence, Cinto Punto Press, El Paso, (1992) 379
- <sup>231</sup> E. Bringuier, Electroluminescence proceedings of the Eight International Workshop on Electroluminescence, Cinto Punto Press, El Paso, (1996) 19
- <sup>232</sup> Y. A. Ono, "Electroluminescent Displays", in H.L. Ong (Ed.), Series on Information Display, World Scientific (1995), Vol 1 48
- <sup>233</sup> N. T. Gordon, *IEEE Transactions on Electron Devices*, Vol., ED-28 4 (1981) 434
- <sup>234</sup> J. W. Allen, *Journal of Luminescence*, 48&49 (1991) 18
- <sup>235</sup> A. H. Kitai, *Journal of Luminescence*, 39 (1988) 227

- 
- <sup>236</sup> N T Gordon, IEEE Transactions on Electron Devices, 24, 4 (1981) 343
- <sup>237</sup> S Sze, Physics of Semiconductor Physics, Wiley, New York, (1981), 149
- <sup>238</sup> H-E Gumlich, H-Ch Mertins, Ch Jung, J of Crystal Growth, 159 (1996) 1041
- <sup>239</sup> M Ogawa, S Nakada, M Sakurai, T Yoshioka, J of Luminescence, 29 (1984) 11
- <sup>240</sup> A F Cattel, A G Cullis, Thin Solid Films, 92 (1982) 211
- <sup>241</sup> E A Masio, C B Thomas, W M Cranton, E Fogarassy, Appl Surface Sc 157 (2000) 74
- <sup>242</sup> J Zhou, H Goto, N Sawaki, I Akasaki, J of Luminescence, 35 (1986) 255
- <sup>243</sup> L V Zavyalova, A K Savin, G S Svechnikov, Displays, 18 (1997) 73
- <sup>244</sup> V C Chaudhari, R H Patil, M G Patil, C S Shalgonkar, Materials Chem and Phys , 59 (1999) 162
- <sup>245</sup> R Scheps, J of Luminescence, 42 (1988) 295
- <sup>246</sup> Y F Kononets, R Tornqvist, N A Vlasenko, Electroluminescence proceedings of the Sixth International Workshop on Electroluminescence, Cinto Punto Press, El Paso, (1992) 259
- <sup>247</sup> S Bhushan, A N Pandey, B R Kaza, J of Luminescence 20 (1979) 29
- <sup>248</sup> J Yu, H Liu, Y Wang, W Jia, J of Luminescence, 79 (1998) 191
- <sup>249</sup> O Sahní, P M Alt, D B Dove, W E Howard, D J McClure, Proc 1980 Biennial Display Research Conference, IEEE (1980) 154
- <sup>250</sup> W E Howard IEEE Trans Electron Devices, 24 (1997) 903
- <sup>251</sup> Y A Ono, Electroluminescent Displays, in H L Ong (ed), Series on Information Display World Scientific, Singapore, Vol 1 (1995) 65
- <sup>252</sup> D Crakner, Information Display 13 (1997) 10
- <sup>253</sup> Y H Lee, I J Chung, M H Oh, Appl Phys Lett , 58 (1991) 962
- <sup>254</sup> K Chen, G R Yang, M Neilson, T M Lu, E J Rymaszewski, Appl Phys Lett , 70 (1997) 399
- <sup>255</sup> R Ludeke, H J Wen, Appl Phys Lett 71 (1997) 3123
- <sup>256</sup> J C Lambropoulos, S S Hwang Proc Mater Res Soc Symp , 284 (1993) 133
- <sup>257</sup> T Shibata, K Hirabayashi, H Kozawaguchi, B Tsujiyama, Jpn J Appl Phys , 26 (1987) L1664
- <sup>258</sup> V P Singh S Bhaskaran J C McClure, J SID 4/2 (1996) 59
- <sup>259</sup> A N Krasnov, R C Bajcar, P G Hofstra, Appl Phys Lett , 73 (1998) 351

- 
- <sup>260</sup> P Thioulouse, *Electrochem Soc Spring Meeting Extended Abstracts*, 83/1 (1983) 910
- <sup>261</sup> D H Smith *J Luminescence*, 23 (1981) 209
- <sup>262</sup> A N Krasnov, *Thin Solid Films*, 347 (1999) 1
- <sup>263</sup> Y W Lam, H C Lam, *J Phys D Appl Phys*, 9 (1976) 1677
- <sup>264</sup> S McCulloch, G Stewart, R M Guppy, J O W Norris, *Intr J of Optoelectronics*, 9/3 (1994) 235
- <sup>265</sup> R B Pettit, C J Brinker, *Solar Energy Materials*, 14 (1986) 269
- <sup>266</sup> S K Gupta C G Audain, *SPIE*, 269 (1984) 179
- <sup>267</sup> C J R Gonzales-Oliver, P F James, H Rawson, *J Non-Cryst Solids*, 48 (1982) 129
- <sup>268</sup> A C Adams, C D Capio, *J Electrochem Soc* 126/6 (1979) 1042
- <sup>269</sup> S Bruynooghe, F Bertin, A Chabli, J-C Gay, B Blanchard, M Couchaud, *Thin Solid Films* 313-314 (1998) 722
- <sup>270</sup> J -Y Zhang I W Boyd, *Met Sci in semiconducting Processing* 3 (2000) 345
- <sup>271</sup> P M Glaser, C G Pantano, *J Non-Cryst Solids*, 63 (1984) 209
- <sup>272</sup> K A Andrianov, *Organic Silicon Compounds Moscow (1955)*, Translation 59-11239 U S Dept of Commerce Washington D C
- <sup>273</sup> S Sakka, K Kamiya, in *Materials Science Research Vol 17, Emergent Process methods for High-Technology Ceramics*, eds T Davis, H Palmer, T Porter (1984) 83
- <sup>274</sup> A McEvoy, PhD Thesis Dublin City University, Dublin 1996
- <sup>275</sup> M Matsui, H Nagayoshi, G Muto, S Tanimoto, K Kuroiwa and Y Tarui, *Jpn J Appl Phys Part 1* (1990), 29
- <sup>276</sup> Y Nakagawa and T Okada *J Appl Phys*, 68 (1990), 556
- <sup>277</sup> J -Y Zhang, L -J Bie and I W Boyd *Jpn J Appl Phys Part 2*, 37 (1998), L27
- <sup>278</sup> H Terui and M Kobayashi *Appl Phys Lett*, 32 (1978), p 666
- <sup>279</sup> N Rausch, E P Burte, *Microelectron Eng* 19 (1992) 725
- <sup>280</sup> F Z Tepehan, F E Ghodsi, G G Tepehan and N Ozer, *Solar Energy Materials and Solar Cells*, Volume 46, Issue 4, July 1997, Pages 311
- <sup>281</sup> L Young, *Proc R Soc London*, A244 (1958) 41
- <sup>282</sup> F Vratny, *J Electrochem Soc* 114 (1967) 505
- <sup>283</sup> T Kato, T Ito, *J Electrochem Soc* 135 (1988) 2586

- 
- <sup>284</sup> M Pessa, R Makela, T Suntola, Appl Phys Lett 38 (1981) 131
- <sup>285</sup> T Takahashi, H Itoh, J Less-Common Met 38 (1972) 211
- <sup>286</sup> T J Rehg, J A Ochoa-Tapia, A Knoesen, B G Higgins, Appl Opt 28 (1989) 5215
- <sup>287</sup> T Oishi, T Nakazawa, A Katou, Electron Comp Jpn 76 (1993) 50
- <sup>288</sup> F E Ghodsi, F Z Tepehan and G G Tepehan, Thin Solid Films, Volume 295, Issues 1-2, 28 February 1997, Pages 11-15
- <sup>289</sup> C Chaneliere, J L Autran, R A B Devine, B Balland, Mat Sc & Eng R22 (1998) 269
- <sup>290</sup> Y Kavanagh, M J Alam, D C Cameron, (in print Thin Solid Films)
- <sup>291</sup> J -Y Zhang, B Lim and I W Boyd, Thin Solid Films 336, (1998) 340
- <sup>292</sup> R A B Devine, Appl Phys Lett 68 (1996) 1924
- <sup>293</sup> C Chaneliere, J L Autran, R A B Devine, B Balland, Mat Sc & Eng R22 (1998) 269
- <sup>294</sup> J Aranovich et al J Vac Sc Technol 16(4) (1979) 994
- <sup>295</sup> Th Aeugle et al , Thin Solid films, 201 (1991) 293
- <sup>296</sup> S Saito et al , J Am Ceram Soc , 68 [1] (1985) 40
- <sup>297</sup> M J Alam, Preparation and Characterization of Insulating and Transparent Conducting Thin Films for Thin Film Electroluminescent Devices by Sol-Gel Process, PhD Thesis DCU (2001)
- <sup>298</sup> W J JeOng, Solar Energy Materials and Solar Cells, 65 (2001) 37
- <sup>299</sup> P Nunes, E Fortunate, R Martins, Thin Solid Films, 383 (2001) 277
- <sup>300</sup> F C M Van De Pol et al , Thin Solid Films, 204 (1991) 349-364
- <sup>301</sup> B S Panwar et al , Thin Solid Films, 168 (1989) 291
- <sup>302</sup> J F Chang, M H Hon, Thin Solid Films, 386 (2001) 79
- <sup>303</sup> M F Ogawa et al , J of Materials Sc Letters, 9 (1990) 1354
- <sup>304</sup> J S Kim et al , Thin Solid Films, 217 (1992) 133
- <sup>305</sup> A K Gyani et al Thin Solid Films, 182 (1989) L1
- <sup>306</sup> A S Riad, S A Mahmoud, A A Ibrahim, Physica B, 296(2001)319
- <sup>307</sup> D Goyal et al , Jpn J Appl Phys , 31 (1992) 361
- <sup>308</sup> Y Segawa, Phys Stat Sol , (b) 202 (1997) 669
- <sup>309</sup> L Armelo, Thin Solid Films, 394 (2001) 90
- <sup>310</sup> W Tang, D C Cameron, Thin Solid Films, 238 (1994) 83



- 
- <sup>311</sup> N I Kovtyukhova, E V Buzaneva, C C Waraksa & T E Mallouk, *Mat Sc & Eng B* 69-70 (2000) 411
- <sup>312</sup> S K Ghandhi, *VLSI Fabrication Principles silicon and gallium arsenide*, Wiley New York, (1983)
- <sup>313</sup> J M Liu, C K Ong, L C Lim, *Ferroelectrics*, 231 (1999) 223
- <sup>314</sup> P M Alt, *Proc SID* 25 (1984) 123
- <sup>315</sup> C N King, 1985 SID Seminar Lecture Notes Vol 1 S-4 (1985) 4 1/1
- <sup>316</sup> P M Alt, *SID Digest* (1984) 79
- <sup>317</sup> D H Smith *J Luminescence* 23 (1981) 209
- <sup>318</sup> D C Krupka, *J Appl Phys* , 43 (1972) 476
- <sup>319</sup> T Inoguchi and S Mito in *Electroluminescence*, ed J I Pankov, (Topics in Applied Physics, Vol 17) Springer-Verlag, Berlin (1977) 196
- <sup>320</sup> E Bringuier, A Geoffroy, *Appl Phys Lett* , 48 (1986) 1780
- <sup>321</sup> H Diamant, K Dranck, R Pepinsky, *Rev Sci Instrum* , 28 (1957) 30
- <sup>322</sup> C N King *Journal of the Society of Information Display* 1 (1996) 1
- <sup>323</sup> S K Tiku, G C Smith, *IEEE Trans Electron Devices* ED-31 (1984) 105
- <sup>324</sup> A A Douglas, J F Wagner, *SID Digest of the 1992 SID International Symposium* (1992) 356
- <sup>325</sup> J F Wagner, A A Douglas, D C Morton in *Electroluminescence Proceedings of the Sixth International Workshop on Electroluminescence* eds V P Singh and J C McClure Cinto Puntos Press, El Paso (1992) 387
- <sup>326</sup> G O Mueller in *Electroluminescence Proceedings of the Sixth International Workshop on Electroluminescence* eds V P Singh and J C McClure Cinto Puntos Press, El Paso (1992) 102
- <sup>327</sup> Y A Ono, H Kawakami, F Fuyama & K Onisawa, *Jpn J Appl Phys* , 26 (1987) 1482
- <sup>328</sup> W Tang, D C Cameron, *Thin Solid Films*, 280(1996) 221
- <sup>329</sup> W Tang, *Electroluminescent Displays by Sol-gel Process*, PhD Thesis, DCU (1994) 163
- <sup>330</sup> Y A Ono, "Electroluminescent Displays", in H L Ong (Ed ), *Series on Information Display*, World Scientific (1995), Vol 1 31
- <sup>331</sup> M H Song, Y H Lee, T S Hahn, M H Oh, K H Yoon, *Solid State Electronics*, 49, 9 (1998) 1711

- 
- <sup>332</sup> K Vanheusden, C H Seager, W L Warren, D R Tallant, J Caruso, M J Hampden-Smith, T T Kodas, *J Luminescence*, 75(1997) 11
- <sup>333</sup> K H Yoon and J Y Cho, *Mater Res Bull*, 35 (2000) 39
- <sup>334</sup> K Ohmi, S Tanaka, Y Yamano, K Fujimoto, H Kobayashi, R H Mauch, K O Velkhaus and H W Schock, *Jpn , Display S19-4* (1992) 725
- <sup>335</sup> K Ohmi, S Tanaka, H Kobayashi and T Nire in *Electroluminescence Proceedings of the Sixth International Workshop on Electroluminescence*, eds , V P Singh and J C McClure, Cinto Punto Press, El Paso, (1992) 309
- <sup>336</sup> T Suzuki, Y Uno, J Sakurai, Y Saito, S Kyojuka, N Hiji and T Ozawa, *Digest of 1992 SID International Symposium*, (1992) 344